FP7-ICT-2007-C
Objective ICT-2007.8.0
FET-Open 222107

NIW
Natural Interactive Walking

Deliverable 7.3

Book on ecological foot based interfaces and interactions

F. Fontana (UNIUD)
Y. Visell (UPMC)

Sep. 30, 2011
v. 1.0

Classification: PU

INTRODUCTION

This deliverable contains an edited book, authored by key persons and collaborators in the NIW project along the three years.

The book will be entitled “WALKING WITH THE SENSES - Perceptual techniques for walking in simulated environments“ and is edited by Federico Fontana (UNIUD) and Yon Visell (UPMC). It will be published by Logos Verlag (Berlin) under the ISBN 978-3-8325-2967-3. The publisher will sell printed copies, along with putting the book content available online at no charge for the readers.

Although still in draft version, especially concerning some stylistic polishing as well as a number of minor issues of integration and referencing, the book core content is already in conclusive form. The production of this book occurred within a necessarily highly constrained schedule, which required, among other things, that relatively fresh research contents be digested and organized quickly in order to finalize the publication prior to the completion of the project itself.

The editors are confident to see the result of their efforts ready in a few weeks from now, meanwhile counting on the patience and comprehension of the project reviewers and the scientific officer for the unavoidable delay in finalizing this deliverable.

Federico Fontana
Yon Visell

Udine and Paris, Sep. 30, 2011.

Preface

The first inspiration to collectively study technologically-mediated interactions between the feet and ground, and the possibility to influence these interactions through novel human-computer interfaces, arose on while we were navigating the streets of Venice toward the railway station, after the conclusion of a research project meeting. The first ideas emerged while waiting for the "Vaporetto" water bus, as the boat stop bobbed gently under our feet on the waters of the lagoon, where we hypothesized preliminary directions for a research project on walking. Only later did we note the special position Venice occupied as it was evoked by Marcel Proust in his *Remembrance of Things Past* (*À la recherche du temps perdu*). The narrator of the book recalls a time when, while stepping into the courtyard of the Princess de Guermantes' residence in Paris, he is caught in a moment of accidental imbalance between two uneven flagstones, which joyfully evoked a similar experience he felt while walking at the baptistry of Piazza San Marco in Venice.

Of course, there was a more pragmatic impetus as well. Separate investigations at McGill University (on haptic interactive floors) and at the University of Verona (on footstep sound synthesis) spoke compellingly toward new possibilities that might emerge through such a joint collaboration. Although these technological tools were available, along with further expertise in areas including immersive virtual reality display and haptic engineering (at Univ. Paris 6, INRIA IRISA, and Aalborg University), the act of bringing these pieces together raised as many challenges as it solved. This included both pragmatic questions, such as how to effectively integrate different technologies, and more fundamental ones, related to the evaluation of novel, often multimodal perceptual effects that related to an interactive setting (human locomotion augmented with virtual multimodal stimuli) that had been seldom studied. The latter fit the goal of our investigation, which, complementing preexisting work on the design of walking interfaces for navigation in primarily visually rendered virtual environments, instead directed attention to the rich variety of multisensory phenomena that emerge when the foot and body enter into contact with a firm ground surface composed of complex, natural materials. The sounds, bodily movements, and tactile sensations we experience as a result signify the spaces we traverse in an intuitive and familiar way, and communicate to us their characteris-

tics. The ecological information we thus acquire allows us to balance, navigate and orient during everyday tasks in unfamiliar environments, by making use of the invariant ecological meanings that we have learned through extensive prior experience with walking tasks.

The ambitious and wide-ranging research plan we embarked on in the *Natural Interactive Walking* project is reflected in the contents of the present volume. Its goals included the design, prototyping and evaluation of multimodal floor-based machine interfaces for the interactive augmentation of otherwise "neutral" (i.e., flat, silent, and visually homogeneous) ground surfaces; the study of multisensory effects and cross-modal illusions, involving the senses of touch, kinesthesia, audition, and vision, that were made possible by the novel interfaces that were explored; the realization of rich interaction contexts based on ensembles of the previous interface designs; the study of foot-floor interaction paradigms occurring in these contexts, and of the opportunities that they may offer thanks to the high sensitivity of the human feet. Applications of such paradigms may include active signalling for simplified navigation in functional spaces, support to human labor in hostile environments, and healthcare applications for aiding people with reduced foot sensitivity and during rehabilitation of impairments affecting locomotion.

To innovate within a field encompassing such a wide spectrum of knowledge requires competence and technical skills in a diverse array of topics that are not accessible to any single scientific or engineering researcher, that are essentially collaborative and interdisciplinary. However, we took encouragement from the existence of compelling research in related interdisciplinary research areas, including haptic interaction for the hands and human interaction in virtual reality environments. Indeed, several of the technologies and methodologies described in the chapters of this book can be said to be borrowed, at least in part, from those fields. Success in this endeavor could only be achieved through the collaboration of an ensemble of researchers organized around an ambitious set of interrelated goals, which also permitted sufficient independence for them to develop constituent competencies. The research plan was enriched with further components having an orientation toward applications in virtual reality: among these, the development of novel interfaces for navigation in virtual spaces.

The Natural Interactive Walking project was realized thanks to funding from the European Union and the Québec Ministère de Developpement Economique, Innovation, et Exportation which permitted a team of researchers to collaborate on the themes described above for a total of three years. In providing a survey of the most interesting results of this project, the present book represents one of the most important products of the project itself. The result is far from free of defects, as the strong interdisciplinary character of the research makes it difficult to integrate it into a global view. As a result, and in spite of the editorial efforts made in bringing together the present content, we expect that the reader will notice the discontinuities that we, as principle project investigators, have endeavored to smooth out during the course of evolution of the research.

Finally, the production of this book occurred within a necessarily highly constrained schedule, which required, among other things, that relatively fresh research

contents be digested and organized quickly in order to finalize the publication prior to the completion of the project itself. While this may have diminished the quality, it has allowed us to make this book available in the public domain. Ultimately, we think this is a worthy outcome, one of its most dear qualities.

As one final note at the outset, as editors, we agreed that we would be listed in the bibliographic data in alphabetic order, since any classification based on the order of names included would not be able to acknowledge the joint effort we have both made on the book, acknowledging from the beginning that neither editor's work was more important to realizing this book.

Udine, Paris — *Federico Fontana*
September 2011 — *Yon Visell*

Contents

List of Contributors

Laurent Bonnet
INRIA, Rennes, France, e-mail: laurent.bonnet@inria.fr

Gabriel Cirio
INSA / INRIA, Rennes, France, e-mail: gabriel.cirio@inria.fr

Marco Civolani
DIMI, University of Udine, Udine, Italy, e-mail: marco.civolani@uniud.it

Jeremy Cooperstock
CIRMMT, McGill University, Montreal, Canada, e-mail: jer@cim.mcgill.ca

Mathieu Emily
Université Rennes 2, Rennes, France e-mail: mathieu.emily@uhb.fr

Federico Fontana
DIMI, University of Udine, Udine, Italy, e-mail: federico.fontana@uniud.it

Vincent Hayward
UPMC, Université Paris 06, Paris, France, e-mail: vincent.hayward@isir.upmc.fr

Anatole Lécuyer
INRIA, Rennes, France, e-mail: anatole.lecuyer@inria.fr

Maud Marchal
INSA / INRIA, Rennes, e-mail: maud.marchal@inria.fr

Rolf Nordahl
Medialogy, Aalborg University Copenhagen, Copenhagen, Denmark, e-mail: rn@media.aau.dk

Stefano Papetti
DI, University of Verona, Verona, Italy, e-mail: stefano.papetti@univr.it

Rishi Rajalingham
CIRMMT, McGill University, Montreal, Canada, e-mail: rishi@cim.mcgill.ca

Stefania Serafin
Medialogy, Aalborg University Copenhagen, Copenhagen, Denmark, e-mail: sts@media.aau.dk

Severin Smith
CIRMMT, McGill University, Montreal, Canada, e-mail: sparky@cim.mcgill.ca

Léo Terziman
INSA / INRIA / DGA, Rennes, e-mail: leo.terziman@inria.fr

Luca Turchet
Medialogy, Aalborg University Copenhagen, Copenhagen, Denmark, e-mail: tur@media.aau.dk

Yon Visell
UPMC, Université Paris 06, Paris, France, e-mail: yon@zero-th.org

Acronyms

Use the template *acronym.tex* together with the Springer document class SVMono (monograph-type books) or SVMult (edited books) to style your list(s) of abbreviations or symbols in the Springer layout.

Lists of abbreviations, symbols and the like are easily formatted with the help of the Springer-enhanced `description` environment.

ABC	Spelled-out abbreviation and definition
BABI	Spelled-out abbreviation and definition
CABR	Spelled-out abbreviation and definition

Chapter 1
Introduction: New technologies for walking with the senses

F. Fontana and Y. Visell

In a 1939 paper, J. A. Hogan analyzes the incident in which Marcel Proust entered the courtyard of the Princess de Guermantes' residence in Paris when:

> His feet came to rest on two uneven flagstones, and as he balanced from one to the other a delicious sensation swept through his body. Proust continued to exploit this sensation which brought him so much joy [...] he swayed back and forth on the two uneven flagstones, oblivious to his surroundings. But what? Where? How came he by these sensations? [...] Then suddenly it was revealed to him. It was Venice. One day, long since past, he had stood in the baptistry of St. Mark's in Venice, balanced on two uneven flagstones. His present experience balancing on the stones in the Guermantes' courtyard was sufficiently like that one in the past to call up from within him that day in Venice, which he had for so long a time kept buried deep inside him. [122]

The experience Proust felt upon walking into this courtyard is regarded as fundamental to the creation of his celebrated *Remembrance of Things Past* and to the aesthetic theory that pervades all his Recherche. Leaving the significance of this event to Proust's aesthetic universe aside, it is worth noting the impact that the activity of exploring the flagstones with his foot had in awakening pieces of his previously acquired experience. Significantly, the association he makes is strongly non-visual. It is moreover unlikely that the two flagstones he depresses in Paris are particularly similar in shape, size or configuration to those he earlier encountered at the baptistry of St. Mark's in Venice. These few observations can also be read as containing the essential seeds that this book attempts at fertilizing, from a quite different, scientific, perspective.

The activation of memory through interaction with the external world lies near the core of Proust's experience. Compared to the experiences, visual, olfactory, and gustatory, that achieved this during other incidents of his books – as he was looking through the trees of the church spires of Martinville, and, most famously, while dipping a madeleine cake in herbal tea – at least two major differences can be noted. First, the experience is strongly kinesthetic, linked to the perception and active movement of his body. Second, it is non-visual, stemming from somatosensations involving touch, equilibrium, proprioception, and perhaps even reinforced

by the sounds that were produced during the acts of movement and walking. Later, Proust's sensations would be overwhelmed by the sound of traffic in Paris, causing him to open his eyes, and to become present, attending to his immediate surroundings. The interaction depicted in the passage can also be described as "natural". Proust is fed by a number of stimuli pertaining to his everyday experience. They did not need to be mediated by any training, adaptation, or cultural translation. Any part of the Venetian experience that may have had a linguistic component, for example, would not have naturally linked to the Parisian environment. The two experiences gave rise to perceptual ecologies with significant common elements, and, through this overlap, the subject established a mental window into his memory.

Finally, Proust's perception was facilitated by means of an especially sensitive human interface that has not received enough attention in prior literature on human-computer interaction: the feet. By directly exploring certain characteristics of the surface he walked on he was able to uncover the non-visual perceptual invariants that were related through his remembrance.

Many aspects of touch sensation in the feet, including its roles in the sensorimotor control of balance and locomotion over different terrains, have been studied in prior scientific literature. Considerably less is known about how the nature of the ground itself is perceived, and how its different sensory manifestations (touch, sound, visual appearance) and those of the surroundings contribute to the perception of properties of natural ground surfaces, such as their shape, irregularity, or material composition, and our movement upon them. Not surprisingly then, in human-computer interaction and virtual reality little research attention has been devoted to the simulation of multisensory aspects of walking surfaces in ways that could parallel the emerging understanding that has, in recent years, enabled more natural means of human computer interaction with the hands, via direct manipulation, grasping, tool use, and palpation of virtual objects and surfaces. These advances have been greatly supported by the improved level of understanding of human hand function and behavior, at scales ranging from the microphysiology and biomechanics of the skin to high-level perceptual processes and neural or cognitive activity involved during object manipulation.

To support the collection of similar knowledge and to identify suitable mechanisms of interaction with the feet, we launched a research effort aimed at uncovering salient roles played by multisensory, and especially non-visual, perceptual information during locomotion and other interactions with the feet, and to apply the results of this investigation to advance the state-of-the-art in human-computer interaction with the feet. The present book summarizes the results of this effort, in presenting devices, methods, and interactive techniques that aim to reproduce virtual experiences of walking on natural ground surfaces, enabled primarily through the rendering and presentation of virtual multimodal cues of ground properties, such as texture, inclination, shape, material, or other affordances, in the Gibsonian sense. As suggested by the discussion above, the results presented here are organized around the hypothesis that walking, by enabling rich interactions with floor surfaces, consistently conveys enactive information that manifests itself through multimodal cues, and especially via the haptic and auditory channels. In order to better distinguish

this investigation from prior work, we adopt a perspective in which vision plays a primarily integrative role linking locomotion to obstacle avoidance, navigation, balance, and the understanding of details occurring at ground level. The ecological information we obtain from interaction with ground surfaces allows us to navigate and orient during everyday tasks in unfamiliar environments, by means of invariant meanings that we have learned through prior experience with walking tasks.

On the side of interactive technology, the realization of novel interfaces of any kind proceeds, ideally, through design and evaluation cycles, often involving several iterations and multiple layers, including basic engineering, design, and perceptual and usability assessment. For highly interactive and multimodal interfaces such as those presented in this volume, the challenge of evaluation from either of these perspectives is especially pronounced, and this is even more true when the interactions themselves are intended to have an ecological character – that is, preserving, as far as possible, the complex perception-action relationships encountered in real world environments. Due to the developmental and scientific challenges involved, the results described here constitute, in many ways, pointers to directions of departure for this research – first steps, so to speak, toward the realization of natural walking interfaces.

This book is organized in a way that reflects the heterogeneity of the topical area it addresses. The engineering of tactile interfaces for the foot represents a new, and still nascent, development in haptics, and this novelty is reflected in the contents of the chapter by Hayward et al., which introduces new actuator and display technologies for presenting vibrotactile stimuli to the foot. The two chapters by Visell et al. treat applications of computationally augmented floor surfaces for basic tasks in human-computer interaction - namely, interaction with floor-based touch surface interfaces and tracking of persons via in-floor force sensors. Chapters by Terziman and Marchal respectively describe methods for navigating in immersive virtual reality environments and for rendering "pseudo-haptic" effects, which are capable of modulating the perceived kinesthetic sense of slope, ground shape, or material by means of visuo-haptic or visuo-vestibular cross modal interactions. In their chapter, Serafin et al. review some of the methods available for synthesizing the sound of virtual footsteps in response to real-time data specified by either movements of an individual in a virtual environment or by another real-time control process. They also describe the use of such synthetic stimuli in experiments on the perception of walking sounds and soundscapes containing them. In contrast to these unimodal assessments of the perception of walking, the chapter by Nordahl et al. presents the results of a number of multi- or cross-modal perceptual effects related to walking in virtual environments. These may be useful for render specific effects in an immersive virtual environment (e.g., ground slope, softness) or for increasing the level of realism, immersion, or presence felt by users of such an environment. Finally, the chapter of Cirio et al. presents physically-based techniques, and a number of evocative interactive scenarios, for realizing fully multimodal, interactive experiences of walking on virtual ground surfaces.

It is hoped that this collection may prove interesting for researchers in related fields of engineering, computing, perception, and the movement sciences, and, fur-

ther, that a positive result of the incomplete nature of the results presented here may lie in its ability to suggest directions for future research.

Chapter 2
Novel haptic displays for walking interactions

V. Hayward, Y. Visell, S. Serafin, F. Fontana, and M. Civolani

Abstract This chapter describes three approaches to hardware design for foot-oriented haptic devices. The first approach entails tiling a floor and actuating each individual tile according the movements of the walkers and the effects that are desired. Each tile is responsive to the forces applied by the foot. The second approach is to embed vibrotactile transducers in shoes. Interaction forces resulting from foot pressure are sensed with a view to produce virtual interactions with ground surfaces. A wireless communication architecture is described that makes it possible to eliminate the cumbersome cables that may reduce the applicability of worn devices in a virtual reality settings. A third approach is to haptically enable an existing interface. Here, this approach is exemplified by haptically enabling an exercise device known as a wobble board.

2.1 Introduction

When the shoed foot hits the ground, a series or mechanical events ensue. There can be an impact, or merely a soft landing, according to the type of shoe, the type of ground, and the stride of the walker. Once the initial transitory effects have vanished and until the foot lifts off the ground, there can be crushing, fracturing, or hardly anything at all if the ground if stiff. There can also be slipping if the ground is solid, or soil displacement if the ground is granular. There can be other mechanical effects, such as soil compacting.

The question of what form of haptic signal to reproduce in virtual reality applications is therefore not so simple to answer. The sense of touch, which in the foot has properties comparable to that in the hand, is not easy to fool. It has, in fact, great discriminative acumen, even through a sole [113]. But like vision or audition, in accordance to the perceptual task, it may be satisfied by little. Simply think of carrying a conversation on a portable phone—which is far from providing any amount

of fidelity—or watching a black and white TV which dispenses an optical field that is hardly realistic.

The success of these transducers is first and foremost linked to their ability to deliver a minimal level of temporal and spatial information. Anything above this level is enhancement. In the case of foot, our habit to wear shoes plays in our favor since shoes filter out most of the distributed aspects of the haptic interaction with the ground, save perhaps for a distinction between the front and back of the foot at the moment of the impact. In that sense, wearing a shoe is a bit like interacting with an object through a hand-tool. The later case, as is well known, is immeasurably easier to simulate in virtual reality than direct interaction with the hand.

When it comes to stimulating the foot, the options are intrinsically limited by the environmental circumstances. While it is tempting to think of simulating the foot by the same methods as those used to stimulate the hand [115, 116], this option must be discarded in favor of approaches that are specific to the foot. In particular, options involving treadmills, robot arms and other heavy equipment will remain confined to applications where the motor aspects dominate over the perceptual aspects of interacting with a ground [139, 237, 60, 74].

The fidelity of a haptic device depends on a number of factors, including the selection and arrangement of sensing and actuating components, and on its structural mechanical design. The structural design of vibrotactile (VT) displays has, in the past, received less attention. In addition to the devices described in other sections of this chapter, the vibrotactile augmentation of touch surfaces has been widely investigated for HCI applications [244, 103, 204], although design issues affecting their perceptual transparency have often been neglected.

In the following, we describe two, non necessarily exclusive, approaches to stimulating the foot with the simulated high-frequency components, viz. 30–800 Hz, of a foot-ground interaction. As it turns out, a great deal of sensation can be obtained this way, including sensations that tradition would normally ascribe to kinesthesia [312]. One approach is to tile a floor and actuate each tile according to the movement and interaction of the walker or the user. Another approach is to provide the walker with shoes augmented with appropriate transducers. Three foot-stimulating devices are now described, starting with floor-based stimulator, continuing with a shoe-based stimulator, and ending with a haptically augmented training device.

2.2 Vibrotactile floor display

The first design is based on a high fidelity vibrotactile interface integrated in a rigid surface. The main application for which this was envisioned is the vibrotactile display of virtual ground surface material properties for immersive environments. The device consists of an actuated composite plate mounted on an elastic suspension, with integrated force sensors. The structural dynamics of the device was designed to enable it to accurately reproduce vibrations felt during stepping on virtual ground materials over a wide range of frequencies. Measurements demonstrated that it is

capable of reproducing forces of more than 40 N across a usable frequency band from 50 Hz to 750 Hz.

In a broader sense, potential applications of such a device include the simulation of ground textures for virtual and augmented reality simulation [314] or telepresence (e.g., for remote planetary simulation), the rendering of abstract effects or other ecological cues for rehabilitation, the presentation of tactile feedback to accompany the operation of virtual foot controls, control surfaces, or other interfaces [315], and to study human perception. In light of the latter, an effort was undertaken to ensure a high fidelity response that would avoid artifacts and enable the presentation of carefully controlled stimuli in experiments involving human vibrotactile perception.

This device represents the first systematically designed vibrotactile floor component for haptic human-computer interaction. Passive floor-based vibrotactile actuation has been used to present low frequency information in audiovisual display applications, for special effects (e.g., vehicle rumble), in immersive cinema or VR settings [298]. The fidelity requirements that must be met by an *interactive* haptic display are, all things being otherwise equal, higher, since its users are able to actively sample its response to actions of the feet.

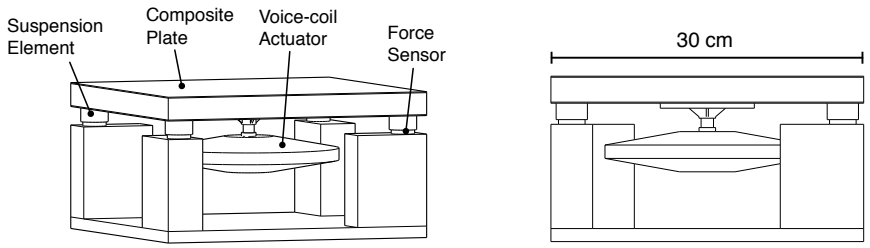

Fig. 2.1: Vibrotactile floor interface hardware for a single tile unit. Middle: View showing main components. Right: Side view with top dimension.

The interface of the device (Figure 2.1) consists of a rigid plate that supplies vibrations in response to forces exerted by a user's foot, via the shoe. The total normal force $F(t)$ applied to the plate by a user is measured. It can be assumed to consist of two components: isolated transients with high frequency content, generated by foot impacts with the plate, and low-frequency forces generated by active human motions, limited in bandwidth to no more than 10 Hz [51, 310]. Vibrotactile feedback is assumed to be constrained, due to actuator limitations, to frequencies greater than a minimum value on the order of 40 Hz. A haptic simulation provides feedback approximating the vibration response felt during interaction with a virtual object. The rendering algorithms are of admittance type, computing displacements (or their time derivatives) in response to forces applied to the virtual object.

The top plate of the tile provides an interface to the body, which in the case of this device is assumed to consist of a foot wearing a shoe. Statically, the device must resist bending when loaded vertically by a force of several hundred Newtons. The rigid deflection of the plate under this load must be minimized subject to the

constraint that the plate be able to vibrate freely, which can be used to infer suitable values of the mechanical parameters of the suspension elements [308].

The top plate consists of aluminum honeycomb sandwich panel component (dimensions $30.4 \times 30.4 \times 2.5$ cm, mass 400 g). This material was selected for its high bending stiffness to weight ratio. The plate is supported by cylindrical SBR rubber elastic elements positioned as shown in Figure 2.1. In dynamic or multi-tile configurations, a retaining socket surrounding the elastic support (not present in the figure) is used to keep the plate from changing position. The actuator is mounted via an aluminum bracket bonded to the center underside of the plate.

Force sensing is performed via four load cell force transducers (Measurement Systems model FX19) located below the vibration mount located under each corner of the plate. Although the cost for outfitting a single-plate device with these sensors is not prohibitive, potential applications of this device to interaction across distributed floor surface areas (see Chapter 3) may involve two dimensional $m \times n$ arrays of tiles, requiring a number $N = 4mn$ of sensors. As a result, in a second configuration, four low-cost resistive force sensors are used in place of load cells. After conditioning, the response of these sensors to an applied force is nonlinear, and varies up to 25% from part to part (according to manufacturer ratings). A measurement and subsequent linearization and force calibration of each is performed, using a calibrated load cell force sensor (details are provided in a separate publication [314]), and ensuring a linear response accurate to within 5%. Analog data from the force sensors is conditioned, amplified, and digitized via a custom acquisition board, based on an Altera FPGA, with 16-bit analog-to-digital converters. Data from each sensor is sampled at a rate of 1 kHz and transported to a host computer over UDP via the board's 10 Mbps Ethernet interface.

The tile is actuated by a single Lorentz force type inertial motor (Clark Synthesis model TST429) with a nominal impedance of 6 Ohms. The actuator has a usable bandwidth of about 25 Hz to 20 kHz, and is capable of driving the plate above strongly enough to quickly produce numbness in the region of the foot that is in contact with the tile. Digital to analog conversion of the signal driving the actuator is performed using a 24-bit, 96 kHz audio interface (Edirol model FA-101). Amplification is performed using a compact, class-D audio amplifier capable of providing 100 W to a nominal 4 Ohm actuator impedance. The resulting device is illustrated in Figure 2.2.

The magnitude frequency response was measured with a piezoelectric accelerometer (AKG model CP-411, calibrated) bonded to the top surface of the plate, as described in the caption of Figure 2.3. Frequency response measurements were taken for several different foot-plate contact conditions, while the foot was wearing a rubber soled shoe. These contact conditions modify the impedance of the display, altering its response. The results are shown in Figure 2.3.

An inverse filter H_c was further designed to equalize the device response in the frequency range from $f = 50$ Hz to 750 Hz, based on a digital IIR filter of order N, that was estimated to match the desired inverse filter using the least p-th norm optimization method [292]. Figure 2.3 compares the original (free) frequency response

Fig. 2.2: Photo with large mens' shoe, showing representative size. The model shown is based on the low-cost force sensing resistor option. The cable in the foreground interfaces the sensors with the data acquisition unit.

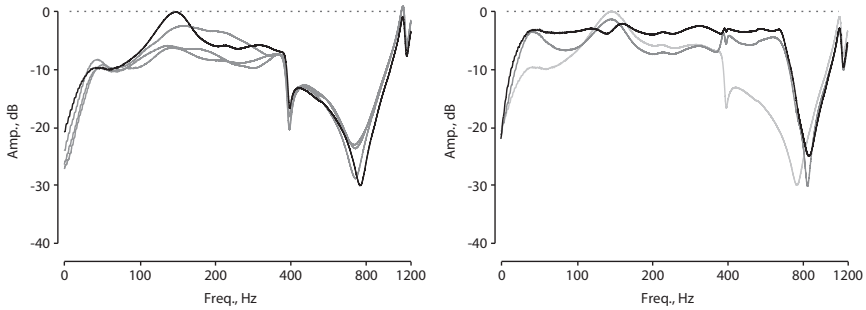

Fig. 2.3: Left: Measured log-scale magnitude frequency response of the display. Measurements were taken at a point equidistant from the plate center and edge, on a line through the center, 15 degrees from the diagonal. The free response is shown with a black line, and other foot-floor contact conditions with varying load applied via the foot are shown in gray. Right: Measured device response without foot contact, uncorrected (lightest gray) and with correction by digital IIR filters of order $N = 10$ (medium gray) and $N = 14$ (black).

of the device with those corrected by filters of order $N = 10$ and 14. In the latter case, the response is flat in a passband with -10 dB roll off near 50 Hz and 750 Hz.

2.3 Haptic shoes

In order to provide haptic feedback, haptic shoes enhanced with pressure sensors have been developed. A pair of light-weight sandals was procured (Model Arpenaz-50, Decathlon, Villeneuve d'Ascq, France). This particular model has light, stiff foam soles that are easy to gouge and fashion. Four cavities were made in the thickness of the sole to accommodate four vibrotactile actuators (Haptuator, Tactile Labs Inc., Deux-Montagnes, Qc, Canada). These electromagnetic recoil-type actuators have an operational, linear bandwidth of 50–500 Hz and can provide up to 3 G of acceleration when connected to light loads.

As indicated in Figure 2.4 and Figure 2.5, two actuators were placed under the heel of the wearer and the other two under the ball of the foot. They were bonded in place to ensure good transmission of the vibrations inside the soles. When activated, vibrations propagated far in the light, stiff foam. In the present configuration, the four actuators were driven by the same signal but could be activated separately to emphasize, for instance, the front or back activation, to strike a balance, or to realize other effects such as modulating different, back-front signals during heel-toe movements.

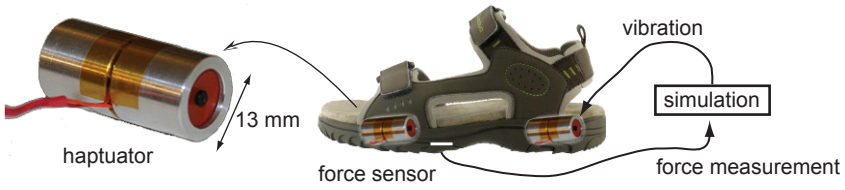

Fig. 2.4: System (one shoe shown). Left: recoil-type actuation from Tactile Labs Inc. The moving parts are protected by an aluminum enclosure able to bear the weight of a person. Middle: approximate location of the actuators in the sandal. Right: system diagram showing the interconnections.

Fig. 2.5: Photograph of pressure sensor and of two actuators embedded in the shoes.

The sole has two force sensitive resistors (FSRs) pressure sensors (Model I.E.E. SS-U-N-S-00039) aimed at detecting the pressure force of the feet during the locomotion of a subject wearing the shoes. The two sensors are placed in correspondence to the heel and toe respectively in each shoe.

The analogue values of each of these sensors are digitized by means of an Arduino Diecimila board (`http://arduino.cc/`) and used to drive the audio and haptic synthesis.

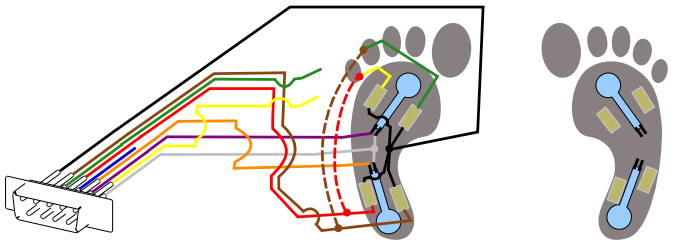

Fig. 2.6: Schematic representation of the cabling required to run sensors and actuators for one shoe.

A cable transports the signals for the pressure sensors and for the actuators to a breakout board which contains trimmers, that form voltage dividers with the FSRs, which then interfaces to an Arduino board. Another cable carries the actuator signals from stereo amplifiers (Model PCA1, Pyle Pro), driven by outputs from a soundcard (FireFace 800, RME Intelligent Audio Solutions). Each stereo amplifier handles 4 actuators found on a single shoe, each output channel of the amplifier driving two actuators connected in parallel. The PC handles the Arduino through a USB connection, and the FireFace soundcard through a FireWire connection.

The vibrotactile feedback has amplitude and bandwidth that are beyond the perceptual thresholds for the feet [195, 146]. However, much of the resulting perception depends on objective and subjective factors, such as type of stimulus, weight of the user, and foot position. By adjusting the coupling between the transducers and the feet, especially the second and third factors are responsible for major changes of the amplitude and bandwidth of the vibrotactile feedback.

Prototypes were equipped with TactileLabs TL002-14-A haptuators. When driven at high amplitudes, close close to distortion levels, and loaded with a normally-weighted person standing still, the sandal was measured to vibrate at the heel with the following peak amplitudes: longitudinal axis 1.5 μm; lateral axis 1.7 μm; orthogonal axis 0.9 μm. The magnitude peak in that prototype amounted to 2.4 μm. The measurements were not repeated for the new prototype, due to the large variability of the coupling depending on the foot position with respect to the ground. Similar peak amplitudes would be expected for a normally-weighted person standing still with her feet firmly adhering to the ground.

2.3.1 Wireless implementation

This section describes the design of wireless communication architecture and shoe interface capable of ensuring a reliable, low latency tactile feedback response to forces sensed underfoot. These features allowed to test algorithms for simulating ground surfaces, as described in subsequent chapters.

The sandals on which this architecture was tested are similar to those described above; they have force sensing resistors (Interlink FSR model 402) fixed under the insole: one at the toe and one at the heel. The sensors were connected to four analog inputs of an acquisition board (Arduino model Duemilanove) via a voltage divider. The force signals were digitally converted using a polling procedure. For every channel, each sample was encoded in 10 bits and encapsulated within two bytes [64].

As demonstrated in previous work, despite its low cost, the Arduino Duemilanove board could function as an adequately high performance front-end for signal acquisition on personal computers through appropriate customization of the firmware [64]. By using native AVR instructions with an optimized interrupt policy, efficient operation of the micro controller's onboard ADC can be ensured. Up to six analog channels can be reliably acquired at constant sampling rate with 10 bits resolution each. Moreover, the serial-over-USB interface could be forced to send synchronous data continuously, thus obtaining uniform sampling also at the host application side.

In the wireless data acquisition setup, packets are sent from the microcontroller board through serial communication to a 2.4 GHz wireless transceiver module (`http://www.sparkfun.com/products/152`) based on the Nordic Semiconductor nRF2401A chip. At the other end, an identical nRF2401A module received the data stream, providing fast and reliable paired wireless communication. The receiver forwarded the data to a second micro controller board, which in turns communicated with a personal computer via USB connection. The setup is depicted in Figure 2.7.

This setup was tested using a computer running an instance of the Pure Data real-time environment which fetches and processes the stream, synthesizing the audio-tactile signals. Since each shoe embedded two audio-tactile transducers, the software synthesizer provided four discrete output channels: a multichannel audio interface was thus required (RME Fireface 400). This way, the stereo signal originally generated for each shoe could be mixed to mono and routed into a two-channels bus. This setup allowed to use a stereo audio interface in the same manner as the internal chips available on ordinary laptop computers.

The audio four channels were grouped in two stereo pairs, one for each shoe, and were also transmitted wirelessly. Each pair was forwarded to an E-MU PIPEline wireless transceiver. Each transceiver was paired with an identical one working at the receiver side. Overall, a four channel audio simplex wireless connection was obtained. The line output of each E-MU at the receiver end fed a 15 W Dayton Audio DTA-1 Class D digital amplifier, driving two Dayton Audio DAEX32 transducers

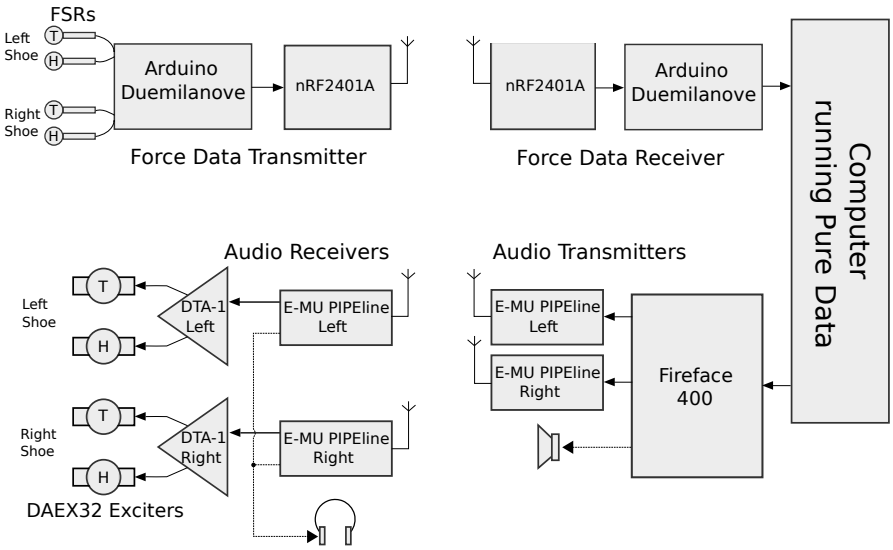

Fig. 2.7: Wireless communication architecture.

fixed under each sandal, one at the toe and one at the heel, closing the interaction loop. The transducers are visible in Figure 2.8, embedded in the sole.

Fig. 2.8: Instrumented shoes (bottom and top view).

Measurements performed on a previous prototype using the same data acquisition procedure [227] showed that the sensor sampling rate per analog channel depends on the speed of the serial communication and on the number of channels: with 115,200 bps, a sampling rate $F_s = 5882$/channels Hz was obtained, which corresponds to approximatively 1,470 Hz per channel using four sensors. After properly adjusting the audio buffer size, the input-output latency of the entire system including the synthesis, (i.e., from the acquisition board analog inputs to the analog outputs of the audio card) amounted to 15 ms.

2.4 Haptic wobble board

A wobble board, see Figure 2.9, is an exercise device primarily intended to strengthen one's ankles, to train the sense of balance, and to help in certain rehabilitation techniques [185]. It is also fun to master and is a favorite of surf and skate board enthusiasts. One common type is just a wooden disk with a rubbery coating on top. It has a half-spherical stand that makes it unstable. Standing on these devices requires, like in surfing, a very skilled postural behavior.

Frequent and regular use of the wobble board exercises both proprioception and motor skills. This exercise has been reported to enhance sensorimotor coordination in general and the sense of balance. In its basic form, the sensory inputs are restricted to kinesthetic signals, vestibular inputs and visual inputs. Highly skilled users can achieve balance with their eyes closed.

Since the wobble board is intended to be used repetitively at home, it can also become boring and tiresome. This motivated us to add sensors and actuators to the wobble board in such a way that it could be programmed to respond to its movements in a great variety of way, beyond and above its basic mechanics. This way, the board can be programmed to respond visually, acoustically and mechanically in variety of ways that may or may not be physically lawful, providing it with hyper realistic capabilities. During exercises, users can watch a screen, listen to sounds and feel high-fidelity vibrotactile stimuli which are all under computer control, while the kinesthetic and vestibular inputs are produced naturally. This way, a hyper-reality wobble board could be constructed at low cost, and provide a possibility to build exercises which are less tedious, while exploiting the possibilities offered by different kinds of feedback.

As shown in Figure 2.9, a traditional Wobble board was designed, with integrated sensors and actuators. Specifically, two vibrotactile actuators (Haptuator, Tactile Labs Inc., Deux-Montagnes, Qc, Canada) were accommodated between the two wooden circular layers of the board. The board on which one stands was replaced by two boards connected by specially designed structural elements that provide optimal compliance in the lateral direction independently from the load that they support, see Figure 2.9. The system also included a 2-axis accelerometer (from Phidgets Inc.) located between the two boards and which provides tilt information. This information can be used to drive the audio, visual and haptic synthesis algorithms.

Fig. 2.9: Actuated and instrumented wobble board.

2.5 Conclusion

We have described three approaches to the design of devices enabling the simulation of foot-ground interaction, each having advantages and shortcomings. The floor-based approach is versatile, but more expensive owing to the increased amount of hardware that must be deployed. It primarily appropriate for fixed installations that are typical of virtual reality settings. The shoe-based approach has a fixed cost per user, is straightforward to implement, and the problem of cables can be solved through wireless communication architectures. Finally, many devices with which people interact through the foot can be "hapticized". Here, we described how a training wobble board can be "haptically enabled".

Chapter 3
Distributed human-computer interaction with augmented floor surfaces

Y. Visell, S. Smith, and J. Cooperstock

Abstract This chapter presents techniques for interactive via the feet with touch sensitive floor surfaces that are augmented with multimodal feedback. After a discussion of prior research in this area, it discusses an approach based on an array of instrumented floor tiles distributed over an area of several square meters, capable of sensing forces and rendering visual, vibrotactile and acoustic feedback. Aspects of the basic usability of such displays for human-computer interaction are also discussed, and we present the results of a preliminary usability evaluation with a target selection task, which was conducted to provide preliminary indications of the appropriate size and layout for foot-operated controls rendered through the floor tile interface. Potential applications for such interfaces are also reviewed, including a novel interactive scenario involving the navigation of immersively presented geospatial data navigated via the feet.

3.1 Introduction

To date, there has been limited research on foot-based interaction for computationally augmented environments. Arguably, one reason for this has been a lack of efficient interfaces and interaction techniques capable of capturing touch via the feet over a distributed display. In the present chapter, we describe techniques for interacting with computationally augmented floor surfaces, including the design of an interface based on a distributed network of low-cost, rigid floor tile components, with integrated sensing and actuation. Taking advantage of the particular structure of this interface, we draw on contact sensing techniques, through which we capture foot-floor contact loci with finer resolution than would be achieved if a single tile were regarded as the smallest relevant spatial unit.

The techniques described here may also be used to mediate interactions between a walker and a virtual ground surface. Several interactive scenarios are described in

Chapter 8, with users enabled to walk on a virtual frozen pond or along a virtual seaside beach.

3.2 Background

3.2.1 Application domains for foot-floor human computer interaction

Foot-based human-computer interaction is gaining interest as a new means of interacting in virtual reality or in ambient computing spaces, with potential applications in areas such as architectural visualization, immersive mission training, or entertainment. Although many of these applications may be amenable to interaction within traditional mouse-click and scrolling or finger-based multitouch paradigms, we believe that manipulation and parsing of the immersive data sets involved could benefit from novel interaction paradigms that leverage the naturalness of interaction on foot and the greater number of degrees of freedom possible via sensing of body movements.

Virtual floor controls could be advantageous in areas of man-machine interaction in which foot operated controls or interfaces are already commonplace, such as manufacturing assembly and repair, mass transportation, vehicle operation, or dentistry. A virtualized display can be used to provide access to instrumentation or machine controls in a way that is flexible to different contexts of use (e.g., different dental procedures). Such an approach may overcome acknowledged problems with the proliferation of physical foot pedals and other controllers in medical interactions [324]. Applications to pedestrian navigation or map-based visualization could emerge as particularly salient, insofar as they may integrate the role of the foot in self-motion. Previously investigated applications of immersive virtual reality, such as architectural walkthroughs or training simulation, may benefit from the addition of context-based interactive maps or menus, as in the investigation of LaViola et al. [160]. Other relevant application fields could include entertainment, music performance, gaming, or advertising, where companies such as Gesturetek and Reactrix have successfully commercialized interactive, floor-based visual displays for marketing purposes.

3.2.2 Techniques and technologies

Examples of the use of foot-controlled input in HCI, interactive arts and video gaming date at least to the early 1980s, with Amiga's Joypad (1983) being one widely known example [273]. In the mid 1980s, Pearson and Weiser investigated foot input devices for desktop PCs, and invented a pedal-like device called the Mole [233].

However, despite the high-level of interest in touch screens for the hands, less research and development has targeted touch-sensitive interfaces for the feet. Interactive floor-based displays can be implemented using direct video capture of the feet (as in the Gesturetek and Reactrix systems), but such interfaces provide no direct information about foot-floor contact forces or contact areas. This information is arguably important for rendering interactions with virtual objects or controls, or for simulating highly contact-dependent interactions with virtual materials.

Direct tactile sensing for interaction with floor surfaces has conventionally been accomplished with surface-mounted force sensing arrays (e.g., [228, 267]). Such interfaces have been applied to applications including person tracking, activity tracking, or musical performance. Floor-mounted tactile sensing arrays are commercially available, but costs are high and support for real-time interaction is limited, since the predominant application areas involve offline gait and posture measurement.

Augsten et al. adapted the method of optical sensing via frustrated total internal reflection to enable the dynamic capture of foot-floor contact areas through back-projected translucent floor plates [20]. This method provides direct imaging of contact area, although it does not directly reveal forces. The main drawback to this approach is that it requires the installation of cameras and projectors within a potentially large recessed space that must be available beneath the floor. The authors implemented and evaluated the usability of foot-floor touch surface interfaces using this approach (Figure 3.1).

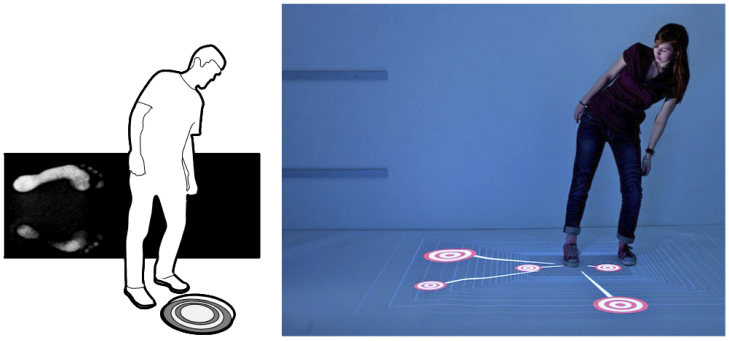

Fig. 3.1: The Multitoe interface of Augsten et al. [20] is based on the optical sensing of foot floor contact regions captured through back-projected translucent floor plates (image reproduced from [20]).

Sensations accompanying walking on natural ground surfaces in real world environments (sand in the desert, or snow in winter) are rich, multimodal and highly evocative of the settings in which they occur [310]. However, floor-based multimodal (visual, auditory, tactile) information displays have only recently begun to be investigated [313]. Related research on virtual and augmented reality environments has focused on the problem of natural navigation in virtual reality environments.

Solutions such as walking in place [293] and redirected walking techniques [253] map body movements sensed through kinematic tracking onto a user's coordinates in a virtual environment (VE). The shoe-based Step WIM interface of LaViola et al. [160] introduced additional foot gestures for controlling navigation in a larger VE via a floor map, but required special shoes and did not provide auditory or haptic feedback. A number of haptic interfaces for enabling omnidirectional in-place locomotion in VEs have been developed [123], but known solutions either limit freedom in walking, or are highly complex and costly.

Fig. 3.2: Left: The floor interface is situated within an immersive, rear projected virtual environment simulator. Right: Visual feedback is provided by top-down video projection (in the instance shown, this corresponds to a virtual, multimodal sand scenario — see Chapter 8).

3.3 A distributed multimodal floor tile interface

The interface developed by the authors [316] consists of an array of rigid tiles, each of which is instrumented with force sensors (four per tile) and a vibrotactile actuator. The prototype shown in Figure 3.3 comprises a square array of 36 tiles, with an area of approximately four square meters. The floor is coated in reflective projection paint, and a pair of overhead video projectors is used for visual display, with redundant projection making it possible to reduce the effect of shadows cast by users. The individual tile interfaces are rigid, plywood plates with dimensions $30.5 \times 30.5 \times 2$ cm, supported by elastic vibration mounts, and coupled to a vibrotactile actuator (Clark Synthesis, model TST229) beneath each plate [308]. Actuator signals are generated on personal computers, output via digital audio interfaces, and amplified.

Normal forces are sensed at locations below the corner vibration supports of each tile using a total of four resistive force sensors (Interlink model 402 FSR). Analog data from the force sensors is conditioned, amplified, and digitized via a 32-channel, 16-bit data acquisition board based on an Altera FPGA. Each sensor is sampled at a rate of up to 1 kHz transmitted over a low-latency Ethernet link. An

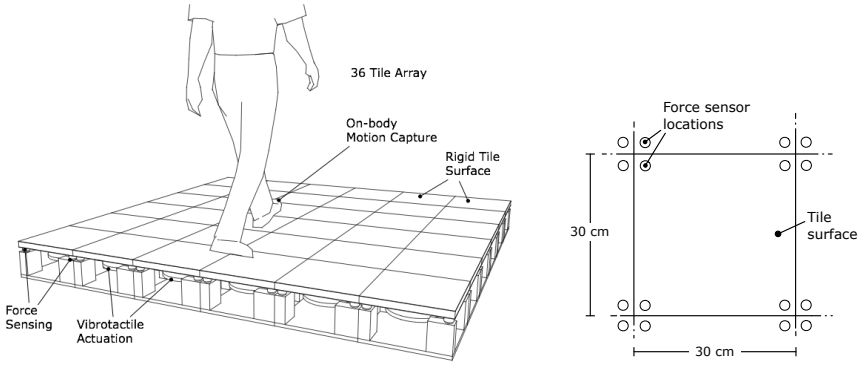

Fig. 3.3: Left: Diagrammatic view of the interface. Sensing and actuating components are integrated beneath the floor. Right: View from above showing sensor locations.

array of six small form factor computers is used for force data processing and audio and vibrotactile rendering. A separate, networked server is responsible for rendering visual feedback and managing user input.

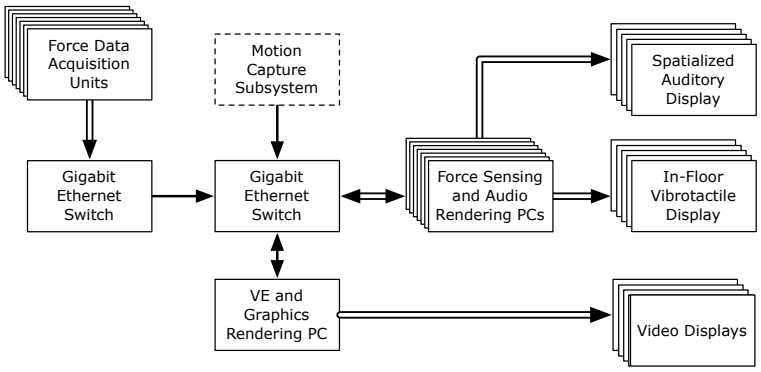

Fig. 3.4: Overview of system components and logical connections between them.

3.4 Contact sensing

For processing sensor data, we draw on intrinsic contact sensing, which aim to resolve the locations of contact, the forces at the interface, and the moment about the contact normals using internal force and torque measurements [36]. It is assumed to involve contact between a rigid object and a soft body (here, a foot), and has been previously used for robotic manipulation. Here we use it for capturing foot-ground

interactions via in-floor force sensors. It requires a number of sensors on the order of the number of rigid degrees of freedom of the structure, far fewer than are needed for tactile sensing via surface mounted arrays. Since a tile has fewer sensors than rigid body degrees of freedom, we make the simplifying assumption of frictionless contact via a normally directed pressure distribution, and further assume that the relative displacement of the suspension elements in the tile is negligible. The problem is then to resolve the location of a contact centroid $\mathbf{x}_c$ associated with a normal force distribution $p_R(\mathbf{x})$ within an area R. In our context, $\mathbf{x}_c$ is a contact point such that a normal force F_c at $\mathbf{x}_c$ gives rise to the same measurements as $p_R(\mathbf{x})$ does [36]. For a floor tile with sensor locations $\mathbf{x}_j$ where measurements f_j are taken (j indexes the tile sensors), $\mathbf{x}_c$ and the normal force $\mathbf{F}_c = (0,0,F_c)$ can be recovered from scalar measurements $\mathbf{F}_j = (0,0,f_j)$ via the force and torque equilibrium equations,

$$\sum_{j=1}^{4} f_j + F_c + f_p = 0 \tag{3.1}$$

$$\sum_{j=1}^{4} \mathbf{x}_j \times \mathbf{F}_j + \mathbf{x}_c \times \mathbf{F}_c + \mathbf{x}_p \times \mathbf{F}_p = 0\,. \tag{3.2}$$

$\mathbf{F}_p = (0,0,f_p)$ is the weight of the the plate and actuator at the tile's center $\mathbf{x}_p$. The three nontrivial scalar equalities (3.1, 3.2) yield:

$$F_c = \sum_{i=1}^{4} f_i - f_p, \quad \mathbf{x}_c = \frac{1}{F_c}\left(\sum_{i=1}^{4} (\mathbf{x}_i - \mathbf{x}_p) f_i + f_c \mathbf{x}_p\right) \tag{3.3}$$

The contact centroid lies within the convex hull of the contact area (dashed line, Figure 3.5) at the centroid of the pressure distribution [36], and thus provides a concise summary of the foot-floor contact locus, but not about shape or orientation. When the foot-floor contact area R overlaps multiple tiles, a pressure centroid $\mathbf{x}_c$

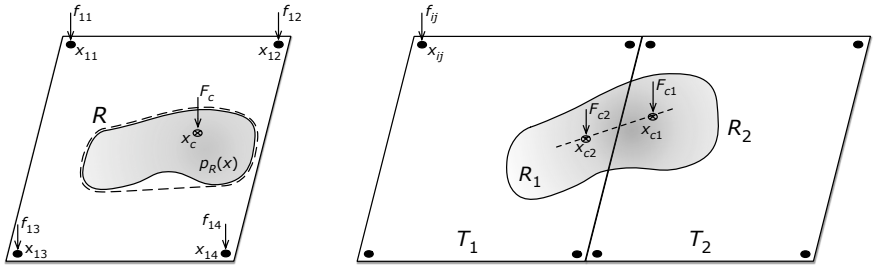

Fig. 3.5: Left: A normal force distribution $p_R(\mathbf{x})$ and associated contact centroid position $\mathbf{x}_c$. Right: A pressure distribution $p_R(\mathbf{x})$ on a region R spanning adjacent tiles. The weighted sum of centroids $\mathbf{x}_c$ is the centroid location for the distribution with support $R = R_1 \bigcup R_2$. It lies on the line segment connecting $\mathbf{x}_{c1}$ and x_{c2}. The difference $\delta\mathbf{x} = \mathbf{x}_{c1} - \mathbf{x}_{c2}$ provides information about contact shape

for the entire area can be computed from those $\mathbf{x}_{ck}$ for each tile (computed from Eq. (3.3)), via $\mathbf{x}_c = w_1\mathbf{x}_{c1} + w_2\mathbf{x}_{c2}$, where $w_k = F_i/F$. The domain-independence of this result makes it possible to continuously track contact across tile boundaries. The difference vector $\delta\mathbf{x} = \mathbf{x}_{c1} - \mathbf{x}_{c2}$ provides additional shape information about the orientation of the contact distribution at the boundary. For a linear pressure distribution spanning the two tiles, the direction vector $\mathbf{n} = \delta\mathbf{x}/|\delta\mathbf{x}|$ is the orientation, and $|\delta\mathbf{x}|$ is half of the length of R. For convex contact shapes that are less sharply oriented (such as those of a foot), the range of angles is compressed around the edge normal direction.

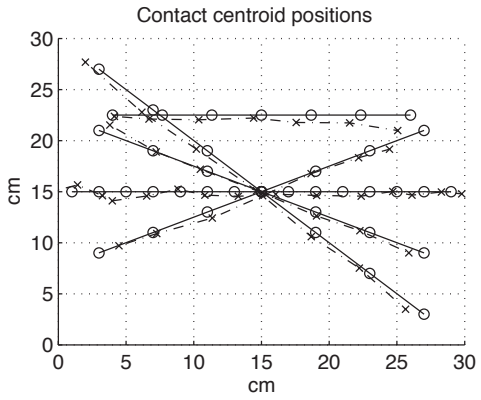

Fig. 3.6: Results of 50 measurements comparing true normal force positions (circles) with contact centroid estimates (Xs).

Figure 3.7 shows the sequence of contact centroid locations produced by an individual walking across the floor. When there is multi-tile foot-floor contact, as illustrated here, we use a simple clustering algorithm to associate nearby contact centroids that are assumed to belong to the same foot.

Figure 3.6 presents measurements of 50 estimated contact positions determined by the method of Eq. (3.3), using a single calibrated floor tile. Despite distortion near tile edges, contacts were localized with a typical accuracy of 2 cm, and worst-case values of ≈ 3 cm, smaller than the linear dimensions of the tile (30 cm) or the typical width of an adult shoe.

3.5 Floor touch surface interfaces

The sensing methods presented above can furthermore be employed to implement virtual floor-based touch interfaces. One set of examples we have created consists of an array of standard UI widgets to be controlled with the feet (Figure 3.8). Input is based on a multi-touch screen metaphor mediated by a set of interaction points

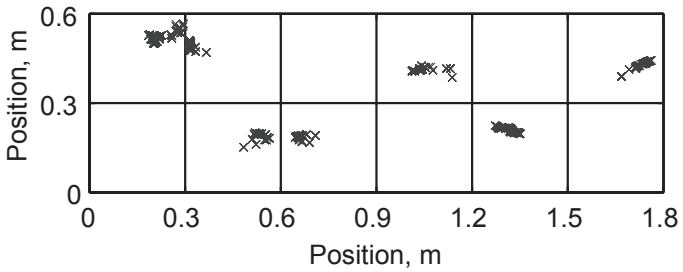

Fig. 3.7: A recorded sequence of contact centroids produced by an individual walking across the floor. Data was sampled each 100 ms to produce the figure. Each square corresponds to one floor tile. When the foot lies on a single tile, as weight shifts from heel to toe, an array of centroids is produced, moving in the direction of travel. At inter-tile boundaries, at each instant one centroid is produced on each tile that there is contact with.

(cursor locations), which are defined as the contact centroids $\mathbf{x}_c$ with the largest forces. Force thresholds associated with a control are used to determine selection. The controls provide positive tactile feedback supplied by the actuators, in the form of synthesized click-like transient vibrations or sliding (friction) vibrations.

3.5.1 Interface design toolkit

We developed a software layer and network protocol to facilitate the design of interactive applications using the floor surface. It abstracts the hardware systems, which are accessed over a local Ethernet network, and connects them to the user interface. The software layer also processes the sensor data to extract foot-floor contact points that are used for interaction, and provides them with unique IDs that persist while contact is sustained. Additionally, it allows to remotely cue and present localized vibrotactile feedback in response to activation or control of user interface objects on the floor. The design of this software layer is based, in part, on the TUIO protocol for table-top touch interfaces [145]. Figure 3.8 illustrates a virtual floor-based touch interface, consisting of sliders, buttons, toggle switches, and similar elements. The controls can be operated without consideration for the location of the tile boundaries, since we track interaction points continuously across tile boundaries. Normal force thresholds are used to determine when buttons or other controls are being engaged. Concurrent audio and vibrotactile feedback, in the form of clicks, taps, or rubbing sounds or vibrations, can be assigned to be supplied in tandem with the discrete or continuous response of a control.

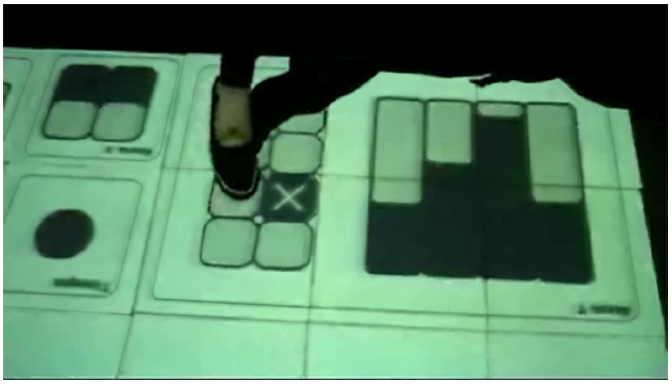

Fig. 3.8: A user interacting with floor-based interface widgets implemented with the interface design toolkit described here.

3.5.2 Usability of foot-floor touch surface interfaces

Due to the novelty of floor-based touch surface interfaces, a question that is soon encountered when beginning to design applications for them concerns the appropriate size and layout of virtual controls, and related features, such as informational overlays or menu structures. As in manual touch surface interaction, the appropriate size likely depends on a range of factors, including sensing limitations, users' motor abilities, target parameters, and feedback modalities, as has been extensively studied and modeled in the human-computer interaction literature [180, 142] and the subset of literature on touch screen usability [34, 10]. The size appropriate for touch screen controls has been shown to depend on the interaction technique adopted. Precision control strategies can enable single pixel accuracy in finger-based touch screen interaction [10, 243], and related techniques may prove effective for use with the feet. Limited research to date has addressed the usability of floor based touch interfaces. However, since the feet play very different roles in human movement than the hands do, the extent to which the kinds of techniques that have been adopted for use with the fingers may be useful for interaction via the feet is questionable.

Human movement research has investigated foot movement control in diverse settings. Visually guided targeting with the foot has been found to be effectively modeled by a similar version of Fitts' law as is employed for modeling hand movements, with an execution time about twice as long for a similar hand movement [121]. However, for many interfaces, usability is manifestly co-determined by both operator and device limitations (e.g., sensor noise or inaccuracy), providing a window on both.

Augsten et al. enabled users to select keys on an on-screen keyboard projected on the floor using precision optical motion capture tracking of the foot location and a crosshair display to indicate the location that was being pointed to, and a pressure threshold to determine pressing. They that found users were able to select target

buttons (keyboard keys) having one of the three dimensions 1.1×1.7, 3.1×3.5, or 5.3×5.8 cm with respective error rates of 28.6%, 9.5%, or 3.0%. Sensing accuracy was not a factor in this study, since the motion capture input provided sub-millimeter accuracy. The authors undertook further studies to determine the optimal part of the foot to be used for selection, and to determine the extent to which non-intentional stepping actions could be discriminated from volitional selection operations.

Visell et al. investigated users' abilities to select on-screen virtual buttons of different sizes presented at different distances and directions using the interface described in the preceding section [316]. In this task, the limited resolution of the force sensors (Figure 3.6) was one factor that could influence performance. Users could activate a button by pressing it in a way that resulted in a contact centroid within the area of the button exceeding a force threshold of about 35 N. The buttons were round, ranged in diameter from 4.5 to 16.5 cm, and were presented at four distances, on lines radiating from between their feet, oriented at one of two angles. Upon selection, the buttons provided visual feedback in the form of a 20 cm white disc centered in place of the original appearance. All buttons provided the same feedback. Only the buttons and foot locations were displayed. No audio or vibrotactile feedback was provided. Summaries of the success frequencies are presented in Figure 3.9.

Users were determined to have selected larger targets within the allotted two-second interval at a significantly higher rate of success than smaller ones. Performance with the largest was very high (98%), and that for the smallest was low (44%). Small targets pose two potential problems. First, they can be occluded by the foot during selection. This problem was somewhat mitigated because when this occurred, they were often visible projected on top of the foot. Second, limitations on precise control can arise from factors such as shoe width, human motor abilities, and sensor positioning errors. Six out of eight participants in this study reported finding a strategy to activate the small buttons by using a feature of the shoe or changing the applied force. Nearby targets (distances of D = 15 to 25 cm) were selected at a higher rate. However, performance was better at 25 cm than at the nearest distance of 15 cm (98.5% vs. 84%). One apparent reason was that when an interface element was too close, it could be occluded from view by the body, or could present a difficult viewing angle. Due to such effects selection time T might not be expected to to follow a Fitts' Law relation, $T = a + b\log_2(D/W)$, but this was not tested here.

Although a mobile user might be able to avoid visibility problems, they seem to be an important consideration. For our device, position sensing is most accurate near the centers of the tiles, as indicated in the preceding section. This was noticed by users of the system, two of whom volunteered that they had learned to better activate small buttons that were close to edges by pressing them off-center. Neck fatigue was a frequently cited source of discomfort, suggesting that displacing the visual feedback relative to the foot-based interaction point might be beneficial.

Further work in this area is clearly needed in order to characterize the usability aspects of floor based touch screen displays. A greater understanding of factors such as control element size, display scale, motor abilities, modalities, and other aspects salient to the use of such a device will certainly be needed. In addition, it would be

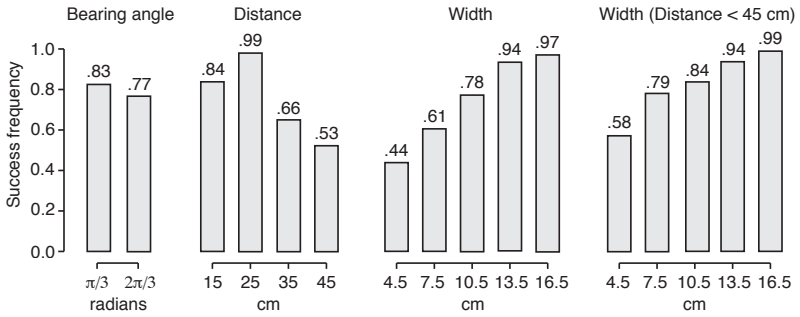

Fig. 3.9: Successful target selection rate vs. distance, angle of presentation (measured away from preferred foot), and button width, inclusive and exclusive of the farthest targets.

valuable to know to what extent usability might be improved through the use of auditory or vibrotactile feedback. Although Augsten et al. were able to identify some strategies that could be used to avoid selecting controls that are walked across, there remain open questions concerning concerns the interplay between users' movements on foot and their interactions with the touch surface. A novel aspect of interacting on foot is that, implicitly, both feet are involved in touching the interface, due to requirements of movement and of maintaining balance. In everyday actions, like striking a soccer ball, weight is often shifted onto one foot, which specifies an anchored location, while the opposite is used to perform an action. Thus, floor interfaces that involve movement may share similarities to bimanual interaction in HCI, a connection that provides another potential avenue of future investigation.

3.6 Application to geospatial data navigation

The ubiquity of multi-touch mobile devices and computers has popularized the use of two-finger gestures to navigate and control zoom level in the display of data via a touch screen. Such an approach focuses on the fingers as a means of providing input and may not be appropriate for settings in which the display surface is not amenable to finger-based interaction, when the hands are occupied, or when the data visualization application occupies a larger volume of space. We argue that this focus has limited the possibilities for carrying out complex exploration tasks in ways that leverage the capabilities we exploit naturally in the physical world.

For target acquisition tasks, e.g., menu and object selection, the accuracy and speed of the input primitives are important. In contrast, for spatial navigation tasks, e.g., panning and zooming, using dragging, resizing, and scrolling operations, less accuracy is often acceptable. Consequently, spatial navigation is likely an appropriate candidate for foot-based input, leaving the hands free, in parallel, to specialize on the more time- and accuracy-critical operations [222]. For instance, in the context of

collaborative design or decision making, e.g., urban and architectural planning, or emergency and crisis management [251, 7, 179], different roles are appropriate for foot input and hand input. Specifically, the feet could be used to specify approximate location while the hands perform other more critical or complex input tasks such as target selection, annotation, or drawing in the virtual design space, or dispatching tasks in emergency situations. Moreover, this represents a compelling alternative for scenarios where use of the hands is inconvenient. For example, in the context of airport information kiosks, where users are often carrying luggage, it may be desirable and appropriate to obtain directions to one's gate through a foot-based interface.

3.6.1 Foot-based gestures for geospatial navigation

Using the distributed floor tile interface described above, we implemented an application and several foot-based interaction methods for navigating geospatial data sets presented through a multitouch-sensitive floor surface in an immersive virtual reality environment. In contrast to prior work, focused on foot-based interaction at a fixed location, our work explores the benefit of such interaction in a distributed floorspace. This approach can be seen as an alternative to desktop computer interfaces for navigating geospatial data, and may be particularly suitable for situations in which an immersive display is involved or in which users' hands are occupied with other tasks.

We developed these interactive techniques for exploring geospatial information by navigating with a floor-based map interface, presented via the multitouch floor surface. The application was developed with the user interface framework presented above. As participants navigated to specified locations using the map, via one of the foot-floor interaction techniques, the images of the streets for the locations visited were presented in real time via the wall surfaces whenever applicable. The available data was acquired from existing internet-based mapping applications from Google and Microsoft.

The interaction techniques investigated included a "pivot" interface, which uses relative foot position as a navigational input, a "magic tape" interface that uses absolute foot position within the workspace, a "sliding" interface that allowed users to virtually push themselves within the mapping interface, and a "classic" approach using virtual buttons and sliders to provide a comparison with a more conventional user interface paradigm. Additional gestures allowed participants to control the zoom level of the map.

3.6.1.1 Classic interface

The "classic" interface transposes the basic design used for spatial navigation in mouse-based applications to the setting of floor-based interaction. Four buttons in a cross arrangement control position and a discrete-valued slider provides control

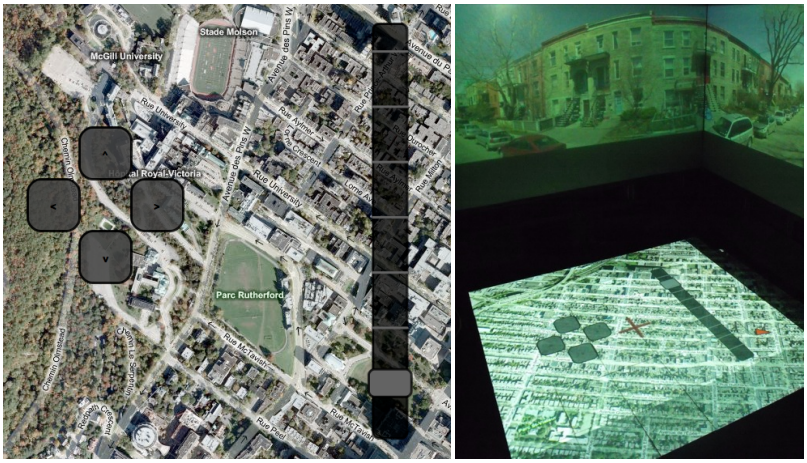

Fig. 3.10: Four button arrows (left) corresponding to panning in the cardinal directions and a slider (right) for zoom.

over the zoom level. The discrete slider levels match those used for the whole body gestures in the subsequent interfaces.

3.6.1.2 Pivot interface

The users establishes a pivot point by standing still for a short period. Placing one foot outside of the pivot area, indicated by a circle around the feet, pans in the direction specified as the vector from the pivot center to the outside foot. The participant can, at any time, exit the pivot area and establish a new one elsewhere.

3.6.1.3 Sliding interface

As with the bezel interface, the users first establishes a pivot point by standing still for a short period. Then, by placing one foot outside the pivot area and using sliding or dragging gestures, akin to touch-screen scroll on an iPhone, the user can pan the map.

3.6.1.4 "Magic tape" interface

The Magic-Barrier-Tape interface, inspired by the work of Cirio et al. (see Chapter 5), takes advantage of the larger floor surface by employing an interaction paradigm based on absolute foot position. This metaphor allows users to navigate freely in the center of the floor space, without altering the displayed map contents. However,

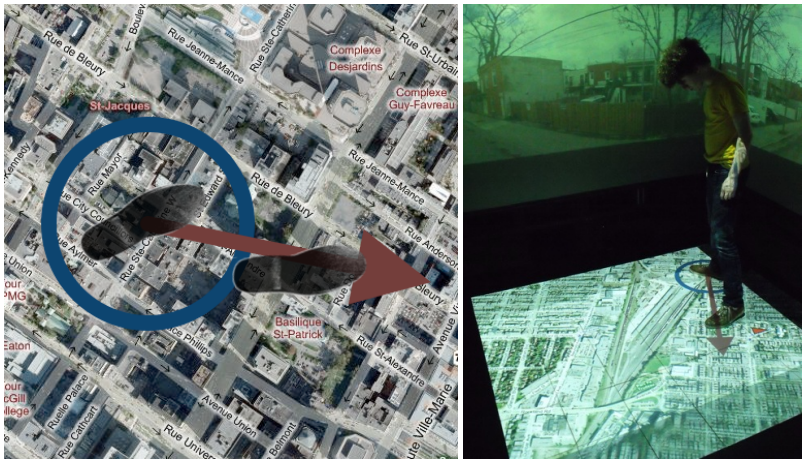

Fig. 3.11: The first foot to remain still establishes the pivot point, surrounded by a blue circle. The second foot then specifies the vector, relative to the pivot, for panning.

Fig. 3.12: In the sliding interface, the first foot establishes a pivot point, and the second foot slides or drags the display in a scrolling motion, with inertia.

when participants walk past the boundary region of the floor surface, the map pans in the direction designated by the user's position. The farther the user from the center, the greater the panning speed. The rate of panning is determined by a quadratic function of the magnitude of the vector from the center to the user's position.

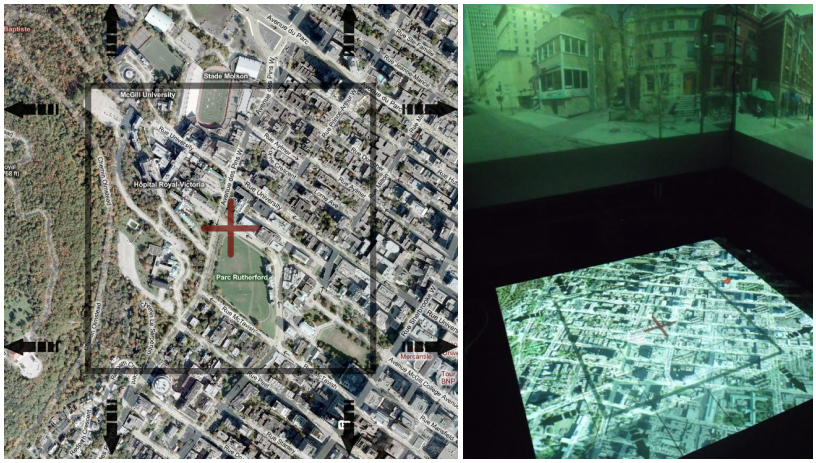

Fig. 3.13: The "magic tape" interface: A rectangular outline indicates the magic tape boundary, beyond which, the user's footstep will result in panning in the direction formed by a vector from the center crosshair and the user's foot.

3.6.2 Gesture recognition: Crouch and zooming

Unlike the direct-manipulation inspired control actions described above, gestures are recognized to allow temporally extended body movements, such as jumping, to affect the application state in a way that is not directly or instantaneously linked to changes in the user interface.

In the geospatial data navigation application, short body gestures can be used in conjunction with the control actions described above to control zooming. A curt "crouching" gesture zooms the map in, while a curt "jumping" gesture (raised onto the toes) zooms out.

Since such gestures have distinctive normal-force profiles trough time they can be matched to a reference signal. The use of a dynamic time warping algorithm for the matching in conjunction with preprocessing normalization allows for variations in gesture speed and amplitude from the user.

The analysis of these gestures, which relate to shifts in the weight and posture of users, is based on recognizing distinct sequences of whole body movements based on dynamic force signals sensed as a result of the weight shifts and posture changes. Many such movements are characterized by distinctive transient force signal from the floor sensors, due to the reaction forces the user generates when moving. A larger gestural vocabulary based on such movements could include crouching, jumping, leaning and tapping. Such movements are accompanied by force impulses as the user lifts and moves his or her body weight.

There are two challenges to detecting such gestures. First, they can vary in amplitude due to the manner and intensity of execution, and to the weight of the user. This issue can be resolved by normalizing the data. Secondly, the timing of sub-steps

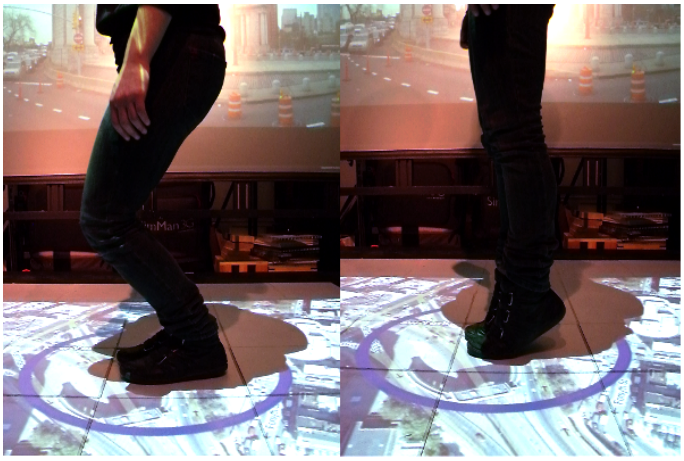

Fig. 3.14: Crouching and jumping gestures for zoom control.

comprising such movements may vary between users, resulting in signals that appear distorted in their progression in time. For instance, one user's "curt jump" might consist of a quick rise to the toes followed immediately by a drop, while another user may pause briefly at the peak the rise, stand on tiptoe, and then slowly drop down. While both inputs will share a common distinctive shape, they are stretched and distorted in time relative to each other.

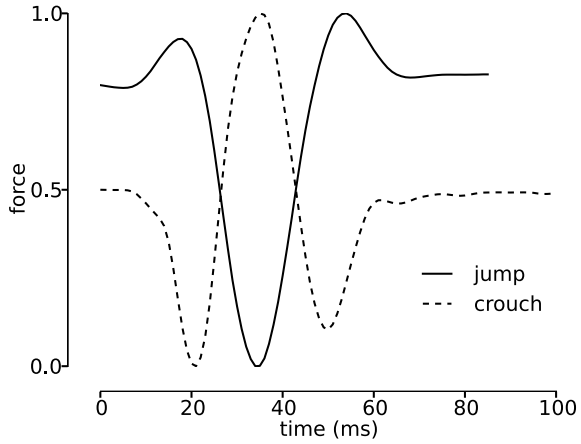

Fig. 3.15: Characteristic normal force profile of the jump and crouch gestures.

In order to compensate for this, we use standard techniques from time series recognition. A dynamic time warping algorithm (DTW) is used to match reference

gestures to the input data series. The system performs a continuous windowed DTW analysis of the force input from the sensor with respect to a number of reference force waveforms, generated beforehand from a training data set. Given an input data series $i(t)$ and a reference data series $r(t)$, the DTW algorithm builds a 2D graph such that every point $p(t,y) = |i(t) - r(y)|$, and seeks to optimize the temporal alignment between the two signals, by assigning the value of the mapping function $y(t)$. The sum of all the values of p along any monotonic and continuous path (moving forward in time only) provides the matching cost of the given path, with lower costs representing better matches.

Since the "start" of any gesture can be difficult to determine prior to analysis, we relax the typical DTW constraint which requires proceeding through each sample of the input in its entirely, and instal allow the matching algorithm to enter anywhere along the bottom edge ($p(x_a,0)$) and to exit anywhere along the top ($p(x_b,y_{max}), x_b > x_a$), which accommodates cases in which the input gesture may have been performed much faster than the reference. Once the path of least cost through the graph is computed, the similarity of the reference and input data series are obtained with allowances for time warping, allowing users flexibility to vary the speed of different segments of the gesture, as long as the overall transient characteristics are still present.

The same algorithm could be adapted for recognizing a variety of bodily gestures sensed through the floor surface.

3.7 Conclusions

This chapter reviewed approaches to interacting with computationally augmented ground surfaces, for purposes such as those of realizing virtual ground material simulations or foot-based touch surface interfaces. It described a particular approach to realizing such interactions via a distributed, multimodal floor interface, which is capable of capturing foot-floor contact information that is highly useful in the aforementioned settings. It presented interaction methods that are low in cost and complexity, and that can be made accessible to multiple users without requiring body-worn markers or equipment. In addition, this chapter presented examples in which these interaction techniques are used to realize generic virtual control surfaces or immersive geospatial data navigation applications. Further applications to the realization of multisensory simulations of virtual ground surfaces are presented in Chapter 8 of this book. We also reviewed guidelines for the use of such a display, based on a usability evaluation applied within a graphical user interface target selection paradigm. It is thus hoped that this contribution succeeds in demonstrating some potential uses and design considerations for floor-based touch surfaces in virtual reality and human-computer interaction.

Chapter 4
A review of nonvisual signatures of human walking with applications to person tracking in augmented environments

Y. Visell, R. Rajalingham, and J. Cooperstock

Abstract Walking can be considered to generate a rich variety of multimodal information that can be made available to ambient sensing systems. Much of this information can be considered to be non-visual in nature, consisting of acoustic and vibration signatures of walking, foot-ground forces, and bodily movements. This chapter reviews techniques for tracking the movements of pedestrians from such signals. We first review the mechanisms through which the latter are generated, then discuss algorithms that can be used to intelligently filter such signals and to extract information from them, through a review of prior literature on human activity and movement tracking, focusing primarily on non-visual sensing modalities. Finally, we discuss one approach to tracking the movements of pedestrians by means of a force-instrumented floor surface.

4.1 Introduction

Walking is fundamental to our experience of the world, and is relevant to many of the immersive conditions that virtual reality (VR) systems aim at simulating. It holds also promise for applications in ubiquitous computing, based on the idea that human locomotion and navigation can function as effective and natural means for interaction with digital information [1, 102].

Most work involving the computational understanding of walking activities has been focused on visual sensing paradigms. However, non-visual channels, consisting of sound, force, and vibrational signatures it produces, are also rich in information. Such signatures are suited to revealing the contact phase of the walking cycle, during which the foot and ground are subject to large mutual forces. Information about this phase is only indirectly reflected in data acquired pertaining to motions of the body, filtered through its inertial mass and structure. As a result, much of the literature on modeling walking dynamics within the vision community has tended

to ignore the (relatively nonlinear) contact phase, and has preferred to model locomotion as a linear (smooth) dynamical process.

Walking can be regarded as a dynamic activity that is highly structured in time and space. This chapter mainly considers the way it is reflected through acoustic, inertial and force signatures, acquired through electronic sensors located in the environment. It discusses recent developments in visual and non-visual (in particular, audio) information processing, and applies techniques from statistical time series modeling. The algorithms that are described here can be used to design novel methods for pedestrian interaction within everyday indoor (e.g., office buildings) and outdoor (e.g., park trails) environments, as reviewed below.

This chapter particularly addresses the modeling of contact dynamics of walking as reflected through its remote signatures. From an application standpoint, the resulting systems may be useful for the design of display methods for "virtual walking" experiences for otherwise neutral surfaces. Such displays interactively synthesize and present, through their actuators, synthetic walking signatures, in the form of auditory and vibrotactile stimuli, that would normally associated to real world ground surfaces; see Chapters 2, 3, and 8.

Some examples of end-user scenarios may help to ground the discussion that follows:

- Eldercare patients are able to move freely about a smart home or shared living facility. The home acquires information about their locations and activities via inexpensive and minimally-intrusive acoustic and seismic sensors in order to provide context-sensitive cognitive assistance, or medical aid, in the case of emergency.
- A visually impaired pedestrian in a noisy urban environment arrives at a crosswalk. Upon stepping on the area of sidewalk near the direction she wishes to cross, she receives an intuitive vibrotactile warning from the ground surface, felt by her foot, indicating that it is not yet safe to do so. A moment later, when the crosswalk indicator changes, she receives a second cue indicating that it is safe to cross.
- Visitors to a historical site or museum are guided toward nearby features of interest via virtual trails, supplied by the ground or via footwear. These trails dynamically form, merging their assumed routes toward potential destinations that are consistent with their position, heading, and any prior information.

4.2 Non-visual signatures of human locomotion

4.2.1 Contact interactions in walking

The recognition or tracking of walking from the the forces, vibrations, and sounds it generates is naturally informed by the characteristics of normal human locomotion and the physical interactions between the foot and ground. This topical area in the

movement sciences is extensive, including areas of biomechanics and sensorimotor control in locomotion. A large literature exists on the analysis of gait in terms of body posture and movement over time. Some gross features and terminology surrounding human locomotion are reviewed below.

4.2.2 The human gait cycle

The systematic measurement of human locomotion began near the end of the 19th century, when French scientist E. J. Marey began to study human gait using sequenced multiple camera photography [25]. He developed the first myograph (a device for measuring muscle activity), as well as a foot-switch system the measure the magnitude and timing of planar contact. Analysis of normal and pathological human gait continued to be developed over subsequent decades. Measurement techniques were developed based on motion pictures (film), sensor-instrumented walkways, on-body instrumentation, including electromyographics (EMG) and goniometry, and later using video and motion capture.

Walking is a periodic activity, and a single period is known as the gait cycle. Typical human walking rates are between 75 and 125 steps per minute (about 1.25 to 2 Hz) [238]. It can be divided into two temporal phases – those of stance and swing (Figure 4.1). The former comprises approximately 60 percent of the cycle, during which some part of the walker's weight is carried by that foot, and can be characterized in terms of foot position and contact, decomposed into initial heel strike, followed by foot flat, heel off, knee flexion, and toe off. The subsequent swing phase spans the period from when the toe first clears the ground until ground contact is reestablished. Thus, the gait cycle is characterized by a mixture of postural attributes (e.g., the degree of flexion at the knee) and contact attributes (e.g., toe on or off). Several time scales are involved, including those of the walking tempo or pace, the footstep, encompassing an entire swing-stance cycle, and discrete events such as heel strike and toe slap.

The net force $\mathbf{F}$ exerted by the foot against the ground is a vector with components tangential and normal to the ground surface. One can distinguish between low and high frequency force components, above and below about 50 Hz. The former is referred to as the Ground Reaction Force (GRF), and is responsible for the center of mass movement of the individual and the support of his or her weight. Although approximately independent of footwear type, it varies between individuals and walking styles [107]. High-frequency forces are due to material-dependent transient, noise-like, or oscillatory interactions between the shoe and ground surface, and are responsible for airborne acoustic and mechanical vibrations generated during walking [172, 87, 323, 69, 88, 107]. Since these high-frequency signals depend energetically on walking movements that generated them, the gait frequency is readily detected in remote measurements via seismic and acoustic sensing [128, 88, 107, 86]. Signatures of individual footsteps are marked by the two key events: the heel strike and toe slap [172, 87] (Figure 4.1). The time between the two

is on the order of 100 ms for stereotypical walking. However, depending on the shoe type, activity, and ground surface shape, a more complex temporal dependence may be observed.

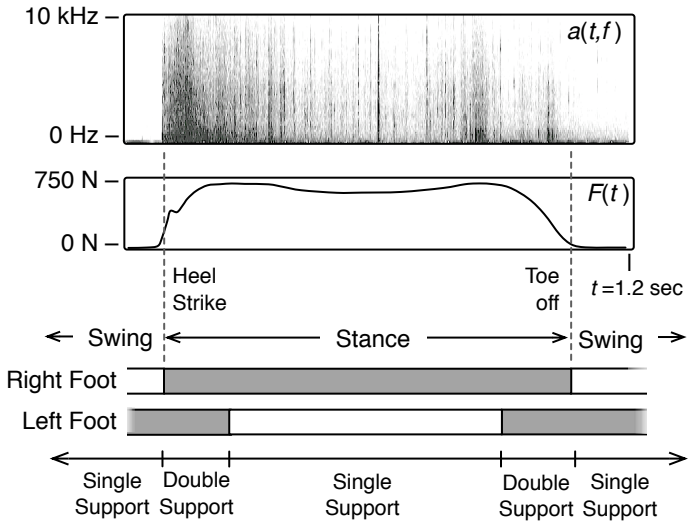

Fig. 4.1: Vibration spectrogram $a(t, f)$ and low-frequency normal foot-ground force $F(t)$ measured at the hard sole of a men's shoe during one footstep of a walker onto rock gravel, together with the corresponding foot contact states within the gait cycle (author's measurements). The dark vertical stripes in the spectrogram correspond to discrete impact or dislocation events that are characteristic of dynamic loading of a complex, granular medium.

4.2.3 Mechanical interactions and materials

Stepping onto a natural or man-made surface produces rich multimodal information, including mechanical vibrations that are indicative of the actions and types of materials involved. Footsteps in hard-soled shoes onto solid materials are typified by transient impacts due to initial heel strike with the floor surface and subsequent slap of the toe area, while sliding can produce either frictional squeaking (when surfaces are clean) or textured noise. In indoor environments, the operation of common foot operated switches, used for lamps, dental equipment, or other machines, is often accompanied by transient contact events between solid mechanical elements.

The discrete quality of these mechanical signals can be contrasted with the more temporally extended nature of those generated by steps onto natural ground coverings, such as gravel, dry sand, or branches. Here, discrete impacts may not be as apparent, and can be accompanied by both viscoelastic deformation and com-

plex transient, oscillatory, or noise-like vibrations generated through the inelastic displacement of heterogeneous materials [120]. A few of the processes that can be involved include brittle fracture and the production of in-solid acoustic bursts during rapid micro-fracture growth [120, 9, 5], stress fluctuations during shear sliding on granular media [26, 73, 206, 205], and the collapse of air pockets in soil or sand.

Thus, foot-ground interactions are commonly accompanied by mechanical vibrations with energy distributed over a broad range of frequencies. High-frequency vibrations originate with a few different categories of physical interaction, including impacts, fracture, and sliding friction. The physics involved is relatively well understood in restricted settings, such as those involving homogeneous solids, but less so when disordered, heterogeneous materials are involved. Due to the random nature of stress-strain fluctuations in these materials, statistical modeling approaches have seen considerable success in describing them [9, 120]. Chapter 8 discusses the interactive simulation of stepping onto such materials in virtual reality.

4.3 Extracting information from vibrational, GRF, and intertial walking signatures

The processing of information in vibrational signatures of walking has been accomplished using data from a diverse array of sensors, including seismic geophones, MEMS accelerometers, piezoelectric accelerometers or other vibration sensors. As noted above, ow frequency components of such signals (below about 300 Hz) are characteristic of the gait pattern, while higher frequency components are indicative of the footwear and ground material types involved.

Research in the mining of information from such signals has aimed at developing suitable feature extraction methods for these data sources [129, 221]. Wavelet based representations and blind wavelet denoising (a signal processing method for the reduction of noise in data, based on the estimation of noise contributions at different scales) has been applied to seismic footstep data by several prior authors [198, 330]. The identification of promising inference or classification algorithms is another active area of research [40, 288, 287, 284, 240].

Seismic signals in the ground can be detected over long distances given amenable conditions, and this has spurred interest in the analysis of such signals for human surveillance [330, 87, 89]. Further work in this area has addressed human distance estimation from seismic footstep data [220]. Specific methods have been developed for footstep detection via distributed sensor networks in uncontrolled environments [184].

Several research groups have investigated classification of inertial sensing and low frequency foot-ground force profiles (ground reaction forces acquired via force sensing floors), for applications such as biometric authentification. Mostayed, Kim, Mazumder, and Park studied the recognition of walker identity from ground reaction force profiles acquired through a force plate [198], as did Headon and Curwen [117]. Orr and Abowd, and Addlesee [3] performed similar research aimed at the

development of a floor for a smart home environment. Several other research groups have carried out work in this area.

Another area of research centers on gait recognition using wearable inertial sensors, or those embedded in handheld computers. Gafurov et al. utilize a sensor pack attached to the lower leg [105] or hip [106]. Ailisto et al. used a sensor pack attached to the waist [8] or the accelerometer of a handheld computer [182]. Both sets of authors experimented with simple, hand-crafted linear discriminant classifiers based on human inspection of the statistics of the data.

One promising application in this area is the early identification of at-risk gait in aging populations from foot-ground force measurements. Holtzreiter and Kohle [127] used artificial neural network to classify normal and pathological gait using force platform recordings. Other researchers have studied the identification of pathological gait patterns using non-contact based sensing. Begg et al. [33] use a support vector machine classifier (SVM) to identify pathological gait using features derived from the minimum foot clearance, which is a local minimum of the vertical distance between the shoe and ground that occurs after toe off in the gait cycle. The required data is typically acquired through motion capture, which has also been used in many other studies on gait classification. Indeed, video based motion capture data likely provides better information for the identification of potential gait pathologies than can be obtained through indirect sensing methods based on non-visual walking signatures.

Chau [55, 56] reviews techniques for analysis and classification of gait data from a movement sciences perspective, with an emphasis on algorithms as opposed to sensing methods. Most examples cited in these surveys utilized motion capture or electromyography for sensing. The volume edited by Palaniswami et al. [223] provides a broad review of machine learning techniques applied to the analysis of human motion from a clinical and movement sciences perspective, emphasizing algorithms and analysis techniques, as distinct from sensing methods and data sources.

4.3.1 Multimodal context and activity recognition

The computational understanding of human activities from multimodal sensors has been widely investigated in ubiquitous and wearable computing research. Some of this research aims at classifying human activities, locations, or other contextual information from several heterogeneous sensor data sources.

4.3.1.1 Multimodal wearable computing systems for activity recognition

Multimodal sensing of walkers movements has also been accomplished with wearable computing devices. One difficulty with evaluating and comparing published results on human activity recognition from wearable sensors is the lack of standard tasks and data sets, and the distinct applications (such as context recognition vs. ac-

tivity recognition) or metrics (such as retrieval precision and recall vs. classification error rate) that have been addressed, and different data sources that are used.

Lester and Choudhury address activity recognition and tracking using a wearable multi-sensor unit, including an accelerometer, microphones, light sensors, barometric pressure, humidity, temperature, and compass sensors. They begin with a large number of features (651 in all) calculated from this data, and apply boosting (an ensemble classifier method based on the consistent combination of classifiers [101, 186]) to select a fraction for use in classification by hidden Markov models (HMMs). These HMMs are trained on posterior probabilities computed from simple ("stump") classifiers for each of the selected features. Subramanya et al. adopt a dynamic Bayesian network (DBN) approach to the recognition of activities and spatial context from a wearable sensor system comprising a global positioning system (GPS) unit, accelerometer, microphones, light, temperature, and barometric pressure [283]. The DBN models employed allow their system to model relationships between locations, GPS measurements, state, environment, and other sensor measurements, through time. Dynamic Bayesian networks are generalized probabilistic graphical models structured over time. They can be implemented as Bayesian filters, and special cases include the HMM, the conditional HMM and the Kalman filter. DBNs make it possible to encode a wide range of types of conditional probabilistic dependencies between state variables and observations over time [202].

Inertial sensors are inexpensive, and increasingly available on commonly used mobile digital devices, such as telephones. They provide a simple way to capture bodily movement. Nonetheless, this data is highly sensitive to the body location at which they are located, which can be addressed through the design of the physical device in relation to the body, and through the extraction of features that can be interpreted despite variation in location. Kunze et al. addressed an unusual problem in this regard: the automatic recognition of the location on the body at which the accelerometer is located [156]. Many researchers have recently studied user activity recognition from accelerometer data [27, 28, 119, 132, 147, 153, 158, 168, 171, 182, 252, 250, 157, 291, 148]. A few recent reviews of the analysis and recognition of human activities via accelerometers exist [183, 11, 150]. Cheng and Hailes investigated the use of accelerometers mounted near the foot for identifying activities performed by their wearer [58]. Huynh and Schiele aimed to extract more informative representations from accelerometer data [132]. They evaluated short-time spectral and average temporal features of body-worn accelerometer data, as well as measures of pairwise correlation between components. Several window lengths were investigated. Evaluation was performed using unsupervised (clustering) and supervised (recognition) methods. Differences were found in feature salience between static and dynamic activities. Heinz and Kunze also assessed features extracted from accelerometer data [119]. Intille et al. have carried out a wide range of research aimed at recognizing activities in domestic environments. Tapia and Intille combined data from wireless accelerometers and heart monitors for real-time recognition of physical activities [290]. Kunze et al. addressed an unusual problem in this regard: the automatic recognition of the location on the body at which the accelerometer is located [156].

Audio data from microphones is used in mobile and ubiquitous computing to providee structured records of environments and activities in them, being less obtrusive than video sensing, and less sensitive to bodily location than video or inertial sensing. Pärkkä et al. studied classification of human movement activities such as walking, running and cycling from wearable sensors, using 35 body worn sensors [229]. The latter ranged from microphones to physiological sensors, barometric pressure, temperature, and accelerometers. Short-time temporal and spectral features were extracted from these sources. Additional features were calculated from stump classifiers designed to identify particular attributes via single sensor modalities (e.g., speech from sound). Features known to be relevant to certain of the measurement modalities (such as physiological sensors) were also calculated. Feature selection was performed in a heuristic manner, using examination of the statistical distributions of the features, and domain-specific knowledge. Temporally stationary classifiers, based on manually and automatically constructed decision trees, and artificial neural networks, were applied to a seven activity classification task. High accuracy was reported on this task. The authors also report that, contrary to expectations, physiological signals such as heart rate and respiration did not prove very useful for activity recognition. Korpipää et al. utilized a wearable sensor pack, including microphone sensor, for classifying 19 environmental contexts encountered by its wearer [152]. Features were derived from the audio data using methods specified in the MPEG-7 standard, including psychoacoustic features and short time spectrum representations. Features were subjected to vector quantization, using fuzzy logic and heuristics. Classification was performed using a naïve Bayes network classifier, without a model of structure on timescales longer than the analysis frame. Recognition results were reported to be relatively high, using a proprietary dataset. Staeger, Lukowicz, et al. focus on sound recognition with a low-power, low-cost miniature, wearable acoustic sensor [277, 177]. They extract a set of short-time spectral and temporal features, perform feature selection using linear discriminant analysis (LDA) and principle components analysis (PCA), and perform evaluation by classifying the location of the wearer, or the dominant sound source, using k-nearest neighbors or learning vector quantization (LVQ) classifiers. These classifiers were selected over more powerful algorithms, due to their suitability for implementation on low power portable electronic devices. Sound source classification has also been investigated with the aim of improving hearing aids [50].

4.3.1.2 Walking sound classification

A handful of published studies have reported on the classification of walking sounds. The subject has arisen in the automatic classification of everyday sounds, walking sounds typically representing one of several categories to be identified, or in auditory scene recognition, where walking sounds are characteristics of certain scenes. It has also been studied in the context of biometrics, surveillance and ambient intelligence.

Walking sound classification studies can be distinguished, in part, by the taxonomies of types of sound that are employed. Several have focused on differentiating walking sounds from other sound categories. Some address the classification of walkers according to their unique identities, or attributes such as gender, weight, or footwear. Others attempt to classify walking style or the affective state or intent of the walker. Still others concern themselves with the classification of environmental properties such as ground material or location.

Casey [52] studied the classification of sounds into 19 different categories, ranging from female speech, to telephones, footsteps, and piano sounds, using the MPEG-7 Audio Framework sound classification tools [53]. Features were determined from an ICA decomposition of the log spectral energies of the signals. These were fed to 19 single Gaussian HMMs with full covariance matrices, trained using a Bayesian maximum a posteriori (MAP) procedure. The mean recognition rate on the experiments was more than 92%. Footstep sounds were classified with an accuracy of about 90%, while a few sounds (such as telephones, at around 65%) were mis-classified much more often.

Mitrovic [191] studied combinations of features and classifiers for everyday sound retrieval. Five environmental sound categories were included , labeled “cars”, “crowds”, “footsteps”, “signals”, and “thunder”. Data was taken from public internet sources. This study evaluated psychoacoutic features, time-domain measures, and spectral features, such as linear predictive coding (LPC) coefficients and Mel Frequency Cepstral Coefficients (MFCCs). Classification was performed with three classifiers: the k-nearest neighbor algorithm, learning vector quantization, and the support vector machine. Retrieval recall and precision were highest with MFCC features in combination with a support vector machine classifier. The author also applied feature selection (based on a posteriori retrieval performance) to determine promising combinations of features.

Peltonen et al. [236] and subsequently Eronen et al. [92] studied the classification of real-world acoustic environments from audio recordings, unlike many other studies on everyday sound classification that use composed studio recordings of different soundscapes. Several of the environments in their study (e.g., indoor hallways) included walking sounds, although none was uniquely characterized by the presence of walking. 27 contexts and six high-level categories were represented. The authors studied recognition performance as a function of features, feature selection methods, HMM configuration and training method. They achieved their best results using PCA or ICA transformation of MFCC features, and found that performance remained near its highest level (around 58% for context recognition) even when a low (four-) dimensional feature vector was used. Their results were compared with human performance on the same tasks, and they found that humans performed only moderately better (at 69% on the context recognition task). Several other authors have studied everyday soundscape classification [19, 18].

A number researchers have investigated features and classifiers for biometric authentification or walker identification from footstep sounds. Many of the results presented in the literature to date are limited by the use of small or studio-recorded datasets. Itai and Yasukawa [136] focused on psychoacoustic parameters such as

loudness, roughness, and fluctuation strength, as well as MFCC features, using a vector quantization based classifier. They reported 88% recognition rates on an identification experiment with 5 different walkers. The same authors later investigated classification based on dynamic time warping [138] and wavelet based features [137]. Shoji et al. [271] and Tanaka and Inoue [289] also carried out classification experiments using spectral features without time information.

Annies et al. [12] studied the automatic classification of walking sounds according to the footwear or the ground material type (snow, sand, metal, etc.), using recordings from a commercial sound design database. They compared classification performance using two feature types and two classifiers. Both features were derived from an auditory signal processing model due to Patterson and Holdsworth [230]. One was oriented toward capturing fine temporal information in the sounds, and the other toward short-time spectral information. An HMM classifier was trained using the feature sequences for the different recordings, while the SVM classifier was trained using aggregated features without sequential information. In nearly all cases, the SVM approach outperformed the HMM.

Bland [40] explored simple methods for detecting footstep events via seismic sensors and microphones. An autoregressive process (i.e., an all-pole IIR filter) was adapted on each window of an overlapping series of windowed footstep recordings, and rough examination of the resulting coefficient paths was used to guide a qualitative analysis of differences between footstep types.

Abu-El-Quran et al. [2] developed a microphone array surveillance system. Their system includes a module for classifying non-speech audio using MFCC features and a time-delay neural network, together with a classifier for distinguishing speech and non-speech audio. Evaluation was performed using a database of recordings acquired under controlled (studio) conditions. They report average error rates of around 5% on a five class classification task including speech, door sounds, fan noise, glass breaking, and wind. Footstep sounds were evaluated only in the context of speech-nonspeech audio classification, where they were never confused with speech.

Itai et al. investigated psychoacoustically-motivated features for the classification of walker identity, in a study in which walkers performed on a wood floor inside a house [136]. In the context investigated, the authors reported mixed success in clustering walker identities within a multidimensional space whose dimensions were loudness, sharpness, fluctuation strength, and roughness.

4.3.1.3 Ambient sensing of human activities using acoustic information

Zou and Bhanu studied the tracking of walkers' location using walking-generated acoustic signals captured from a pair of microphones, as well as video input [35]. Zou and Bhanu found that a (stationary) Bayesian network outperformed a time-delay neural network (which is able to model temporal correlations explicitly) on a walker localization task.

Radhakrishnan and Divakaran applied generative background models normally used for visual background modeling, to the modeling of background audio processes. Their approach, based on Gaussian mixture models and short-time cepstral features, was applied to an audio surveillance problem aimed at novelty detection [247]. Lukowicz, Ward et al. utilized a set of body worn microphones and accelerometers for recognizing activities performed by their wearer over time, in a wood workshop context [178, 321, 322]. Classification decisions were formed using the output of separate models for audio and accelerometer data. Microphone pairs were used to distinguish others' activities from those performed by the wearer. Minnen, Starner, Lukowicz, et al. focused on the recognition of human actions, at the level of individual gestures, using similar data [190]. Chen et al. developed and evaluated a system for monitoring bathroom activities from acoustic information. Their method employed Mel-frequency cepstral coefficient audio features with an HMM classifier, an approach that is typically used for automatic speech recognition [57].

4.3.1.4 Acoustic source separation and localization

Acoustic source localization a long history in SONAR and ballistics imaging, and related research has been carried out in RADAR localization. The localization of humans via such information has been most comprehensively addressed in the literature on speaker tracking from microphone arrays [331, 169, 242, 259], either in a unimodal or multimodal setting (the latter typically also utilizing video sensing).

Interest in distributed sensor networks and ubiquitous computing has led several researchers to study the localization and identification of human activities from acoustic information captured through sensors embedded in everyday artifacts or environments. Dalton explored algorithms for passive acoustic source localization using indoor sensor networks [72]. Westner and Bove examined the separation of acoustic events using microphone arrays in rooms, using blind source separation techniques (described in section **??**, below) [327, 326]. Acoustic source localization also holds potential for improving computational auditory scene analysis systems [90]. Weinstein et al. report on the development of a large scale (1020-node) microphone array and acoustic localization system (beamformer) for intelligent environment applications [325]. Other researchers have approached acoustic source localization using wearable computing (and microphone array) devices, for audio annotation and retrieval [31, 65], or for situation analysis by auditory scene recognition [236].

4.3.1.5 GPS-based activity tracking

Contact-based sensing of walking activities may be applicable to settings in which other sources of data, such as GPS, have traditionally been used for human activity tracking [175, 173, 15]. Due to the coarser spatial resolution of GPS data, activities

recognized are typically long in time scale. Ashbrook and Starner focus on movement between locations, without considering the activity context or route choices involved [16]. Bennewitz et al. demonstrate learning of motion paths between places. Liao et al. address the problem of annotating a user's daily activities [175], and that of jointly modeling place and activity from such data [174].

4.3.1.6 Interface design with acoustic sensing

Murray-Smith and Williamson developed an input method based on real time classification of acoustic information generated through contact events between a user's fingers and the plastic case of a handheld information appliance, using data from inexpensive acoustic sensors, features derived from the magnitude short-time Fourier transform (STFT), and a neural network classification algorithm [203]. A few research projects, including the European Commission sponsored TAI-CHI project, have investigated the extraction of position information from human contact with flat surfaces, using array based signal processing techniques applied to in-solid acoustic signals acquired from contact microphones [70].

4.4 Walking signatures: Dynamic information processing

As reflected in the scenarios and choice of examples presented above, one theme of this chapter is that of modeling pedestrian positions and activities as they evolve over time. The attributes that might be used to describe such pedestrian states are not only time-varying, but express intrinsic temporal structure and dynamics, due from the physical constraints that determine the biomechanics of locomotion, the (discontinuous) temporal evolution of foot-ground forces through the gait cycle, and the physics of contact interactions between foot and ground. Thus, one should not assume that a static classification task is to be solved, but rather should benefit from the structured nature of these interactions. Models suited to systems that evolve through time have been progressively developed in the machine learning community during recent decades.

Two problems relevant to this research concern tracking pedestrian states (activities or positions) over time, and constructing prior models of their activities or trajectories from observations. Here, observations are assumed to consist of contact-generated walking signatures. The term *pose* is used in the literature on computational perception to refer to the complete configuration of a system of interest, including any unobserved aspects of its state. A typical problem to be solved is that of determining pose from partial observations. This may mean reconstructing a complete description of the position or activity of one or more individuals. Such problems arise in many location-aware applications of pervasive and ubiquitous human computer interaction. The problem is typically addressed by combining information from continuously updated data, acquired from sensors, to make inferences about

the expected position or activity of the individual. Such estimates are improved if a good prior model of the behavior or dynamics of the individual is available to guide estimation. This section introduces algorithms and models that are applicable to such a setting.

4.4.1 Probabilistic inference with dynamical models

State space models provide a compact framework for describing the evolution of a dynamical system through time, and they can be elegantly integrated with probabilistic machine learning methods for pattern classification, as shown below.

4.4.1.1 Discrete time dynamical system formulation

The goal is to model time series of walking activities. The time series is represented by a sequence of hidden states x_t (p-dimensional vectors), inputs u_t (r-dimensional vectors), and outputs y_t (k-dimensional vectors). The system evolves in discrete time (the subscript t is the time index) according to a stationary Markov dynamical system:

$$x_{t+1} = f_\theta(x_t, u_t; w_t) \tag{4.1}$$

$$y_t = g_\theta(x_t, u_t; v_t) \tag{4.2}$$

The functions f_θ and g_θ are vector valued, possibly nonlinear functions of their arguments. Often they are parametrized by a set of values θ.[1] w_t and v_t are noise processes. In the simplest nontrivial case, these are taken to be zero mean additive Gaussian processes (Figure 4.2). The system is assumed to be stationary, in the sense that neither the noise statistics or the functions f_θ and g_θ depend on time. In case

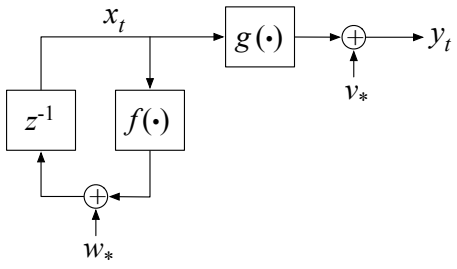

Fig. 4.2: Discrete time nonlinear dynamical system model, assuming additive noise. The control input is suppressed.

[1] Interesting nonparametric nonlinear state space models also exist.

these quantities depend on time, it is preferable to represent this time dependence in the system state. The following definitions are needed:

- x_t: The state vector at time t
- u_t: The (known) control vector, if present, used to drive the state from x_{t-1} to x_t
- y_t: The observation of the state x_t taken at time t
- The state history to time t, $x_{1:t} = (x_1, x_2, \ldots, x_t)$
- The observation history to time t, $y_{1:t} = (y_1, y_2, \ldots, y_t)$
- The similarly defined history of control inputs (if present), $u_{1:t}$

y_t are the observations of what is taking place; here, they will be observations of pedestrian positions, activities, or other walking events, as captured through contact-based sensors. x_t are hidden variables responsible for the observed variation; in this chapter, these will represent pedestrian positions or activity labels. Depending on the inference problem, the inputs u_t may or may not be present. Since it is assumed that walkers act autonomously, u_t will not typically be relevant.

Equation (4.2) is a parametrized control system model of the dynamics of interest. Separating the system state dynamics and observation descriptions provide a conceptually clearer, and in many cases simpler, description. The system may be viewed as a probabilistic latent variable model, in which the states x are thought of as hidden variables, furnishing an informative lower dimensional explanation of complex variations observed in the outputs y. Equation (4.2) can be thought of as specifying a dynamical prior probability distribution over the latent space. A unified view of such models was presented by Roweis and Ghahramani [260]. The form and parameter values of the dynamical function f_θ and the observation function g_θ, together with the noise distributions, determine the qualities of the observed time series y_t. The system dynamics depend both on the dynamical function's specification and on the state description. The former may be inferred from data, or based on a priori considerations, such as physical models.

4.4.1.2 State and model estimation from observations

Assuming an observed input-output time series (u_t, y_t) to be given, and assuming the parametrized form f_θ, g_θ of the system to be appropriate, one would like to determine values of the system parameters θ that best explain the observations, providing a compact representation of the observations. The problem of determining the values of θ in this way is called *model estimation*. (*System identification* is a name commonly used in the engineering literature.)

If a time series model has been estimated from a sequence of observations up to the present time (which can be compactly denoted as $y_{1:t} = \{y_1, y_2, \ldots, y_t\}$), one can ask what unobserved state sequence $x_{1:t}$ is implied. More generally, one may wish to know how well a given state sequence fits with the observations, best addressed within a probabilistic setting (section 4.4.1.3). This is the *state estimation* problem (also referred to as *tracking, filtering* or *smoothing* in the engineering literature). Tracking and filtering attempt to infer the hidden state at time t from observations

up to time t, while smoothing takes into account all available observations, up to and beyond time t. As an example, y_t might be noisy measurements of a walker's position, from which one wishes to estimate the true spatial position x_t.

Various techniques have been developed over the last half century for solving state and model estimation. Many of them can be understood from the viewpoint of Bayesian filtering, a probabilistic framework for updating such predictions continuously as new information is acquired from one or more sources.

4.4.1.3 Probabilistic formulation

Realistic dynamical system models have a stochastic quality, because the systems of interest have observations that are noisy functions of the inputs, and possess noisy dynamics. In such a model, process noise w_t and observation noise v_t are meant to reflect uncertainty in observed and hidden state space variables. An additional advantage of noise is that a wide variety of system outputs can be captured by a simple model (avoiding, for example, the need to explicitly modeling complex microscopic disturbances).

The system state in the presence of noise can be represented through the use of probabilities, which reflect the uncertainties involved, and provide a calculus for updating state estimates and uncertainties as new information is received [98, 297]. A common approximation is to assume that v_t and w_t represent additive, white (temporally uncorrelated), zero-mean Gaussian distributed noise sources, i.e., that the noise sources are distributed as $p(v_t) = N(0,Q)$ and $p(w_t) = N(0,R)$, where $N(\mu,\Sigma)$ is a multivariate normal probability density with the indicated mean and covariance matrix, and Q and R are the noise covariances of v_t and w_t. Under this assumption, and suppressing the control inputs, the system equations (4.2) can be written in terms of the conditional densities for the state and output:

$$p(x_t|x_{t-1}) = \exp\left\{-\frac{1}{2}[x_t - f_\theta(x_{t-1})]^T Q^{-1}[y_t - f_\theta(x_{t-1})]\right\} \det(2\pi Q)^{-1/2} \quad (4.3)$$

$$p(y_t|x_t) = \exp\left\{-\frac{1}{2}[y_t - g_\theta(x_t)]^T R^{-1}[y_t - g_\theta(x_t)]\right\} \det(2\pi R)^{-1/2} \quad (4.4)$$

T in the exponent denotes the transpose, and $\det(A)$ is the determinant of A. This set of equations has the interpretation of a dynamic probabilistic latent variable model, with potentially nonlinear dynamics (Eq. 4.3) and latent space embedding (Eq. 4.4). If f or g are assumed to be linear, the respective densities are Gaussian under the noise assumptions given above. If both are linear, the result is a dynamic, probabilistic linear latent variable model – a type that has been well-studied.

The Markov assumption means that the joint probability can be factored

$$p(x_{1:t}, y_{1:t}) = p(x_1)\prod_{t=1}^{T} p(x_t|x_{t-1})\prod_{t=1}^{T} p(y_t|x_t)\,. \quad (4.5)$$

If the initial state density is assumed to be a Gaussian $p(x_1) = N(\pi_1, V_1)$ with mean π_1 and covariance V_1, then the joint log probability can be written as a sum of terms having the following form [110]

$$\begin{aligned}\log\{p(x_{1:t}, y_{1:t})\} = &-\sum_{t=1}^{T}\left(\frac{1}{2}[y_t - g_\theta(x_t)]^T R^{-1}[y_t - g_\theta(x_t)]\right) - \frac{T}{2}\log|R| \\ &-\sum_{t=2}^{T}\left(\frac{1}{2}[x_t - f_\theta(x_{t-1})]^T Q^{-1}[y_t - f_\theta(x_{t-1})]\right) - \frac{T-1}{2}\log|Q| \\ &-\frac{1}{2}[x_1 - \pi_1]^T V_1^{-1}[x_1 - \pi_1] - \frac{1}{2}\log|V_1| - \frac{T(p+k)}{2}\log 2\pi \quad (4.6)\end{aligned}$$

This (nonlinear) expression is general under the Gaussian noise assumptions above. If the system is assumed to be linear, the log probability is a sum of quadratic terms. Often, neither assumption holds.

4.4.1.4 Forecasting and belief

A basic question concerns how likely any given future observation is, given past observations and (known) control inputs. It is embodied by the forecasting distribution $p(y_{t+h}|y_{1:t}, u_{1:t+h})$. h represents a prediction time horizon. Another quantity of interest is the total probability of an observation sequence given the model, $p(y_{1:T}|\theta)$, (written here to explicitly show the dependence on the model parameters θ).

The state space model assumes the existence of the hidden state x_t whose evolution explains the observations. Computing interesting quantities such as $p(y_{1:T}|\theta)$ is aided if the value of the hidden state of the system can be determined under different conditions. This goal can be embodied by the aim of computing a *belief distribution*, which is given by the posterior density over x_t conditioned on the prior observations $y_{1:t}$ and control inputs $u_{1:t}$

$$\mathrm{Bel}(x_t) = p(x_t|y_{1:t}, u_{1:t}) \quad (4.7)$$

The belief distribution embodies the knowledge of the system at the present time t given all past observations and control inputs.

As Murphy notes [202], a rationale for belief representations as the objective for estimation using stochastic dynamical systems was provided in the 1960s, when Aström [17] proved that $\mathrm{Bel}(x_t)$ is a sufficient statistic for prediction and control, provided the hidden state is rich enough. The implication is that nothing that is not already reflected in the belief state at time t is gained by retaining a longer record of past observations.

Since this chapter is not primarily concerned with control, control inputs u_t to the system will be suppressed during the rest of the discussion.

4.4.1.5 Statistical decision making

One aim of this research is to provide models that are both interpretive and that are capable of enabling statistical decision tasks. Interpretive models allow to make inferences as to the continuous states associated to a pedestrian, while decision tasks permit inferences of a discrete nature to be made, such as classifications of identity, activity and gait type. One advantage of the use of probabilities is that they provide a normalized measure of fitness, namely the total likelihood of the observation sequence given the model, $p(y_{1:T}|\theta)$. Although explicitly discriminative approaches, which would provide additional comparisons of relative fitness between models, are not discussed here, such approaches can be developed within the same framework.

4.4.1.6 Sequential state estimation by belief propagation

The belief distribution is influenced by evidence represented by the observation history $y_{1:t}$. The Markov assumption allows to iteratively compute $\mathrm{Bel}(x_t)$ (given an amenable system and belief representation) as the number of sensor observations that have been received grow over time. Inference is accomplished via Bayes' rule[2], cast in a form suitable for recursive state estimation:

$$p(x_t|y_{1:t}) = \frac{p(y_t|x_t, y_{1:t-1})p(x_t|y_{1:t-1})}{p(y_t|y_{1:t-1})} \tag{4.8}$$

using the Markov assumption on y_t and the fact that the denominator is a state-independent value, one can write this as

$$p(x_t|y_{1:t}) = Cp(y_t|x_t)p(x_t|y_{1:t-1}) \tag{4.9}$$

(The state-independent value C ensures that the posterior distribution integrates to one over the state space.) The last factor can be expanded through the intermediate state x_{t-1} to give

$$p(x_t|y_{1:t}) = C\,p(y_t|x_t)\int p(x_t|x_{t-1})p(x_{t-1}|y_{1:t-1})dx_{t-1} \tag{4.10}$$

Using this formula, belief is updated at each time step, in two stages. Upon a state transition to x_t, it the **prediction** formula is applied, combining the posterior density $\mathrm{Bel}(x_{t-1}) = p(x_{t-1}|y_{1:t-1})$ at the prior timestep with the system dynamics distribution $p(x_t|x_{t-1})$:

$$\mathrm{Bel}^-(x_t) \leftarrow \int p(x_t|x_{t-1})\,\mathrm{Bel}(x_{t-1})\,dx_{t-1} \tag{4.11}$$

The superscript $(-)$ denotes that the belief is a prediction for the future which does not account for the current observation. When an observation y_t is made, the estimate is fused with the new information, via the **correction** formula:

[2] Bayes' rule: $p(x|y) = p(y|x)p(x)/p(y)$

$$\mathrm{Bel}(x_t) \leftarrow C\, p(y_t|x_t)\, \mathrm{Bel}^{-}(x_t) \tag{4.12}$$

4.4.2 State spaces, belief representations and state inference

The foregoing formulation is abstract, and how it is implemented depends on the system dynamics, observation process, statistics, and representations of $\mathrm{Bel}(x_t)$ and $p(y_t|x_t)$. For certain models, sequential state estimation is tractable, through the calculations given above.

Belief representations can be categorized according to assumptions on the state space, belief state, and other factors [98, 188]. They include:

A. Continuous belief distributions

Gaussian distributions with linear dynamics: The belief takes the form of a normal distribution

$$\mathrm{Bel}(x_t) = N(x_t; \mu_t, \Sigma_t) \tag{4.13}$$

Optimal sequential state estimation can be solved exactly, and is accomplished by the Kalman filter update equations [144]. The process is tractable because Gaussian distributions are closed under joint conditioning and marginalization (that is, multiplication and integration).

Gaussian distributions with linearized dynamics: A nonlinear system can often be treated as locally linear. Linearization is accomplished by first order Taylor expansion around the current state. The Kalman filter is applied to this locally linear model. Additional errors arising from linearization are not modeled in the noise variance. The result is called the extended Kalman filter (EKF) [317].

Gaussian distributions with statistical linearization: This model, known as the unscented Kalman filter (UKF), represents a Gaussian state distribution through a set of $2L+1$ weighted samples $x_t^i, i = 1, 2, \ldots, L$ (L is the state space dimension), called *sigma points*, that encode its sufficient statistics. These samples are propagated through the true nonlinearity, and are used to reconstruct an updated estimate of the state distribution via mean and covariance data computed from the propagated samples. The same procedure is applied to the observation model. The UKF can be implemented as efficiently as the EKF, is simpler to implement (requiring no Jacobians to be calculated), and has proved to be more accurate [318].

Mixture of Gaussians: The belief representation consists of a weighted sum of M hypotheses, each of them a normalized Gaussian distribution:

$$\mathrm{Bel}(x_t) = \sum_{i=1}^{M} w_i N(x_t; \mu_t^i, \Sigma_t^i) \tag{4.14}$$

Methods in this family can be distinguished according to how they propagate the density forward in time, and how the hypotheses are weighted or selected at successive time steps. Many proposed algorithms are based on heuristics. One configuration consists of M linear Kalman filters, with a prescription for reweighting and/or reallocating filters after temporal updates.

B. Discrete belief distributions:

Monte-Carlo (particle) filters: The state distribution is modeled by a set of discrete samples. They are capable of capturing linear or nonlinear dynamics, and of operating within a continuous or discrete state-space. While similar to weighted mixture of Gaussian models, in Monte Carlo approaches maintaining an optimal set of hypotheses can be done in a theoretically justified way, using importance resampling [14].
Sampled state spaces: Dynamics in such models can be constructed to take place on a regular grid. Since the domains are all discrete, probabilities may be represented by histograms, which makes the relevant computations tractable.
Discrete and nonmetric state spaces: The best-known example is the hidden Markov model (HMM), which assumes that x_t is a discrete random variable. The transition function is no longer continuous, the observation function at any state is any continuous density, and state inference is efficiently performed using the Viterbi algorithm [246].

C. Hybrid continuous-discrete models:

Switching linear dynamical systems can represent systems that are linear in distinct, discretely-parametrized regimes. A discrete state variable (analogous to the discrete state of an HMM) may be used to parametrize the current regime, while a continuous state variable is used to describe dynamics in that regime. Discrete state transitions are typically treated as Markov chains. Examples of systems of this type include models of animal behavior, where several distinct sub-behaviors are observed (e.g., sequences of patterns of movements in populations of bees), or human juggling [214]. For Gaussian-distributed belief representations, learning can be performed through iterative approximation, using the EM algorithm [111]. This family of models has been applied in diverse disciplines, ranging from control, to geosciences, economics, and aerospace engineering, and consequently a broad range of approximate inference methods have been developed.

4.4.3 Locomotion as a piecewise-continuous process

Systems of the last type described above are relevant to the subject matter of this chapter, because of the discontinuous (or, better stated, piecewise-continuous) nature of foot-ground interactions during locomotion. In related research by Bissacco et al. kinematic data acquired during locomotion was viewed as having been generated by a hybrid continuous-discrete dynamical system [39, 38]. In their models, kinematic gait patterns are captured through a switching linear dynamical system consisting of a continuous system (an autoregression process, as described in section 4.4.4) designed to capture the motion of the leg during the free swing phase, and a discrete transition, which provides a simplified representation of the nonlinear phase during which foot and ground are in contact. These distinctive properties of a gait pattern are regarded as arising from different parameter settings of the continuous model, and from a different discrete transition process. The model estimation and tracking algorithms these authors developed are reviewed in section 4.4.4, below.

By comparison, the present chapter focuses primary attention on the contact phase. Time evolution within this phase is modeled through observations of the acoustic and vibrational signatures that it produces. The non-contact phases can be viewed as discontinuities during which no observations are available, as footstep signatures are not being produced.

4.4.4 Model estimation from data

The discussion above focused on the problem of state inference, i.e., the consistent calculation of belief distributions about the hidden system state as a function of observations. From a learning standpoint, the complementary problem is that of determining the system model f, g that best fits the evidence. For a parametric system model, this means determining the value of the system parameters θ. The approach taken to learning depends substantially on the model form that is assumed. The two most common families of model estimation algorithm rely on gradient descent optimization or the expectation-maximization (EM) algorithm. Other approaches to learning system models from data, which do not directly fit within these two categories, have also been developed in recent years.

4.4.4.1 System identification

Input-output time series models, such as autoregression processes, and certain black-box models, such as time-delay neural networks, have predominantly relied on gradient based methods for learning model parameters from data.In this form of parameter estimation, model parameters are directly adapted via iterative gradient descent so as to best explain the observed time series Y. An error function is defined

between the predictions of the model and the observations – for example, between the average one-step predicted observations and the subsequent true observations, given the model parameters θ. A gradient descent algorithm is used to find the values θ^* of theta that yield a local minimum of this error function.

More modern versions of system identification, that seek to learn parameters of state space system models from input and output observations in a non-probabilistic setting also exist, but a comprehensive review of other methods from system identification is not attempted here.

4.4.4.2 Expectation maximization

The expectation maximization (EM) algorithm is applicable to the estimation of a wide class of probability models. It provides a method for determining the parameters θ that maximize the log likelihood of a set of observed data $\log p(Y|\theta)$, without knowledge of the values of the hidden state variables X [77]. It assumes a joint distribution $p(Y,X|\theta)$ over the observed and unobserved variables to be given, dependent on θ. The algorithm proceeds as follows [37].

1. Choose an initial value of the parameters, θ_{old} .
2. **E-Step:** Evaluate the posterior distribution of the observations, $p(Y|X,\theta_{\text{old}})$.
3. **M-Step:** Determine θ_{new} to maximize the complete data log likelihood $Q(\theta,\theta_{\text{old}})$

$$\theta_{\text{new}} = \arg\max_{\theta} Q(\theta,\theta_{\text{old}}) \tag{4.15}$$

   where

$$Q(\theta,\theta_{\text{old}}) = \sum_{Y} p(Y|X,\theta_{\text{old}}) \log p(Y,X|\theta)\,. \tag{4.16}$$

4. Check for convergence of Q or of θ. If convergence is not met, let $\theta_{\text{old}} \leftarrow \theta_{\text{new}}$ and return to step 2.

Each cycle of the algorithm is guaranteed to increase the likelihood of the observed data. When the EM algorithm is applied to time series model estimation [272], the E step is solved using state estimation to infer the distribution over the hidden state sequence. The M step uses the result of the state estimation step to optimize the values of the parameters. Applied to the HMM, this results in the widely used Baum-Welch training algorithm [32]. The algorithm can also be used to learn the parameters of a linear dynamical system (Kalman filter) [111]. In this case, state estimation in the M step is performed using Kalman filtering or smoothing.

Several authors have applied the EM algorithm to the estimation of nonlinear state-space models. Roweis and Ghahramani [261] combined the EKF and EM algorithms to estimate the parameters of a model consisting of a linear-Gaussian system combined with a parametric nonlinearity given by a radial basis function (RBF) network, i.e., a state-space function

$$z = \sum_{i=1}^{I} h_i \rho_i(x) + Ax + b\,, \quad \rho_i(x) = \det(2\pi S_i)^{-\frac{1}{2}} \exp\left\{ -\frac{1}{2}(x-c_i)^t S_i^{-1}(x-c_i) \right\}. \tag{4.17}$$

The authors parametrize this nonlinearity as a superposition of Gaussian basis functions, characterized by a set of weights h_i, centers c_i in state space, and covariances S_i. The same form of nonlinearity is used to represent the system evolution function f and/or the observation function g, with appropriate replacements of x and z for x_t, x_{t-1}, and y_t.

4.4.4.3 Bayesian multimodal fusion

When data from multiple sensor channels is available, it is desirable to combine it in ways that allow to improve state estimates. This can be accommodated within the Bayesian filtering viewpoint [85]. Assume the observation vector y to consist of data derived from k distinct sources $y_t = (y_t^{(1)}, y_t^{(2)}, \ldots, y_t^{(k)})$. Provided these measurements are conditionally independent [85], i.e.

$$p(y_t^{(1)}, y_t^{(2)}, \ldots, y_t^{(k)} | x_t) = p(y_t^{(1)}|x_t) p(y_t^{(2)}|x_t) \cdots p(y_t^{(k)}|x_t) \tag{4.18}$$

then the y's form what is known as an independent likelihood pool,

$$p(x|y) = C p(x) \prod_{i=1}^{k} p(y^{(k)}|x) \tag{4.19}$$

and the state and model estimation discussions presented above go through without modification. Thus, one major advantage of the Bayesian filtering viewpoint is that multisensor data fusion can, given amenable measurements, be handled within a unitary formalism.

4.4.4.4 Other approaches to model estimation for human motion

Ijspeert et al. [134, 133] developed a state space dynamical system model for human motion, called Dynamic Movement Primitives (DMP). These models consist of one of two canonical linear systems, reproducing either discrete movements (with bell-shaped velocity profiles similar to typical trajectories seen in human point-to-point movements) or periodic, rhythmic movements, based on limit cycle attractors. These basic linear models are augmented with a locally-weighted RBF nonlinearity that can be learned from data to fit a demonstrated kinematic trajectory. From a biological movement control perspective, the DMP is thought of as an elementary predictive (forward) model for quickly executing a previously learned movement in a way that is adapted to the requirements of context (for example, with variation in execution speed, scale, or endpoints of the trajectory). The approach estimates model parameters by integrating the hidden state using the linear part of the model

matched to the gross features of the trajectory (e.g., start and end configuration), and applies a form of subspace regression to fit the RBF nonlinearity to the observed kinematic trajectory.

Visell et al. extended the approach of Ijspeert et al. to a Bayesian filter framework by augmenting the dynamical model with a Monte-Carlo sampled belief distribution. The latter is used to perform state inference for new observation sequences [307], and, within a multiple motion models framework, to maintain a continuously updated belief state over the joint set of motion possibilities, which can be used as a filter for interpreting the observed motion pattern in real-time.

Bissacco [39] developed a closed-form, but sub-optimal, model learning algorithm for switching linear dynamical systems, based on subspace system identification ideas. In this model, each linear system is conceived to correspond to the non-contact phase of a gait pattern, while the switch is meant to correspond to the ground-contact phase. This algorithm estimates both model-switching event distributions, and parameters of the models themselves, from data. The model was applied to human gait dynamics, as represented in joint angles acquired via motion capture data. It was found to compare qualitatively and quantitatively favorably to iterative learning methods. However, decision-making tasks such as classification were not implemented.

Bissacco and Soatto [38] developed hybrid continuous-discrete autoregressive (AR) models for human motion. They apply a Bayesian approach to learning posterior distributions $p(\theta|y_{1:t})$ over the parameters of continuous (non-switching) AR models, and develop a model distance using these posterior distributions, based on the Wasserstein-Mallows ("Earth-mover's") distance. Extending this model to the switching case (hybrid autoregressive models) involved applying the distance measure to multimodal distributions. They use their model to learn time series derived from video sensing of human locomotion patterns, and demonstrate the superior classification performance of the resulting hybrid models over simpler linear models. In subsequent work they have developed kernel-based distance measures for the space of autoregressive processes, to support statistical decision making among estimated models (e.g., classification of learned time series). As a question of style, these methods are more closely linked to stochastic control, whereas the foregoing discussion has emphasized a probabilistic viewpoint.

Others have developed approaches to motion dynamics modeling based on Bayesian models with Gaussian Process priors that are capable of jointly performing dimensionality reduction and state space model regression. Wang et al. [320, 319] developed a machine learning model of human movement known as the Gaussian process dynamical model (GPDM). As in the model of Roweis and Ghahramani, the GPDM represents a movement pattern as a probabilistic dynamical model consisting of a linear Gaussian system with an RBF nonlinearity. However, whereas Roweis and Ghahramani learn a parametric model from data, using the EM algorithm, Wang et al. adopt a fully Bayesian approach, and marginalize over (integrate out) the model parameters, with a Gaussian process prior. The marginalization is performed explicitly in closed form, leading to a nonparametric model which can be learned from data. They trained the GPDM on high dimensional motion capture

sequences of human walking and evaluated the results of learning using different training algorithms. Related approaches have been developed based on regression with reproducing kernel Hilbert space models [248].[3]

4.5 Application to pedestrian tracking via in-floor force sensing

This section presents a probabilistic approach to the tracking and estimation of the lower body posture of users moving on foot over an instrumented floor surface of the type described in Chapter 3. We use force measurements from the floor to track body posture in 3D space using Bayesian filters with a switching state-space model. Potential applications of this work to person tracking and human-computer interaction are briefly discussed.

4.5.1 Background on 3D person tracking

3D human posture tracking is a classic challenge in computer vision and pattern recognition. Computer vision techniques have been the most widely used for this purpose [192, 193], although several researchers have investigated human tracking via in-floor sensor arrays [201, 218, 4]. Common challenges of person tracking in these domains include the loss of 3D pose information through observation via the sensor array, and the underlying complex dynamics of human motion. Missing information plays an important role in both settings. Losses due to occlusion in video-based tracking are somewhat analogous to the loss of observations while feet are out of contact with the ground during tracking via a floor-based array. Overcoming such missing information has, in part, motivated the approach presented here.

Although motion capture and video can provide high-resolution 3D position information for human tracking, they are not always available and are prone to visual occlusion. Furthermore, state of the art methods for inferring human contact interactions from video provide inaccurate information about interaction forces between body and ground [48]. Such forces are highly characteristic of the individuals and activities generating them (as evidenced in the references given below).

Bayesian filtering provides a unifying view of diverse probabilistic tracking methods. It has been extensively applied to problems in object, person, or context tracking [97, 296]. The effectiveness of such methods stems from their ability to integrate information acquired over time in ways that respect the structure and dynamics of the object or individual being tracked. Nonparametric Bayesian filtering techniques, like the particle filter based model used here, make it possible to perform tracking without making unnecessary assumptions about the form taken by

[3] These approaches are promising but would derail the present proposal too much to discuss here.

those distributions or the dynamics governing them, by maintaining many hypotheses in parallel.

The system presented here consists of a posture tracking system based on a distributed, sparse in-floor sensing array. Prior literature on the analysis of foot-floor contact forces has addressed applications to immersive interactive media [228], pedestrian identification [218, 286], gait and dance analysis [239], among others [332, 267, 196, 187]. Here, similar data is used for 3D kinematic tracking of users' lower bodies, a task that has received less attention in prior research on floor-sensing arrays. Murakita et al. utilized a Markov Chain Monte Carlo method to track pedestrians via an array of binary pressure sensors [201], albeit with much larger errors (typically 0.6 m) than what we achieve here (Sec. 4.5.5). Yin and Pai tracked whole-body movements via a high-resolution (and costly) floor sensing array, based on the similarity of force patterns to those recorded in a database of movements [332]. However, their system was limited to tracking relative to a predefined set of static poses.

Our intended applications involve both person tracking and interaction with floor-based touch displays via the feet [315]. In both cases, we are interested in tracking the 3D kinematics of the lower body of moving persons, with an emphasis on the locations of their feet. Although existing force sensing arrays can provide accurate information about foot-floor contact forces, the achievable resolution is often limited by cost constraints. In addition, mappings from patterns of foot-floor forces to body posture are complex and one-to-many. Effective use of prior knowledge about body structure, movement, and walking mechanics is required in order to track posture accurately.

4.5.2 System configuration

The sensing floor used in the experiments is described more fully in Chapter 3 (Figure 4.3). It consists of a 6×6 array of rigid tiles, 30 cm on each side. Each tile is instrumented with four resistive force sensors (Interlink model 402), which are located at the corners. Thus, the nominal linear sensing resolution of this array is 15 cm. In addition, each tile includes a wide bandwidth vibrotactile actuator [308], which although unused here, does modestly influence the sensor measurements, due to its weight [315]. Analog data from the force sensors are conditioned, amplified, and digitized via 32-channel, 16-bit data acquisition boards. Each sensor is sampled at a rate of up to 1 kHz transmitted over a low-latency Ethernet link. An array of six small-form-factor computers is used for force data processing.

For applications that do not require kinematic tracking, we infer foot-floor contact loci using intrinsic contact sensing techniques (see Chapter 3 and [315]), attaining an effective resolution of about 2 cm. However, such methods are incapable of tracking the location of a foot once it leaves the floor surface, and cannot resolve situations in which the feet overlap onto a single tile. Moreover, inference of lower body pose from in-floor force sensor data is challenging due to the loss of informa-

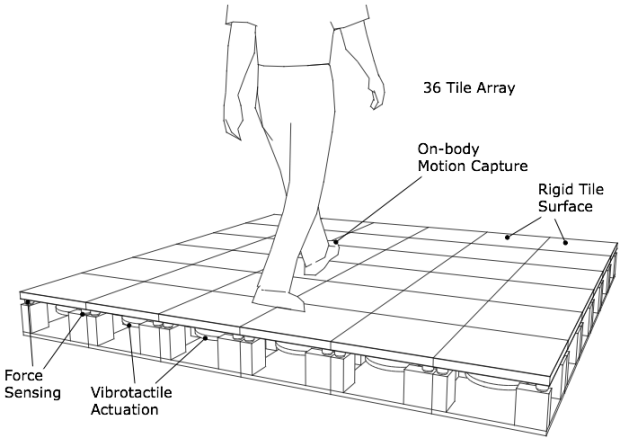

Fig. 4.3: Illustration of the distributed floor interface, with components labelled.

tion inherent in this complex mapping. Such limitations have, in part, motivated the present work. In particular, we adopt the framework of Bayesian filtering in order to maintain continuity of lower body position estimates in dynamic settings, such as walking, where foot-ground contact is regularly interrupted.

Within this framework, our task remains challenging due to the high dimensional mapping from an articulated pedestrian pose to the observed force sensor values. In particular, this map is discontinuous for a sensing infrastructure consisting of independent, rigid tiles, as poses that are similar in nature, i.e. with footprints of similar 2D position and orientation, will lead to drastically different force observations when tile boundaries are crossed.

4.5.3 Tracking problem and algorithm

Consider a dynamic system with states x_t and observations y_t, both indexed by time. A Bayesian filter probabilistically estimate at time t the state x_t by sequentially updating a belief distribution $\mathrm{Bel}(x_t)$ over the state space, defined by $\mathrm{Bel}(x_t) = p(x_t|y_t, y_{t-1}, y_{t-2}, ...) = p(x_t|y_{1:t})$. Assuming the states comprise a Markov process, the Belief distribution at each subsequent time step can be obtained, using Bayes' Theorem, in terms of the belief state at the prior time step $t-1$, the assumed motion model $p(x_t|x_{t-1})$, and the likelihood $p(y_t|x_t)$ of the newly acquired observation y_t given the state x_t:

$$\mathrm{Bel}(x_t) \propto p(y_t|x_t) \int p(x_t|x_{t-1})\mathrm{Bel}(x_{t-1})\, dx_{t-1} \tag{4.20}$$

Bayesian filters can be distinguished, in part, by the form of the Belief distribution $\mathrm{Bel}(x_t)$ that is assumed. Here, we adopt a Monte-Carlo approach, in which $\mathrm{Bel}(x_t)$ is represented by a set of weighted samples, or particles, given by $S_t = \{(x_t^i, w_t^i), i = 1,2,\ldots N_s\}$. Our method uses the Sampling-Importance-Resampling (SIR) algorithm [99], described in Alg. 1, and schematically illustrated in Fig 4.4.

For each new observation, SIR re-weighs the set of particles depending on their likelihood, evolves them in time using the assumed dynamic model, and updates the particle set S_t by resampling based on these weights.

Specifically, the likelihood function $L(x_t) = p(y_t|x_t)$ is computed in two steps as follows.

1. Using the observation model $\mathbf{H}$, defined in Section 4.5.3.1, that maps states into the observation space, generate expected observations $y_t^* = \mathbf{H}(x_t)$.
2. Using the similarity measure $S(z,z') = p(z|z')$, defined in Section 4.5.3.2, compute the likelihood as $L(x_t) \equiv S(y_t^*, y_t)$.

As seen in Eq.4.21, each particle is weighted according to its likelihood while also considering a prior distribution $p(x_t)$. As described in Section 4.5.3.2, the prior distribution $p(x_t)$ is useful for encoding constraints on states x_t, thus leading to an efficient search of the state space.

The attributed weight is then used to resample the particle set (see Eq. 4.22). This step distinguishes SIR from SIS (Sampling Importance Sampling), and is meant to eliminate degeneracy of particles; by concentrating on high weighted particles to create a new uniformly distributed particle set, the extreme case where most particles have negligible weight is avoided. The opposite extreme, consisting of a single strong hypothesis, can be avoided by the inclusion of a roughening process. Roughening consists of the addition of random, zero-mean, normally distributed noise to all particles after resampling (Eq. 4.24), to allow for a thorough search of the solution space. Additionally, particles are propagated forward in time based on the assumed dynamic model (see Eq.4.23), which implicitly defines the motion probability $p(x_t|x_{t-1})$. Our dynamic model consists of two processes, accounting for the continuous and discrete aspects of the motion of interest. The dynamic model and roughening process are defined in detail in Section 4.5.4.

In our system for tracking via in-floor force measurements, the relevant variables consist of:

- Observations $\mathbf{y}_t$, consisting of a 12×12 array of force values, f_i.
- States, $\mathbf{x}_t$, describing kinematic lower-body poses, are 19-dimensional vectors: $\mathbf{x}_t = (\phi_{l,t}, \dot{\phi}_{l,t}, \dot{\phi}_{l,t-1}, \phi_{r,t}, \dot{\phi}_{r,t}, \dot{\phi}_{r,t-1}, \beta)$. They include planar midpoint coordinates $\mathbf{u}$ and orientations θ for each foot, where $\phi_l = (\mathbf{u}_l, \theta_l)$ and likewise for ϕ_r, along with first time derivatives. The state $\mathbf{x}_t$ also includes a binary-valued vector $\beta = (\beta_l, \beta_r)$, implemented as a quaternary variable, which indicates the foot-floor contact condition ($\beta_i = 1$ if there is contact) for the left and right feet.

Figure 4.5 illustrates this state description within a skeletal model. The algorithm definition is completed by specifying the observation model $\mathbf{y}_t = \mathbf{H}(\mathbf{x}_t)$, the likelihood model $p(\mathbf{y}_t|\mathbf{x}_t)$, and the motion model, $p(\mathbf{x}_t|\mathbf{x}_{t-1})$.

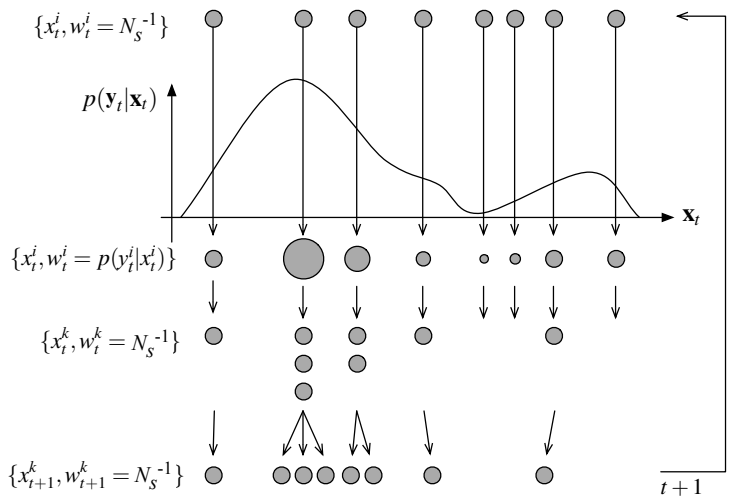

Fig. 4.4: The SIR particle filter algorithm.

Algorithm 1 Sampling Importance Resampling

Initialize particles randomly: $S_0 \sim N(\mu_S, \sigma_S)$
while $t > 0$ **do**
  Observe y_t.
  for $i = 1$ to N_s **do**

$$\text{Likelihood:} \quad p(y_t|x_t^i) = S(y_t, H(x_t))$$
$$\text{Weight:} \quad w_t^i = p(x_t^i) \times p(y_t|x_t^i) \tag{4.21}$$

  end for
  for $i = 1$ to N_s **do**

$$\text{Normalize:} \quad W = \textstyle\sum_i w_t^i, w_t^i \leftarrow W^{-1} w_t^i$$
$$\text{Resample:} \quad x_t^i \sim p(x_t^{i*}|w_t^i), w_{t+1}^i = N_s^{-1} \tag{4.22}$$
$$\text{Draw:} \quad x_{t+1}^i \sim p(x_{t+1}|x_t^i) \tag{4.23}$$
$$\text{Roughen:} \quad x_{t+1}^i \leftarrow x_{t+1}^i + \eta_{t+1}, \eta \sim N(0, \sigma_x) \tag{4.24}$$

  end for
  $S_{t+1} = \{(x_{t+1}^i, w_{t+1}^i)\}_{i=1}^{N_s}$
end while

4.5.3.1 Observation model

We model expected observations $\mathbf{H}(\mathbf{x}_t)$ for a state $\mathbf{x}_t$ by simulating the mechanical forces associated with a pose. Ignoring shear forces, foot-tile contact results in a normal pressure distribution $p(\mathbf{u})$, where $\mathbf{u} = (u, v)$ are 2D coordinates on the floor. The pressure distribution on a tile is conveniently summarized by a contact centroid $p_c = (\mathbf{u}_c, F)$, where $F = \int d\mathbf{u}\, p(\mathbf{u})$ is the net normal force and $\mathbf{u}_c$ is the pressure

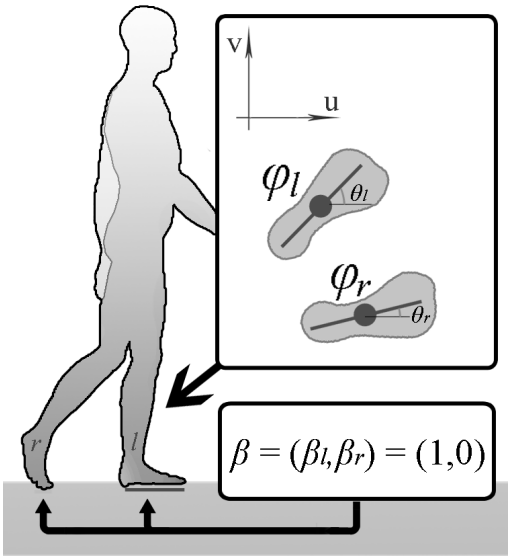

Fig. 4.5: State description of lower body poses: $\mathbf{x}_t$ defines feet and foot-floor contact.

centroid. A normal force with magnitude F, applied at $\mathbf{u}_c$, would give rise to the same force measurements f_i as $p(\mathbf{u})$ [315, 36] (Fig 4.6). Our observation model associates a pose $\mathbf{x}_t$ to a set of contact centroids, $p_{c,j}, j = 1,2,\ldots,N_c$. One centroid is placed on each tile that a foot pose is determined to be in contact with ($\beta_i > 0$), and the total weight F of the user is partitioned among these centroids. The placement of a contact centroid is determined by the average position of foot to tile contact. Expected sensor readings f_i are obtained from the static equilibrium equations for each tile. Each pressure centroid p_c yields a contribution $f_{i,c} = d_i^{-1}(\sum_{j=0}^{4} d_j^{-1})^{-1}$, where $d_j = |\mathbf{u}_c - \mathbf{u}_j|$, and $\mathbf{u}_j$ is the sensor location. In this way, we predict observed force values $\mathbf{y}_t^* = \{f_{i,t}\}$ for a state $\mathbf{x}_t$.

4.5.3.2 Likelihood model

The likelihood function $L(\mathbf{x}_t) = p(\mathbf{y}_t|\mathbf{x}_t)$ describes the probability of observing force values $\mathbf{y}_t$ given the state $\mathbf{x}_t$. As described above, we use the observation model to generate expected observations, $\mathbf{y}_t^* = \mathbf{H}(\mathbf{x}_t)$. The likelihood function is then defined in terms of a normalized similarity measure $p(\mathbf{y}_t|\mathbf{x}_t) = S(\mathbf{y}_t^*, \mathbf{y}_t)$ between true force pattern observations $\mathbf{y}_t$ and expected force observations $\mathbf{z}_t^*$.

4.5.3.3 Similarity measure S

The similarity measure $S(\mathbf{z}, \mathbf{z}') = p(\mathbf{z}|\mathbf{z}')$ models the probability of observing $\mathbf{z}$ if the true observation is $\mathbf{z}'$. Conventional similarity measures make use of metrics

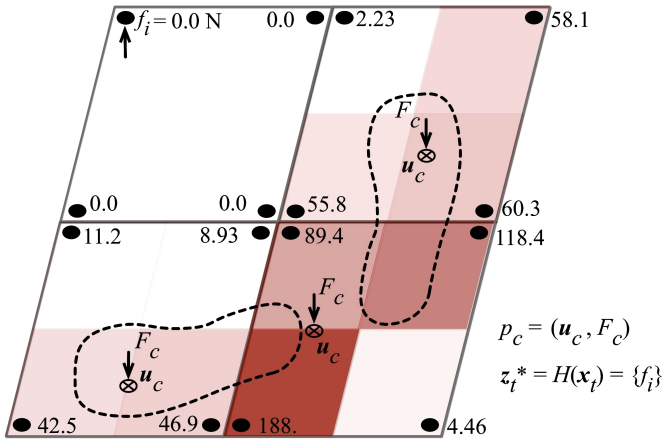

Fig. 4.6: The observation model $H(\mathbf{x}_t)$ maps a pose $\mathbf{x}_t$ (illustrated here as two feet) to a set of contact centroids ($\mathbf{u}_c$). These are then converted to force sensor readings $\mathbf{y}_t = \{f_i\}$. Expected force observations are illustrated as grids, with each quadrant intensity proportional to corresponding force sensor value (given in Newtons).

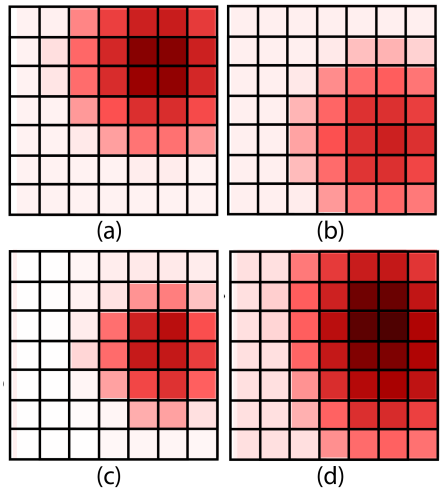

Fig. 4.7: Computations of the similarity measure from the 2D pressure distributions for: (a) $\mathbf{y}_t$, (b) $\mathbf{y}_t^*$, (c) $\mathbf{y}_t \cap \mathbf{y}_t^*$, (d) $\mathbf{y}_t \cup \mathbf{y}_t^*$. Pressure distributions are illustrated as grids, with each quadrant intensity proportional to corresponding force sensor value. The intersection ($\cap$) and union ($\cup$) of force observations are used in computing similarity $S(\mathbf{y}_t, \mathbf{y}_t^*)$.

such as Euclidean or Mahalanobis distance functions. However, since $\mathbf{H}$ is a high-dimensional discontinuous map from states $\mathbf{x}_t$ to observations $\mathbf{y}_t$, these measures cannot properly gauge similarity between observation vectors $\mathbf{y}_t$, $\mathbf{y}_t^* = \mathbf{H}(\mathbf{x}_t)$. Moreover, the force observations are comparatively sparse, with most values being zero. As an alternative, we compute pair-wise similarity between such patterns, based on a measure of their area of overlap. Specifically, we employ a similarity measure that

has proved useful in tracking via binary image masks [257], computing $S(\mathbf{z}^*, \mathbf{z})$ as the relative area of overlap between the true and expected 2D pressure distributions,

$$S(\mathbf{y}_t^*, \mathbf{y}_t) = \frac{\cap(\mathbf{y}_t^*, \mathbf{y}_t)}{\cup(\mathbf{y}_t^*, \mathbf{y}_t)} = \frac{1}{N_z} \sum_{i=1}^{N_z} \frac{\min(\mathbf{y}_t(i), \mathbf{y}_t^*(i))}{\max(\mathbf{y}_t(i), \mathbf{y}_t^*(i))}$$

Figure 4.7 illustrates conceptual examples of observations $\mathbf{y}_t$, $\mathbf{y}_t^*$ as 2D pressure distributions, as well as their intersection $\cap(\mathbf{y}_t^*, \mathbf{y}_t)$ and union $\cup(\mathbf{y}_t^*, \mathbf{y}_t)$.

We note that the average overlap of these resulting pressure distributions is an effective metric for capturing similarities between force observations as a probability:

$$\begin{aligned} S(\mathbf{z}, \mathbf{z}) &= 1 \\ \mathbf{y}_1 \neq \mathbf{y}_2 \Rightarrow 0 &< S(\mathbf{y}_1, \mathbf{y}_2) < 1 \\ S(\mathbf{y}_1, \mathbf{y}_2) &= S(\mathbf{y}_2, \mathbf{y}_1) \end{aligned} \tag{4.25}$$

4.5.3.4 Postural constraints

The likelihood model is modified to encode human postural constraints, via a prior distribution $p(\mathbf{x}_t)$. The latter is defined to consist of a set of independent postural priors for human walking, in the form of univariate Gaussian distributions $N(\mu_\varsigma, \sigma_\varsigma)$, $N(\mu_\Theta, \sigma_\Theta)$ over stance width $\varsigma = \|\mathbf{u}_l - \mathbf{u}_r\|$ and relative orientation $\Theta = |\theta_l - \theta_r|$ respectively. The postural prior is introduced as the product $p(\mathbf{x}_t) = N(\varsigma; \mu_\varsigma, \sigma_\varsigma) N(\Theta; \mu_\Theta, \sigma_\Theta)$. The prior distribution $p(\mathbf{x}_t)$ is applied when computing the particle weights from the likelihood L (see Eq. 4.21).

4.5.4 Dynamics model

We model the movements of the lower body of a walker via the motion probability $p(\mathbf{x}_t | \mathbf{x}_{t-1})$. The state x_t consists of continuous configuration variables ϕ_i and discrete contact variables β_i. We therefore approximate foot motion in a hybrid (stochastic) framework, incorporating continuous, linear movements of the limb coupled to discrete state transitions reflecting changes of the foot-floor contact conditions.

4.5.4.1 Continuous, linear dynamics

The state representing the left or right foot is denoted respectively by a vector $\phi_i = (\mathbf{u}_i, \theta_i)$ giving the midpoint and orientation of either the left ($i = l$) or right ($i = r$) foot at time t (Figure 4.5. The dynamics used in our algorithm can be described by the following linear, discrete time system:

$$\phi_{i,t} = \phi_{i,t-1} + \beta_i \Gamma_i (\dot{\phi}_{t-1} dt + \eta_t^0) \tag{4.26}$$

$$\dot{\phi}_{i,t} = \beta_i [\alpha \dot{\phi}_{i,t-1} + (1-\alpha)(\dot{\phi}_{i,t-2} + \eta_{t-1}^1)] \tag{4.27}$$

The parameter β_i is the binary contact variable for foot i. Thus, ϕ_i is constant when there is contact ($\beta_i = 0$) and otherwise drifts, with position and velocity driven by additive Gaussian noise processes η_t^0 or η_t^1, where $\eta \sim N(0, \Sigma)$. For efficiency, we parametrize drift via a single noise process, defining $\eta \equiv \eta_t^0 = \eta_t^1 dt$ for all t. The noise covariance Σ is a 3×3 diagonal matrix with diagonal entries $\sigma_u, \sigma_v, \sigma_\theta$. To mimic walking, velocity drift in the direction that the foot is oriented is assumed to be larger. This non-isotropic drift is implemented through the factor Γ_i, a diagonal matrix with entries $(\cos\theta_i(\gamma + \sqrt{1-\gamma^2}), \sin\theta_i(\gamma - \sqrt{1-\gamma^2}), 1)$, where $0 < \gamma < 1$ is a dimensionless scalar defining the longitudinal bias. α is a dimensionless scalar defining the velocity noise mixing rate. It approximates the dynamics of a free foot during walking by means of a saturating linear drift velocity.

Although this continuous dynamic model violates the Markov assumption made in Eq.4.20, we note that there exists a Markov representation of this system, via the following change of variables:

$$\Phi_t = \begin{bmatrix} \dot{\phi}_t \\ \dot{\phi}_{t-1} \end{bmatrix} = \begin{bmatrix} \alpha & 1-\alpha \\ 1 & 0 \end{bmatrix} \Phi_{t-1} \tag{4.28}$$

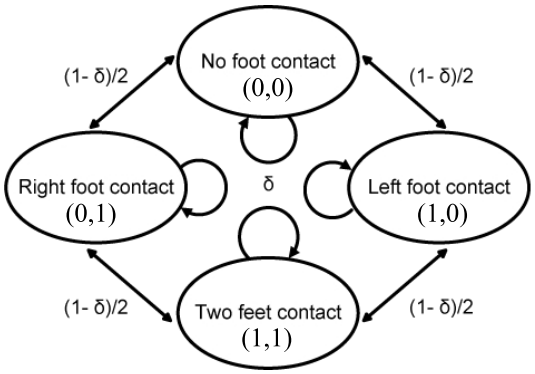

Fig. 4.8: Stochastic state transition diagram approximating stepping motion.

4.5.4.2 Roughening

As presented in (Alg. 1), noise $\eta \sim N(0, \sigma_x)$ is added to the continuous state components ϕ_i at each SIR step in order to avoid particle degeneracy.

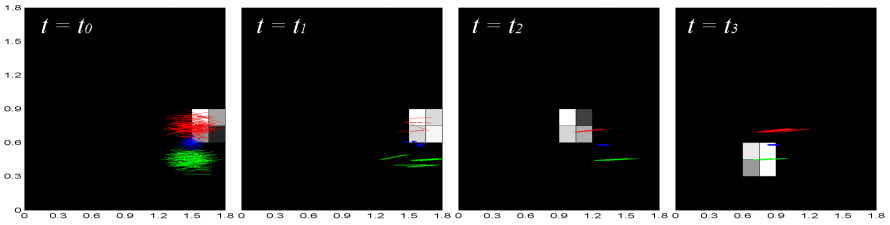

Fig. 4.9: Force observations and pose estimates at 4 stages of the sample walking sequence. Observations are shown as 2D pressure distributions, with quadrant intensity proportional to force sensor readings. Poses are illustrated as green and red lines, corresponding to a top view of left and right feet estimates respectively, with blue circles corresponding to inferred center of mass.

4.5.4.3 Discrete state transition model

The dynamic model includes discrete transitions from the foot-floor contact states $\beta = (\beta_l, \beta_r)$, where $\beta = 0$ or 1, via the stochastic process, shown in Figure 4.8. Despite its simplicity, this model is effective in approximating discrete stepping motion. δ is an empirically determined probability of no change in contact state β. All remaining transitions are symmetric, with transition probability $\frac{1-\delta}{2}$.

4.5.5 Experiment and results

The system described above was evaluated by measuring the absolute positions of the feet of pedestrians using data acquired synchronously via motion capture (Vicon Motion Systems). Reflective markers were attached to the walkers' shoes, providing an accurate estimate of 3D foot positions. Five recordings of walking sequences between 5.7 and 12.4 seconds in length were acquired via the apparatus described in previous reports. Synchronous motion capture and force data were recorded. Errors were computed based on maximum a posteriori (MAP) foot position estimates obtained from the tracking algorithm.

Figure 4.9 shows the state estimates and force observations at four stages of the walking sequence: the initial particle set has high variance, but is quickly narrowed down to a few hypotheses which are evolved based on our motion model. Figure 4.10 shows the resulting motion trajectories and errors for the two foot locations, in planar coordinates. Average RMS error values are reported in Table 4.1. The experimental parameters are given in Table 4.2. Position errors during foot-floor contact are found to be slightly less on average than when a foot is not in contact with the floor. Temporal alignment mismatches were found to have a large effect, so we also performed a windowed error calculation in which an acceptable time shift of 10 samples (at 20 Hz) was permitted. This greatly reduced RMS position errors (see Table 4.1), suggesting that system tracking per-

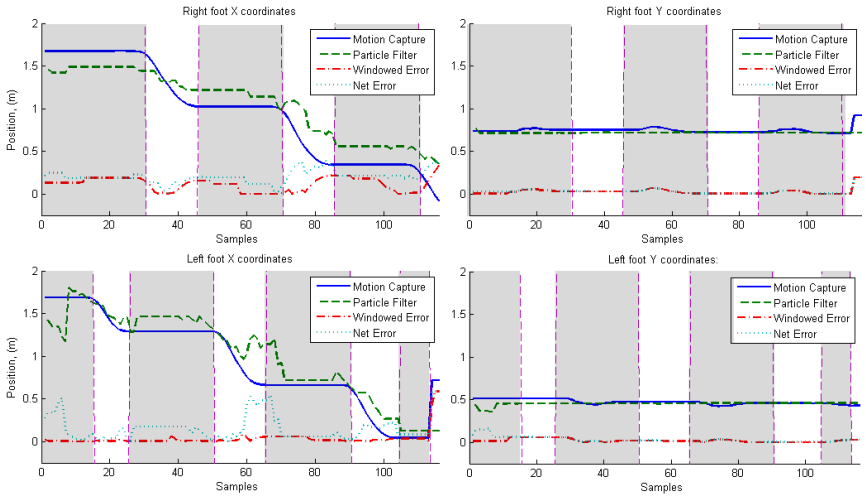

Fig. 4.10: Sample results for a pedestrian crossing the apparatus, comparing measurements from motion capture data and estimates obtained from the particle filter. Results are shown for both feet ϕ_l, ϕ_r. The shaded domains illustrate contact states, with grey and white corresponding to $\beta_i = 1$, $\beta_i = 0$ respectively.

Foot	Error (m)	Windowed error (m)
Right (no contact)	0.1901	0.1245
Left (no contact)	0.1649	0.0336
Average (no contact)	**0.1775**	**0.0791**
Right (contact)	0.2025	0.1058
Left (contact)	0.1406	0.0306
Average (contact)	**0.1716**	**0.0682**
Right (all)	0.1982	0.1122
Left (all)	0.1490	0.0316
Average (all)	**0.1736**	**0.0719**

Table 4.1: RMS Position Error

formance may be most acceptable in situations in which temporal accuracy is not important. Tracking performance in more temporally demanding settings might be greatly improved if a better alignment can be achieved. Video documentation of these results is provided in the supplementary material, and available online at `http://www.cim.mcgill.ca/~rishi/video.swf`.

In addition to position estimates, this system provides continuous labels identifying the walker's right and left feet. During tracking of the sequences used for evaluation, left and right feet were continuously and coherently identified with 100% accuracy. The capability of this system to maintain and propagate these labels may be useful for applications including floor-based touch screen user interfaces, where it may be desirable to assign each foot a different functional operation, or to render a different response to left and right foot [315].

SIR Algorithm	
Number of particles	$N_s = 200$
Initial Noise	$\sigma_S = 4.572$ cm
Roughening Position Noise	$\sigma_x = 0.003048$ cm/rad
Likelihood Model	
Postural prior stance size	$(\mu_\varsigma, \sigma_\varsigma) = (30.48, 30.48)$ cm
Postural prior stance angle	$(\mu_\Theta, \sigma_\Theta) = (0, \pi/2)$ rad
Dynamic Model	
Additive Position Noise	$\sigma_{u,v} = 0.3048$ cm
Additive Angle Noise	$\sigma_\theta = 0.003048$ rad
Longitudinal bias	$\gamma = 0.9$
Velocity mixing rate	$\alpha = 0.55$
Probability of no β change	$\delta = 0.55$

Table 4.2: Experimental parameters

4.5.6 Person tracking from in-floor force measurements: Conclusions

This section described the application of Bayesian filtering techniques to the problem of tracking the lower body pose of a pedestrian from foot-floor interaction forces acquired via a coarse array of in-floor force sensors. The system developed achieves continuous and labeled tracking of the lower limbs of a walker via a coarse sensor array, by combining prior knowledge about the mechanical structure of the interface and a simple, but consistent, model of the dynamics of the feet during walking. In the experiment described above, our system never confused the left and right feet of the walker, and was able to track the locations of each with an average resolution on the order of 15 cm, and with improved resolution when feet are in contact with the surface. Potential applications of these techniques include tracking in smart environments in which motion capture is impractical (due to occlusion or other factors), and to interaction with distributed, floor-based touch surface interfaces for the feet [315, 314].

Despite the promising nature of these results further experiments are needed to evaluate the quality of the tracking. In addition, it is clear that the system itself can be improved in several respects. A higher-density sensor network would improve position estimates during contact, albeit at greater cost. A model for the non-contact portion of walking movement that is more sophisticated than the random drift model used in our system could significantly improve estimates in foot tracking when a foot is not in contact with the floor. The incorporation of additional prior knowledge about the kinematic constraints on lower limb positions during walking would also be expected to contribute improvements. In ongoing work, we are exploring the possibilities for optimally fusing information from in-floor force sensors with motion capture or other video sensors, in order to resolve data loss due to camera occlusion, or to provide contact forces and timing information that cannot be accurately estimated from video.

4.6 Conclusion

This chapter discussed aspects of the problem of tracking of pedestrian movements in augmented environments, reviewing the selection of ambient sensing modalities and devices, the extraction of information from walking-generated sensor data, and a selection of the wide variety of algorithms that have been used for mining the resulting data and for tracking the movements of persons in space. In the last section, a sample application was described based on tracking pedestrians from in-floor force sensor measurements, using an interface that is described more fully in another chapter of this book.

Chapter 5
Novel Interactive Techniques for Walking in Virtual Reality

L. Terziman, G. Cirio, M. Marchal, and A. Lécuyer

Abstract In this chapter we present a state of the art of the natural interactive walking in restricted workspaces. Then we focus on three novel navigation techniques which achieve, in different ways, the challenging objective of proposing an interactive virtual navigation in large virtual environments with a restricted workspace. These three techniques were developed in a continuum, engaging progressively more physical walking from the user, and from a more hardware to a more software-based technique.

5.1 Introduction

Navigation is one of the main interaction tasks in Virtual Environments (VE). Most Virtual Reality (VR) applications provide the users with a way to walk and/or move in the virtual world.

However, one main issue that is often faced with Virtual Reality setup is the restricted workspace in which the user is physically walking. Real walking motions are indeed constrained and bounded by either the walls of the (real) room or the range of the tracking system. Virtual navigation technique must therefore cope with the challenge of this restricted workspace.

In this chapter we present three novel navigation techniques which achieve, in different ways, the challenging objective of proposing an interactive virtual navigation in large virtual environments with a restricted workspace. These three techniques were developed in a continuum, engaging progressively more physical walking from the user, and from a more hardware to a more software-based technique.

The first technique is an input device called the “JoyMan” which can be seen as a “human-scale joystick”. It is a novel hardware based on user’s equilibrioception, i.e., user can lean to control the speed of her virtual navigation with her body orientation. The second technique, called “Shake-Your-Head”, implies more walking, as the user can “walk in place” to control a potentially infinite virtual walk. Interest-

ingly enough, Shake-Your-Head can make use of a low-cost and basic webcam to sense head motions when walking in place. The third technique called the "Magic Barrier Tape" is a software technique which uses a virtual barrier tape to display the limits of the restricted workspace straightforwardly in the virtual world. This enables safer and optimized physical walking inside the workspace. The user can push on the virtual tape to switch to rate-control mode of her navigation and reach out-of-reach locations.

In the remainder of this chapter we will first describe related work in the field of walking and navigation in VR. We will then describe our three novel techniques. Last, we will discuss and summarize the relative strengths and weaknesses of each so that it could help VR developers choose the appropriate approach depending on their application needs.

5.2 State of the art: Natural interactive walking in restricted workspaces

There is an important body of work on navigation approaches for virtual reality. We first review techniques which either allow navigation with no physical motion of the user (static navigation) or no spatial displacement (walking in place). We then discuss navigation techniques involving natural walking, which are more relevant to our work.

5.2.1 Static navigation and walking in place

There are several known Virtual Reality (VR) locomotion metaphors where the user is not required to walk [43], and therefore does not need to overcome restricted workspace problems. Examples of these include *teleportation* i.e., an instantaneous change of position to a new location. *Worlds In Miniature* (WIM) [232] is a metaphor where the user has a copy of the virtual world in his hands. Users can choose a location in the copy and be smoothly taken there in the "real" virtual world. Probably the most common navigation technique is the *Flying Vehicle* where the environment is not manipulated. The illusion is that the user can move through the world, either by using a mock-up, a wand or other device.

Walking in place [274, 294] simulates the physical act of walking without forward motion of the body; a virtual forward motion is introduced. Visual optical flow of navigation, that should be matched by proprioceptive information from the natural walking gait, is instead matched by proprioceptive information from a gait close to natural walking. The sense of presence is greatly increased compared to static navigation techniques [305], but other sensory data related to walking, mainly vestibular cues, are still missing.

5.2.2 Natural walking

Several studies have shown the benefits of using natural walking for the navigation of virtual environments, in terms of task performance [262, 118, 333], presence [305] and naturalness [154, 305, 333]. Hence, several techniques try to adapt natural walking to restricted size workspaces.

In *Step WIM* [159] a user invokes a miniature version of the world at their feet, allowing distances greater than the physical environment to be traveled. The user can walk on the WIM to a new position and trigger a rescaling command that will scale up the WIM until it reaches the virtual world size. When used in a CAVE, where the field of view is restricted by the missing screen, a 360° mapping of the scene to the system display field is used. The effect of the technique is noticed by the user, requiring a small adaptation time to adjust, and does not entirely solve the missing screen problem.

Resetting techniques [328, 329] try to overcome the limited working environment problem with natural walking using head-mounted displays (HMDs). They reset the user's position or orientation in the real world when reaching workspace limits, without breaking spatial awareness of the virtual world. In the freeze-backup technique, the virtual world is frozen and the user takes steps backwards to re-center her real world position inside the workspace. In the freeze-turn technique, the orientation of the user is frozen while she physically pivots 180°. In the 2:1-turn technique, a 360° virtual rotation is mapped to a 180° real world rotation, and the user also physically pivots 180°. These resetting techniques are performed consciously by the user following a warning signal, which implies a break in immersion. Moreover, the resetting itself might feel unnatural.

The *Seven League Boots* [135] allows natural walking in virtual worlds larger than the real space. It scales the user's speed only along their intended direction of travel, using gaze and previous displacement direction. Although appreciated, it does not entirely solve the limited workspace problem.

The *Magic Barrier Tape* [63] explicitly displays the boundaries of the real environment within the virtual environment as virtual barrier tape. It allows natural walking navigation within the space delimited by the tape, as well as rate control at the boundaries by pushing on the tape. It provides an easy, intuitive and safe way of navigating in a virtual scene, without breaking the sense of immersion, but does not solve the missing screen problem if used in a CAVE.

5.2.3 Redirection techniques

Redirected Walking [254, 279, 151] and *Motion Compression* [207, 91, 282] techniques "trick" the user into walking in a curved path in the real world when walking in a straight line in the virtual world through the progressive rotation of the scene around them. In a sufficiently large workspace, and with a straight virtual path, the user can walk endlessly without reaching the limits of the real workspace. These

techniques are natural and in some cases imperceptible. However, they require large workspaces, can be confusing when doing unpredictable or quick changes of direction, and may require distracting events [234]. In practice, they are more suited for HMDs and wide area tracking systems.

Redirected Walking was used in combination with a walking in place technique in a CAVE environment to avoid looking at the missing screen [255]. Experiments showed that the frequency of looking at the missing screen was not reduced compared to hand-held navigation, although the variance was.

In the specific case of architectural virtual walkthroughs, the *Arch-Explore* interface [49] allows the use of redirection techniques in small environments such as CAVEs. A virtual door mechanism is combined to increased (perceptible) redirection gains and the splitting of virtual rooms considered too large for redirection into smaller sized rooms. The missing screen problem is not addressed in this work.

In recent work, *change blindness redirection* [285] redirects users wearing HMDs by making dynamic changes to the environment, such as changing the configuration of doors and corridors while the user is focusing on a distracting task. The fact that the technique is not noticeable renders these results very promising.

There is clearly a lack of adequate navigation techniques allowing immersive real walking and infinite exploration for CAVE-like environments. Existing techniques exhibit many limitations, and there is no convincing solution for the missing screen problem. Although very promising, redirection techniques require specific real and virtual environments in order to work correctly. In this work, we address these issues by proposing three novel navigation techniques for safe, natural and enjoyable navigation within CAVE-like environments.

5.3 JoyMan: Navigating in virtual reality using equilibrioception as a human joystick

The JoyMan is a new interface to navigate into virtual worlds. One main objective of this interface is to go towards realistic locomotion trajectories in the virtual environment. The JoyMan meets this objective by combining two components: a peripheral device allowing users to indicate the desired direction of locomotion and a control law which transforms the device state into a virtual velocity vector.

5.3.1 Description of the JoyMan interface

The mechanical design of the device is based on the metaphor of a human-scale joystick and mainly consists of a board upon which the user stands. The inclination of this board can be changed by the user. Thus, the user indicates the desired locomotion direction by tilting the platform in the corresponding direction. The mechanical design of the platform allows the user to change the platform inclination

by leaning and prevents him from falling, whereas repealing forces tend to maintain the platform horizontal. The control law transforms the device state (pitch and roll angles) into a virtual locomotion velocity vector. The proposed law ensures that humanly feasible velocities are achieved during virtual locomotion. Particularly, the tangential velocity is bounded and depends on the desired angular velocity. These two components are detailed below.

5.3.1.1 Device mechanical design

The proposed mechanical design of the interface is proposed in Figure 5.1.

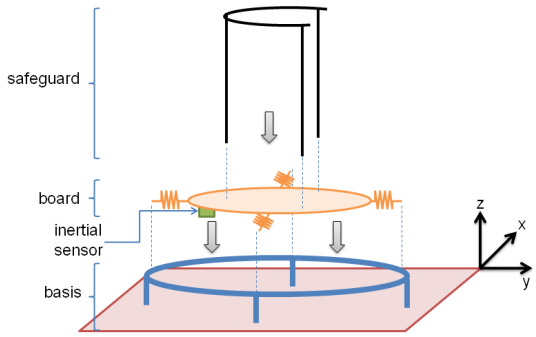

Fig. 5.1: Schematic representation of the main elements forming our peripheral device. The board and the basis are articulated using springs. Springs generate repealing forces that tend to maintain the board in the horizontal plane, however, the board can be freely oriented around the two horizontal axis (pitch and roll) with limited range. Users act on the device by standing on it, and apply forces in order to tilt the board by leaning. The board inclination is measured using an inertial sensor. The safeguard prevents users from falling when leaning.

The key principle of the JoyMan is to let the user indicate the desired direction of his virtual locomotion by leaning in the corresponding direction. In other words, our objective is to let a user control his locomotion from his equilibrioception. This main functionality stressed at first the mechanical design of the JoyMan device.

The main properties of our design are :

- the user should be able to stand on the platform, which is the natural position in the task of locomotion;
- the user should feel perfectly safe when using the platform which, as a result, should prevent him from falling;
- the user should be able to lean over the limit of his own balance in order to increase the amplitude of vestibular sensations;
- the device should tend to bring the user back in vertical position to avoid highly tiring manœuvers during its use.

We also carefully considered other criteria during the device design process: the most important was to build an affordable interface. Exploring the equilibrioception in place of proprioception to control oneself locomotion in the virtual world is a promising direction to lower these costs. However, we did not want to lower the costs by degrading the feeling of immersion provided by the interface. We aim at building a new interface that does not involve any active mechanical device in its movement and does not imply the use of sophisticated and complex tracking devices. We meet the objectives listed above based on a simple mechanical device as illustrated in Figure 5.1.

The device is made of 4 components:

The basis supports the whole device. It is made of a flat square platform lying on the ground and of a circle shaped steel frame linked to the board by legs. The legs and the platform are fixed together and the board is large enough to prevent the device from tipping over.

The board is the element supporting users. It is circle shaped and linked to the frame by springs. As a result, the board is free relatively to the frame within limited range of motion. We can approximately but reasonably consider that the board is articulated to the frame by two degrees of freedom which are rotations around the x and y axis as illustrated in Figure 5.1.

The safeguard is rigidly fixed to the board and prevent users from falling.

The inertial sensor is rigidly attached to the board and acquires the current orientation of the board.

The basis is made of a square woodcut platform. The steel frame is the one of a trampoline where the springs have also been retrieved (1 m diameter). The basis is a machined plastic plate (0.55 m diameter) equipped with 18 hooks on its rim. A rigid rope is tied up between the hooks and the springs attach the board to the frame. Finally, the safeguard is made of welded iron tubes. Its height can be adapted to each user (height between 0.8 m and 1.2 m). Building costs did not exceed $ 500 in spite of the fact that this device is a unique prototype excluding the inertial sensor.

Illustrations of the peripheral device in use are provided in Figure 5.2. The user can stand straight on the platform and has to lean in any direction to start the locomotion in the virtual world. The control law that allows to navigate in a VE with the new interface is described in the next paragraph.

5.3.1.2 Virtual locomotion control

The main steps of the virtual locomotion control are summarized in Figure 5.3. The control is composed of two elements detailed in the following paragraph: a locomotion model and a control law.

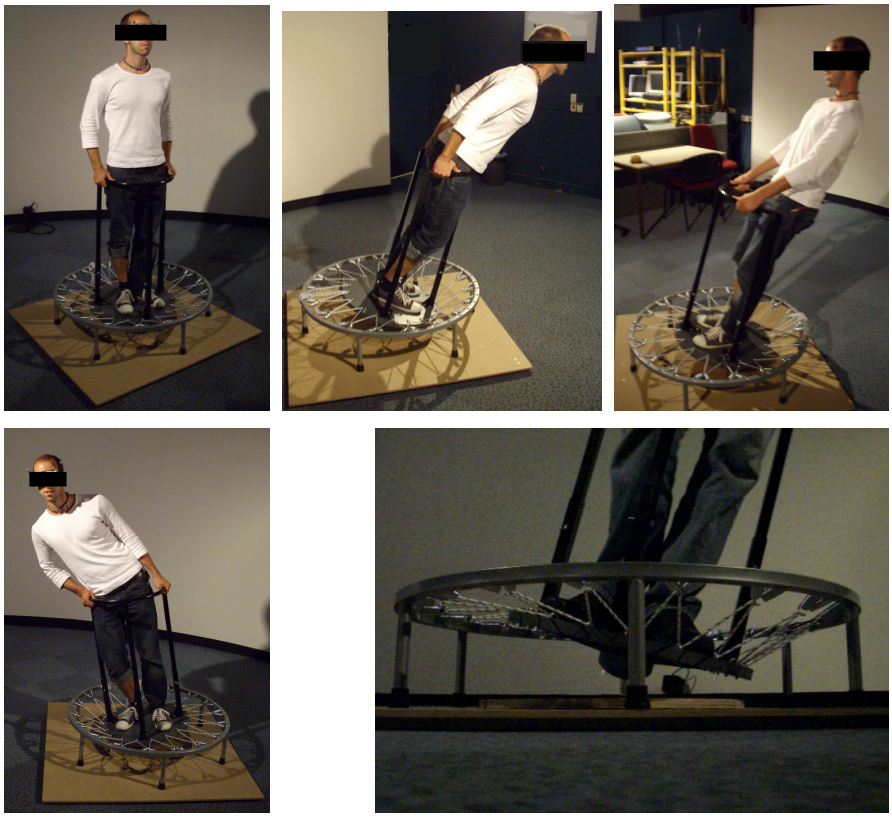

Fig. 5.2: Illustration of the peripheral device in use. Users can stand straight on the board, repealing forces make easy keeping the platform inclination. Users have to lean to start locomotion in virtual worlds. All the possible leaning directions are displayed.

Locomotion model

The locomotion model allows to translate the position and orientation of the platform into a virtual motion in the VE. We exploited experimental observations of the walking human trajectory to build our model [13].

We model the position P of the user in the virtual space as an oriented point moving in a horizontal plane (see Figure 5.3):

$$P = \begin{bmatrix} x \\ y \\ \theta \end{bmatrix}. \tag{5.1}$$

The virtual motion is velocity controlled. We assume the virtual trajectory is nonholonomic, which means that the velocity vector orientation and the body orienta-

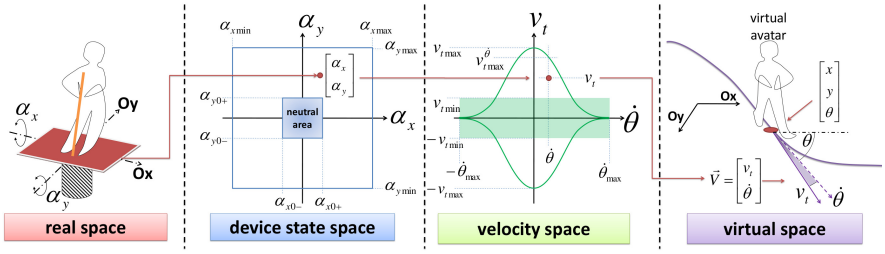

Fig. 5.3: Summary of the different steps for the virtual locomotion control. From the position and orientation of the JoyMan, we can compute the virtual velocity vector by using our locomotion model and control law.

tion are always identical. The non-holonomic nature of walking human trajectory has been experimentally observed in [13].

Non-holonomy constraint allows us to decompose the velocity vector V as follows:

$$V = v_t . \begin{bmatrix} cos(\theta) \\ sin(\theta) \end{bmatrix}. \tag{5.2}$$

Such a decomposition allows us to independently control the tangential speed v_t and the orientation θ. Human tangential velocity is limited. We denote $v_{t_{max}}$ the maximum tangential velocity bound. By default, we set this bound at $v_{t_{max}} = 1.4$ m/s. It has equally been observed that very slow walking velocities are never reached: such velocities are humanly feasible but not used in practice. We thus define $v_{t_{min}} = 0.6$ m/s. It has been however observed that changing orientation θ affects the amplitude of v_t during human locomotion [335]: humans decelerate when turning. In order to take into account such an observation, we define $v^{\dot{\theta}}_{t_{max}}$ the bound of the tangential velocity knowing the current turning velocity $\dot{\theta}$. $v^{\dot{\theta}}_{t_{max}}$ is defined as follows:

$$\begin{aligned} v^{\dot{\theta}}_{t_{max}} &= a.v_{t_{max}}.e^{-b.\frac{\dot{\theta}}{c}} \\ v^{\dot{\theta}}_{t_{min}} &= a.v_{t_{min}}.e^{-b.\frac{\dot{\theta}}{c}} \end{aligned} \tag{5.3}$$

where a, b and c are parameters. As a result, we model the reachable tangential velocity $v^{\dot{\theta}}_{t_{max}}$ as a Gaussian function of the current turning velocity $\dot{\theta}$. The higher $\dot{\theta}$, the lower the tangential velocity bound. By default, we arbitrarily choose: $a = 1.07$, $b = 0.5$ and $c = 0.7$. Such values match the experimental observations provided in [335]. Finally, the absolute value of the angular velocity is also bounded to $\dot{\theta}_{max}$. We arbitrarily choose $\dot{\theta}_{max} = 1$ rad/s.

Control Law

The control law allows users to modify the virtual velocity vector V by standing on the device and leaning. The modification of the platform orientation affects the state of the device s_d. s_d is defined by the orientation of the board α_x and α_y relatively to the two horizontal axis **Ox** and **Oy**, as measured by the inertial sensor:

$$s_d = \begin{bmatrix} \alpha_x \\ \alpha_y \end{bmatrix}. \tag{5.4}$$

We neglect the orientation around the **Oz** axis. During calibration stage, we ask the user to stand on the platform and to successively firmly lean towards all the cardinal directions. We estimate the reachable bounds of the board orientation by averaging the reached orientation over a short period of time, $\alpha_{x_{min}}$, $\alpha_{x_{max}}$, $\alpha_{y_{min}}$ and $\alpha_{y_{max}}$. We also ask the user to stand straight on the platform and define a neutral area bounded by $\alpha_{x_{0+}}$, $\alpha_{x_{0-}}$, $\alpha_{y_{0+}}$ and $\alpha_{y_{0-}}$.

We want the user to control his tangential velocity v_t by leaning in forward or backward direction, i.e., by playing on α_x, whilst angular velocity $\dot{\theta}$ is controlled by leaning on the sides, i.e., by playing on the α_y value. The angular velocity is controlled as follows:

$$\begin{cases} \dot{\theta} = \dot{\theta}_{max} . \frac{\alpha_{y_{max}} - \alpha_y}{\alpha_{y_{max}} - \alpha_{y_{0+}}} & \text{if } \alpha_y > \alpha_{y_{0+}} \\ \dot{\theta} = \dot{\theta}_{max} . \frac{\alpha_y - \alpha_{y_{min}}}{\alpha_{y_{0-}} - \alpha_{y_{min}}} & \text{if } \alpha_y < \alpha_{y_{0-}} \\ \dot{\theta} = 0 & \text{otherwise} \end{cases} \tag{5.5}$$

which allows to deduce $v_{t_{max}}^{\dot{\theta}}$ and $v_{t_{min}}^{\dot{\theta}}$ according to equation (5.3) and finally v_t:

$$\begin{cases} v_t = v_{t_{min}}^{\dot{\theta}} + (v_{t_{max}}^{\dot{\theta}} - v_{t_{min}}^{\dot{\theta}}) . \frac{\alpha_{x_{max}} - \alpha_x}{\alpha_{x_{max}} - \alpha_{x_{0+}}} & \text{if } \alpha_x > \alpha_{x_{0+}} \\ v_t = -v_{t_{min}}^{\dot{\theta}} + (v_{t_{max}}^{\dot{\theta}} - v_{t_{min}}^{\dot{\theta}}) . \frac{\alpha_x - \alpha_{x_{min}}}{\alpha_{x_{0-}} - \alpha_{x_{min}}} & \text{if } \alpha_x < \alpha_{x_{0-}} \\ v_t = 0 & \text{otherwise} \end{cases} . \tag{5.6}$$

At each time step n, the virtual velocity vector $V_n = [v_{t_n}, \dot{\theta}_n]$ is thus deduced from s_d, the state of the device. Before updating the simulation accordingly, we check that no unbelievable acceleration is performed. Thus, given the previous velocity vector V_{n-1}, we finally compute the effective velocity vector V_f:

$$V_f = V_{n-1} + \lfloor \frac{V_n - V_{n-1}}{\Delta t} \rceil \tag{5.7}$$

where Δt the simulation time step, and $\lfloor \rceil$ a function that truncates the velocity vector variation so that the absolute tangential acceleration does not exceed 1 m/s^{-2} and the angular one does not exceed 1 rad/s^{-2}.

5.3.1.3 JoyMan interface

The JoyMan interface is designed for immersive virtual locomotion into virtual worlds. Our main aim was to explore the possibility of an interface that tends to preserve the equilibrioception in place of proprioception, in contrary to many current interfaces. The mechanical design of our platform is relatively simple. We showed how the proposed device allows a user to safely perform exaggerated leaning motion, over the limit of balance, in order to indicate his virtual navigation wills. We here remind our long-term objective to be able to perform realistic locomotion trajectories into the virtual world. What can we expect from the JoyMan interface?

Immersion

The device does not limit technical choices about visual or audio feedback. Typically, the device can be directly used in any immersive environment. More important, the initiation of the locomotion is made by leaning ahead. This corresponds to the real motion to initiate walking, which is considered to be a constant loose of balance and succession of falling ahead. We expect this interaction mode, where vestibular sensory system stimulation is preserved, to be greatly immersive.

Realism

We expect that the dynamics of the required manœuvers to operate the JoyMan are close to the ones of real walking motions. As an example, using the JoyMan, users perform a left turn following a right turn by changing the platform orientation toward its opposite using their whole body. Involved inertias and frictions prevent from performing this change of state immediately: this reproduces the walking behavior during which the inclination of the body is naturally adapted to face centrifuge force. We clearly do not expect users to achieve efficient navigation (in terms of task completion time) using the JoyMan.

5.3.2 Preliminary evaluation

As a preliminary evaluation, we propose to compare our interface to the joystick, a classical peripheral often used in VR applications. The joystick can be considered as one of the most performing interface to achieve efficient navigation in terms of task completion time. Thus, the first objective of our evaluation was to quantify the loss of performances of our interface compared to the joystick (our interface involves namely the whole body compared to the joystick where only hands and arms are used). The experiments were conducted using 3D VE displayed either on a screen or on a Head-Mounted Display (HMD). We investigated the effectiveness of our

interface to travel complex paths composed of different gates placed in the VE. The second objective of our evaluation was to verify if we can obtain a more immersive navigation with our interface compared to classical peripherals already used in VE, i.e. the joystick. Thus, a subjective questionnaire was proposed to the participants to evaluate their subjective preferences in terms of quality of the VE navigation.

5.3.2.1 Performances: Task completion time and accuracy

For each participant, the task completion time of each trial was measured for the different experimental conditions. A repeated two-way ANOVA was performed on the two different interfaces and the two visual conditions. The ANOVA accounting for the visual conditions and the task completion time revealed a significant effect ($F(1,526) = 11.63$, p-value< 0.001). A significant effect was also found for the interfaces and the task completion time ($F(1,526) = 54.47$, p-value< 0.001). As expected, the results reveal that the joystick was better than the JoyMan in terms of speed of the navigation. The mean value for the completion time of a path was 187 s (standard deviation=13 s) for the joystick and 321 s (standard deviation=89 s) for the JoyMan.

A specific analysis was developed to study the learning effect of the two configurations (JoyMan and Joystick). A linear model where all conditions are mixed was fitted to explain the relation between the task completion times and the trial number. For the JoyMan configuration, it revealed that the slope of the linear regression was significantly lower than zero (p-value < 0.000001), reflecting a significant decrease in the task completion time as the number of trials increases. The same analysis, where the first trial was removed, showed that the slope was not significantly different from zero anymore (for both visual conditions). Figure 5.4 illustrates the task completion time of the different trials for the JoyMan configuration.

For each participant and for each trial, the percentage of errors for the different paths was measured. There was no error at the end, for both configurations (JoyMan and Joystick) and both visual conditions.

5.3.2.2 Subjective questionnaire

A preference questionnaire was proposed in which participants had to grade from 1 (low appreciation) to 7 (high appreciation) the two configurations (JoyMan and Joystick) according to 8 subjective criteria : Fun, Intuitive, Accuracy, Presence, Rotation realism, Fatigue, Cybersickness and Global appreciation. The grade 7 for Fatigue and Cybersickness respectively means that the interface does not induce any fatigue and does not imply any cybersickness feeling.

After performing an ANOVA on the two different conditions, we found a significant effect for 6 criteria: Fun ($F(1,30) = 17.77$, $p < 0.001$), Intuitive ($F(1,30) = 21.25$, p-value< 0.001), Accuracy ($F(1,30) = 23.52$, p-value< 0.001), Presence ($F(1,30) = 13.35$, p-value< 0.001), Rotation realism ($F(1,30) = 6.63$, p-value=

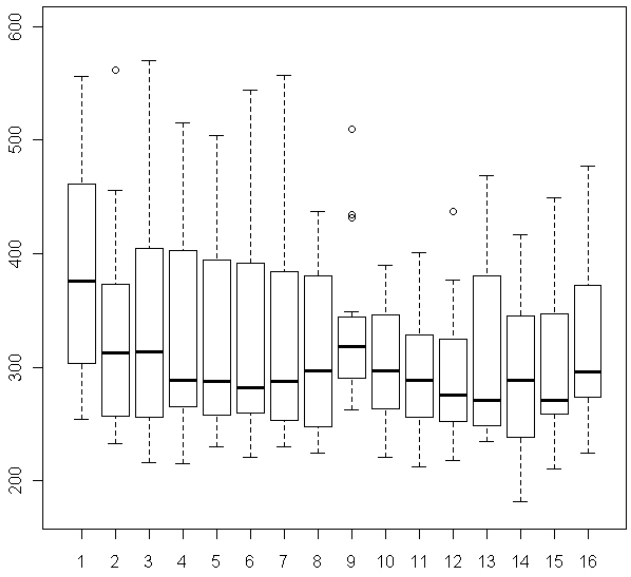

Fig. 5.4: Task completion time (in seconds) for the JoyMan configuration (16 trials). The first trial was left to illustrate the learning effect. Each box plot is delimited by the quartile (25% quantile and 75% quantile) of the distribution of the condition over the individuals. The median is also represented for each trial.

0.015) and Fatigue ($F(1,30) = 87.51$, p-value< 0.001). In particular, our new platform was better ranked for Fun, Presence and Rotation realism. No significant effect was found for Cybersickness ($F(1,30) = 4.01$, p-value=0.054) and Global appreciation ($F(1,30) = 0.69$, p-value$= 0.411$).

5.3.3 Discussion and perspectives

As a global conclusion of the preliminary evaluation of the JoyMan, we can state that the feeling of immersion in the virtual world is significantly improved - in comparison with traditional joystick-based techniques - at the cost of some easiness of use. The JoyMan is still at a early stage of development, however, first results are promising and open a large set of possible directions to improve usability and the level of realism of virtual navigation. This section discuss as exhaustively as possi-

ble these directions as well as future work to meet our objectives: an easy, intuitive, immersive interface allowing realistic locomotion in virtual worlds.

5.3.3.1 Interface calibration

The navigation with the JoyMan implies the whole body and, as expected, the task completion times were higher for our interface compared to the joystick where only the arms and hands are involved. The use of the whole body, implying more movements, is also a reason for the lower rating for the Accuracy criterion in the subjective questionnaire. However, the results concerning the evaluation of our interface in terms of performances are encouraging as the participants always succeeded to complete the navigation task during the evaluation. One way of improvement for the performances of our interface could be the interface calibration. The control law directly transforms the angle of the interface platform into virtual walking velocities. 3 types of parameters were proposed to design our control law: those define the active angles area into the device state space ($\alpha_{x_{min}}$, $\alpha_{x_{max}}$, $\alpha_{y_{min}}$ and $\alpha_{y_{max}}$, $\alpha_{x_{0+}}$, $\alpha_{x_{0-}}$, $\alpha_{y_{0+}}$ and $\alpha_{y_{0-}}$), those controlling the reachable virtual velocities ($\dot{\theta}_{max}$, $v_{t_{min}}$ and $v_{t_{max}}$) and finally those controlling the dynamics of the relation between tangential and angular velocities (a, b, and c, see Equation 5.3). Ideally, the first type of parameters should be calibrated for each user. Indeed, given his size, weight and strength, each user provides relatively different efforts to reach a same given platform inclination angle (i.e., a given walking velocity). The slight fatigue reported by participants in the results of our experiments confirms the need for individual calibration. Currently, calibration process consists in recording leaning motions as well as neutral positions to define the bounds of the effective zone for the platform. We made such a calibration before experiments, but kept a unique one all along our evaluation in order to have the same behavior of our interface for all participants. For VR applications, we could envisage to explore various calibration techniques as well, such as by displaying a virtual environment with a moving point-of-view and to ask users to apply the effort on the platform they believe to be corresponding to the motion.

5.3.3.2 Mechanical design

The results of the subjective questionnaire suggest that the participants enjoyed the navigation with the JoyMan. They namely gave a higher rating for the Fun criterion but also for Presence criterion and Rotation Realism criterion. Specifically, the higher rate given to this last criterion confirms that our mechanical design was appreciated for locomotion tasks in the virtual environment. A way of improvement for our mechanical design could concern the linkage between the platform and the basis. The proposed prototype implements this linkage using an inextensible rope and a set of springs (see Figure 5.2) as we wanted to have a simple mechanical design. However, we could envisage to modify the linkage to increase the possibility

of movements of our interface. Ideally (mechanically speaking), the linkage could be a 2 rotational degrees of freedom, one with a restoring force proportional to the platform inclination.

5.3.3.3 Control law

Experimental evaluation reveals that the proposed control law is intuitively grasped by users: establishing a relation between linear and angular velocities seems to be naturally accepted by users, and is consistent with observations of human locomotion trajectories. Future work will deal with potential modifications of the control law, for example by using a law that can lower vestibular and visual sensory conflicts.

The device state vector is currently two dimensional: the two angles that describe the platform inclination. With some experience, it appears that the device can be fully and accurately controlled by involving the lower body only, it is not even required to hang on to the barrier (except for moving backward in the current state of the device). Such a property opens interesting perspectives and makes possible to increase the dimension of the device state space. Possible extensions are numerous, and immediately within reach if the VR system is equipped with tracking abilities: hands remain free to achieve secondary actions in the virtual worlds (grasping, touching, pointing tasks, etc.), view direction and locomotion control can be decomposed, etc. Nevertheless, we observed during experiments that most of the participants intuitively attempts to control their locomotion also by moving their upper body, in spite of the inefficiency of such motions to significantly increase the inclination of the platform. We however could use this input (i.e., the orientation of the spine relatively to the hips) to control navigation based on an holonomic locomotion model: as opposed to the non-holonomic one, lateral velocities are allowed in addition to tangential and angular ones by removing the constraint imposed by (5.2)—lateral velocities here correspond to side-steps.

5.3.3.4 Immersion and sensory feedback

Evaluation showed that the JoyMan provides a satisfying level of immersion into the virtual world. In addition, the Presence criterion was better ranked for our interface, compared to the joystick. As future work, we could envisage to improve the level of immersion by adding other interaction techniques. Thus, the visual perception of motion could be improved by adding camera motions like in [295] for example. Thus, having oscillating view point could reinforce the accuracy of the perception of the traveled distance by reproducing the natural oscillations of the head during human locomotion. This could also lower the feeling that locomotion is too slow as reported by participants in the subjective questionnaire.

5.3.4 Conclusion

In this section, we presented a novel interface to control locomotion into a virtual world while remaining globally static in the real space. The JoyMan interface is composed of a new peripheral device and a dedicated control law which transforms the device state into a virtual locomotion velocity vector. Our main contributions are (1) to explore the users ability to exploit equilibrioception to control their virtual locomotion and (2) to maintain a high level of immersion compared to hand-held devices (e.g., joysticks).

After a preliminary evaluation, we obtained promising results as the users enjoyed the navigation with our new interface. Presence and realism in the virtual rotations were also underlined. The evaluation also opened several future work directions to improve and extend our interface. Various VR but also real applications could be envisaged, when navigating in a 3D world. Our interface could be used for example for videogames, rehabilitation, training tasks or virtual visits.

5.4 Shake-Your-Head: Walking-in-place using head movements

The Shake-Your-Head technique is a new implementation of the Walking-In-Place (WIP) paradigm designed to be compatible with desktop VR applications. Moreover, this technique can be implemented using low cost devices, contrarily to the classical WIP techniques.

5.4.1 Shake-Your-Head: Revisiting WIP for desktop VR

We propose to revisit the whole pipeline of the Walking-In-Place technique to match a larger set of configurations and apply it to the context of desktop Virtual Reality. Our approach is illustrated in Figure 5.5. The Figure highlights the main differences between our approach and the classical and existing WIP techniques.

With the Shake-Your-Head technique, the user can be standing or sitting (such as in traditional video games or desktop VR configurations). The user interacts with the system by means of head movements. These head movements can be captured using different tracking interfaces, but we insist on the use of low-cost optical tracking with standard webcams. The locomotion simulation proposes not only the computation of a virtual walking motion but also turning, jumping, and crawling possibilities. As a result, the user can perceive the locomotion in the virtual world by means of integrated virtual camera motions on the three axes of motion, to further enhance the sensation of walking.

In the following section we will describe the different parts of our approach, namely: (1) the 3D user interface input/output, (2) the interaction techniques de-

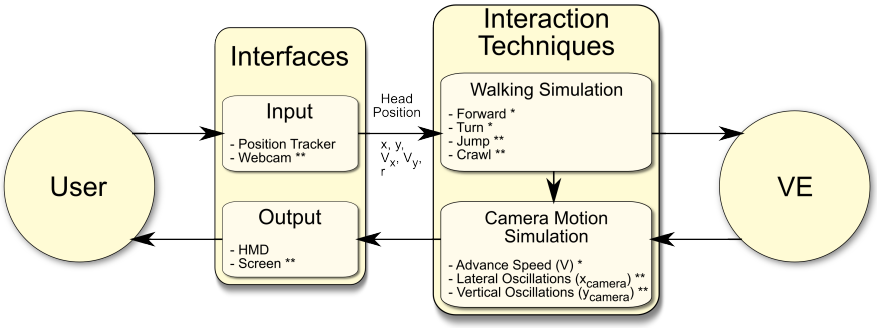

Fig. 5.5: Overview the proposed approach for Walking-In-Place (one star stresses improvement of existing component, two stars stress additional components).

veloped for the computation of the virtual locomotion, and (3) the visual feedback relying on camera motions.

5.4.1.1 Input/Output interfaces

Our method proposes new features in terms of interfaces in order to extend the set of configurations where WIP can be applied, especially for Desktop VR. Thus, we propose to incorporate new devices for both input and output user interfaces in the VE.

Input: Tracking based on head motions

The input interface of our method is only based on head motions. In our implementation, the input interface is reduced to a webcam, allowing the use of our method for Desktop configuration without any additional peripheral. However, our method can also be implemented with other classical VR tracking systems.

Use of head movements

The main concept of our method is to exploit the head oscillations as a transposition of the one observed during natural walking. While walking, the head of the user oscillates along the lateral, vertical and forward axes [165]. The oscillations are strongly correlated to gait events and foot steps. Moreover, these oscillations also occur while walking in place and can be measured.

The head motions are classically retrieved in the existing WIP techniques thanks to the use of regular position trackers [274]. More generally, any tracking device can be used, as long as its accuracy is within the range of 1 cm. Moreover, the acquisition process of the required position does not have any influence, as long

as the real time constraint is maintained. In our method, we propose the use of a video camera system to handle the tracking of the user head. Thus, our interaction technique can be deployed on a large scale at low cost for training purpose or video games for example.

Extracted data

In our method, we propose to use 3 Degrees of Freedom (DOF) that can be easily accessed in the image frame provided by the webcam:

- the lateral position x (and the computed speed V_x);
- the vertical position y (and the computed speed V_y);
- the rotation of the head in the frontal plan r.

These three head motions are illustrated in Figure 5.6.

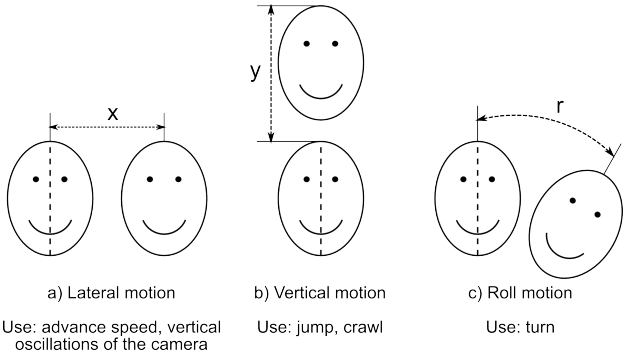

Fig. 5.6: Extracted head motions: (a) lateral motion, (b) vertical motion, (c) roll motion.

Implementation

The use of the webcam to track the 3D position of the user head without using markers requires the implementation of real time constraints for the algorithms, i.e. more than 25 frames per seconds. Our implementation is based on the Camshift (Continuously Adaptive Mean Shift) algorithm [44] implemented in the OpenCV library. This algorithm is based on color tracking and is well-suited for real-time tracking of features of a given color, such as the face of the user.

While the user is standing in front of the webcam, our algorithm recognizes him as an ellipsoid. The position of the head (x,y) can be deduced from the center of the ellipse and the orientation angle of the head r is given by the angle with the vertical of the ellipse. However, x and y depend on the resolution of the used webcam. Thus, we compute a normalized position (x_n,y_n) on [-1; 1] on both axes. From the normalized positions of the head (x_n,y_n), we compute the instantaneous speeds V_x

and V_y, and we use Kalman filters on all values to reduce the noise produced by the algorithm.

Output: Immersive and desktop visual displays

Our method can be used with both immersive and regular screens as output interface with the VE. A requirement of desktop VR applications was to propose a technique that is usable with a limited Field of view (FOV). In regular WIP techniques, the provided FOV is always 360°, except in [255] where they used the redirected walking technique to simulate a 360° FOV in a 4-walls CAVE. In this paper, our technique is evaluated with both LCD laptop screens to fulfill the Desktop VR pre-requisite or video projected output. Our method can also be used with the classical output used with WIP, i.e. with HMDs or CAVEs.

5.4.1.2 Walking simulation

Walking states

The main goal of our interaction technique is to translate the inputs of the user, i.e. head motions, into virtual motions in the VE. The user should be able to perform various motions while navigating in the VE. We implemented different locomotion states: walking, turning, jumping and crawling. To manage these different states, we added a state automaton to our algorithm. The state transitions are governed by the user head motions and the main inputs are the lateral velocity V_x and the vertical velocity V_y.

Forward state

The forward movements in the VE are governed by the lateral oscillations as main input. Our technique is designed to emphasize the idea of walking with a varying speed depending on the user head motions. The speed V_a oscillates regularly, accordingly to the lateral head motions. One head oscillation period corresponds to one step. The footstep events are simulated by a null advance speed and correspond to a modification of the lateral velocity sign of the user's head. Thus, when the user's head reaches the maximal amplitude of the oscillations, the oscillating speed is null, as well as the advance speed simulating a foot step.

For more realistic movements, we introduced two thresholds T_{min} and T_{max}. The former threshold allows to stop the forward movements when the lateral head motions are too small. The latter allows to avoid unrealistic high speed walks. The advance velocity V_a is computed in two steps in order to test these thresholds. The equations of V_a are:

$$V_{n_1} = \frac{min(abs(V_x), T_{max})}{T_{max}}$$

$$V_{n_2} = \begin{cases} 0 & \text{if } V_{n_1} < T_{min} \\ V_{n_1} & \text{otherwise} \end{cases} . \tag{5.8}$$

$$V_a = V_{n_2} * V_{max}$$

Finally, the advance speed V of the camera inside the VE is adapted depending on the current locomotion state and is given by:

$$V = \begin{cases} V_a & \text{if state = walk} \\ 0.4 * V_a & \text{if state = crawl} \\ V_{max} & \text{if state = jump} \end{cases} . \tag{5.9}$$

We chose normalized thresholds with the following values: $T_{min} = 0.05$ and $T_{max} = 0.5$. We also set V_{max} to 3.5 m/s, corresponding to the maximal speed that can be achieved.

Jump and crawl states

Comparing to existing WIP techniques, we chose to add 2 new states to the navigation possibilities in the VE: Jump and Crawl motions. The jump and crawl states are governed by the vertical oscillations of the user's head. If the vertical velocity exceeds normalized thresholds T_{jump} in upward direction and T_{crawl} in downward direction, the user can jump and crawl respectively in the VE. In practice, it means that the user will need to slightly jump or bend forward if he is seated, or jump or crouch down if he is standing. The user has to stand-up to stop crawling.

When a jump is detected, the vertical position of the camera is set to follow a classical parabolic trajectory defined by:

$$y_{camera} = \frac{1}{2} * g * t^2 + V * t \tag{5.10}$$

with g the gravity acceleration and t the time. The jumping state is left automatically while landing, i.e. when the camera reaches again its normal height H (known as the reference state when the algorithm starts). After preliminary testings, we set $T_{jump} = 0.3$ and $T_{crawl} = 0.4$. While the crawling state is activated, the vertical position of the virtual camera y_{camera} is lowered by 1 m.

Turn state

In parallel to Forward, Jump and Crawl states, the user has the possibility to turn inside the VE in order to modify his navigation direction. During a turn in a normal walk, the human body leans slightly in direction of the center of the turn to compensate the centrifugal force [68]. This phenomenon is often reproduced by video

games players which can tend to lean in the direction of the turn even if it does not have any influence on their in-game trajectory. Thus, we choose to use this property to implement turns in our system as a control law based on the head orientation on the roll axis. To turn in the VE, the user has to lean his head in the left or right side respectively to turn left or right in the VE. The rotation speed V_r of the virtual camera is given by:

$$V_r = \begin{cases} V_{r_{max}} & \text{if } r > r_{max} \\ -V_{r_{max}} & \text{if } r < -r_{max} \\ 0 & \text{otherwise} \end{cases} \tag{5.11}$$

where r_{max} is the minimum angle of head inclination to start the rotation and $V_{r_{max}}$ is the maximal angular speed of the rotations. In our experiment, we set $r_{max} = 15^\circ$ and $V_{r_{max}} = 45^\circ/\text{s}$.

5.4.1.3 Visual feedback based on camera motions

To further emphasize the perception of walking in the VE, we extended the visual rendering of the WIP using camera motions driven by the user's head oscillations. There are existing models in the literature that make the virtual camera oscillating along the three axes [165]. However, the oscillations are totally independent from the user interactions.

We introduce a new model of camera motions adapted to the user's head motions. The camera oscillations along the different axes must follow the user in real time to maintain the coherency of the system. Thus, we have implemented a novel visual feedback with camera motions along the vertical, lateral and advance axes.

Advance oscillations

The advance speed V of the view point already oscillates. The camera motions are indeed intrinsically linked to the advance velocity of the control law presented in 5.4.1.2. As a result, extra camera motion is not necessary along this axis and the advance camera velocity corresponds exactly to V.

Lateral oscillations

In order to move in the VE, the user has to make his head oscillating from left to right. Thus, as the user moves in front of the screen, his view point of the scene is modified to follow the head oscillations.

The lateral oscillations of the camera are computed as a function of the user's position. If d is the distance of the user to the screen and α and β the opening angles of the webcam, the real world position of the user in front of the screen depends on the normalized coordinates x_n and y_n. The real world position of the user's head is given by the following coordinates:

$$\begin{cases} x_{real} = x_n * d * \tan(\alpha/2) \\ y_{real} = y_n * d * \tan(\beta/2) \end{cases}. \tag{5.12}$$

Finally, the virtual camera is moved along the lateral axis by a distance x_{camera} equals to: $x_{camera} = A_x * x_{real}$. We set the scale factor A_x to 1 to match the user's head displacement and thus generate the illusion that the screen is a window through which the user can observe directly the VE. However, other values can be used to amplify the camera motions for example. The webcam parameters used during the experiment were set to $\alpha = 60°$ and $\beta = 45°$.

Vertical oscillations

The vertical oscillations of the camera can not be computed with the same algorithm as for lateral oscillations. In a desktop VR context the user can sit, hence being unable to produce high vertical oscillations.

In our method, we propose to generate pseudo-sinusoidal vertical camera oscillations based on the current phase of the virtual gait cycle. Similarly to the advance speed control law, the vertical amplitude y_{camera} of the camera oscillations is given by:

$$y_{camera} = V_{n_2} * y_{camera}^{max} \tag{5.13}$$

where y_{camera}^{max} is the amplitude of the vertical oscillations for velocities greater or equal to the T_{max} threshold. For smaller speeds, the amplitude of the oscillations is proportional to this maximum, thus increasing the perception of the variations in advance speeds. Using the same factor between the camera motions and the advance velocity forces the synchronization, resulting in a smooth final visual rendering. In our implementation, we set $y_{camera}^{max} = 15$ cm.

5.4.1.4 Discussion

To summarize, our approach is composed of (1) an input interface based solely on the user's head movements, (2) a locomotion simulation in the VE composed of various possibilities such as jumping, crawling, turning, and (3) a visual feedback of walking relying on oscillating camera motions. The head motions are tracked along 3 DOF: lateral, vertical and roll axis (Figure 5.6). These different physical motions are transposed in virtual movements thanks to a locomotion automaton. We then added oscillating camera motions (Equations 5.9, 5.12 and 5.13) to the visual feedback to enhance the walking sensation. The different control laws were parameterized after preliminary testings. But of course some parameters can be modified in order to amplify/decrease some effects during the locomotion simulation. Besides, other movement possibilities could also be envisaged and added to our automaton such as running state or backward movement.

5.4.2 Evaluation

The evaluation of the proposed technique was performed using a comparison with classical techniques in Desktop VR. We chose keyboard and joystick peripherals for sitting and standing users respectively as they are often used in Desktop VR context. The experiments were conducted using 3D VE displayed on a screen and we investigated the effectiveness of our technique to travel complex paths composed of different gates placed in the VE.

In this paper, we choose to not compare our technique to existing WIP techniques, and instead used more common interfaces that followed our low cost requirement. We conducted the evaluation of the proposed technique in both immersive Standing Up (SU) position and Desktop Sitting Down (SD) position. The keyboard and joystick were chosen respectively as the control conditions in the SD position and the SU position. Both keyboard and joystick peripherals are referred as Control techniques (Ctrl) in the following paragraphs. Our technique is referred with the "WIP" suffix.

5.4.2.1 Task completion time

For each participant, the task completion time of each trial was measured for the different experimental conditions. An exploratory analysis was first performed. A Principle Component Analysis revealed the presence of one spurious individual who was taken out from the analysis. A specific analysis was developed to study the learning effect of the two conditions (Joystick/Keyboard and WIP techniques). A linear model where all conditions are mixed was fitted to explain the relation between the task completion times and the trial number. It revealed that the slope of the linear regression was significantly lower than zero (p-value < 0.000001), reflecting a significant decrease in the task completion time as the number of trials increases. The same analysis, where the first trial was removed, showed that the slope was not significantly different from zero anymore. In the following paragraph, the first trial was removed from the analysis as it corresponds to a learning effect.

A two-way ANOVA was performed on the 2 different conditions (Joystick/Keyboard and WIP techniques) and the 2 different positions (Sit-Down and Stand-Up). A post-hoc analysis using Tukey's procedure was then performed. The ANOVA was achieved separately for the two different types of paths (normal/steeple).

Concerning the normal path, the two-way ANOVA accounting for the conditions and the positions revealed a significant dependency between the position and the task completion time ($F(1,11) = 31.9981$, $p < 0.0001$) and between the condition and the task completion time ($F(1,11) = 6.0449$, $p = 0.0143$). Interaction between condition and position was also considered as a significant factor to discriminate task completion time ($F(1,11) = 27.1921$, $p < 0.0001$). Post-hoc analysis showed that the task completion time in the SD-WIP configuration ($M = 55.67$ s) was significantly lower than in the SD-Ctrl configuration ($M = 61.72$ s), adjusted p-value < 0.0001, in the SU-Ctrl configuration ($M = 62.06$ s), adjusted p-value < 0.0001,

and in the SU-WIP configuration ($M = 64.23$ s), adjusted p-value < 0.0001. The other pairs of effects did not give any significant adjusted p-values.

The results concerning the different conditions are represented in Figure 5.7 for Sit-Down and Stand-Up experiments respectively, for the normal path only. The results are ordered in function of the trials. The first trial was kept to illustrate the learning effect.

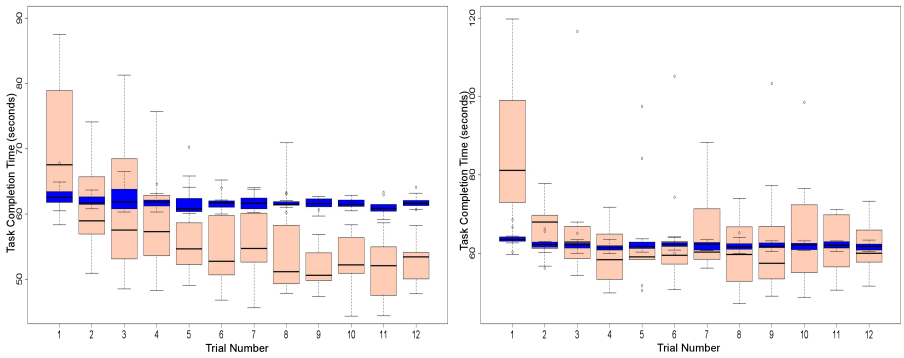

(a) Sit-Down Experiment (b) Stand-Up Experiment

Fig. 5.7: Task completion time for the two different techniques on normal paths for (a) SD experiments and (b) SU experiments. The blue and red light colors correspond to the Ctrl and WIP conditions respectively. Each box plot is delimited by the quartile (25% quantile and 75% quantile) of the distribution of the condition over the individuals. The median is also represented for each condition.

For the steeple path, the pre-analysis suggested the presence of a spurious individual and the existence of one learning trial. The two-way ANOVA accounting for the conditions and positions revealed a significant dependency between the position and the task completion time ($F(1,11) = 8.5665$, $p < 0.005$), and the condition and the task completion time ($F(1,11) = 11.8925$, $p < 0.001$. Interaction between condition and position was also considered as a significant factor to discriminate task completion time ($F(1,11) = 8.7647$, $p < 0.005$). Post-hoc analysis showed than the task completion time in the SU-WIP configuration ($M = 86.07$ s) was significantly higher than in the SD-Ctrl configuration ($M = 74.78$ s), adjusted p-value < 0.0001, in the SU-Ctrl configuration ($M = 74.72$ s), adjusted p-values < 0.0001 and in the SD-WIP configuration ($M = 75.64$ s), adjusted p-values < 0.0001. The other pairs of effects did not give any significant adjusted p-values.

5.4.2.2 Accuracy

For each participant and for each trial, the percentage of errors for the different paths was measured. The two types of path (Normal and Steeple) are separated. The result-

ing percentages are for the normal path: 0.61% of error for SD-WIP configuration, 0% of error for SD-Ctrl configuration, 1.39% of error for SU-WIP configuration, 0.09% of error for SU-Ctrl configuration.

The resulting percentages are for the steeple path: 20.49% of error for SD-WIP configuration, 7.81% of error for SD-Ctrl configuration, 27.28% of error for SU-WIP configuration, 13.19% of error for SU-Ctrl configuration. We found a significant effect between Ctrl and WIP techniques for the steeple path.

5.4.2.3 Subjective questionnaire

After Sit-Down and Stand-Up configurations, a preference questionnaire was proposed in which participants had to grade from 1 (low appreciation) to 7 (high appreciation) the four different conditions (SD-Ctrl, SD-WIP, SU-Ctrl, SU-WIP) according to 9 subjective criteria: (a) Fun, (b) Easiness of Use, (c) Intuitive, (d) Accuracy, (e) Presence, (f) Walking realism, (g) Fatigue, (h) Cybersickness and (i) Global appreciation. Figure 5.8 shows the results concerning the grades (Likert-scale) obtained by the two different techniques for each of the subjective criteria, for the two experimental conditions (SD and SU). The grade 7 for Fatigue and Cybersickness respectively means that the technique does not induce any fatigue and does not imply any cybersickness feeling.

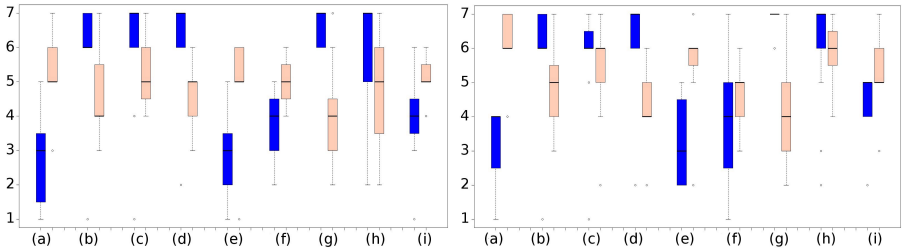

(a) Sit-Down Experiment (b) Stand-Up Experiment

Fig. 5.8: Results for subjective rating for the two different techniques for (a) SD experiments and (b) SU experiments. The blue and red light colors correspond to the Ctrl and WIP conditions respectively. The subjective criteria are (a) Fun, (b) Easiness of Use, (c) Intuitive, (d) Accuracy, (e) Presence, (f) Walking realism, (g) Fatigue, (h) Cybersickness and (i) Global appreciation. Each boxplot is delimited by the quartile (25% quantile and 75% quantile) of the distribution of the condition over the individuals. The median is also represented for each condition.

Concerning SD configuration, no significant effect was found for the following criteria: Intuitive ($p = 0.052$) and Cybersickness ($p = 0.12$). Concerning SU configuration, no significant effect was found for the following criteria: Intuitive ($p = 0.3$), Walking realism ($p = 0.19$) and Cybersickness ($p = 0.21$). We found a significant

effect for all other criteria. In particular, our technique was better ranked for Fun, Presence and Global Appreciation, for both configurations.

5.4.3 Discussion

The results suggest that the technique can allow efficient navigation even compared with standard and well-known input devices such as keyboards and gamepads. The participants could sometimes go even faster with WIP, without any strong loss in precision. The WIP-based interaction seems also fast to learn, after only a couple of trials. The technique is well appreciated and perceived as more immersive and more fun than classical configurations.

The quick learning of our technique could be explained by the fact that interfaces based on webcam are generally intuitive and simple to learn [241]. After the learning phase, WIP tends to become faster than the keyboard in sitting condition. One explanation could be that with the technique (but also with the joystick in the standing condition) we could observe that participants tended to turn without stopping their advance motion. On the contrary, with the keyboard condition, participants tended to walk and turn sequentially, which might have globally increased the task completion time. Another explanation could be that, in the implementation of WIP, the advance speed is influenced by the speed of lateral movements. The seated position allows the user to make faster oscillations than the standing position, and thus to accelerate the walking motion by making fast lateral oscillations. Interestingly, these faster motions did not impair the precision of users.

The longer task completion time observed for WIP in the steeple paths (involving jumping and crawling motions) could be due to unexpected behaviors which induced incorrect transitions in our locomotion automaton. Indeed, some participants acted as if they were ”anticipating” the jumps and bent down prior jumping. The problem could easily be fixed in the future by using additional conditions in the automaton based on both speed and position.

Results from the questionnaire are very consistent with previous subjective evaluations of WIP [305]. In the study, the WIP is more appreciated, and is perceived as more fun, and improving presence. As expected, more standard techniques (i.e. joystick and keyboard) are found easier to use, more precise, and less tiring (as they induce less physical movements). Interestingly, impression of cybersickness is not increased by WIP. This could be due to our desktop (and thus less immersive) configurations. Last, realism of walking in the VE was significantly improved only in the sitting condition. The perception of walking with WIP is actually quite complex, as participants wrote: ”we have the impression to be a video game character”, ”the motions are exaggerated, or ”we really have the sensation of walking, and not running”. In the standing condition, some participants found that the physical motions were closer to ”skiing or ”skating, as they noticed that they did not lift their feet from the ground but only oscillated their body. For these people we could further stress in the future that our implementation of WIP still works very well when lift-

ing the feet and walking in place, as the oscillations of the head can be captured the same way in both situations (lifting the feet or not).

Taken together, the results suggest that the Shake-Your-Head technique could be used in a wide range of applications, when navigating in a 3D world, in sitting or standing configurations. It seems to be both a low-cost and an efficient paradigm that can match a lot of walking motions. It could thus be used for training in VR with more physical engagement (military infantry, vocational procedures), or more realistic virtual visits such as for project review in architecture or urban planning.

5.4.4 Conclusion

We presented the Shake-Your-Head, a technique designed to revisit the whole pipeline of the Walking-In-Place technique to match a larger set of configurations and apply it notably to the context of Desktop Virtual Reality. The Shake-Your-Head technique acquires solely the head movements of the user. It can be used in a desktop configuration with the possibility for the user to sit down and to navigate in the VE through small screens and standard input devices such as a basic webcam for tracking. Various motions have been implemented such as turning, jumping and crawling in the locomotion simulation. Additional visual feedback based on camera motions to enhance the walking sensation were also introduced.

An experiment was conducted to evaluate the technique compared to standard techniques such as keyboard and joystick. In this experiment, participants had to walk through a series a gates forming a slalom path. The evaluation was performed both in an immersive and desktop configurations. It was notably found that WIP only requires a small learning time to allow faster navigation in seated position compared to the keyboard. Moreover, the technique was more appreciated and considered as more fun and inducing more presence than traditional techniques.

5.5 Magic-Barrier-Tape: Walking in large virtual environments with a small physical workspace

The Magic Barrier Tape is a novel interaction metaphor that brings a solution to immersive infinite walking in a restricted workspace through a natural and efficient metaphor.

5.5.1 The Magic Barrier Tape

Walking workspaces of virtual reality systems are often bounded by the tracking area, the display devices or by the walls of the immersive room. Hence, the Magic

Barrier Tape has two fundamental objectives. The first one is to inform and display the limits of the workspace in a natural way, without break of immersion, in order to avoid the collision with physical objects outside the workspace boundaries or leaving the tracking area. The second one is to provide an integrated navigation technique to reach any location in the virtual scene, beyond the walking workspace.

To overcome the mismatch between the restricted size workspace and the potentially infinite size of the virtual scene, we followed the concept of hybrid position/rate control [82], used in a different context for object manipulation, where position control is used inside the available workspace for fine positioning, while rate control is used at the boundaries for coarse positioning. This concept can be found in common desktop applications and games where the mouse switches to rate control when it reaches the edge of the screen: in a file manager when doing multiple selection, or in top-view strategy games such as Starcraft when panning on the map. In our context, we applied the concept to navigation, with the available workspace being the walking workspace. The boundaries of the workspace are represented by a virtual barrier at mid body height textured with slanted black and yellow stripes, evoking the use of barrier tape and its implicit message: "do not cross".

The real workspace, delimited by the physical boundaries, is mapped to a virtual workspace inside the scene, delimited by the virtual barrier tape. Inside the workspace, we use position control: the user can freely walk, and objects inside the virtual workspace can be reached and manipulated through real walking and real life movements. When reaching the boundaries of the workspace, we switch to rate control: the user can move farther in the scene by "pushing" on the virtual barrier tape, hence translating the virtual workspace in the scene. He can then perform a task inside the virtual workspace at the new location.

The Magic Barrier Tape concept is not subject to a specific technology. It can be implemented in many different virtual reality systems. Any object or body part can be used as an actuator for the virtual barrier tape, depending on the application, and the rate control law can be fitted to specific behavioral needs. In the remaining of this section, we detail the Magic Barrier Tape concept. We take as implementation example our own virtual reality environment, consisting of a HMD with a 1.5 m radius cylindrical tracking space, and one of the user's hands as actuating object.

5.5.1.1 Display of the workspace limits

The boundaries of the workspace are displayed through 3 complementary visual cues: the main virtual barrier tape, the warning virtual barrier tape, and their grey shadow on the floor.

The main virtual barrier tape is presented as a band that matches the shape of the workspace boundaries, such as a square for a CAVE or a circle for a cylindrical tracking system. It is positioned at a safe distance ahead of them, high enough from the virtual floor so that the user does not need to look down to see the barrier tape, and low enough so that it does not occlude the user's forward vision. The boundaries of the workspace are therefore clearly and continuously visible. The tape is made

slightly translucent so what would have been normally hidden by the tape is still discernible.

The warning virtual barrier tape appears when the user's body is close to the main tape, as a warning signal. This second tape has the same shape and origin than the main one, and has a red glow to capture the user's attention. For the same reason, it is positioned at the user's eyes height. The tape is fully transparent when the user is at a reasonably safe distance from the main tape, and becomes progressively opaque as the user gets closer, therefore making the warning signal also progressive, from dim to strong. The warning virtual barrier tape is complementary to the main tape, since it is triggered as a safety measure, and it gives an idea of when to stop walking and start "pushing".

The tapes shadow is drawn on the floor as if the barrier tapes were lit from above, in order to have a visual cue about the limits of the workspace when the user looks down. Hence, at least one of the 3 visual components is always visible at almost any viewing direction, which is particularly helpful with an HMD setup where there is usually a narrow field of view. Figure 5.9 shows the three components of the Magic Barrier Tape: the main barrier tape, the warning barrier tape (here visible) and the tapes' shadow.

In our virtual reality environment implementation, the main virtual barrier tape is 30 cm high and at 30 cm from the boundaries. It is shaped as a ring with a 1.2 m radius and the center of the tracking area as origin. It is positioned at 1.3 m from the virtual floor. The warning tape is activated when the user is at 30 cm from the main tape.

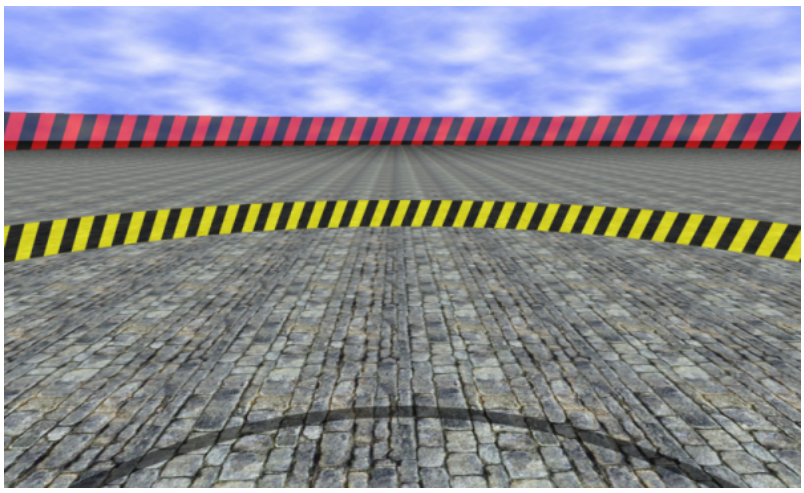

Fig. 5.9: The three Magic Barrier Tape visual cues to show the workspace boundaries: the main virtual barrier tape (middle), the warning tape (top) and the tapes shadow (bottom).

5.5.1.2 Navigation through rate control

The Magic Barrier Tape allows the use of position control inside the workspace, and rate control at the boundaries. The user is switched from position control to rate control whenever his hand (or any other tracked body part) penetrates the boundaries represented by the virtual barrier tape. The speed of the resulting translation in the virtual scene is a function of the hand penetration distance. When the user's hand is pulled back inside the workspace, the user is switched back to position control.

The virtual barrier tapes (main and warning) are deformed when the user's body (preferentially, the hand) penetrates the boundaries. This elastic behavior allows the user to see how deep he is "pushing", and therefore to evaluate how fast he will move in the virtual scene. A visual feedback on the rate control is also important so the user can know where the neutral position is located [82].

The deformation follows the shape of a centered Gaussian curve D, of equation:

$$D(p) = p\frac{1}{\sigma\sqrt{2\pi}}e^{-\frac{x^2}{2\sigma^2}}$$

where p is the penetration length (in meters), and σ the standard deviation, which controls the "width" of the deformation. The virtual barrier tape is rotated so that the center of the Gaussian curve matches the penetration point P, the collision point between the hand and the virtual barrier tape. Therefore, as shown in Figure 5.10, the Gaussian deformation is centered around the penetration point, and its symmetry axis is given by the $\overrightarrow{OP}$ direction, where O is the center of the virtual barrier tape. Since the deformation follows the user's hand, the Gaussian curve has to be shifted to take into account the lateral deviation of the hand position H with respect to the Gaussian axis, as shown in Figure 5.10. The final result gives the impression of having an elastic region around the penetration point than can be deformed in any direction. This deformation direction, $\overrightarrow{PH}$, gives the travel direction of the virtual workspace (Figure 5.10).

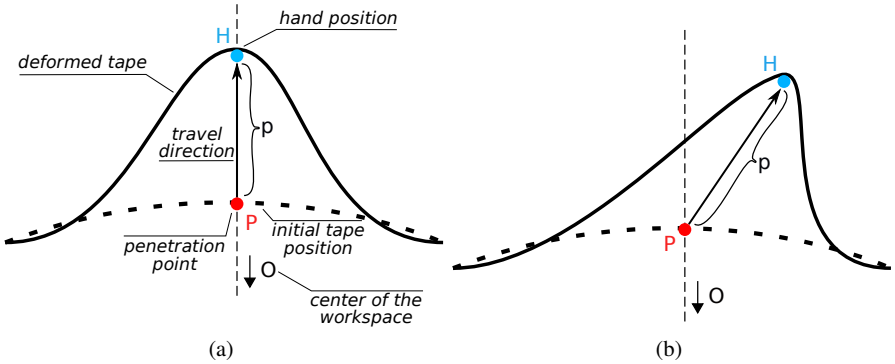

Fig. 5.10: The Gaussian deformation of the Magic Barrier Tape in top-view (a) and its shifted version (b) to follow the hand position.

The velocity V, a function of p, gives the speed of travel. It has the following equation:

$$V(p) = k * p^n$$

where k and n are constants. We use a polynomial function in order to have both slow speed when the user is close to the boundaries for small distances, and high speeds to move fast for distant targets. In our implementation, after preliminary testing, we used $\sigma = 0.15$, $k = 1.4$ and $n = 3$.

Our Magic Barrier Tape implementation provides both a safe walking environment and a natural and efficient navigation technique.

5.5.1.3 Extending resetting techniques for omni-directional walking

In order to conduct the evaluation of the Magic Barrier Tape, we chose similar purpose techniques among existing navigation techniques. Among the surveyed active navigation techniques, based on real walking, only the resetting techniques developed by Williams et al. [328] provide collision free and infinite navigation capabilities. However, the resetting techniques were originally designed for straight paths and right angle turns, where in most virtual reality applications the user is allowed to freely explore his surrounding virtual environment, taking arbitrary paths and freely rotating around him. For fair comparison throughout the evaluation, since our Magic Barrier Tape technique enables such a navigation, we propose to add visual cues to these techniques in order to make them well suited for omni-directional navigation.

Extended Freeze-backup technique

In the original Freeze-backup technique, in order to reset his position the user has to walk backwards in a straight line, until he reaches the resetting position. Since he is not guided while walking backwards, paths can only be straight. Otherwise, he could reach the workspace boundaries prematurely and find himself "locked" in a very short path resetting loop.

In the extended Freeze-backup technique, backups now need to take the user to the center of the real workspace. Before the reset, the user can be at any position in the real workspace, and with any orientation. Hence, we propose to add visual cues to guide the user through his resetting motion, which is divided in two steps. First, the body needs to be oriented towards the resetting position. An horizontal segment is drawn on the screen representing the user's orientation with respect to the resetting position, like his shoulder line seen from above in the real workspace reference frame. The user has to change his orientation until the segment becomes parallel to his body. Then, as a second step, the user has to walk to the resetting position by following an arrow direction. The arrow becomes smaller as the user gets closer to the resetting position, indicating how far he is from his target. Through

this mechanism, the user can reach the center of the real workspace from anywhere in the real workspace.

Extended 2:1-Turn technique

In the original 2:1-Turn technique, a 180° real rotation of the user is mapped to a 360° virtual turn, and the user stays on the same real path but on the opposite direction. Since real turns are always of 180°, walking paths need to be straight with eventually right angle turns to avoid the same "locking" problems mentioned above.

In the extended 2:1-Turn technique, real turns can no longer be of only 180°. The resetting angle is given by the non oriented angle between the viewing direction and the body position - resetting position vector. The virtual angle remains the same, 360°. For any orientation before resetting, two turning directions are possible: to the left and to the right. To each direction corresponds an angle, with usually one greater than the other. The direction with the largest angle is chosen, so that the rotation gain when mapping the turn to a 360° virtual turn is lower, and the illusion is therefore less perceivable. An arrow drawn at the top of the screen indicates the turning direction to the user.

5.5.2 Evaluation

In order to demonstrate its suitability for infinite navigation within a restricted workspace, we evaluated the Magic Barrier Tape by comparing it to two other existing navigation techniques that enable collision free infinite walking within a restricted workspace, namely the Freeze-Backup and the 2:1-Turn resetting techniques [328] with our extensions for omni-directional walking. We conducted two experiments, a pointing task and a path following task.

5.5.2.1 Experiment #1

In Experiment #1, our goal was to compare the 3 techniques over a pointing task where the user had to move from a central initial location to a new location, indicated by a target, as fast as possible. We a priori assumed that the Magic Barrier Tape will be faster, since rate control allows speeds greater than the average walking speed.

For the different comparison analyses, a correction for experiment-wise error was realized by using Bonferroni-adjusted alpha level ($p = 0.05$ divided by the number of tests). Thus, in order to compare the Barrier Tape technique to the two other techniques (Freeze-backup and 2:1-Turn) the alpha level was adjusted to $p = 0.025$.

Completion time

Using the completion time data collected during the experiment, we conducted a statistical analysis. For each participant, statistics (mean M, standard deviation SD) were computed on the 18 trials in each condition. A one-way within subject design ANOVA (Techniques: Barrier tape, Freeze-backup, 2:1-Turn) on the mean completion time (in seconds) revealed a significant main effect of the technique ($F(2,22) = 183.22$, $p < 0.001$). Follow up t tests revealed that completion time in the Barrier Tape technique ($M = 6.37$ s, $SD = 1.30$ s) was significantly shorter than in the Freeze-backup technique ($M = 21.49$ s, $SD = 3.11$ s, $t(11) = -19.15$, $p < 0.001$). Similarly, completion time in the Barrier Tape technique was significantly shorter than in the 2:1-Turn technique ($M = 14.54$ s, $SD = 2.41$ s, $t(11) = -14.61$, $p < 0.001$).

Amplitude of walking in the real world

An ANOVA on the mean amplitude of walking in the real world (in meters) revealed a significant main effect of the technique ($F(2,22) = 434.75$, $p < 0.001$). Follow up t tests revealed that the amplitude of walking in the real world in the Barrier Tape technique ($M = 1.46$ m, $SD = 0.16$ m) was significantly shorter than in the Freeze-backup technique ($M = 4.42$ m, $SD = 0.30$ m, $t(11) = -30.13$, $p < 0.001$). Similarly, the amplitude of walking in the real world in the Barrier Tape technique was significantly shorter than in the 2:1-Turn technique ($M = 3.37$ m, $SD = 0.23$ m, $t(11) = -20.80$, $p < 0.001$).

5.5.2.2 Experiment #2

In the second experiment, our goal was to compare the 3 techniques over a path following task where the user had to follow a path delimited by two virtual walls, as fast as possible and as accurately as possible by trying to stay right between the two walls. We a priori assumed that the Magic Barrier Tape would be faster, as in Experiment #1, but less precise due to the controllability of rate control [334].

For the different comparison analysis, a correction for experiment-wise error was realized by using Bonferroni-adjusted alpha level ($p = 0.05$ divided by the number of tests). Thus, in order to compare the Barrier Tape technique to the two other techniques (Freeze-backup and 2:1-Turn) the alpha level was adjusted to $p = 0.025$.

Completion time

An ANOVA on the mean completion time (in seconds) revealed a significant main effect of the technique ($F(2,22) = 84.01$, $p < 0.001$). Follow up t tests revealed that completion time in the Barrier Tape technique ($M = 31.62$ s, $SD = 9.71$ s) was sig-

nificantly shorter than in the Freeze-backup technique ($M = 99.54$ s, $SD = 21.63$ s, $t(11) = -12.06$, $p < 0.001$). Similarly, completion time in the Barrier Tape technique was significantly shorter than in the 2:1-Turn technique ($M = 52.33$ s, $SD = 6.59$ s, $t(11) = -6.48$, $p < 0.001$).

Path deviation

An ANOVA on the mean path deviation (in square meters) revealed a significant main effect of the technique $F(2,22) = 4.77$, $p = 0.019$. Follow up t tests revealed that the path deviation in the Barrier Tape technique ($M = 3.46$ m^2, $SD = 1.76$ m^2) was not significantly different from the path deviation in the Freeze-backup technique ($M = 2.45$ m^2, $SD = 1.04$ m^2, $t(11) = 1.72$, $p = 0.1143$.). By contrast, the analysis indicated that the path deviation in the 2:1-Turn technique ($M = 1.93$ m^2, $SD = 0.54$ m^2) was significantly lower than in the Barrier Tape technique, $t(11) = 2.81$, $p = 0.017$.

Amplitude of Walking in the Real World

An ANOVA on the mean amplitude of walking in the real world (in meters) revealed a significant main effect of the technique ($F(2,22) = 379.81$, $p < 0.001$). Follow up t tests revealed that the amplitude of walking in the real world in the Barrier Tape technique ($M = 6.81$ m, $SD = 1.33$ m) was significantly shorter than in the Freeze-backup technique ($M = 19.03$ m, $SD = 1.25$ m, $t(11) = -32.63$, $p < 0.001$). Similarly, the amplitude of walking in the real world in the Barrier Tape technique was significantly shorter than in the 2:1-Turn technique ($M = 13.61$ m, $SD = 1.54$ m, $t(11) = -13.17$, $p < 0.001$).

5.5.2.3 Subjective questionnaire

After both experiments, a preference questionnaire was proposed in which participants had to grade from 1 to 7 the 3 techniques according to 6 subjective criteria: *easiness of use*, *fatigue*, *navigation speed*, *navigation precision*, *general appreciation* and *naturalness*. Figure 5.11 shows the means and standard deviations of the 3 techniques for each of the subjective criteria.

Wilcoxon signed rank tests with Bonferroni correction showed significant differences: for the *fatigue*, between the Barrier Tape and the Freeze-backup techniques ($z = 2.69$, $p = 0.007$) and between the Barrier Tape and the 2:1-Turn techniques ($z = 2.41$, $p = 0.016$); for the *naturalness*, between the Barrier Tape and the Freeze-backup techniques ($z = 2.77$, $p = 0.006$) and between the Barrier Tape and the 2:1-Turn techniques ($z = 2.53$, $p = 0.011$); for the *navigation speed*, only between the Barrier Tape and the Freeze-backup techniques ($z = 2.82$, $p = 0.005$); and for the

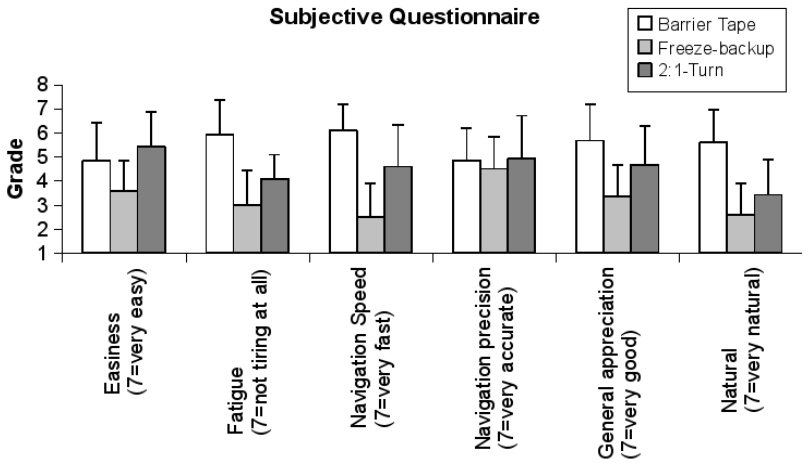

Fig. 5.11: Mean and standard deviation of subjective ratings about the different criteria for the three techniques.

general appreciation, only between the Barrier Tape and the Freeze-backup techniques ($z = 2.65$, $p = 0.008$).

5.5.3 Discussion

Both experiments showed that the Magic Barrier Tape is faster compared to the other techniques. Indeed, results show that Experiment #1 trials were completed more than 3 times faster with the Magic Barrier Tape than with the Freeze-backup technique, and more than 2 times faster than with the 2:1-Turn technique. In Experiment #2, completion time using the Magic Barrier Tape was also roughly 3 and 2 times faster respectively. This result is consistent with the user's impression from the questionnaire regarding the navigation speed of the different techniques (Figure 5.11). It is mainly due to the fact that there is no time lost in the resetting of the position when using the Magic Barrier Tape, and that the control law allows navigation speeds greater than the average walking speed. Completion times could be further reduced by tuning the control law for greater speeds, although controlling the Magic Barrier Tape could become increasingly difficult, as testified by 3 users which complained about an acceleration behavior that was sometimes hard to control.

The experiments also showed that users walked less when using the Magic Barrier Tape than with the other 2 techniques, which was expected due to the use of rate control at the boundaries of the workspace. However, an interesting observation can be made when considering that trials were completed significantly faster with the Magic Barrier Tape. If we compute the ratio between the amplitude of walking

in the real world and completion time, in a per user basis, we obtain similar values for the Magic Barrier Tape ($M = 0.24$, $SD = 0.04$), the Freeze-backup ($M = 0.21$, $SD = 0.04$) and the 2:1-Turn ($M = 0.24$, $SD = 0.04$) techniques in Experiment #1, as well as in Experiment #2 with ($M = 0.22$, $SD = 0.036$), ($M = 0.20$, $SD = 0.037$) and ($M = 0.26$, $SD = 0.052$) respectively. Hence, the amount of "useful walking", contributing to moving forward in the virtual world, relative to time is as large with the Magic Barrier Tape as with the other techniques. If we consider that walking speeds are the same for the 3 techniques, users spend roughly the same percentage of the total time doing useful walking with the Magic Barrier Tape technique than with the other 2 techniques.

Experiment #2 showed that the Magic Barrier Tape was less precise when following a given path, with a higher path deviation when compared to the 2:1-Turn technique (roughly 2 times less precise). We cannot reach firm conclusions on the comparison with the Freeze-backup technique, since results were not significantly different. Again, these results were expected. By its nature and design, the use of the Magic Barrier Tape is meant for coarse positioning. The user gets close enough to the navigation target in order to have it inside his workspace, and can then reach it by fine positioning navigation through real walking. As explained by one of the subjects of the Experiment #2, when asked about the strategies he used: "I sent the barrier tape as far as possible without going into the walls in order to take advantage of the workspace". However, path deviation could be improved by allowing users to customize their control law, like when they choose the mouse speed in desktop computers. Moreover, Zhai [334] observed that, with sufficient training, rate control and position control can achieve similar performances. Hence, further user training on the Magic Barrier Tape rate control might improve its mean path deviation.

Overall, users graded the Magic Barrier Tape higher in all criteria of the questionnaire where comparisons were significantly different. We emphasize that 6 subjects complained about having cybersickness when using the 2:1-Turn technique, while 2 said it made them loose balance. Many subjects found the Freeze-backup technique exhausting and frustrating. It is also important to note that 2 subjects had a very hard time using the Magic Barrier Tape. They used an inadequate strategy, and complained about the control law. They might have needed a longer training time, or more guidance on the strategy to adopt. They consistently graded it lower than the other techniques in every criteria of the questionnaire.

In a nutshell, the Magic Barrier Tape is faster than the Freeze-backup and the 2:1-Turn techniques, but is less precise when using it in rate control. The 2:1-Turn technique is the most precise, but seems to induce cybersickness to users, as well as equilibrium issues. There is a general dissatisfaction with the Freeze-backup technique, mainly due to its physical exertion and slow speed, leading to a frustrating experience. People generally prefer the Magic Barrier Tape, and find it more natural and less tiring.

5.5.4 Perspectives

Through user feedback on the experiments and our own observations, we found some ways of potentially improving the Magic Barrier Tape.

The user could use any part of his body in order to "push" on the virtual barrier tape. One could think about using the shoulders, the pelvis or the feet, since we often naturally use these body parts when we are unable to use our hands.

In their "Bubble" technique [82], a hybrid position/rate control haptic interaction technique for devices with restricted workspace, Dominjon et al. successfully used haptic feedback to represent the workspace boundaries and their virtual elasticity. In the RubberEdge technique [54], Casiez et al. used a passive haptic feedback through an elastic ring on top of a tracking surface such as a touchpad to allow the user to switch from position to rate control when reaching the elastic boundaries. Similarly, the Magic Barrier Tape could be augmented with haptic feedback when "pushing" on the tape. A possibility could be the use of passive haptics through tangible objects such as queue barriers with retractable belts as one could find in airports and queue-up places. The queue barriers could follow the workspace boundaries, and the virtual barrier tape would match the queue barriers position. Since retractable belts are elastic, the haptic feedback of the virtual barrier tape elastic deformation would be straightforward. Many users complained about the translation speed when using the Magic Barrier Tape, since the acceleration could be hard to control. A solution to this problem could be the use of a discrete approach. The control law, according to the hand penetration, would deliver one of three discrete velocities, corresponding to a human walking, jogging or running. Side-stepping human velocities could be used when moving in a direction orthogonal to the body orientation. The translation speed would therefore be more predictable, although capped by the running speed.

Last, although the barrier tape is made semi-transparent to reduce occlusion, visibility might be reduced in environments were the dominant color is close to the tape color. A way to enhance visibility in such cases would be to use different tape textures using complements of the dominant colors of the surrounding environment, in order to emphasize the presence of the Magic Barrier Tape while increasing the visibility of the scene.

5.5.5 Conclusion

This section introduces the Magic Barrier Tape, a new interaction metaphor for navigating in a potentially infinite virtual scene while confined to a restricted walking workspace. Using the barrier tape metaphor and its "do not cross" implicit message, the walking workspace is surrounded with virtual barrier tape in the virtual scene. The technique uses a hybrid position/rate control mechanism: real walking is used inside the workspace, while rate control navigation is used to move beyond the boundaries by "pushing" on the virtual barrier tape. Moreover, the technique natu-

rally informs the user about the boundaries of his walking workspace, providing a walking environment safe from collisions and tracking problems.

We conducted two experiments in order to evaluate the Magic Barrier Tape by comparing it to other state-of-the-art navigation techniques previously extended for omni-directional navigation. In Experiment #1 participants had to walk to a target, while in Experiment #2 they had to navigate inside a scene following a path. Results showed that the Magic Barrier Tape was faster than the other techniques. Experiment #2 results confirmed that, by design, navigation through rate control with the Magic Barrier Tape is not meant for precise path following, but rather for coarse positioning between fine positioning tasks. Overall, the Magic Barrier Tape was more appreciated, while being more natural and less tiring.

Future work will focus on exploring the different perspectives highlighted in this paper, namely the use of haptics for a more compelling and immersive experience, and the use of discrete velocities to produce a more predictable and realistic motion in rate control.

5.6 Conclusion

Restricted workspace in which the user is physically walking is one main issue that is often faced with Virtual Reality setup. Real walking motions are indeed constrained and bounded by either the walls of the (real) room or the range of the tracking system. Therefore this restricted workspace is a challenge the Virtual navigation technique must cope with.

In this chapter we presented three novel navigation techniques which achieve, in different ways, the challenging objective of proposing an interactive virtual navigation in large virtual environments with a restricted workspace. The “JoyMan” technique is a new input device which can be seen as a “human-scale joystick”. It is a novel hardware based on user’s equilibrioception, i.e., user can lean to control the speed of her virtual navigation with her body orientation. With the “Shake-Your-Head” (SYH) technique, the user can “walk in place” to control a potentially infinite virtual walk. Interestingly enough, Shake-Your-Head can make use of a low-cost and basic webcam to sense head motions when walking in place. Finally, the “Magic Barrier Tape” (MBT) is a software technique which uses a virtual barrier tape to display the limits of the restricted workspace straightforwardly in the virtual world. This enables safer and optimized physical walking inside the workspace. The user can push on the virtual tape to switch to rate-control mode of her navigation and reach out-of-reach locations. The characteristics of the three techniques are summarized in the table 5.1.

Thus, the JoyMan and MBT techniques are more immersive than the SYH. Moreover, of the three techniques, the MBT provide the more realistic type of walk. On the contrary, the JoyMan is the less realistic technique for simulating the walk, but it can be used in CAVE environments and its cost is moderate. Finally, the low cost

	Output hardware	Type of walk	Cost	Control law
MBT	HMD	Real walk	High	Hybrid rate/position control
JoyMan	HMD, CAVE	Static	Average	Rate control
SYH	Desktop	Walking-In-Place	Low	Position control

Table 5.1: Characteristics of the three presented techniques.

of the SYH technique can make it very interesting for some applications, like video games or large scale training applications.

The presented techniques have all their pros and cons. In the end, the choice of one navigation technique should be made carefully based on the targeted application and technical constraints.

Chapter 6
Pseudo-haptic walking

M. Marchal, G. Cirio, L. Bonnet, M. Emily, and A. Lécuyer

Abstract Pseudo-haptic feedback allows the simulation of haptic sensations in virtual environments using only visual feedback and properties of human visuo-haptic perception. The technique is mainly used for providing haptic feedback in the hands. In this chapter, we propose an extension of the concept for the feet. We introduce novel interactive techniques to simulate the sensation of walking up and down in immersive virtual worlds based on visual feedback. Our method consists in modifying the motion of the virtual subjective camera while the user is really walking in an immersive virtual environment. The modification of the virtual viewpoint is a function of the variations in the height of the virtual ground. Three effects are proposed: (1) a straightforward modification of the camera's height, (2) a modification of the camera's navigation velocity, (3) a modification of the camera's orientation. They were tested in an immersive virtual reality setup in which the user is really walking. A Desktop configuration where the user is seated and controls input devices was also tested and compared to the real walking configuration. Experimental results show that our visual techniques are very efficient for the simulation of two canonical shapes: bumps and holes located on the ground. Interestingly, a strong "orientation-height illusion" is found, as changes in pitch viewing orientation produce perception of height changes (although camera's height remains strictly the same in this case). Our visual effects could be applied in various virtual reality applications such as urban or architectural project reviews or training, as well as in videogames, in order to provide the sensation of walking on uneven grounds.

6.1 Introduction

Virtual Reality technologies immerse users inside a 3D synthetic world simulated in real-time by a computer. In such a virtual world, the user is given the possibility to manipulate virtual objects, and/or walk and explore virtual scenes.

Surprisingly, most current virtual reality (VR) setups restrict users to walk on flat workspaces. Whilst this might seem appropriate for walking inside virtual buildings or virtual streets, which are often flat, it becomes rapidly counter-immersive and inappropriate for any outdoor walking experience, such as when exploring a natural landscape. A main reason lies in the current difficulty to simulate, in the physical workspace, uneven grounds by means of mechanically actuated interfaces. As for today, few achievements have been reported on the design of devices that can render uneven grounds such as locomotion interfaces [124, 125, 140]. These interfaces remain costly, cumbersome and difficult to spread at the moment.

In videogames, the user is generally seated and interacts through input devices. Mouse and keyboards are often used to control avatar and walk in the 3D virtual world in "first-person view". In this case, a technique commonly employed when navigating on uneven grounds consists in constraining the motion of the virtual camera to follow the terrain. The camera stands always at the same height relative to ground level. This results in a continuous change in height of the view point, as if the user was "sliding" on the virtual ground.

In this chapter, we study the use of such kind of visual techniques to simulate uneven terrains and provide the sensation of walking up and down in an immersive virtual environment (VE) while walking on flat real ground. The proposed techniques use only visual feedback and consist in modifying the motion of the camera as function of the relief of virtual grounds. Three techniques are proposed: (1) a modification of the camera's height, (2) a modification of the camera's advance speed, (3) a modification of the camera's orientation. These techniques are implemented and tested in two different configurations. The first one is an immersive virtual reality setup in which the user is really walking while visual feedback of an Head Mounted Display (HMD) is automatically modified by superimposing one or more of the aforementioned visual effects. The second configuration is a desktop setup in which user is seated and controls the 3D walking with mouse/keyboard such as in videogames. We use these two setups to evaluate the influence of the different visual effects (and their combination) within various applications. The Desktop configuration can be considered as a control condition, in order to compare the use of visual techniques in an immersive situation (i.e., when the user is really walking) with a more classical desktop situation.

The remainder of the chapter is organized as follows. First, the chapter begins with a description of related work in the field of simulation of walking in virtual environments. Then, we describe the concept of our visual effects and how they were implemented for the simulation of two simple shapes: a bump and a hole. In the following parts, we describe the results of the experiment conducted to evaluate the efficiency of the techniques for simulating uneven terrains. The chapter ends with a conclusion and a description of potential perspectives and applications.

6.2 Related work

As of today, the simulation of the physical sensation of walking on uneven grounds has mainly been proposed through locomotion interfaces. When using these locomotion devices, the user is engaged in a repetitive gait, while his motion is compensated with an inverse motion produced by the device. Hence, the interface directly controls the position of the user in the virtual world. Most of the devices try to enable natural walking. In spite of the fact that there is a significant amount of locomotion devices specifically designed for VR systems and exploration of virtual worlds, most of them can only enable walking on flat surfaces, without obstacles. However, the action of walking over uneven terrain and cluttered environments is fundamental in our daily life (e.g. walking up and down the stairs), and critical on some occasions, such as when exploring outdoor environments. To date, only a few systems are capable of simulating human walking on non-flat ground.

The Sarcos Treadport [126], a treadmill with a mechanical tether attached to the back of the user, is an example of an attempt to provide a feeling of climbing slopes. Originally, the mechanical tether was used to compensate missing inertial forces and to simulate obstacles in the virtual path by applying forces on the user's torso. The concept was then extended so that the tether could also render the forces required to simulate a slope [124, 125]. A force on the opposite direction of motion was used when simulating walking uphill, with a magnitude equal to the horizontal component of the force in the real world case, and, analogously, a force was applied on the direction of motion when going downhill. Simulation of side slopes was also possible when applying lateral forces.

Leaving the kinesthetic simulation and entering the haptic realm, the ATLAS [208] treadmill, mounted on an actuated spherical joint, was able to provide slopes by allowing the pitching and rolling of the platform. With a different approach, the Ground Surface Simulator GSS [209] was able to simulate uneven terrain through a linear treadmill with a deformable belt. Six long platforms could locally raise the belt, allowing the display of small bumps up to 5° in slope. The Sarcos Biport and the GaitMaster [140], both made of foot motion platforms, could simulate uneven terrains but not inclined floors.

While these devices offer uneven terrain rendering to some extent, they all suffer from common limitations that restrict their widespread use, such as their huge size and weight, their cost or their lack of accuracy and degrees of freedom. Therefore, they have not yet been widely adopted outside the laboratory. Other smaller, less complex and more affordable locomotion devices exist that enable locomotion following the same motion compensation principle. Foot-wearable devices like the Powered-Shoes [141] and, more recently, the Gait Enhancing Mobile Shoe [75], compensate the user's motion without being attached to a bulky structure. However, they cannot render slopes or any kind of uneven terrain.

In order to simulate haptic sensations without haptic interfaces, other solutions have thus been proposed such as sensory substitution and pseudo-haptic feedback [162]. Pseudo-haptic feedback was notably studied through the modification of the speed of a mouse cursor according to the "height" of a texture [163]. As the mouse

cursor explored an image representing a top view of a texture, an acceleration (or deceleration) of the cursor indicated a negative (or positive) slope of the texture. Experimental evaluations showed that participants could successfully identify macroscopic textures such as bumps and holes, by simply using the variations of the motion of the cursor. Approaches using camera movements were also proposed in order to modify the locomotion sensations in virtual environments. For instance, Steinicke et al. [278] used redirected walking techniques in order to modify the trajectory orientation of the user in the real environment. Lécuyer et al. [164] used camera oscillations to improve the sensation of walking in VE. However, these approaches are not dedicated to walking sensations on uneven grounds.

In some "first-person view" videogames, the camera velocity is progressively scaled up or down whether the avatar is going up or down a hill, providing a slope information. This effect could be considered as a straight transposition of the aforementioned pseudo-haptic texture. However, to the authors' best knowledge there has been no study of the influence of such visual effects on the user's perception of heights and slopes in virtual environments, and these effects have never been implemented within an immersive VR setup when physically walking.

6.3 Novel interactive techniques based on visual feedback

6.3.1 Concept of the interactive techniques

The objective of the interactive techniques is to reproduce the sensation of walking on an uneven ground without the use of any haptic or locomotion interface. The main idea consists in modifying the motion of the subjective camera while the user is walking in the VE. The concept is to control the camera position and orientation, depending on the uneven virtual terrain displayed either on the screen or on a HMD. The camera motion is adjusted as a function of the simulated height of the terrain on which the user is walking. The variations of the camera motion are used here to transpose the perception of climbing or descending a slope.

Three different types of modifications to the camera motion have been studied: height variation, orientation variation and velocity variation. The amplitude of the different effects is computed using the height information of the 3D virtual environment. Thus, the techniques can be used to simulate any uneven 3D terrain, assuming that we know its height map. The implemented algorithm computes an iterative solution (depending on the user motion) for the modification of the camera motion. When the user is moving in the VE, a theoretical displacement is measured and the amount of the camera motion is computed using this measurement. Then, the new position of the user is computed and transmitted to the camera position and/or orientation. The visual techniques described here recall the ones used in videogames. However, unlike most gaming situations, our intention is to use them when the user is actually walking, i.e. superimposed to the visual feedback of the virtual scene.

6.3.2 Implementation

The different effects (Height, Orientation, Velocity) are displayed in Figure 6.1. The combination of the three effects was also implemented.

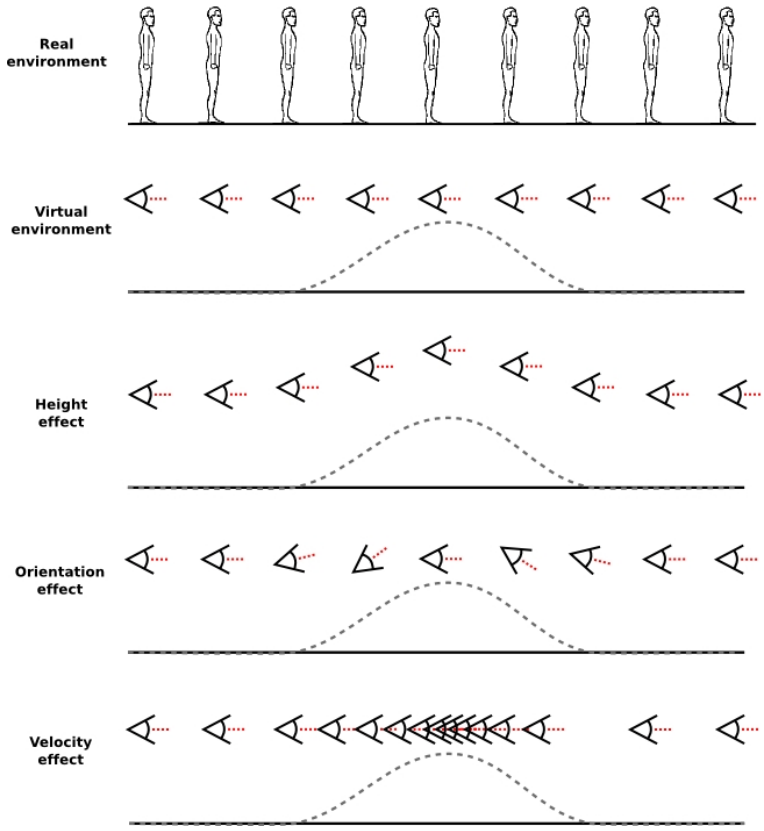

Fig. 6.1: Principle of the three different effects: the user is walking on a flat environment while the VE is composed of a bump. The camera motion is modified in three different ways: height variation (the camera moves with a constant orientation and a constant distance to the virtual ground surface), orientation variation (the camera is oriented following the curvature of the slope), velocity variation (the camera velocity decreases as the user is going up a virtual bump and increases as the user is going down with a run up at the end of the bump).

6.3.2.1 Height variation

The height effect consists in modifying the subjective camera height with a translation along the vertical axis. This effect allows the user to move parallel to the ground surface during his navigation in the virtual world. This approach is already used in a lot of demos and videogames. The height variates following the equation:

$$\text{Height}^t = \text{Height}^{t-1} + \Delta_{\text{Height}} \,.\, R_{\text{Height}} \tag{6.1}$$

where Height^t represents the camera height value at time t where the image is updated. R_{Height} is the ratio applied to the difference of height Δ_{Height} between times $t-1$ and t. In our implementation, we introduced ratios in order to parameterize the amplitude of the different effects. In our experiment, we chose $R_{\text{Height}} = 0.5$.

6.3.2.2 Orientation variation

The orientation effect consists in applying a variation in pitch angle to the subjective camera in order to look down when descending and up when ascending. This effect is supposed to mimic postural changes when walking on uneven grounds: the subject would have to compensate the orientation modification and adopt a new postural position. The camera angle at time t, Angle^t, is proportional to the tangent angle of the Gaussian curve α^t where the user is at time t:

$$\text{Angle}^t = \alpha^t \,.\, R_{\text{Orientation}} \tag{6.2}$$

where $R_{\text{Orientation}}$ is the ratio applied to the angle. In our experiment, we chose $R_{\text{Orientation}} = 0.5$.

6.3.2.3 Velocity variation

The velocity effect is based on the variation of the camera velocity. In a real environment, a subject is generally going slower on ascending slopes, and faster on descending slopes. We try to transpose this effect in our experiment by modifying the camera motion when the user is walking in a VE. Thus, the camera velocity is decreased when the user is going up and increased when the user is going down. This effect could be considered as a straightforward transposition of the pseudo-haptic textures effect [163], adapted here to the simulation of walking on uneven reliefs at a first-person view. We used a different algorithm for the ascending and descending cases. The algorithms compute the ratio R_{Velocity} applied between the real user velocity and the virtual camera velocity. The camera velocity is then modified following the equation:

$$\text{Velocity}^t = \text{Velocity}^{t-1} \,.\, R^t_{\text{Velocity}} \tag{6.3}$$

- Ascending case:

$$R^{t}_{\text{Velocity}} = exp(-R_{\text{AscendingV}} \,.\, \alpha^{t}) \tag{6.4}$$

  where α is the tangent angle of the Gaussian curve and $R_{\text{AscendingV}} = 0.1$ in our experiments.
- Descending case:
  This algorithm is designed to give a run up for a while after the bump or at the beginning of the hole. At time t, the ratio is updated regarding the difference between the user height in scene at times $t-1$ and t :

$$R^{t}_{\text{Velocity}} = R^{t-1}_{\text{Velocity}} + \Delta_{\text{Height}} \,.\, R_{\text{DescendingV}} \tag{6.5}$$

  where the ratio $R_{\text{DescendingV}}$ is equal to 2.0 in our experiments. When the subject reaches the end of the descent, his speed is at a maximum. If he is walking in a hole, then he starts to go up and his speed value will be given by the ascending algorithm. If the subject is on a bump, he will reach the plane ground after the bump. His speed ratio R_{Velocity} will start decreasing at 0.1 unit per second, until another bump/hole is reached or the ratio is back to normal.

6.3.3 Simulating bumps and holes

Our visual techniques were used to simulate two classical shapes: a bump and a hole. Our simulations used a known mathematical profile: a Gaussian profile, which defines the height maps of the shapes during the evaluations. It corresponds to a mathematical distribution of heights along a line perpendicular to the walking path. The same profile was used for the simulations of holes and bumps.

6.4 Evaluation: Efficiency of visual effects to simulate bumps and holes

The investigation of the perception of 3D holes and bumps while walking in a VE was performed using an experimental protocol consisting of a comparison of the different effects. The experiments were conducted using 3D virtual environments displayed either on a HMD or on a screen.

6.4.1 Virtual environment

The virtual environment is a simple corridor with given dimensions (height = 3.0 m, length = 19.0 m, width = 2.0 m). There is a part in the center of the corridor where the height can be modified during the experiments: the user can walk either

on a bump, a hole or a plane. To symbolize this variable part of the corridor, a transparent cube is represented on the ground with a height of $0.5m$ and a surface of $3m \times 2m$, as illustrated in Figure 6.2. The variable height of the ground is not visible in order to exclude visual cues from the scene.

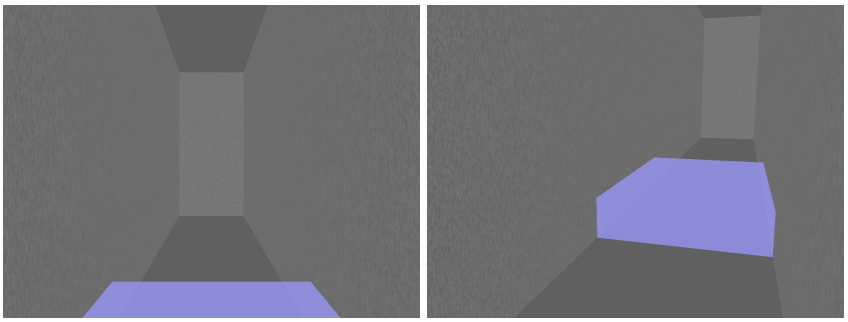

(a) (b)

Fig. 6.2: (a) Description of the virtual environment composed of a corridor; (b) a transparent blue cube is placed in the center in order to represent to the participant the location of the height modifications on the ground surface.

6.4.2 Population and visual conditions

6.4.2.1 Group 1: Immersive VR configuration with HMD

Twelve participants (4 females and 8 males) aged from 21 to 59 (mean = 28.7, std = 11.0) were in Group 1 and exposed to a first visual condition. One of them was left-handed, and none of them had known perception disorders. They were all naïve to the purpose of the experiment.

For this group, the experiments were conducted in an immersive room large enough to walk straight forward almost 6 meters. We used the eMagin Z800 Head Mounted Display as display device, at 60 Hz and with stereoscopy enabled. The user was wearing an opaque fabric on top of the HMD to hide the surrounding real world. An unique wire was transmitting the data, allowing the user to move freely during the experiments, as illustrated in Figure 6.3. The user's head was tracked by an ART ARTtrack2 infrared tracking system with 9 surrounding cameras for tracking the entire path of the experiment (corresponding to the virtual corridor). The available tracking space dimensions were: height = 2.5 m, length = 6 m, width = 3 m.

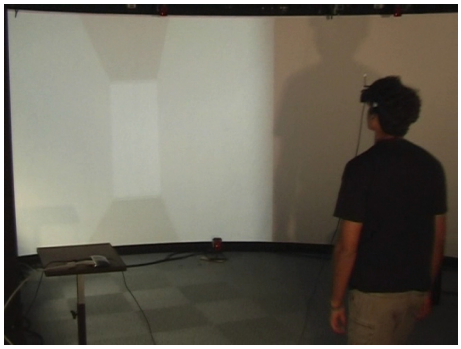

Fig. 6.3 Configuration of the immersive room for the experiments using the HMD. The scene displayed on the HMD is also displayed on the screen in this picture as an illustration of what the user can see during the experiments.

6.4.2.2 Group 2: Desktop configuration with monitor screen

Twelve participants (12 males) aged from 21 to 59 (mean = 27.8, std = 6.1) were in Group 2 and exposed to a second visual condition. The twelve participants were all different from participants of Group 1. One of them was left-handed, and none of them had known perception disorders. They were all naïve to the purpose of the experiment and they were different from the experiments conducted with a HMD.

For this group, the experiments were conducted with a PC, by using a classical keyboard for the answers. There was no stereoscopic effect. This second group can be considered as a control population, to compare the use of visual techniques in an immersive configuration, i.e. when the user is really walking, with the desktop case. The different fields of view for the rendering process for Desktop and HMD configurations were identical.

6.4.3 Experimental plan

In the experiment, our goal was to evaluate and compare the three different effects (Height, Orientation and Velocity) for the simulation of two canonical shapes: bumps and holes located on the surface ground of an immersive virtual environment. We also evaluated a fourth effect which is a combination of the three effects.

We used:

- three different *profiles*: Bump, Hole and Plane;
- two different types of walking locomotion: Forward and Backward *movements*;
- four visual *effects*: Height (H), Orientation (0), Velocity (V) and a combination of the three effects (HOV).

The experimental plan was made of the combinations [Profile x Movements] x 9 trials, for each effect (54 trials per effect). The subject alternates Forward and Backward movements, within a random sequence of [Bump, Hole, Plane] x [Forward, Backward] = 6 combinations. We performed between-subject design. The 4 series

(one for each effect) are presented using a Latin square and a defined sequence [H-O-V-HOV], counterbalanced with 4 sub-groups. The 12 participants of each Group (Group 1 with HMD and 2 with PC) were thus equally divided into 4 sub-groups of 3 people each.

The motivation for testing backward movements relies on the fact that gait postures of human bodies are generally different when moving forward or backward on a slope. Thus, our hypothesis was that backward movements could potentially lead to different physical sensations for our visual effects.

6.4.4 Procedure

The experiment consists of 216 trials per participant (54 per effect). The subject has to go forward and then backward in the virtual corridor. At the end of each movement (either forward or backward), a black screen appears (either on the HMD or on the screen) and the participant can give his answer concerning the identified shape (hole, bump, or plane).

6.4.5 Results

For each participant, the percentage of correct answers was estimated for the different experimental conditions. An ANOVA on the 4 different effects was conducted on the percentage of correct answers. A post-hoc analysis using Tukey's procedure was then performed. ANOVA were achieved separately for the two experimental configurations (HMD and Desktop) and by differentiating Forward and Backward movements. The results concerning the different effects are represented in Figure 6.4 for the HMD and the Desktop configurations. Results concerning Forward and Backward movements are distinguished for each group, as they gave different values. The order in the sequence had no significant effect on the results.

In the following paragraph, we present the results obtained for the four different configurations as a combination of HMD and Desktop groups, Forward and Backward movements.

The ANOVA accounting for the four different effects revealed a significant dependency between the effect and the probability of giving a correct answer for all the configurations.

For the Forward movement performed with the HMD configuration, the ANOVA performed between the four different effects revealed significant results for the effect ($F(3,11) = 19.447$, $p < 0.0001$). Post-hoc analysis showed that the percentage of correct responses in the Height condition ($M = 73\%$) was significantly higher than in the Velocity condition ($M = 37\%$), adjusted p-value < 0.001; the percentage of correct responses in the Orientation condition ($M = 85\%$) was significantly higher than in the Velocity condition, adjusted p-value < 0.001; and the percentage

of correct responses in the HOV condition ($M = 87\%$) was significantly higher than in the Velocity condition, adjusted p-value < 0.001. The other pairs of effects did not give any significant adjusted p-values.

For the Backward movement performed with the HMD configuration, the ANOVA performed between the four different effects revealed significant results for the effect ($F(3,11) = 11.646$, $p < 0.0001$). Post-hoc analysis revealed also significant differences: the percentage of correct responses in the Height condition ($M = 67\%$) was significantly higher than in the Velocity condition ($M = 37\%$), adjusted p-value $= 0.0004$; the percentage of correct responses in the Orientation condition ($M = 65\%$) was significantly higher than in the Velocity condition, adjusted p-value $= 0.0010$; and the percentage of correct responses in the HOV condition ($M = 75\%$) was significantly higher than in the Velocity condition, adjusted p-value < 0.0001. The other pairs of effects did not give any significant adjusted p-values.

For the Forward movement performed with the Desktop configuration, the ANOVA performed between the four different effects revealed significant results for the effect ($F(3,11) = 7.77$, $p = 0.0003$). Post-hoc analysis showed that the percentages of correct responses are significantly higher in Height condition ($M = 100\%$), HOV condition ($M = 99\%$), Orientation condition ($M = 98\%$) than in the Velocity condition ($M = 89\%$). Adjusted p-values are respectively 0.0008 (Height vs Velocity), 0.0012 (HOV vs Velocity) and 0.0072 (Orientation vs Velocity). The other pairs of effects did not give any significant adjusted p-values.

For the Backward movement performed with the Desktop configuration, the ANOVA revealed significant results for the effect ($F(3,11) = 3.8508$, $p = 0.016$). Post-hoc analysis revealed that the percentage of correct responses are significantly higher in the Height condition ($M = 99\%$) than in the Velocity condition ($M = 89\%$) with an adjusted p-value equals to 0.015. The other pairs of effects did not give any significant adjusted p-values.

At first glance, regarding the percentage of correct answers for the different effects, it seems that the sensation of bumps and holes was perceived among the participants. HMD and Desktop configurations give relatively different results. The Velocity effect with Desktop configuration gives namely higher percentages of correct responses compared to HMD configuration. Forward and Backward movements are distinguished for both configurations. Experiments conducted with a HMD and Backward movement globally obtained lower results compared to the experiments conducted with the same experimental configuration but with Forward movements. We can particularly notice the lower results for the two effects containing the Orientation effect (O and HOV) for Backward movements.

For HMD group, we can also notice the presence of two individuals (represented by individual dots on Figure 6.4.a and 6.4.b). These two individuals have obtained lower percentages of correct answers for the HOV effect and higher percentages for the Velocity effect, compared to the rest of the population, and could be considered as outliers.

We conducted also an analysis concerning the percentage of correct answers for the different shapes identified (i.e. Hole, Plane and Bump). The results are reported in Figure 6.5 for HMD and Desktop configurations, and detailed for Forward and

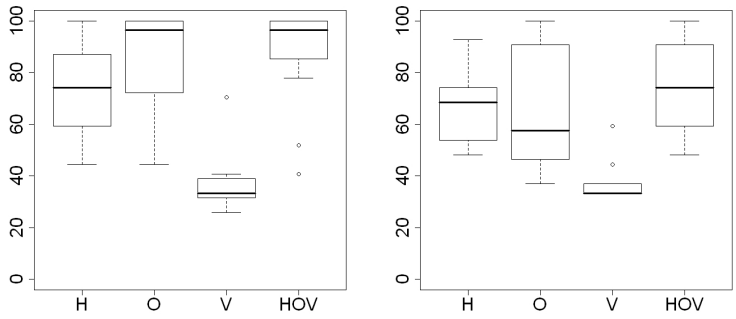

(a) HMD Forward

(b) HMD Backward

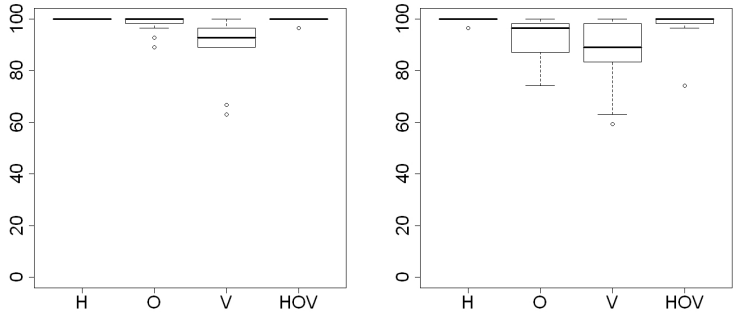

(c) Desktop Forward

(d) Desktop Backward

Fig. 6.4: Results: Percentage of correct answers for HMD configuration ((a) and (b) box plots) or Desktop configuration ((c) and (d) box plots). (a) and (c) represent the results for Forward movements, (b) and (d) represent the results for Backward movements. The 4 different effects are represented on each picture: Height (H), Orientation (O), Velocity (V) and the combination of the three previous effects (HOV). Each box plot is delimited by the quartile (25% quantile and 75% quantile) of the distribution of the effect over the individuals. The median is also represented for each effect.

Backward movements. Experiments conducted with HMD contain a higher number of incorrect answers: the higher number of incorrect answers for each effect are Plane shape for Height effect, Bump/Hole shape for Orientation and HOV effects. Thus, the Orientation effect seems to have an influence on the shape perception. For Velocity effect with HMD configuration, almost all answers are incorrect: Plane shape solution is almost always chosen, meaning that holes and bumps are almost never detected. On the opposite side, shapes with Velocity effect on Desktop configuration are well recognized. Thus, Velocity effect in an immersive situation leads to significantly different results, as observed also in Figure 6.4. Concerning backward movements with HMD configuration, we can notice that the percentage of incorrect

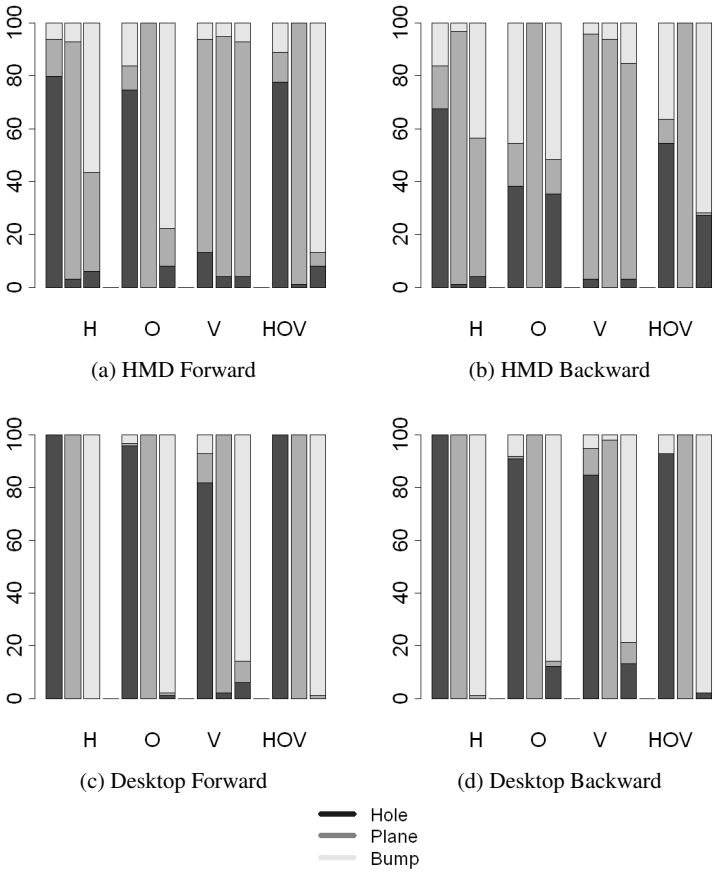

(a) HMD Forward (b) HMD Backward

(c) Desktop Forward (d) Desktop Backward

Fig. 6.5: Results: Percentage of correct answers. Results are given for the 4 effects and the 3 different shapes (Hole, Plane and Bump in this order). The percentage of answers is decomposed for each shape, displaying additionally the incorrect shapes identified for each shape. The Forward and Backward movements are distinguished.

answers is higher than for forward movements, for Height, Orientation and HOV effects.

6.4.6 Subjective questionnaire

After both experiments, a preference questionnaire was proposed in which participants had to grade from 1 (low appreciation) to 7 (high appreciation) the four dif-

ferent effects (H, O, V, HOV) according to 4 subjective criteria: ease of judgment, realism, cybersickness and global appreciation. Figures 6.6 and 6.7 show the results concerning the grades obtained by the four different effects for each of the subjective criteria, for HMD and Desktop configurations.

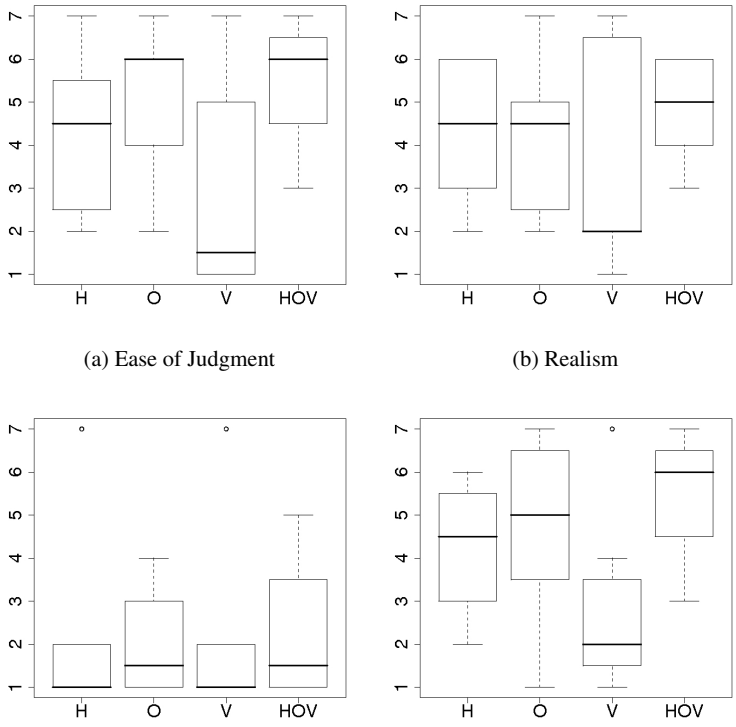

(a) Ease of Judgment

(b) Realism

(c) Cybersickness

(d) Global appreciation

Fig. 6.6: Results for subjective ratings for the four effects for HMD experiments: each box plot is delimited by the quartile (25% quantile and 75% quantile) of the distribution of the effect over the individuals. The median is also represented for each effect. The 4 different effects are represented on each picture: Height (H), Orientation (O), Velocity (V) and the combination of the three effects (HOV).

As the number of modalities is high (7 grades), we assume data to be normally distributed and perform an ANOVA test to compare the four types of algorithm. Thus, an ANOVA on the 4 different effects was conducted on the grade of each criterion. ANOVA were performed separately for the two experimental configurations and were followed by a post-hoc analysis using Tukey's procedure. The ANOVA accounting for the four different effects revealed no significant dependency between

the effect and the grading value for Realism ($F(3,11) = 1.30$, $p = 0.28$) and Cybersickness ($F(3,11) = 0.17$, $p = 0.91$) for HMD experiments.

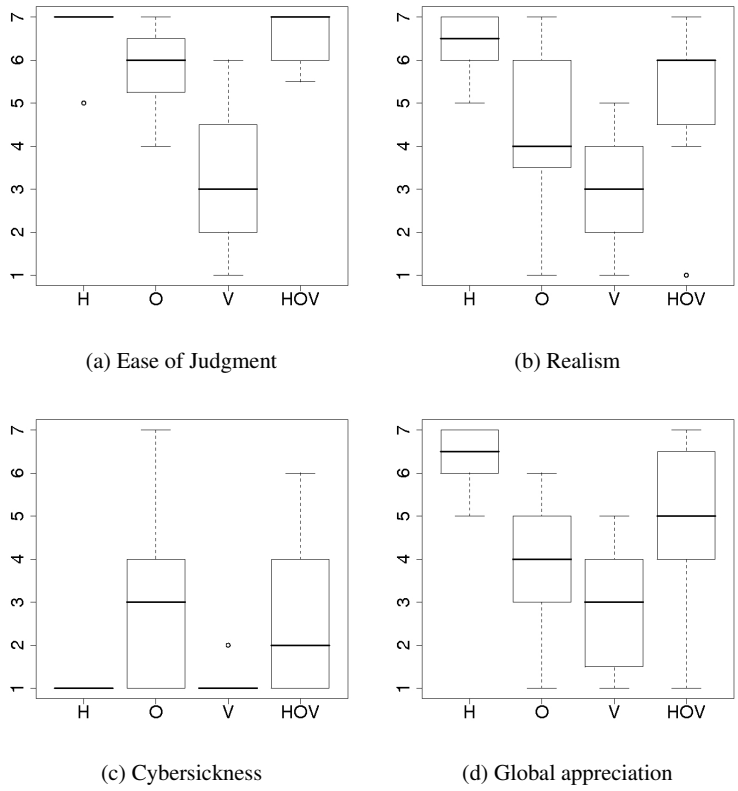

(a) Ease of Judgment

(b) Realism

(c) Cybersickness

(d) Global appreciation

Fig. 6.7: Results for subjective ratings about the different criteria for the four effects for Desktop experiments: each box plot is delimited by the quartile (25% quantile and 75% quantile) of the distribution of the effect over the individuals. The median is also represented for each effect. The 4 different effects are represented on each picture: Height (H), Orientation (O), Velocity (V) and the combination of the three effects (HOV).

Concerning global appreciation, the ANOVA performed between the four different effects revealed significant results for the Effect for both configurations ($F(3,11) = 13.27$, $p < 0.0001$ for Desktop configuration, $F(3,11) = 6.9$, $p < 0.0001$ for HMD configuration). The HOV effect obtains the best global appreciation for HMD experiments, followed by Orientation and Height effects. Post-hoc analysis shows that Velocity is significantly less appreciated than HOV (adjusted p-value 0.0003) and Orientation (adjusted p-value 0.013). The other pairs of effects

did not give any significant adjusted p-values, which argues in favor of a difference between the Velocity effect and the three other effects.

Height effect obtains the best global appreciation for Desktop experiments, followed by HOV effect. Post-hoc analysis revealed that the Height condition is significantly more appreciated than Orientation (adjusted p-value 0.0008) and Velocity (adjusted p-value < 0.0001). The other pairs of effects did not give any significant adjusted p-values. Indeed, Height condition was less appreciated in HMD experiment. On the contrary, the other techniques were better accepted and fairly evaluated for HMD configuration.

Concerning Ease of Judgment criterion, the ANOVA performed between the four different effects revealed significant results for the Effect for both configurations ($F(3,11) = 30.1$, $p < 0.0001$ for Desktop configuration, $F(3,11) = 4.53$, $p = 0.007$ for HMD configuration). Post-hoc analysis for HMD configuration gave similar results as obtained for global appreciation. Velocity effect is significantly less appreciated than HOV effect (adjusted p-value $= 0.0067$) and Orientation effect (adjusted p-value $= 0.036$). The other pairs of effects did not give any significant adjusted p-values, which argues in favor of a difference between the Velocity effect and the three other effects. However post-hoc analysis for Desktop configuration is slightly different than the one obtained for global appreciation. For Ease of Judgment criterion, Velocity is significantly less appreciated than the three other conditions: Height effect (adjusted p-value < 0.0001), HOV effect (adjusted p-value < 0.0001) and Orientation effect (adjusted p-value < 0.0001).

Concerning Cybersickness and Realism criteria, the ANOVA performed between the four different effects revealed significant results for the Effect only for Desktop configurations ($F(3,11) = 6.56$, $p < 0.0001$ for Cybersickness, $F(3,11) = 14.6$, $p < 0.0001$ for Realism). Post-hoc analysis for Realism criterion revealed that Height effect is found more realistic than Orientation effect (adjusted p-value $= 0.0033$) and Velocity effect (adjusted p-value < 0.0001). Furthermore HOV effect is found more realistic than Velocity (adjusted p-value $= 0.0003$). The other pairs of effects did not give any significant adjusted p-values. Post-hoc analysis for Cybersickness criterion showed significant adjusted p-values between Orientation and Height effects (adjusted p-value $= 0.0025$) and between Orientation and Velocity effects (adjusted p-value=0.0058). These results argue in favor of the exaggerated perceptions of the Orientation for Desktop experiments due to parameter values (the different ratios explained in Section 6.3), which seem to play a key role in the subjective appreciation of the participants.

Participants were also asked to evaluate the height of the shapes (Bump or Holes) of the experiments. Means and standard deviations of the participant answers are given in Table 6.1 for HMD configuration and in Table 6.2 for Desktop configuration. The real height of the Bump/Hole was 1.0 meter, with a ratio coefficient equal to 0.5 for Height, Orientation and Combination effects.

The estimated values are globally lower for HMD configuration. Interestingly, participants gave the Orientation effect the highest height for HMD configuration. The Orientation effect is always evaluated with an over-estimation of the correct height, although there is no variation in the camera height. The height values are

	H	O	V	HOV
Bump	0.32 (0.28)	0.79 (0.56)	0.06 (0.15)	0.68 (0.45)
Hole	-0.3 (0.32)	-0.77 (0.55)	-0.05 (0.12)	-0.59 (0.40)

Table 6.1: Means and standard deviations (in brackets) of the heights (in meters) given by the participants to holes and bumps for HMD configuration experiments. The four different effects (H, O, V, HOV) are distinguished.

	H	O	V	HOV
Bump	0.59 (0.52)	0.97 (0.54)	0.42 (0.46)	1.32 (1.12)
Hole	-0.58 (0.52)	-0.99 (0.53)	-0.42 (0.46)	-1.28 (1.10)

Table 6.2: Means and standard deviations (in brackets) of the heights (in meters) given by the participants to holes and bumps for Desktop configuration experiments. The four different effects (H, O, V, HOV) are distinguished.

under-estimated for Height effect for HMD configuration but slightly over-estimated for Desktop configuration. For Desktop configuration, the highest height is given to the experiments conducted with the HOV effect. For HMD configuration, the Velocity effect conducts to a height value near to zero, but it is not the case for the Desktop configuration where the height change perception is better, as already observed in the results in Figures 6.4 and 6.5.

6.5 General discussion

At first glance, results show that slope presence was identified for most effects in the immersive configuration. The slope appreciation greatly varies according to the experimental setup and, in a lesser way, according to the motion direction.

The Height and the Orientation effects yielded highly positive results in an immersive configuration. Users clearly felt a change in height, and could distinguish in most of the cases whether it was a bump or a hole. In the Forward case for the immersive setup, the Orientation effect shows better results than the Height effect. Although there was no change in height, users were able to perceive it more accurately than in trials where the height itself changed. The success and the accuracy of the Orientation effect was confirmed with the subjective questionnaire since users had no trouble in drawing the outline of the shapes they encountered during the experiments. When estimating the height of these shapes, results were not so far from real heights. The sum of the effects did not give better results than one effect taken alone for HMD configuration. However, the HOV effect was more appreciated in the subjective questionnaire for the immersive situation.

On the other hand, Height technique was less appreciated in HMD experiments. A possible explanation might be that users, particularly game players and people

familiar with navigation in VR, are used to see camera height variations when navigating in virtual uneven terrains in desktop environments. The Height effect is used in every desktop simulation involving slopes and landscapes. They have rarely or never been exposed to the other effects. Hence, they find the Height effect more natural and more appreciated. However, these same users have obviously spent less time in immersive simulations, and might not be used to the conditions of an immersive setup. Consequently, they are less trained for the Height effect under these conditions and did not perceive any "real inclines/declines" sensations. Hence, the other techniques were better accepted and fairly evaluated for the immersive configuration.

When immersed in a VE with an HMD setup, it appears that users do not well perceive change in height when subject to the Velocity effect. Hence, one could think that the direct transposition of the pseudo-haptic effect from the 2D to the 3D realm does not provide the expected visual cues in an immersive configuration. Thus, when using the non-immersive Desktop setup, the same Velocity effect, although not as efficient as the others, yields much better results than in the immersive setup, reaching up to an almost perfect score. A possible explanation for this behavior might be related to the optical flow of the virtual scene. In the immersive setup, the walls of the corridor were situated at the sides of the user's field of view due to the use of an HMD, while in the Desktop setup the entire display was largely contained in the field of view. Hence, the optical flow visible on the walls had a greater effect in the Desktop setup. The Velocity effect might have better results with a different virtual scene and/or different HMD optics.

As expected, backward and forward movements led to different results. The different shapes were less identified for backward movements in an immersive configuration. A reason for this difference between the two directions of walking might be the tuning of the different parameters, especially when Orientation effect is used.

Parameters of the different effects seem to play a key role for letting the participant identify a bump or a hole. We chose to tune the parameters of our different effects based on the HMD configuration. This choice led us to non-optimized parameters for Desktop configuration, and could explain some differences in the results and subjective questionnaires (e.g. for the Orientation effect which parameter was probably too high). The choice of our parameter values was arbitrary but could be based on more sophisticated models or on the application objectives. Although a very simple and straightforward implementation of the orientation motion was enough to achieve a good performance with the Orientation effect, other models closer to real life motions and gaits might improve these results. The physically-based model of an avatar representing the user in the virtual world, coupled to the motion of the user in the real world, might provide changes in head orientation, and hence in camera orientation, that are closer to what the user might expect. The use of real data on head orientation of users walking up and down on slopes could also be an alternative solution to tune the camera parameters. Finally, the use of other modalities could also be envisaged with our approach [300].

In future work, it could also be interesting to vary the steepness of the bump/hole. To conclude, a higher degree of realism, something actually criticized by many

users, as shown in the subjective questionnaire results, could improve the efficiency of the Orientation effect.

6.6 Conclusion and perspectives

In this chapter, we introduced novel interactive techniques to simulate the sensation of walking up and down in immersive virtual worlds based on visual feedback. Our method consists in modifying the motion of the virtual subjective camera as function of the variations in the height of the ground. This method has been widely used for desktop applications for videogames for example but never explored for providing real relief sensation when walking in an immersive virtual environment. Three effects were proposed: (1) a straightforward modification of the camera's height, (2) a modification of the camera's navigation velocity, (3) a modification of the camera's orientation. They were tested in an immersive virtual reality setup in which the user is really walking. A Desktop configuration where the user is seated and controls input devices was also used to compare the results.

The experiments were conducted to evaluate the influence of our visual techniques for the perception of simple and canonical shapes: virtual bumps and holes located on the ground. Experiments showed that changes in height and orientation of the camera are very efficient effects in an immersive configuration. The speed effect seems to be less perceived. Interestingly, in the immersive configuration, the consistent combination of all visual effects together led to the best results (although this result was not found significant) and was subjectively preferred by the participants. Experiments suggest also a strong perception of height changes caused by the orientation effect (although camera's height remains strictly the same in this case). This is confirmed by subjective questionnaire in which participants estimated a higher amplitude for bumps and holes simulated with orientation technique. This "orientation-height illusion" opens challenging questions in terms of human perception and challenges our interpretations.

Taken together, our results suggest that our visual techniques could be applied in an immersive virtual environment to simulate the sensation of walking on uneven surfaces. Our techniques could be used in various applications of virtual reality such as for urban and architectural reviews training, as well as in videogames in an immersive configuration.

Chapter 7
Auditory rendering and display techniques

S. Serafin, F. Fontana, L. Turchet, and S. Papetti

Abstract A walking task engages, among others, the sense of hearing. Not only humans perceive their own footstep sounds during locomotion: Walking conveys fundamental auditory cues of recognition also to listeners who are not performing the task. As a result, footstep sounds contribute to keep walkers in the perception and action loop, meanwhile informing external listeners about several characteristics of their actions. After reviewing the literature dealing with auditory aspects of interest for virtual walking, this chapter provides an overview on current techniques for the interactive synthesis and display of footstep sounds. User evaluations conducted on auditory display prototypes applying these techniques are presented, which shed light on their potential to find application in multimodal foot-floor interaction scenarios.

7.1 Introduction

During locomotion, humans are often engaged in parallel tasks preventing from a thorough visual exploration and fine analysis of the floor that must be traversed. This is the case for example of a person walking in the city, while browsing a fresh copy of a newspaper or simply looking around. Symmetrically, it is not uncommon to notice a walking person who cannot permanently focus on a concurrent visual task, due to lack of sensory cues substituting vision meanwhile capable of reporting about the path coming next.

Together, both such situations reveal a constant attempt of humans to keep walking tasks in the periphery of attention, a decision that is at any moment challenged by potential pitfalls that can occur during locomotion [213]. In this perspective, walking represents an interesting application domain in which to study possibilities for empowering the exchange of non visual information between humans and the external world.

The sonic modality, in particular, is at the core of many interactions involving communication through the periphery of one's attention. The physical contacts with grounds that, once pressed or scraped, produce sounds, turn out to be especially informing. They also provide cues to walking persons nearby and to listeners who are outside this loop, meanwhile in the proximity of the interaction touchpoint. Such cues include surface material [113], shoe type and walking style, and enables listeners to make inferences on gender as well as physical, biomechanical, and affective characters of a person [172, 311, 46].

This chapter builds upon the general hypothesis that subsumes the above situations: By providing peripheral meanwhile widely informing cues, interactive walking sounds support hearing subjects in their everyday activities involving self-locomotion.

This hypothesis in principle is applicable to a broad set of contexts and, hence, its implications have potential to span diverse social groups. Specifically, it would be interesting to assess walking sounds as a human factor, and consequently measure their informative value in critical areas such as labor, locomotion across hostile spaces, and also as a navigation aid for people with different abilities [167]. Once available, these measurements may turn useful to establish auditory scenes in which such factors are optimized depending on the specific context of application.

In this chapter, we suggest that effective sonic interactions in walking can be met through proper *augmentations* of the perceived reality. This means that future interactive floor scenarios should increase, rather than substitute the natural possibilities of grounds to convey auditory cues at floor level. In our case, additional cues will be enabled by enriching otherwise neutral floors with "layers" that provide physically-consistent sounds calling for familiar, possibly everyday ground ecologies. Examples will include the superposition over a (real) silent floor surface of sounds capable of rendering virtual aggregate grounds such as gravel, snow or mud.

Fortunately, current sensing and actuation devices allow interaction designers to come up with interface concepts, whose realization can be carried out already today at affordable cost and in reasonable time. Concerning in particular the floor interface domain, a plethora of force sensors as well as sound reproduction devices exist for detecting, then instantaneously responding to human walking through synthetic sonic feedback generated in real time by a laptop, or even smaller computing machines. In parallel it must be remembered that technologies differ in costs and featured specifications, and not all such technologies promise to scale down in price and encumbrance in their future versions.

Specifically in the case of audio reproduction, the hardest constraints are perhaps given by the power consumption and weight of the amplifiers as well as loudspeakers. On the one hand we can opt for small, low-power devices providing fair quality and no bass sound, consequence of their limited acoustic efficiency. On the other hand we can choose large amplification and reproduction devices with generally accurate emission broadband, albeit resulting in bulky, by no means wearable auditory interfaces.

Whether the right soundscapes will be finally achieved through rich and immersive, hence necessarily complex and encumbering systems or, conversely, through

(even not computer-enabled) simple and miniaturized interfaces finding room in a shoe sole, is a question that needs time and further work to be answered. In this perspective, the chapter represents just a starting point toward that answer.

In spite of the current limits of our research activity, we think we have started to move things in the correct direction. Elements in our research methodology that we have tried to always keep in mind include the constant confrontation between engineering solutions and their validity for the users, leading to some virtuous design-and-evaluation cycles also in our case. Furthermore, an eye has been kept constantly open on trading off between accuracy of reproduction, cost, and encumbrance of the devices.

In the meantime, we have restlessly involved the scientific communities of sonic interaction design and sound and music computing in participating to the development of interactive walking sonifications in their various forms, as well as in evaluating the subsequent results in ways to maximize our chance to stay on a constantly productive research track.

7.1.1 Chapter organization

This chapter touches aspects that are crucial during the design and realization process of a soundscape centered around walking sounds.

- Synthesis techniques are proposed which simulate walking events, especially for the creation of virtual sonic layers of aggregate material on top of acoustically neutral floors. Since they are based on the simulation of simplified physical event descriptions, such techniques can be straightforwardly employed to synthesize also the vibrotactile signals that naturally come out as a result of the same descriptions.
- Taken alone, a footstep sound has low perceptual meaning unless a convenient auditory scene is built around it. This scene includes design of soundscapes which simulate different indoor and outdoor spaces.
- The resulting sonic scenarios must be rendered by adopting proper combinations of interactive walking sounds and soundscape descriptions. Not only they must achieve a sufficient degree of realism when displayed using a conventional reproduction arrangement, such as for instance a headset or a couple of stereo loudspeakers: they should be also flexible enough to accommodate for peculiar displays. This flexibility becomes especially interesting in the case of walking sound augmentations, for which some non conventional reproduction sets are presented and then discussed.
- A user-centered evaluation of such scenarios is important in order to assess the ability of the simulations to realistically recreate ground surfaces.

7.2 Sound synthesis of walking

7.2.1 Background

The first systematic attempt to synthesize walking sounds has been proposed by Cook in 2002 [67]. In his pioneering work, he introduced elements of novelty that make his work stimulating and still largely state-of-the art.

The most interesting aspect in his modeling approach was the emphasis on foot-floor interactivity: thanks to an articulate procedure, which included several analysis stages, the model stored essential features from signals which were recorded during foot interactions with diverse floors; then, a reproduction of the same features could be made online by informing a parametric synthesis filter with temporal series of force envelopes, reporting for footstep sequences. This model allowed straightforward connection of the resulting system architecture to floor interfaces like sensing mats, performing a physically-informed interactive synthesis of walking sounds.

The physically-informed approach was further exploited in the synthesis of walking sounds. By making use of physically-based algorithms for the reproduction of microscopic impacts [258], as early in 2003 Fontana designed a stochastic controller that, once parameterized in parameters of force and resistance (respectively against and belonging to the floor), generated realistic sound simulations of footsteps over crumples and similar aggregate materials. Thanks to a higher-level control layer, such sounds were grouped into a footstep sequence once they were triggered by an expressive control model exposing affective parameters and musical performance rules, proposed by Bresin. The resulting real-time software architecture was a patch for Puredata, that allowed continuous control of both some physical floor parameters and gestural intentions of users [95].

An attempt to integrate some biomechanical parameters of locomotion, particularly the GRF, in a real time footstep sound synthesizer was made by Farnell in 2007 [93]. Once again, the result is a patch for Puredata that was furthermore intended to work as an audio engine for computer games, in which walking is interactively sonified.

7.2.2 Synthesizing walking

Acoustic and vibrational signatures of locomotion are the result of more elementary physical interactions, including impacts, friction, or fracture events, between objects with certain shape and surface material properties such hardness, texture etc. The decomposition of complex everyday sound phenomena in terms of more elementary ones has been an organizing idea in auditory display research during recent decades [109].

Specifically, a footstep sound can be considered the result of multiple micro-impacts between a shoe and a floor. Either they concur to form a unique percept

consisting of a single impact, in the case of *solid* materials, or conversely they result in a more or less dispersed, however coherent burst of impulsive sounds in the case of *aggregate* materials. At simulation level, it is convenient to draw a main distinction between solid and aggregate ground surfaces, the latter being assumed to possess a granular structure such as that of gravel.

An impact involves the interaction between an active *exciter*, i.e., the impactor, and a passive *resonator*. Sonic impacts between solid surfaces have been extensively investigated, and results are available which describe the relationship between physical and perceptual parameters of the objects in contact [149, 306]. Such sounds are typically short in duration, with a sharp temporal onset and relatively rapid decay.

The most simple approach to synthesize such sounds is based on a lumped source-filter model, in which a signal $s(t)$ modelling the excitation is passed through a linear filter with impulse response $h(t)$ modelling the resonator, resulting in an output expressed by the linear convolution of these two signals: $y(t) = s(t) * h(t)$.

By borrowing terminology from the kinematics of human locomotion, the excitation force can be identified with the GRF. In our case, GRF signals acquired using microphones or force input devices have been used to control different sound synthesis algorithms, which reproduce solid and aggregate surfaces as listed in the following of this section.

7.2.3 Physics-based modeling

The simulation of the interaction between solid surfaces can be obtained by decomposing the physical phenomenon into its basic constituents, instead of linearizing it into a series of two or more filters. The physics-based modeling approach precisely allows to deal with different kinds of interactions, by preserving their invariant phenomenological properties through this decomposition. According to this approach, situations like a foot sliding across the floor, or conversely walking on it, can be rendered respectively by starting from a friction or impact excitation component, meanwhile preserving the invariant floor properties in the resonant component.

Impact and friction are two crucial categories that affect walking perception [109]. In the impact model, the excitation corresponding to each impact $s(t)$ is assumed to possess a short temporal extent and an unbiased frequency response. A widely adopted physically-based description of this phenomenon considers the force f between the two bodies to be a function of the compression x of the exciter and velocity of impact $\dot{x}$, depending on the parameters of elasticity of the materials, masses, and local geometry around the contact surface [22]:

$$f(x,\dot{x}) = \begin{cases} -kx^{\alpha} - \lambda x^{\alpha}\dot{x}, & x > 0 \\ 0, & x \leq 0 \end{cases} \tag{7.1}$$

where k accounts for the material stiffness, λ represents the force dissipation due to internal friction during the impact, α depends on the local geometry around the contact surface. When $x \leq 0$ the two objects are not in contact.

Friction has been already implemented in sound synthesis as well, by means of a dynamic model in which the relationship between relative velocity v of the bodies in contact and friction force f is represented as a differential problem [24]. Assuming that friction results from a large number of microscopic elastic bonds, also called bristles [84], the v-to-f relationship is expressed as:

$$f(z,\dot{z},v,w) = \sigma_0 z + \sigma_1 \dot{z} + \sigma_2 v + \sigma_3 w \tag{7.2}$$

where z is the average bristle deflection, the coefficient σ_0 is the bristle stiffness, σ_1 the bristle damping, and the term $\sigma_2 v$ accounts for linear viscous friction. The fourth component $\sigma_3 w$ relates to surface roughness, and is simulated as fractal noise.

7.2.3.1 Interaction with aggregate surfaces

For what we have said, the sonic properties of aggregate surfaces can be reproduced by dense temporal sequences of short impact sounds. In most cases sound designers avoid to model these properties at a fine-grained level of detail, since a profound inspection of the microscopic phenomenon does not bring proportional advantages to the quality of the synthesis meanwhile increasing the computational burden to levels that often become intolerable[1].

Rather, these sequences are calculated using probabilistic laws informed by physical parameters. These laws determine the sound production at a macroscopic level, meanwhile introducing stochastic fluctuations to the microscopic events forming the sequence. Such events, in their turn, can be physically inspired like the impacts previously discussed as well as figured out by analyzing recorded signals accounting for ground material "templates" [67]. An example of the latter modeling approach is the PhiSM algorithm [66].

The crumpling algorithm [95, 47] implements a higher-level control, that is put on top of the physically-based impact-resonator model previously seen. In other words, it organizes temporal sequences of physical impacts between microscopic objects, assumed to be solid. Such sequences give rise to crumpling events, each represented by a corresponding group of micro-impacts. At the same time, the energetic evolution of a sequence instantaneously informs the parameters that are responsible for the generation of micro-impacts.

The temporal distribution of the micro-impacts is governed by a Poisson stochastic process, whose inter-arrival times are given by the Poisson distribution $P(\tau) = \lambda e^{\lambda \tau}$ in which λ controls the stochastic density of the micro-impacts. In parallel, the

[1] Note that this simplification cannot be used a general rule holding for all sounds resulting from multiple, small-scale processes. For instance, when substances with varying contact properties are involved such as liquids in motion, more sophisticated simulations must be realized which consider also the transitions across different macroscopic states [83].

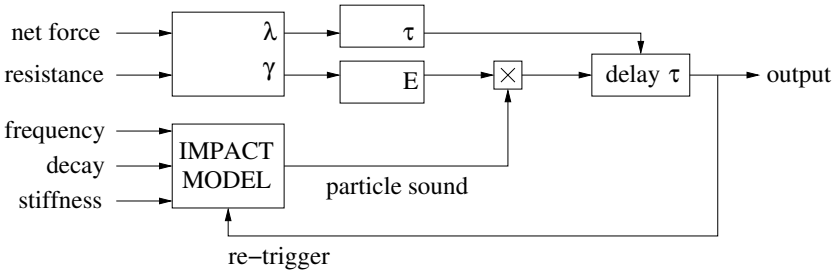

Fig. 7.1: Continuous crumpling algorithm.

power of each micro-impact follows a stochastic law $P(\gamma) = E^{\gamma}$, controlled by the γ parameter, which is derived from the physics of crumpling [269]. As a result, i) the dissipation of energy occurring during an impact, and ii) the temporal distribution of adjacent impacts can be constantly controlled (in stochastic sense) by the energy left to the process.

The crumpling model exposes the *average interval* between micro-impacts and the *average power* of every event as characteristic parameters for the control of sound. Once such controls are instantaneously mapped onto the force signals coming from a foot interface, the model allows continuous control over the generation of crumpling events that can be associated to footstep sounds [47].

Further mapping can be designed in between the interface and the above controls for setting the invariant features of an aggregate ground material, like its *resistance* or *compliance* parameter, having consequences in the perceived granularity of the ground. Together with proper settings of the modal resonator parameters defining the "color" of each micro-impact, these macroscopic controls set the acoustic signature of an aggregate material.

Figure 7.1 illustrates the continuous crumpling algorithm. By considering that aggregate grounds dynamically respond to a foot falling on them or scraping over them, it was hypothesized that the model should provide energy proportionally to the changes in the force, accounting for corresponding variations of the foot compression. To this end, force data streams provided by FSR sensors (see Chapter 2) are conditioned so as to filter out negative variations of the GRF, thus avoiding the generation of feedback when the foot depresses the ground.

7.2.3.2 Ground surfaces as resonant objects

In all cases of interest, a ground surface can be modeled as a linear resonator as opposed to the exciter. The ground properties determine the resonator parameters. Solid and homogeneous floors exhibit a narrow-band (hence longer and possessing definite color) sonic signature, conversely aggregate floors can be synthesized using bursts of short, wide-band (hence more noisy) resonant sounds simulating multiple collisions of the shoe against ensembles of small resonators.

Notably, the former sounds in practice are more difficult to be displayed. In fact, homogeneous floors are inherently large resonators capable of producing spatially diffused, possibly loud oscillations across a wide area (think of walking over a wooden floor or jumping on a metal grate). Conversely, aggregate materials generate localized sounds that normally can not propagate along the ground surface. The former, hence, need a powerful enough sound reproduction system: a constraint that rarely can be satisfied by a wearable interface.

As opposed to reproduction, the computational modeling of an even complex linear resonator is relatively straightforward. Modal synthesis [6] explains how to decompose a resonator that responds to an impulse with a signal $h(t)$ in terms of a number of resonant *modes*. The response, then, is modelled as a filter bank with impulse response $h(t) = \sum_i a_i e^{-b_i t} \sin(2\pi f_i t)$, where a_i represents the amplitude of the ith mode, b_i its decay rate, and f_i the associated modal frequency.

Each resonating filter is equivalent to a second-order damped linear oscillator:

$$\ddot{x}^{(r)}(t) + g^{(r)}\dot{x}^{(r)}(t) + \left[\omega^{(r)}\right]^2 x^{(r)}(t) = \frac{1}{m^{(r)}} f_{ext}(t), \tag{7.3}$$

where $x^{(r)}$ is the oscillator displacement and f_{ext} represents any external driving force, while the parameters $\omega^{(r)}$ and $g^{(r)}$ are the oscillator center frequency and damping coefficient, respectively. The parameter $1/m^{(r)}$ controls the "inertial" properties of the oscillator. Such a one-dimensional model provides a basic description of the resonator in terms of its pitch $\omega^{(r)}$ and quality factor $q^{(r)} = \omega^{(r)}/g^{(r)}$. The parameter $g^{(r)}$ relates to the decay properties of the impulse response of the system (7.3): specifically, the relation $t_e = 2/g^{(r)}$ holds, where t_e is the $1/e$ decay time of the impulse response.

7.2.4 Physics-based sound synthesis using the SDT

The Sound Design Toolkit[2] (SDT) [76] is a software product made up of a set of physically-consistent tools for designing, synthesizing and manipulating ecological sounds [108] in real time. The aim of the SDT is to provide efficient and effective instruments for interactive sonification and sonic interaction design.

The SDT consists of a collection of patches and *externals* for Puredata and Max/MSP.[3] The library is compatible with MacOSX, Windows, and Linux (Puredata only).

In the Puredata and Max/MSP terminology, an *external* is a dynamic library which provides some kind of signal processing. Depending on its communication interface (in the form of a set of *inlets* and *outlets*) an *external* can be linked to other *externals*, arithmetical operators, digital filters, sliders or other GUI elements that

[2] `http://www.soundobject.org/SDT/`

[3] Which is in a sense the advanced, yet commercial, counterpart to Puredata.

are natively provided by such environments. Together, all these elements find place inside patches allowing to define complete digital signal processing procedures.

In particular, each SDT's *external* represents a physically-based or -informed/-inspired algorithm for sound synthesis or control. The SDT patches make use of these *externals* to implement fully functional physically-consistent sound models. Moreover, they provide features for parametric control and routing of I/O signals.

The SDT has been used for synthesizing audio and vibrotactile feedback simulating different ground materials. Following is a brief description of the models, and how they have been used.

7.2.4.1 Realization of solid impacts

In the SDT implementation, a modal resonator can have an arbitrary number of resonant modes, each of which is represented by a linear 2nd-order oscillator in the form given by (7.3). Also, the resonating object can be endowed with a macro-dynamic behavior provided by an *inertial mode* added to the modal resonator structure. The inertial mode describes the macro-dynamics of a modal resonator as that of a pointwise mass, which is described by the Newton's equation of motion:

$$\ddot{x}(t) = \frac{1}{m} f(t) \tag{7.4}$$

where x is the *displacement* of the whole object, m is its *mass*, and f is the external *force* applied to the object. When present, the inertial mode is considered as the first mode of a modal resonator. It is clear that while an inertial mode is undamped, conversely resonant modes are damped. Having described its single components, it is now possible to describe the structure of a modal resonator having N modes of index $l = 1 \ldots N$ by means of the following linear system:

$$\begin{bmatrix} \ddot{x}_1(t) \\ \vdots \\ \ddot{x}_N(t) \end{bmatrix} + G \begin{bmatrix} \dot{x}_1(t) \\ \vdots \\ \dot{x}_N(t) \end{bmatrix} + \Omega^2 \begin{bmatrix} x_1(t) \\ \vdots \\ x_N(t) \end{bmatrix} = \bar{m} f(t) \tag{7.5}$$

where G and Ω are diagonal matrices whose elements are, respectively: $g_{l=1\ldots N}$ and $\omega_{l=1\ldots N}$, and $\bar{m} = [1/m_{l=1\ldots N}]^T$. In case the inertial mode was present, g_1 and ω_1 would be equal to 0, while x_1 would be the displacement of the entire object and m_1 its total mass.

The displacement x_j of a resonating object at a given point $j = 1 \ldots N$ can be calculated as:

$$x_j(t) = \sum_{l=1}^{N} q_{jl} \cdot x_l(t) \tag{7.6}$$

where the coefficients q_{jl} are the *output weights* for each mode $l = 1 \ldots N$ at the output point j. It is clear that, in case an input and an output point coincided (that is, $i = j$), their modal weights $1/m_{li}$ and output weights q_{jl} would also be the same.

The algorithms underlying solid surface sound models share a common structure which is shown in Figure 7.2: two objects interact through what is called an *interactor*, which models the actual contact interaction. The interactor contains most of the art, that is necessary to couple two or more objects in the discrete-time domain.

In principle, in order to implement the algorithm represented in Fig. 7.2 it is sufficient to couple two instances of (7.5) with (7.1) or (7.2). In practice, this elaboration must be performed while converting the same equations to the discrete-time domain. Thus, their coupling needs to solve issues about numerical stability and accuracy, as well as instantaneous propagation of the effects [224].

In the current version of the SDT the bilinear transformation — an A-stable 2nd-order implicit method [245] — is used to translate the continuous-time equations above to the discrete-time domain. In order to discretize the system of 2nd-order differential equations of (7.5) it is useful first to rewrite a single mode (7.3) as an equivalent system of two 1st-order differential equations:

$$\begin{cases} \dot{v}(t) + g v(t) + \omega^2 x(t) = \frac{1}{m} f(t) \\ v(t) = \dot{x}(t) \end{cases} . \tag{7.7}$$

By applying the Laplace-transform to (7.7) we obtain two 1st-order equations in s. The next step is to apply the bilinear transformation, thus obtaining two equations in z, and finally apply the inverse Z-transform in order to obtain the following discrete-time system, expressed in *state-space* form:

$$\begin{bmatrix} x(n) \\ v(n) \end{bmatrix} = A \begin{bmatrix} x(n-1) \\ v(n-1) \end{bmatrix} + \begin{bmatrix} \frac{1}{4m\Delta} \\ \frac{F_s}{2m\Delta} \end{bmatrix} [f(n) + f(n-1)] \tag{7.8a}$$

where the matrix A has the following expression:

$$A = \frac{1}{\Delta} \begin{bmatrix} \Delta - \omega^2/2 & F_s \\ -F_s \omega^2 & 2F_s^2 - \Delta \end{bmatrix} \tag{7.8b}$$

with $\Delta = F_s^2 + gF_s/2 + \omega^2/4$.

As for the inertial mode, the discrete counterpart to (7.4) is easily obtained from (7.8a) and (7.8b) considering $g = 0$ and $\omega = 0$. It follows that the bilinear transformation enables to maintain a unified formulation for both the inertial and resonant modes.

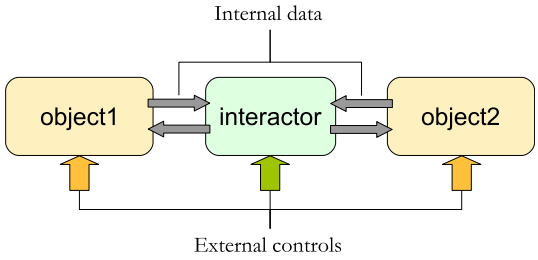

Fig. 7.2 The common structure underlying the SDT algorithms simulating solid surface contacts.

Since the bilinear transformation is an implicit equation, the resulting discrete representation (7.8a) is also in implicit form: an instantaneous dependency between the state variables (displacement x and velocity v) and the input force f is present.

Finally, the discrete-time counterpart to the system made of (7.5) and (7.6), representing an entire modal object, can be written as:

$$\begin{cases} \begin{bmatrix} x_l(n) \\ v_l(n) \end{bmatrix} = A_l \begin{bmatrix} x_l(n-1) \\ v_l(n-1) \end{bmatrix} + \begin{bmatrix} \frac{1}{4m_l\Delta_l} \\ \frac{f_s}{2m_l\Delta_l} \end{bmatrix} [f(n) + f(n-1)] \\ \\ \begin{bmatrix} x_j(n) \\ v_j(n) \end{bmatrix} = \sum_{l=1}^{N} q_{jl} \begin{bmatrix} x_l(n) \\ v_l(n) \end{bmatrix} \end{cases} \tag{7.9}$$

where $l = 1 \ldots N$ and $j = 1 \ldots N$ denote respectively the mode and output point considered. The matrix A_l is as in (7.8b), but now accounts for a different $\Delta_l = F_s^2 + g_l F_s/2 + \omega_l^2/4$ for each mode l.

Due to the implicit form of the bilinear transformation, the resulting discrete-time equations are implicit as well. Hence, an instantaneous relationship is present. For instance, in the case of the impact model, while the modal resonator of (7.9) needs f_{n+1} to compute $[x_{n+1}\ v_{n+1}]^T$, the impact force f_{n+1} also has an instantaneous dependence on x_{n+1} and v_{n+1} given by the discrete-time counterpart of (7.1). Such a *delay-free loop* is not directly computable and, because of the non-linear dependence $f(x,v)$, it needs some special handling in order to be solved. In particular, the *K-method* [42] together with *Newton's method* [245] are used.

The algorithm summarized in Fig. 7.2 can now be seen in more detail: at each temporal step the resonators send their internal state (namely, displacement and velocity at the interaction point) to the interactor, which in turn, after solving the delay-free loop as explained above, can send the newly computed interaction forces back to the objects, thus putting them in condition to perform a computation for the next step. The non-linearities provide richness and improved dynamics to the resulting sounds, even when using low-order resonators.

The solid surface sound models from the SDT allow to set the number of modes of a modal resonator, and the control parameters allow manipulate their modal properties individually.

7.2.4.2 Application to footstep sounds

The SDT realization of solid impacts is a basic building block for synthesizing footstep sounds. A realization of the friction model (7.2) exist in the same library as well, whose discrete-time implementation is left out of this chapter for the peculiar numerical issues that it raises [24].

For the sake of footstep sound synthesis, SDT has been enriched with an alternative impact model implementation, called soft impact. This model allows to synthesize the sound of an impact on a soft surface, or a soft impact between two surfaces. Although avoiding an accurate simulation of the physics of contacts between spa-

tially distributed objects, nevertheless the soft impact algorithm provides effective acoustic results by making use of a dense temporal sequence of tiny signals that excite the resonator described by (7.9). In more detail, no mutual interaction among an interactor and resonating objects is simulated. The interactor, i.e. the force f of (7.9), is instead substituted by a proper static force in the form of a noise burst that finally excites a modal resonator.

This algorithm, hence, realizes a simple feed-forward signal processing procedure. In spite of its simplicity, the idea behind can be qualitatively justified considering that smooth contacts can be reduced to dense temporal sequences of micro-impacts, in a sense modeling the surfaces of the interacting objects as multiple contact areas. Also, the use of specifically filtered noise signals can be motivated considering that such micro-impacts can exhibit a stochastic-like distribution. Besides the modal resonator parameters, the available controls include an ADSR (*attack time*, *decay time*, *sustain gain*, *sustain time*, *release time*) envelope shaper and the *cutoff frequency* parameter of two auxiliary equalization filters (respectively high- and low-pass) which process the noise burst

Finally, SDT puts available an implementation of the continuous crumpling model described in 7.2.3.1.

Practical use of the SDT has been made in the following case studies:

- while simulating impacts between solid surfaces, force data streams provided by the input sensors (see Chapter 2) were pre-conditioned and then analyzed in order to identify foot-floor contact events. Such events have been used to trigger four separate instances of the impact model, corresponding to the heel and toe of each foot: when a contact event was detected, its energy was estimated and the resulting value used to set the initial velocity of the corresponding impact model [226, 227];
- friction has been used while implementing compounds of physically-based building blocks, such as during the synthesis of creaking wood (see Section 7.3);
- concerning soft impacts, the force data stream provided by the FSR sensors (again in Chapter 2) has been treated as in the impact model. In this case however, the energy was used to control the amplitude of the noise burst directly [226, 225, 46, 225];
- as for the continuous crumpling simulations, four pre-conditioned force signals corresponding to the heel and toe of each foot were directly mapped to the respective force parameters of separate instances of the SDT's *crumpling* model. At a lower level, the micro-impacts can be synthesized either by triggering solid or soft impact events. By means of this model, realistic simulations of grounds covered with snow, brushwood or gravel have been obtained [226, 46, 225, 227].

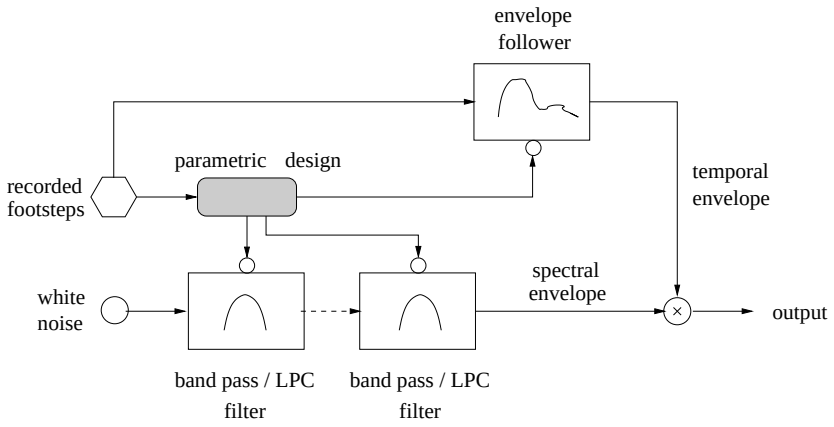

Fig. 7.3: Sketch of the method based on parametric synthesis of footstep sounds.

7.2.5 Parametric modeling

In parallel with the synthesis of walking sounds obtained using physically-based models, more simple models can be realized when there is reasonable expectation to come up with realistic, low-latency sonic interactions.

Parametric synthesis has already been proposed for the synthesis of walking sounds [93]. In this section we describe a method that proved effective in the simulation of floors exposing either homogeneous or aggregate surfaces. This method inherits existing analysis-and-synthesis techniques that have been proposed for the generation of walking and, later, hand clapping sounds [67, 235], furthermore it introduces simple novelties in an effort to make the synthesis process as most intuitive for the sonic interaction designer.

The idea is that of starting from the knowledge contained in a pre-recorded set of walking sounds—that can be downloaded also for free, e.g. from the Freesound online database `www.freesound.org`. This knowledge is used to i) shape noise by means of linear filters, for instance obtained by LPC processing of the source samples or even by manual tuning of the filter parameters, and then to ii) envelope the amplitude of the filtered noise depending on the instantaneous GRF value. Figure 7.3 shows the method in more detail, as well as the design procedure behind.

Concerning the shaping of the noise source, acceptable results can already obtained by manually tuning a series of second-order bandpass recursive digital filters. Typical parameters are shown in Table 7.1.

In parallel, an amplitude weighing function can be obtained for each material by aligning and then averaging the envelopes, each obtained through straightforward nonlinear processing [67] of a corresponding source sample. This function ultimately represents a mean envelope signal, whose standard deviation from the average value is known at each temporal step.

Table 7.1: Second-order filter parameter values for different ground materials

Material	Filters	Bandwidth (Q)	Center frequency	Gain
Snow	IIR BP	50	400 Hz	1
	IIR BP	700	660 Hz	0.4
Dead leaves	IIR BP	50	100 Hz	1
	IIR BP	500	850 Hz	0.5
	IIR BP	5000	6000 Hz	0.33
Metal (heel)	IIR BP	17	220 Hz	1
	IIR BP	500	220 Hz	1
Metal (toe)	IIR BP	12	250 Hz	1
	IIR BP	20	250 Hz	1
	IIR BP	200	400 Hz	0.24
	IIR BP	500	400 Hz	0.24
Wood (heel)	IIR BP	250	250 Hz	1
	IIR BP	250	250 Hz	1
	IIR BP	180	660 Hz	0.01
	IIR BP	550	660 Hz	0.01
Wood (toe)	IIR BP	55	130 Hz	1
	IIR BP	250	130 Hz	1
	IIR BP	200	610 Hz	0.16
	IIR BP	500	610 Hz	0.16

At this point it is not difficult to re-synthesize a sequence of footstep sounds over a distinct material: when a walking event is detected, the GRF onset (typically the initial 3 or 4 ms) is used to estimate the duration of a footstep. By considering that the energy consumed during every footstep varies to a small extent, the amplitude weighing function is shrunk/stretched along the time dimension (for instance using linear interpolation) and proportionally increased/decreased in amplitude depending on the GRF strength. Furthermore, randomness is added to the mean trajectory at every temporal step proportionally to the standard deviation of the average envelope function.

Parametric synthesis has been successfully adopted to generate accurate stimuli for the test appearing in Section 7.5.2, using LPC to compute the shaping filter coefficients starting from envelope-normalized sound source recordings. Although in that case the procedure was performed offline, the parsimonious use of computational as well as memory resources made by the parametric synthesis procedure poses no problems toward the implementation in real time of this method.

In more detail, the online analysis on the GRF signal is not that simple for parametric synthesis purposes. More elaboration in fact would be needed on top of the onset identification, which keeps into account variations in the foot gesture occurring during the walking act: consider, for instance, a person who stops her foot before completing a step. Until this issues of analysis remain unsolved, physics-based models informed by continuous GRF data deserve more appeal compared to parametric synthesis.

Table 7.2: Combination of sound synthesis models for different walking sounds. Note: for some materials, up to three independent instances of PhISM are computed.

Sound	Impact	Friction	PhISM	Crumpling	GRF control	Stochastic control
Creaking wood	YES	YES	-	-	impacts	friction
Metal	YES	-	-	-	impacts	-
Fresh snow	YES	-	YES	YES	PhISM & crumpling	-
Gravel	-	-	YES	-	PhISM	-
Beach sand	-	-	YES	-	PhISM	-
Forest underbrush	-	-	YES	-	PhISM	-
Dry leaves	-	-	YES	-	PhISM	-
Dirt plus pebbles	-	-	YES	-	PhISM	-

7.3 Composition and parameterization of the models

The sound of a footstep potentially depends on a myriad of contextual conditions: the kind of shoes a subject wears and the type of surface a person is walking on characterize just a subspace of the entire set of possible contexts. One assumption that, for instance, can be made to reduce this space is that the shoe has a rigid sole. This assumption has notable consequences in the simulation of interactions with solid floors, whereas bringing minor effects in the case of aggregate grounds.

The algorithms proposed in the previous sections can be qualitatively informed, starting from a spectral analysis of recordings of real footsteps. From the same recordings, characteristic recurrent events can be identified and then reproduced during the re-synthesis, with an aim to simulate their evolution across time and subsequent re-combination into a desired final product.

Some examples are provided in the following, giving empirical evidence of the fact that credible footstep sounds can be obtained thanks to a careful sound design supported by powerful tools, such as the models seen in the previous sections.

The sound produced while walking on dry leaves can be constructed as a combination of sonic events having relatively long duration and spectral energy at both low and high frequencies, with the addition of noisy glitches that confer “crunchiness” to the final sound. A similar example comes from walking on gravel, resulting from the contribution of physical impacts among stones of different mass, which while colliding give rise to sounds having features that depend on this mass.

Such interventions must be properly weighed, to obtain a good match with the components identified in the corresponding real sounds. Finally, an overall loudness must be determined to confer ecological realism to the final sound.

Using different combinations of the models described in the previous section, the following solid and aggregate surfaces have been simulated and tested: wood and creaking wood, metal, deep and low snow, gravel, beach sand, forest underbrush, dry leaves and dirt plus pebbles. [212, 303, 268]. Table 7.2 summarizes how such models have been combined to generate these sounds.

For instance, the sound of footsteps on wood was synthesized by controlling one instance of the SDT impact through GRF data, and superimposing to the impact "creaking" sounds obtained by exciting a friction model through ramp functions driving the external rubbing force. The variation and duration of such ramps was randomly set within certain ranges, before synthesizing every new footstep. The addition of randomness enhances the realism, overall introducing changes in the frequency, amplitude and duration of the sounds.

The examples proposed in this section have been validated through the experiment reported in Section 7.5.1.

7.4 Footstep sounds rendering and displaying

Sounds can be conveyed to the walker through the air and/or bone conduction, by means of speaker, headphone, or contact devices. Concerning the display techniques, and depending on the device, approaches can be followed ranging from the traditional mono or stereophonic reproduction up to solutions affording more precise sound source localization, through binaural listening or physical collocation in space of one or more small loudspeakers reproducing the virtual source.

Several rendering paradigms have been tested for the synthesis of auditory displays [104]. In recent years, some such paradigms have been challenged in the novel context of interactive display, in which the dynamic evolution of an auditory scene can be obtained by trading off real time constraints and computational burden.

Besides common headphone and room loudspeaker systems, more unusual solutions are presented in this book with specific attention to ground-level auditory displays: among these, small speakers or insole shakers that are directly mounted into the shoes, and audio-tactile devices placed under the floor. In some cases, walking sounds are delivered by these devices as a by-product of broadband vibrotactile transduction, resulting also in sound as part of the overall reproduced mechanical energy.

7.4.1 Soundscapes rendering and displaying

When exploring a place by walking, at least two categories of sounds can be identified: the person's own footsteps and the surrounding soundscape. In the movie industry, footsteps sounds represent important elements. Chion writes of footstep sounds as being rich in what he refers to as *materializing sound indices*—those features that can lend concreteness and materiality to what is on-screen, or contrarily, make it seem abstracted and unreal [59]. Studies on soundscape originated with the work of R. Murray Schafer [266]. Among other ideas, Schafer proposed soundwalks as empirical methods for identifying a soundscape for a specific location. In a soundwalk people are supposed to move in a specific location, noticing all the

environmental sounds heard. Schafer claimed that every place has a sound signature. The idea of experiencing a place by listening has been originally developed by Blesser [41]. By synthesizing technical, aesthetic and humanistic considerations, he describes the field of aural architecture and its importance in everyday life.

For virtual reality purposes, three classes of soundscapes can be identified: static, dynamic, and interactive.

- *Static* soundscapes diffuse an auditory scene regardless of any specific localization effect.
- *Dynamic* soundscapes render the spatial position of one or more sound sources, even dynamically in space, regardless of any user input.
- *Interactive* soundscapes render the auditory scene also as a result of the actions and gestures of the user(s), which for instance can be tracked by a motion capture system. As an example of sound interaction, one can imagine the simulation of a forest, with sounds of fleeing animals following by the movements of a listener furthermore engaged in a walking task.

As part of the research done, an engine has been realized in Max/MSP able to provide soundscapes belonging to any of these three classes. To include dynamic and interactive features, the ambisonic tools[4] for Max/MSP were used. Such tools, in fact, allow to move virtual sound sources along trajectories defined on a three-dimensional space [265]. At current, the engine can manage up to sixteen independent virtual sound sources, one to display the user's footsteps and the remaining fifteen handling the external sound sources populating the soundscape.

7.4.2 How to combine footsteps and soundscapes

Virtual reality studies made in the field of sound delivery methods and sound quality have recently shown that the addition of environmental cues can lead to measurable enhancement in the sense of presence [281, 61, 264]. Recently, the role of self-produced sound to enhance sense of presence in virtual environments has been investigated. By combining different kinds of auditory feedback consisting of interactive footstep sounds created by ego-motion with static soundscapes, it was shown how motion in virtual reality is significantly enhanced when moving sound sources and ego-motion are rendered [210].

Specifically in our simulations, a number of soundscapes have been designed according to statistically significant indications given by subjects concerning the sonic ecologies they imagined for a specific environment, e.g. a forest. Such soundscapes were composed mainly by assembling freely available recorded material, like that existing in the Hollywood Edge sound effects library and the Freesound website.

A crucial step for the production of ecologically correct soundscapes consists of balancing the loudness of the background sounds with that of the footsteps, conversely lying in the foreground. This balance was again determined by users during

[4] Available at http://www.icst.net/research/projects/ambisonics-tools/

magnitude-adjustment experiments, in which subjects were asked to find out the correct trade-off between the loudness of their own footsteps and the surrounding sounds.

7.5 Evaluating the engines

This section reports on experiments, that were conducted for evaluating the models and techniques described in the previous sections of this chapter.

7.5.1 Auditory recognition of simulated surfaces

The ability of subjects to identify different synthetic ground materials by listening during walking was investigated. In this experiment, subjects were asked to recognize the sounds in an active setting involving microphone acquisition at foot level and subsequent envelope extraction [67] of the subject's walking action. For this reason, the setting was acoustically isolated and subjects were asked to avoid producing sounds other than those generated by their own walking.

7.5.1.1 Methodology and protocol

Sounds were synthesized in real time using the recipes listed in Section 7.3, while subjects were walking across the isolated environment described above.

Participants were exposed to 26 trials, for a total presentation of 13 stimuli each displayed twice in randomized order. The stimuli consisted of footstep sounds on the following surfaces: beach sand, gravel, dirt plus pebbles (like in a country road), snow (in particular deep snow), high grass, forest underbrush (a forest floor composed by dirt, leaves and branches breaking), dry leaves, wood, creaking wood and metal. To increase the ecology of the experiment, footstep sounds on wood, creaking wood and metal were enriched by including some standard room reverberation.

Fifteen participants (six male and nine female), aged between 19 and 29 (mean 22.13, std 2.47), took part in the experiment. All participants reported normal hearing conditions and were naive with respect to the experimental setup and to the purpose of the experiment. They wore sneakers, trainers, boots and other kinds of shoes with rubber sole.

Participants were asked to wear a pair of headphones and to walk in the area delimited by the microphones. They were given a list of different surfaces to be held in one hand, presented as non-forced alternate choice. The list of surfaces presented to the subjects is outlined in the first row of Table 7.3. It represents an extended list of the surfaces the subjects were exposed to.

	BS	GL	DR	SW	HG	UB	DL	WD	CW	MT	WR	CR	MR	FS	CC	PD	WT	CP	—
BS	15	2		5			1							2				1	4
GL		21	2			1	1							4					1
DR		1	3	2		6	6		1					10					1
SW				24	1									4					1
HG	2	7	3	1	0	3	7			2									5
UB		1	3	1		19	1							3				1	1
DL	1	3	5			5	12							4					
WD			1	2				14		1						1	1		10
CW								1	28					1					
MT								1		24				1	2				2
WR									3	11	6				7				3
CR												28			1				1
MR								1					25	1	1				2

Abbreviations:

WD wood	CW creaking wood	SW snow	UB underbrush
— don't know	FS Frozen snow	BS beach sand	GL Gravel
MT metal	HG High grass	DL dry leaves	CC concrete
DR dirt	PD puddles	WT Water	CP carpet
WR wood reverb	MR metal reverb	CR creaking+ reverb	

Table 7.3: Confusion matrix: recognition of synthesized footstep sounds.

At the end of the experiment, subjects were asked to answer some questions concerning the naturalness of the interaction with the system. Every participant took on average 24 minutes to complete the experiment.

7.5.1.2 Results

Table 7.3 shows the confusion matrix which displays the results of the experiment. The first row lists the materials that could be chosen, while the first column lists the materials simulated in the stimuli subjects were exposed to. The decision of providing a wider choice of materials was taken to minimize the statistical significance of subjects guessing at random.

From this table, it is possible to notice how surfaces such as snow, creaking wood with and without reverberation, gravel and metal with reverberation were correctly recognized in a high number of trials. Recognition of surfaces such as dirt plus pebbles, high grass and wood appeared to be low. An analysis performed on the wrong answers reveals that on average subjects tended to mistakenly spread judgments over surfaces belonging to the same category (e.g., wood versus concrete, snow versus frozen snow, dry leaves versus forest underbrush) while keeping different categories distinct in their judgments (e.g., wood versus water, wood versus gravel, metal versus dry leaves).

Moreover, results show that the addition of reverberation to the sounds resulted in better recognitions for metal, and worse for wood, which was perceived most of

MATERIAL	PHYSICAL PROPERTIES	ACOUSTIC PROPERTIES
C , W	Solid	Spectral Cues
G , T	Aggregate	Temporal Cues

Fig. 7.4: Experimental hypothesis. (C: concrete, W: wood, G: gravel, T: twigs.)

the times as concrete. Overall, recognition rates are similar to those measured on recorded footstep sounds [212].

7.5.2 Salience of temporal and spectral cues of walking

Based on the parametric synthesis model described in Section 7.2.5, an experiment has been performed aiming to understand the salience of auditory cues of walking.

The experimental hypothesis was kept simple, by relying on a classification of such cues in spectral and temporal. Furthermore the experiment itself was made offline, in this way focusing on the auditory feedback alone while excluding vision and touch. The complete report on this activity can be found in [96].

We hypothesized that the perception of solid materials is mainly determined by *spectral* cues, conversely the perception of aggregate materials is mainly determined by *temporal* cues. In particular, we experimented using concrete (C) and wooden (W) floors, representative of solid materials, as well as with gravel (G) and dried twigs (T), representative of aggregate materials. The former, such as concrete, marble, wood, are stiff. The latter, such as gravel, dry leaves, sand, allow relative motion of their constituent units and progressively adapt to the sole profile during the interaction. Now,

- solid materials give rise to short, repeatable impacts having a definite spectral color;
- aggregate materials elicit sequences of tiny impacts having distinctive temporal density, that create a sort of “crumpling”, less resonant sound.

Figure 7.4 illustrates the hypothesis.

7.5.2.1 Methodology and Protocol

Subjects were sitting in front of a Mac Pro PC running a Java application communicating (via the *pdj* library) with Puredata, a free software environment for real

time audio synthesis also enabling simple visualizations (through the *GEM* library). They listened to the auditory stimuli through a pair of AKG K240 headphones.

Thirteen male and three female undergraduate computer science students aged aged 22 to 31 (mean = 24.62, std = 2.55) participated in the experiment. Few of them had some experience in sound processing. All of them reported to usually wear snickers.

At the end of the experiment, every subject completed a subjective questionnaire about the realism and ease of identification of the audio stimuli.

One footstep by a normally walking male wearing leather shoes was repeatedly recorded while he stepped over a tray filled with gravel and, then, dried twigs. Recordings were made inside a silent, normally reverberant room using a Zoom H2 digital hand recorder standing 0.5 m far from the tray. For either material, seven recordings were selected and randomly enqueued to create walking sequences lasting 12 s and containing 13 footsteps. In addition to the in-house recordings, high quality samples of a male walking on concrete and on wooden parquet were downloaded from the commercial database `sounddogs.com`. Using these samples, two further walking sequences were created having the same beat and average Sound Pressure Level as of those based on in-house recordings.

Temporal envelopes were extracted from every sequence, by computing the signal

$$e_M[n] = (1 - b[n])|s_M[n]| + b[n]e_M[n-1] \tag{7.10}$$

out of the corresponding sequence s_M, $M \in \mathscr{M} = \{C, W, G, T\}$. (Refer to Figure 7.4 for the meaning of the C, W, G, and T.) As in previous research on synthetic footsteps, the envelope following parameter $b[n]$ was set to 0.8 when $|s_M[n]| > e_M[n-1]$, and to 0.998 otherwise [67]. By following the input when its magnitude is greater than the envelope, and by in parallel allowing a comparably slow decay of the envelope itself when the same magnitude is smaller, this setting ensures that amplitude peaks are tracked accurately, while leaving spurious peaking components off the envelope signal e_M.

By dividing every sequence s_M by its envelope e_M, we computed signals $u_M = s_M/e_M$ in which the temporal dynamics was removed. In other words, we manipulated the footstep sequences so to have stationary amplitude along time.

What remained in u_M was a spectral color, that we extracted with a 48th-order inverse LPC filter h_M^{-1} estimated in correspondence of those parts of the signals containing footstep sounds. Using this filter order, if training the model using *one* footstep then we could not detect differences between the original sound and the correspondingly re-synthesized footstep. We emphasize that the resulting LPC filter in any case estimated one single transfer function, independently of the number of footsteps taken from the original sequence which informed the model. Since we trained the estimator with the entire sequence, the re-synthesized sound had a slightly different color compared to any other footstep belonging to the original sequence.

In the end, for every material M a highly realistic version $\tilde{s}_M$ of the original sequence s_M could be re-synthesized by convolving digital white noise w by the

"coloring" filter h_M, and then multiplying its output, i.e. the synthetic version $\tilde{u}_M$ of u_M, by the envelope signal e_M:

$$\tilde{s}_M[n] = (w * h_M)[n] \cdot e_M[n] = \tilde{u}_M[n] \cdot e_M[n]. \tag{7.11}$$

This technique draws ideas from a family of physically-informed models of walking sounds [67, 304]. In the meantime it provides a simpler, more controlled re-synthesis process avoiding stochastic generation of patterns as in such models. In our case, the silent parts of the four envelopes were tailored to generate synthetic sequences having identical walking tempos. This simple manipulation ensured seamless mutual exchange of the envelopes among sequences, as explained in the following.

Sixteen stimuli were created by adding twelve *hybrid* re-syntheses to the *native* stimuli $\tilde{s}_C$, $\tilde{s}_W$, $\tilde{s}_G$, and $\tilde{s}_T$. Every hybrid stimulus $\tilde{s}_{M_t,M_f}$, $M_t, M_f \in \mathscr{M}$ was defined as to account for the spectral color of material M_f *and* the temporal envelope of material $M_t \neq M_f$:

$$\tilde{s}_{M_t,M_f}[n] = (w * h_{M_f})[n] \cdot e_{M_t}[n] = \tilde{u}_{M_f}[n] \cdot e_{M_t}[n]. \tag{7.12}$$

For each material M_f, we checked that all hybrid temporal manipulations using $M_t \neq M_f$ did not notably alter the spectral information of $\tilde{s}_{M_f}$, and thus its original color. In fact, an inspection of the spectra $E_M(\omega)$ of the various envelopes made by Fourier-transforming e_M, i.e., $E_M(\omega) = \mathscr{F}\{e_M\}(\omega)$, shows that they all have a comparable spectrum. More precisely, all spectra E_C, E_W, E_G, E_T exhibit similar magnitudes, that are shown in Figure 7.5 after removing the respective dc component for ease of inspection. This means that the spectral differences in $\tilde{S}_{M_t,M_f}(\omega)$ caused by multiplying $\tilde{u}_{M_f}$ by e_{M_t}, that is,

$$\tilde{S}_{M_t,M_f}(\omega) = \mathscr{F}\{\tilde{u}_{M_f} \cdot e_{M_t}\}(\omega) = (\tilde{U}_{M_f} * E_{M_t})(\omega), \tag{7.13}$$

are substantially independent of the material, hence almost identical to those introduced in $\tilde{s}_{M_f}$ by its own envelope e_{M_f}.

Symmetrically, the temporal artifacts which are caused by hybridization between two different materials can be considered minor. In fact, because of the LPC design methodology, all filters h_C, h_W, h_G, h_T do transform white noise into a stationary signal independently of the material.

To become confident with the auditory stimuli, subjects trained for some minutes before starting an individual session by selecting and playing each one of the original sequences s_C, s_W, s_G, s_T for several times. Each sequence could be selected by clicking on the corresponding software button in a graphic interface.

Each individual session consisted of 192 trials, obtained by randomly playing each one of the sixteen synthetic stimuli for twelve times. At each trial the subject listened to a stimulus, and selected one material by clicking the corresponding button in the interface. When the button was released, the screen froze for two seconds and changed color to inform subjects of the conclusion of the trial. After this short pause, a new trial was performed.

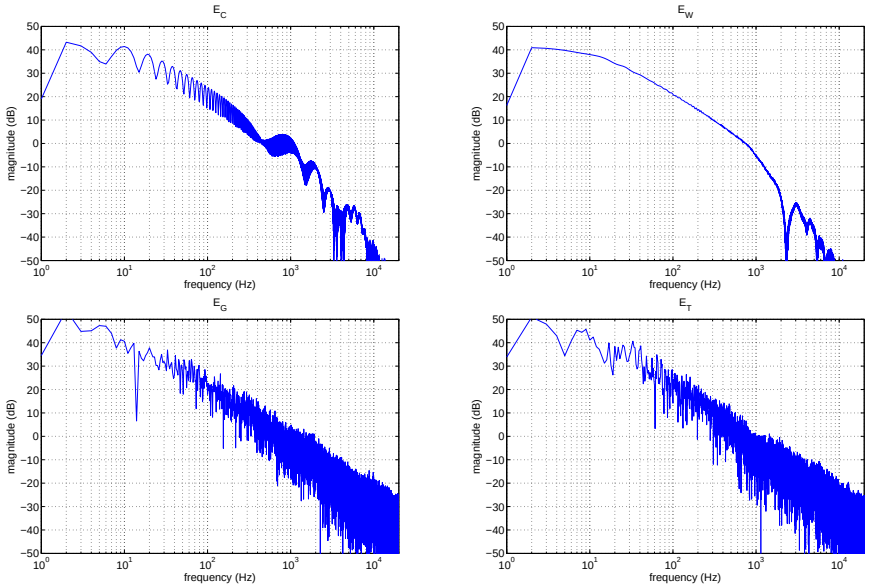

Fig. 7.5: Magnitude spectra of envelopes E_C, E_W, E_G, and E_T. Respective dc components removed for ease of inspection.

The four buttons randomly switched position at each trial. Subjects could temporarily stop the experiment by clicking the pause icon '||' located in the middle of the screen, whenever they wanted to take a short break among trials. It took approximately 45 minutes for each participant to complete the session.

7.5.2.2 Results

For each participant, percentages of selection for the four materials C, W, G, T were analyzed. We considered the fraction of participants who showed significantly correct (random is 25%) material recognitions from the four synthetic stimuli $\tilde{s}_C$, $\tilde{s}_W$, $\tilde{s}_G$, $\tilde{s}_T$, across the twelve repetitions. The critical value (with $\alpha = 0.05$) of the one-tailed binomial test Bin(12,0.25) is 7 trials (i.e., 58.33%): only the participants with an auditory recognition of the original materials higher than 58.33% were included in the analysis. After this check, 16 participants were considered for the recognition of dried twigs, 15 for gravel, 16 for wood, and 10 for concrete.

The results of the analysis are presented in Figure 7.6. In these plots, a bar exhibiting a low percentage means that the correspondingly substituted information (either temporal or spatial) is important for the recognition of the original material, represented by the leftmost bar in the same plot. The difference from random percentage (25%) was tested using one-proportion (two-tailed) z tests.

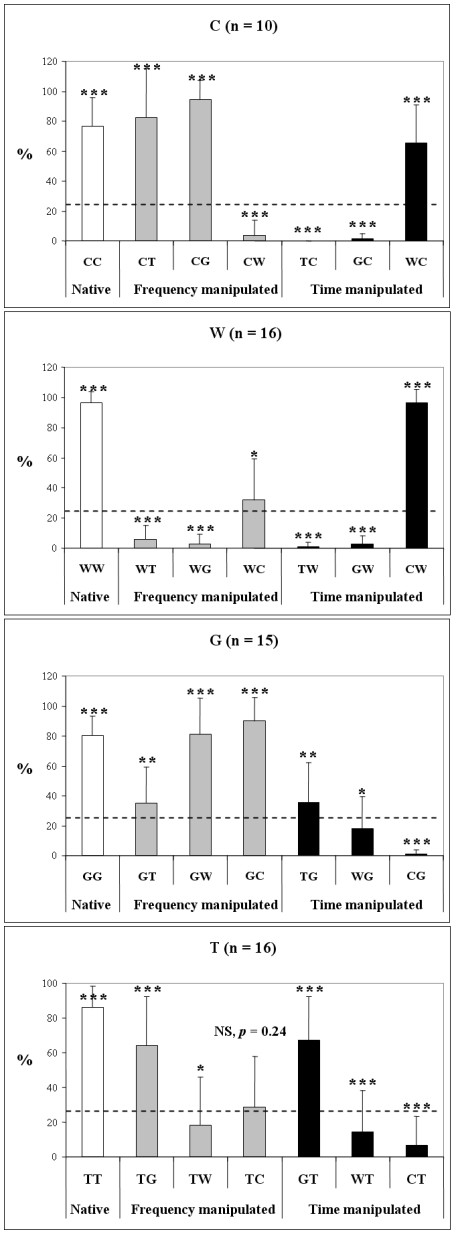

Fig. 7.6: Mean percentages of selection (lines represent std) for C,W,G,T as a function of the auditory stimulus $\tilde{s}_{M_t,M_f}$. The difference from random selection (line at 25%) was tested using one-proportion (two-tailed) z tests. Note: $*: p < 0.05$, $**: p < 0.01$, $***: p < 0.001$, NS: not significant, n: number of subjects.

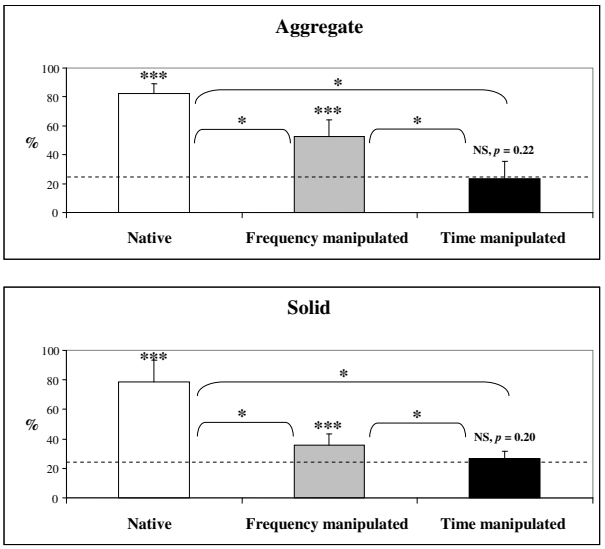

Fig. 7.7: Mean percentages of selection (lines represent std) for material categories (Aggregate and Solid) as a function of the auditory stimulus $\bar{s}_{M_t,M_f}$. The difference from random selection (line at 25%) was tested using one-proportion (two-tailed) z tests. The differences between the three audio conditions were tested with two-proportion z tests (two-tailed and Bonferroni-adjusted alpha level with $p = 0.05/3 = 0.0167$). Note: $*: p < 0.05$, $**: p < 0.01$, $***: p < 0.001$, NS: not significant.

By aggregating the data, we also evaluated the auditory recognition of material categories. Again, this analysis was conducted using data from participants exhibiting an auditory recognition significantly higher than random concerning the two sets of stimuli accounting for the respective categories (24 trials for each category). In this case, the critical value (this time computed by a one-proportion/one-tailed z test to account for the larger number of trials, with $\alpha = 0.05$) is 10 trials, corresponding to 41.67%. All the participants passed the check.

The results of the new analysis are presented in Figure 7.7. For the different percentages of selection, the difference relative to random (25%) was tested using one-proportion (two-tailed) z tests. Thus, for the aggregate category, the percentages of selection in native (82.29%) and frequency manipulated (52.78%) conditions were significantly different from random ($z = 25.98$, $p < 0.001$ and $z = 21.77$, $p < 0.001$, respectively). By contrast, the percentage of selection in the time manipulated condition (23.44%) was not significantly different from random ($z = -1.22$, $p = 0.22$). On the other hand, for the solid category, the percentages of selection in native (78.39%) and frequency manipulated (35.59%) conditions were significantly different from random ($z = 24.16$, $p < 0.001$ and $z = 8.30$, $p < 0.001$, respectively). By contrast, the percentage of selection in the time manipulated condition (26.65%) was not significantly different from random ($z = 1.29$, $p = 0.20$). The differences

between the three audio conditions were tested with two-proportion (two-tailed) z tests.

A correction for experiment-wise error was realized by using Bonferroni-adjusted alpha level (p divided by the number of tests). Thus, in order to compare the three audio conditions (native, frequency manipulated, and time manipulated), the alpha level was adjusted to $p = 0.05/3 = 0.0167$. For the aggregate category, the analysis showed that the native condition was significantly different from the frequency manipulated ($z = 10.23$, $p < 0.05$) and time manipulated ($z = 20.56$, $p < 0.05$) conditions. The difference between frequency manipulated and time manipulated conditions was significantly different ($z = 14.50$, $p < 0.05$) as well. For the solid category, the analysis indicated that the native condition was significantly different from the frequency manipulated ($z = 14.57$, $p < 0.05$) and time manipulated ($z = 17.96$, $p < 0.05$) conditions. The difference between frequency manipulated and time manipulated conditions was also significantly different ($z = 4.63$, $p < 0.05$).

After the experiment, a questionnaire was proposed in which each participant had to grade from 1 to 7 the four native stimuli according to two subjective criteria: realism, and ease of identification. Wilcoxon signed rank (two-tailed) tests with Bonferroni correction showed significant differences only for the realism of sounds: between concrete and dried twigs ($z = -3.28$, $p = 0.001$), and between concrete and gravel ($z = -3.16$, $p = 0.0016$).

7.5.2.3 Discussion and Conclusions

The histograms for concrete and wood in Figure 7.6 show that subjects tolerate swapping between the temporal features of C and W, both belonging to the solid category, conversely the substitution in the same signals with temporal features extracted from aggregate materials (i.e. G and T) harms the recognition. This result is in favor of the initial hypothesis. The effect of spectral manipulations of C and W is more articulate. In this case the hypothesis is essentially confirmed with wood, whose distinctive color cannot be changed using any other spectrum. In parallel, subjects are tolerant to substitutions in C with spectra from aggregate materials. This greater tolerance may be due to the basic lack of distinct color of concrete floors, especially for listeners who usually wear rubber sole shoes such as snickers (indeed the majority of our sample). The same conclusion finds partial confirmation by the greater confidence shown by subjects in recognizing aggregate materials, in the limits of the significance of these data.

The histograms in Figure 7.6 regarding gravel and twigs partially support the initial hypothesis. Time swaps between G and T are tolerated to a lesser extent compared to solid floors. Like before, substituting the temporal features of solid materials in an aggregate sound is not tolerated. Spectral substitutions are not as destructive as they were for solid materials, especially in the case of gravel. The worst situation is when the spectrum of W is substituted in T, again probably due to the distinct color that wood resonances bring into the sound.

Figure 7.7 would further support this discussion. In fact, in spite of the low significance of the data from time manipulations (i.e. black bars), it shows that subjects are primarily sensitive to temporal substitutions between solid and aggregate materials. In parallel, spectral changes are more tolerated during the recognition of aggregate material compared to solid floors.

The proposed experiment has confirmed that solid and aggregate floor materials exhibit precise temporal features, that cannot be interchanged while designing accurate walking sounds. Within such respective categories, spectral color represents an important cue for the recognition of solid materials, conversely sounds of aggregate materials seem to tolerate larger artefacts in their spectra.

7.5.3 Evaluation of soundscapes: interactivity

In two preliminary experiments [301] it was investigated how subjects react to different soundscape dynamics while walking in a virtual auditory scene.

The task of the first experiment was to walk across a circular perimeter inside the walking area in a room. Eight loudspeakers were placed at the angles and middle points of each side of a rectangular floor. The user's position was tracked by a MoCap system, and then used to localize synthetic footsteps along the task through the speakers. Localization was performed using the ambisonics tools for Max/MSP, allowing to move virtual sound sources on a three-dimensional space (refer to Section 7.4.1). During the experiment the loudspeakers were hidden by opaque, acoustically transparent curtains.

During the walk, subjects were exposed to six conditions—again, refer to Section 7.4.1: i) static soundscape; ii) coherent interactive soundscape; iii) incoherent interactive soundscape; iv) static soundscape with static distractors; v) coherent interactive soundscape with dynamic distractors; vi) incoherent interactive soundscape with dynamic distractors. Incoherent means that the footstep sounds were localized opposite to the actual position of the moving subject in the walking area.

Distractors consisted of footstep sounds of a phantom subject walking in the same area. Specifically, static distractors were rendered by displaying their sound with equal intensity from all room loudspeakers, whereas dynamic distractors covered a triangular trajectory inside the circular perimeter.

Participants were exposed to twelve trials, where the six conditions were presented twice in randomized order. Performing each trial took about one minute. Each condition was presented using virtual floors made of wood and forest underbrush. The reason for choosing one solid and one aggregate material was to discern whether the surface type affected the results.

The distractors displayed the same virtual surfaces, but at lower intensity, slightly different timbre, and moderately faster gait cycle.

After the presentation of each stimulus, participants were required to answer the following questions on a seven-point Likert scale:

- How well could you localize under your feet the footstep sounds you produced?

- How well did the sounds of your footsteps follow your position in the room?
- How much did your walk in the virtual environment seem consistent with your walk in the real world?
- How natural did your interaction with the environment seem?
- To what degree did you feel confused or disoriented while walking?

Our hypotheses were that a coherent interactive soundscape would result in improved subjective appreciation and consequent rating; that the incoherent dynamic condition would have been judged as the worst; and that the use of distractors would have decreased the subjective appreciation of the perceived auditory scene, hence its rating.

First, a significant difference was found between the surface materials for what concerns the coherent interactive and static condition, in the case of absence of distractors: the difference between such conditions is negligible in the case of wood, whereas this difference becomes significant in the case of forest underbrush ($p < 0.0001$). Conversely, the same difference was not significant in presence of the distractors.

Secondly, for both materials the incoherent interactive condition gave rise to poorer evaluations in terms of localization, following, consistency and naturalness as well as to less confidence on orientation, both in presence and in absence of distractors. In detail, for both materials significance was found concerning the difference between the coherent and incoherent interactive conditions (for wood: $p < 0.001$ and $p < 0.01$; for forest: $p < 0.000001$ and $p < 0.05$, both respectively with and without distractors), as well as between the static and incoherent interactive conditions (for wood: $p < 0.01$ and $p < 0.01$; for forest: $p < 0.000001$, both respectively with and without distractors).

Thirdly, for both materials the evaluations in absence of distractors were almost always better than in presence of them concerning localization, following, consistency, naturalness and orientation. This difference was significant for the forest underbrush case ($p < 0.05$), whereas for the wood it was not.

For both materials, the disorientation was higher in presence rather than in absence of distractors, but significant differences between these two conditions were found only for the forest underbrush case ($p < 0.05$). The incoherent interactive with distractors condition was rated as the most disorienting for both materials. Conversely, for the forest underbrush case the coherent interactive condition was rated as the least disorienting.

Overall, the coherent interactive condition gave rise to significantly better results than the static one concerning the forest underbrush case in absence of distractors. A subsequent analysis for each of the investigated parameters revealed significant differences between the two conditions only for the "naturalness" parameter ($p < 0.05$).

It is therefore possible to conclude that users can perceive that their interaction with the virtual environment is neither realistic nor natural when the source is not moving coherently with their position. The hypothesis concerning the distractors was confirmed: for both materials, almost always the evaluations in absence of dis-

tractors were better than when the distractors were present, although significant differences were found only for the forest case. In addition, the disorientation was higher in presence of distractors (but significant only for the forest case). This evidence suggests that the use of distractors, i.e., walking sounds evoking the presence of another person walking in the same room as the subject, is likely to influence the perception of self-produced footstep sounds.

Starting from the results of the first experiment we designed a second experiment, investigating in more detail the subjective perception of the static and coherent interactive soundscapes. The task consisted of walking freely inside the walking area. Participants were exposed to fourteen trials, where seven virtual surface materials were randomly presented in presence of both types of soundscapes. Such materials, five aggregate and two solid, consisted of gravel, sand, snow, dry leaves, forest underbrush, wood and metal.

Each trial lasted about one minute. After the presentation of each stimulus participants were required to evaluate, on a seven-point Likert scale, the same questions presented in the first experiment.

The goal of this experiment was to assess whether participants showed a preference for either display method, while exploring the virtual environment during a free walk (i.e., without any predefined trajectory like in the first experiment). Furthermore we were interested in assessing whether the surface property affected the results.

Results show that participants did not show any preference for either method. The answers to the questionnaire were very similar for all the surfaces, with no significant differences. This result suggests that both methods could be used in a virtual environment, to deliver interactively generated footstep sounds. However, other tests should be conducted to add quantitative elements to this conclusion.

7.5.4 Evaluation of soundscapes: ecology

An experiment was conducted aiming at understanding the role of soundscapes in creating a sense of place and context when designing a virtual walking experience [301]. More in detail, the goal of the experiment was to investigate the ability of subjects to recognize the different walking sounds they were exposed to in three conditions: without soundscape, with ecologically coherent soundscape (e.g. footsteps sounds on a soundscape reporting of a beach) and with ecologically incoherent soundscape (e.g. footsteps sounds on a soundscape reporting of a ski slope).

The interactive footsteps were synthesized in real time while subjects were walking using the system described in Section 7.4.1. Offline, the following soundscapes were built: a crowded beach, the courtyard of a farm, a ski slope, a forest, and a garden with trees during fall. All soundscapes were diffused as static.

The task was to recognize the surface material, as well as to evaluate the realism and quality of the footstep sounds. In the conditions with soundscape, participants

were also asked to recognize the surrounding environment in which they were walking.

Results showed that the addition of a coherent soundscape resulted in a better recognition of the surfaces, along with a higher realism and quality of the proposed sound compared to the conditions without and with incoherent soundscape.

For some surface materials, adding a coherent soundscape significantly improved the surface recognition compared to the case in which the soundscape was not provided, and this happened especially with materials whose recognition was difficult without soundscape. Similarly, the percentages of correct answers were higher in the condition with coherent soundscape compared to the condition with incoherent soundscape, significantly for some materials. Furthermore, the same percentages were higher in the condition without soundscape compared to the condition with incoherent soundscape. As expected, adding an incoherent soundscape created an ecological mismatch which often confused the subjects.

The analysis of the wrong answers reveals that in all the experiments none of the proposed aggregate surfaces was confused with a solid one. This means that subjects were able to robustly identify the type of surface.

Regarding the evaluations on the realism and quality of the footsteps sounds in the three conditions, higher evaluations were found in the condition with coherent soundscape compared to the condition without and with incoherent soundscape, as well as for the condition without soundscape compared to that with incoherent soundscape. For some materials these evaluations were statistically significant.

Additionally, the percentages of correct guess of the soundscape were higher with coherent rather than incoherent soundscape.

Overall, subjects observed that soundscapes play an important role in ground surface recognition, precisely for their ability to create a context. Especially in presence of conflicting information, as it was the case with incoherent soundscapes, subjects tried to identify the strongest ecological cues in the auditory scene while performing their recognitions.

This experiment gives strong indication of the importance of context in the recognition of a virtual auditory scene, where walking sounds generated by subjects and soundscapes are combined. Though, it is only a preliminary investigation: further experiments are needed to gain a better understanding of the cognitive factors involved when subjects are exposed to different sound events, especially when a situation of semantic incongruence is present.

7.6 Conclusions

This chapter provided a description of how to synthesize walking sounds using physics-based and physically inspired models, including recipes for constructing and parameterizing model compositions dictated by the designer's experience and taste. Several surfaces have been simulated, both solid and aggregate. The simula-

tions work in real time and are controlled by kinds of input devices such as those described in Chapter 2.

After reporting on current auditory display possibilities, we also described experiments whose aim was to assess the ability of subjects to recognize the simulated surfaces, the saliency of temporal and frequency cues in footstep sounds, the role of soundscapes in enhancing the interactivity and ecological realism of an auditory scene. These experiments validate the quality of the proposed synthesis engines, and testify their possibilities and limits to faithfully recreate virtual walking experiences.

Chapter 8
Multisensory and haptic rendering of complex virtual grounds

G. Cirio, Y. Visell, and M. Marchal

Abstract The addition of vibrotactile and, more generally, multimodal feedback when interacting with a virtual environment is fundamental when aiming at fully immersive and realistic simulations. This is particularly true when using natural navigation paradigms such as walking for the exploration of virtual environments. Tactile perceptual cues generated by a ground surface can provide crucial information regarding the ground material itself, the surrounding environment and specificities of the foot-floor interaction, such as gait phase or forces, and can even reflect user emotions. This chapter addresses the multimodal rendering of walking interactions with virtual ground surfaces, incorporating vibrotactile, acoustic and graphic rendering to enable truly multimodal experiences. Taking advantage of the availability of novel multimodal floor surfaces (see Chapters 2 and 3), we propose different models for the rendering of vibrotactile and multi9modal cues from the foot-based interaction with two categories of complex ground materials that exhibit strong high-frequency components: granular materials and fluids.

8.1 Context

Virtual reality (VR) applications aim at simulating digital environments with which users can interact and, as a result, perceive through different modalities the effects of their actions in real time. In real life, we interact with our surrounding environment with our five senses. Ideally, this should also be the case in a VR simulation. However, most VR simulators built to date contain visual displays, vision-based or mechanical tracking devices to monitor the position of users and props, and spatialized sound displays, but neglect the haptic sense, or sense of touch, not to mention those of olfaction (smell) and gustation (taste). Consequently, current typical VR applications rely primarily on vision and hearing.

Because touching is an integral part of our experience of the world, in order to improve the immersion of users in virtual environments, haptic (force and/or tactile)

feedback is essential, to enable users to touch, feel, and manipulate objects. Virtually all tasks we accomplish in real life involve bodily interaction with the environment. It also appears to be true that a higher sense of presence can be achieved in a VR simulation through the addition of even low-fidelity tactile feedback to an existing visual and auditory display than can be accomplished by improving one particular modality such as the visual display alone [276].

Just as the synthesizing and rendering of visual images defines the area of computer graphics, the art and science of developing devices and algorithms that synthesize computer generated force-feedback and vibrotactile cues is the concern of computer haptics [30]. Haptics broadly refers to touch interactions (physical contact) that occur for the purpose of perception or manipulation of objects [263].

During walking interactions, low-frequency forces due to movements of a walker's lower body generate low-frequency ground reaction forces as well as higher frequency acoustic and vibrotactile signals due to foot interaction with the ground material. In this chapter, we focus on the high frequency components of mechanical signals generated during walking interactions, which are readily reproduced via relatively low cost vibrotactile display devices or by auditory displays. Specifically, we study the the modeling and simulation of different ground materials allowing the multimodal rendering of foot-ground interaction, with special emphasis on the vibrotactile modality, but also incorporating the acoustic and visual sensory channels.

8.1.1 Vibrotactile rendering of virtual materials

Tactile rendering refers to the process by which sensory stimuli are computed using a software algorithm in order to convey information about a virtual object through the tactile modality. Vibrotactile displays primarily address the human haptic ability to perceive high-frequency mechanical stimuli, with frequency content distributed primarily between 30 Hz and 800 Hz. Vibrotactile rendering algorithms gather data from the environment, such as the feet position and the physical attributes of the virtual objects (shape, elasticity, texture, mass, etc), and compute the vibrotactile signals that would result from these interactions. The design of the rendering algorithm is crucial for an accurate stimuli restitution: a simple pre-computed signal (e.g., the playback of a pre-recorded impact force transient signal) is likely to feel different than a more complex signal generated using a physically-based model, since the latter can vary depending on the physical parameters governing the interaction.

Transient signals have been used at the moment of impact to improve the perception of contact with rigid bodies of different material. Okamura et al. [217] recorded real, high resolution acceleration information by tapping on different materials with a measuring instrument. This data was fit to decaying sinusoidal signals of the form $S(t) = A(v) \exp -Bt \sin(\omega t)$, where $A(v)$ is the amplitude depending on the tool velocity, B is a decay constant, and ω the oscillation frequency. Therefore, impacts with each captured material was represented by a different vibration signature. This vibrotactile signal was then rendered by an appropriate vibrotactile transducer at the

moment of impact, successfully conveying perceptual information about the material hardness.

However, transducers do not exactly reproduce what is recorded through other devices. Hence, Okamura's technique was later improved [216] to compensate for device dynamics and rendering bandwidth by applying scaling factors found through human perceptual experiments for a given transducer. This lead to the rendering of realistic signals corresponding to materials such as rubber, wood and aluminum, but had the main drawback of requiring a perceptual tuning step for each transducer. Kuchenbecker et al. [155] addressed this issue by adapting the signal to the dynamic response of the device using an inverted system model of the display. This enabled the rendering of realistic impacts from recorded force patterns. Further studies by Fiene et al. improved this technique by considering the grip force applied to the device [94].

8.1.2 Contributions

In the context of natural walking, prior work has not addressed the vibrotactile rendering of walking interactions with virtual grounds. Yet, including tactile cues when exploring virtual environments would bring major benefits in the fields of medical rehabilitation for gait and postural exercises, training simulations for the recreation of compelling and realistic grounds, and entertainment for improved immersion within rich virtual environments.

Taking advantage of the availability of novel multimodal floor surfaces (see Chapters 2 and 3), we propose different models for the rendering of vibrotactile and multimodal cues from the foot-based interaction with two categories of complex ground materials that exhibit strong high-frequency components: granular materials and fluids.

Footsteps onto granular (aggregate) ground materials, such as sand, snow, or ice fragments belie a common temporal process originating with the transition toward a minimum-energy configuration of an ensemble of microscopic systems, via a sequence of transient events. The latter are characterized by energies and transition times that depend on the characteristics of the system and the amount of power it absorbs while changing configuration. They dynamically capture macroscopic information about the resulting composite system through time. On the other hand, liquid-covered ground surfaces, such as water puddles and shallow pools, have an important kinesthetic component due to pressure and viscosity forces within the fluid, and may, at first, seem to lack high frequency mechanical responses. However, important high frequency components exist, as generated by bubble and air cavity resonances, which are responsible for the characteristic sound of moving fluids. We utilize the fact that vibrotactile and acoustic phenomena share a common physical source by designing our vibrotactile models based on existing knowledge of fluid sound rendering. Both types of ground materials exhibit very interesting high frequency features adequate for their restitution through an actuated vibrotac-

tile floor: as opposed to rigid surfaces, the overall signal is not reduced to transients at the moment of impact, but can produce a signal during the entire foot-floor contact duration.

Although mainly focused on the vibrotactile modality, our approaches are multimodal. The same models can be used to synthetise acoustic feedback, due to vibrotactile and acoustic phenomena common generation mechanisms and physical source. The visual modality is an absolute requirement on its own, since interacting with virtual environments without visual feedback is of little interest, except in very specific cases.

8.2 Walking on disordered natural materials

In this section, we present techniques to enable users to interact on foot with simulated natural ground surfaces, such as soil or ice, in immersive virtual environments, using the interface and interaction techniques described in Chapter 3. Position and force estimates from in-floor force sensors are used to synthesize plausible auditory and vibrotactile feedback in response. Relevant rendering techniques are discussed in the context of specific interactive scenarios, involving walking on a virtual frozen pond or bed of sand.

Sensations accompanying walking on natural ground surfaces in real world environments (sand in the desert, or snow in winter) are multimodal and highly evocative of the settings in which they occur [310]. Limited prior research has addressed foot-based interaction with VR and AR environments [161, 310], perhaps due to a lack of efficient techniques for capturing foot-floor contact interactions and rendering them over distributed floor areas, and the emerging nature of the applications involved.

Here, we present a novel solution using a network of instrumented floor tiles, and methods for capturing foot-floor contact interactions so as to render multimodal responses of virtual ground materials.

8.2.1 Vibrotactile rendering of stepping on disordered heterogeneous materials

Due to the highly interactive nature of the generation of haptic stimuli in response to foot-applied pressure, the display of haptic textures, in the form of high frequency vibrations simulating the feel of stepping onto heterogeneous solid ground materials [309], is a significant challenge to be overcome in the multimodal rendering of walking on virtual ground surfaces. During a step onto quasi-brittle porous natural materials (e.g., sand or gravel), one evokes physical interaction forces that include viscoelastic components, describing the recoverable deformation of the volume of the ground surrounding the contact interface; transient shocks from the impact of foot against the ground; and plastic components from the collapse of brittle struc-

tures or granular force chains, resulting in unrecoverable deformations [80, 280]. Combinations of such effects give rise to the high frequency, texture-like vibrations characteristic of the feel of walking on different surfaces [88]. Figure 8.1 presents an example of force and vibration data acquired by the authors from one footstep on a gravel surface. Because the vibration signature is continuously coupled to the force input over time in such examples, there is no straightforward way to convincingly use recorded footstep vibrations for vibrotactile rendering, although more flexible granular sound-synthesis methods could be used [29, 71]. For the modeling of simpler interactions, involving impulsive contact with solid materials, recorded transient playback techniques could be used [155].

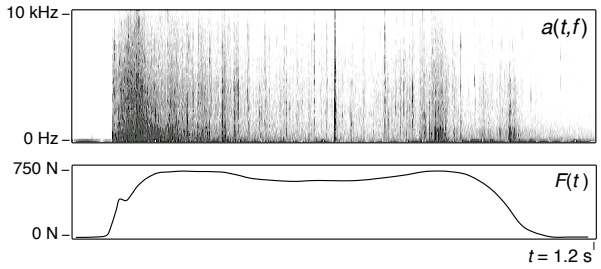

Fig. 8.1: Vibration spectrogram $a(t,f)$ and normal force $F(t)$ measured from one footstep onto rock gravel (Authors' recording). Note the discrete (impulsive) broadband impact events evidenced by vertical lines in the spectrogram.

A simple yet physically-motivated approach we have taken to the haptic synthesis of interaction with such surfaces is based on a minimal fracture mechanics model, drawing on an approach that has also proved useful for modeling other types of haptic interaction involving damage [114, 181]. Figure 8.2 illustrates the continuum model and a simple mechanical analog used for synthesis. In the stuck state, the surface has stiffness $K = k_1 + k_2$, effective mass m and damping constant b. It undergoes a displacement x in response to a force F, as governed by:

$$F(t) = m\ddot{x} + b\dot{x} + K(x - x_0), \quad x_0 = k_2\xi(t)/K \tag{8.1}$$

In the stuck state, virtual surface admittance $Y(s) = \dot{x}(s)/F(s)$ is given, in the Laplace-transformed (s) domain, by:

$$Y(s) = s(ms^2 + bs + K)^{-1}, \quad K = k_1k_2\xi/(k_1 + k_2) \tag{8.2}$$

where $\xi(t)$ represents the net plastic displacement up to time t. A Mohr-Coulomb yield criterion is applied to determine slip onset: When the force on the plastic unit exceeds a threshold value (which may be constant or noise-dependent), a slip event generates an incremental displacement $\Delta\xi(t)$, along with an energy loss of ΔW representing the inelastic work of fracture growth.

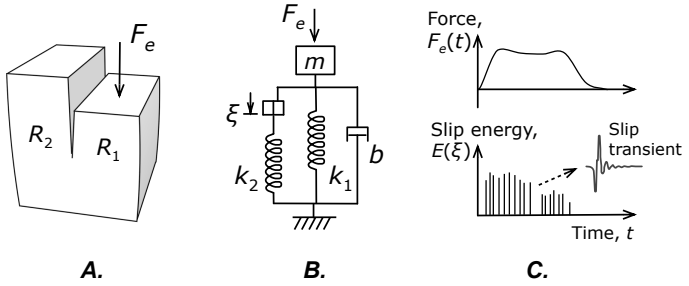

Fig. 8.2: Normal force texture synthesis. *A.* A fracture mechanics approach is adopted. A visco-elasto-plastic body undergoes shear sliding fracture due to applied force F_e. *B.* A simple mechanical analog for the generation of slip events $\xi(t)$ in response to F_e. *C.* For vibrotactile display, each slip event is rendered as an impulsive transient using an event-based approach.

Slip displacements are rendered as discrete transient signals, using an event-based approach [155]. High frequency components of such transient mechanical events are known to depend in detail on the materials and forces of interaction, and we model some of these dependencies when synthesizing the transients [313]. An example normal force texture resulting from a footstep load during walking is shown in Figure 8.3).

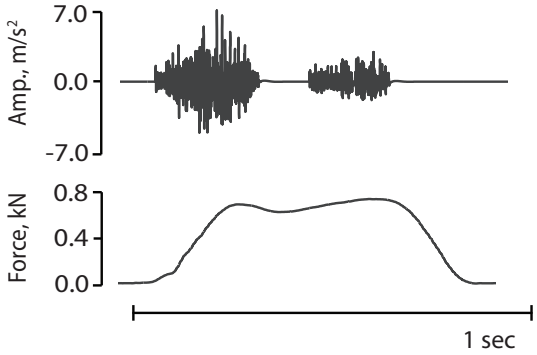

Fig. 8.3: Example footstep normal force and synthesized waveform using the simple normal force texture algorithm described in the text. The respective signals were captured through force and acceleration sensors integrated in the vibrotactile display device described in Chapters 2 and 3.

8.2.2 Multimodal rendering of material interactions with a virtual frozen pond

Based on the interface and interaction techniques presented in Chapter 3, we designed a virtual frozen pond demonstration that users may walk on, producing patterns of surface cracks that are rendered and displayed via audio, visual, and vibrotactile channels (Figure 8.4). The advantage of this scenario is that plausibly realistic visual feedback could be rendered without detailed knowledge of foot-floor contact conditions, which would require a more complex sensing configuration.

Fig. 8.4: Still images of users interacting with the simulated frozen pond.

8.2.2.1 Non-visual rendering

In the demonstration, audio and vibrotactile feedback accompany the fracture of the virtual ice sheet underfoot. The two are derived from a simplified mechanical model. Fracture events are characterized via an event time t_i and energy loss E_i. Figure 8.5 illustrates the local continuum description and a simple mechanical analog used for synthesis. In this model, in the stuck state, the surface has stiffness $K = k_1 + k_2$ and is governed by:

$$F(t) = m\ddot{x} + b\dot{x} + K(x - x_0), \quad x_0 = k_2\xi(t)/K \tag{8.3}$$

where $\xi(t)$ represents the net plastic displacement up to time t. A Mohr-Coulomb yield criterion determines slip onset: When the force F_ξ on the plastic unit exceeds a threshold F_0 (either a constant value or one sampled from a random process), a slip event is generated with energy loss E_i, representing the inelastic work of frac-

ture growth. E_i is sampled from an exponential distribution $p(E) \propto E^{-\gamma}$ with a scale parameter γ that is, for many fracture processes, an approximate invariant of the material medium [310]. Slip displacements are rendered as transients given by a coupled model consisting of a nonlinear impulse coupled with a bank of modal oscillators with impulse response $s(t) = \sum_i a_i e^{-b_i t} \sin(2\pi f_i t)$, determined by amplitudes a_i, decay rates b_i, and frequencies f_i [23, 258]. A transient impulse at time t_0 is modeled phenomenologically as a nonlinear viscoelastic impact with effective force $f(t) \propto \Delta W$, simulated via the Hunt-Crossley impact model [131]

$$f(t) = kx(t)^{\alpha} - \lambda x(t)^{\alpha} \dot{x}(t)\,. \tag{8.4}$$

$x(t)$ is the compression displacement and $\dot{x}(t)$ is the compression velocity. The impact has effective parameters governing stiffness k, dissipation λ, and contact shape α.

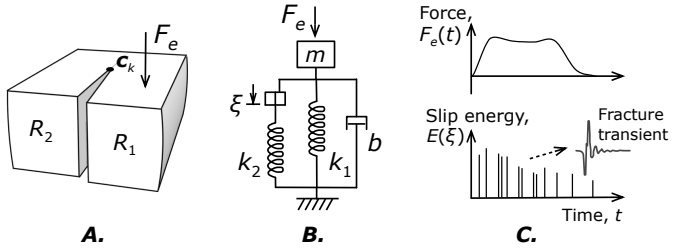

Fig. 8.5: *A.* Behavior at the crack front $\mathbf{c}_k$ is modeled using a simplified fracture mechanics treatment. A visco-elasto-plastic body undergoes shear sliding fracture. *B.* A simple mechanical analog. *C.* Each slip event is rendered as an impulsive transient.

8.2.2.2 Visual animation and control

Brittle fracture in computer graphics is often animated by simulating the inelastic evolution of a distributed stress state [231, 215]. Here, we adopted a simplified simulation technique in order to fuse the local temporal crack-growth model given above with a heuristic for spatial crack pattern growth. The contact centroid $\mathbf{x}_c$ summarizes the local stress due to the load from a foot. A fracture pattern consists of a collection of crack fronts, defined by linear sequences of node positions, $\mathbf{c}_0, \mathbf{c}_1, \ldots, \mathbf{c}_n$. Fronts originate at seed locations $\mathbf{p} = \mathbf{c}_0$. The fracture is rendered as line primitives $\ell_k = (\mathbf{c}_k - \mathbf{c}_{k-1})$ on the ice sheet (Figure 8.6). Seed locations $\mathbf{p}$ are determined by foot-floor contact. A crack event initiated by the audio-tactile process at time t_i with energy $E(t_i)$ results in the creation of a new seed or the growth of fractures from an existing one. In the former case, a new seed $\mathbf{p}$ is formed at the location of the dominant contact centroid $\mathbf{x}_c$ if no existing seed lies within distance Δp. The seed $\mathbf{p}$ is created with a random number N_c of latent crack fronts, $\mathbf{c}_0^1, \mathbf{c}_0^2, \ldots \mathbf{c}_0^{N_c}$. We sample N_c

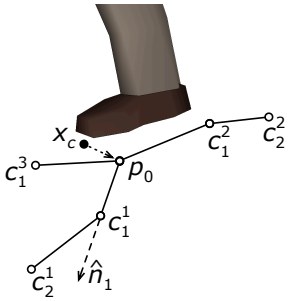

Fig. 8.6: A crack pattern, modeled as a graph of lines between nodes $\mathbf{c}_i$ extending from the seed location p_0.

uniformly in $2,3,\ldots 6$, so that the cracks propagate outward from the initial contact position. A crack front propagates from a seed $\mathbf{p}$ nearest to $\mathbf{x}_c$. With probability $1/N_c$ the jth crack front of $\mathbf{p}$ is extended. Its growth is determined by a propagation vector $\mathbf{d}_m^j$ such that $\mathbf{c}_m^j = \mathbf{c}_{m-1}^j + \mathbf{d}_m^j$. We take $\mathbf{d}_m^j = \alpha E \hat{\mathbf{n}}_m^j$, where E is the crack energy, α is a global growth rate parameter, and $\hat{\mathbf{n}}_m^j$ is the direction. Since we lack information about the principal stress directions at the front, we propagate in a random direction given by $\hat{\mathbf{n}}_m^j = \hat{\mathbf{n}}_{m-1}^j + \beta\hat{\mathbf{t}}$, where $\beta \sim N(\beta;0,\sigma)$ is a Gaussian random variable and $\hat{\mathbf{t}} = \hat{\mathbf{n}}^j \times \hat{\mathbf{u}}$, where $\mathbf{u}$ is the upward surface normal (i.e., $\mathbf{t}$ is a unit vector tangent to $\hat{\mathbf{n}}^j$). The initial directions at $\mathbf{p}$ are spaced equally on the circle.

8.3 Walking on fluids

Water and other fluids have been largely ignored in the context of vibrotactile feedback. For VR simulations of real-world environments, the inability to include interaction with fluids is a significant limitation. The work described here represents an initial effort to remedy this, motivated by our interest in supporting multimodal VR simulations such as walking through puddles or splashing on the beach, as shown in Figure **??**. Further applications include improved training involving fluids, such as medical and phobia simulators, and enhanced user experience in entertainment, such as when interacting with water in immersive virtual worlds.

To this end, we introduced the first physically based vibrotactile fluid rendering model for solid-fluid interaction. Similar to other rendering approaches for virtual materials, we profit from the fact that vibrotactile and acoustic phenomena share a common physical source. Hence, we base the design of our vibrotactile model on prior knowledge of fluid sound rendering. Since fluid sound is generated mainly through bubble and air cavity resonance, we enhanced a fluid simulator with real-time bubble creation and solid-fluid impact mechanisms, and can synthesize vibrotactile feedback from interaction and simulation events. Using this approach, we explored the use of bubble-based vibrations to convey fluid interaction sensations to

users. We render the feedback for hand- or foot-based interaction, engendering rich perceptual experiences of interacting with water features.

8.3.0.3 Acoustic models for fluid rendering

We aim at leveraging real-time fluid sound synthesis algorithms to generate the relevant vibrotactile feedback. Those techniques that are physically based rely on the oscillation of air bubbles trapped inside the fluid volume [256] to produce sound. The first bubble sound synthesis technique was proposed in Van den Doel's seminal work [81] where, based on Minnaert formula [189], he provides a simple algorithm to synthesize bubble sounds based on a few parameters. However, the synthesis was not coupled to a fluid simulation. This is achieved by Drioli et al. [83] through an ad-hoc model for the filling of a glass of water, based on the height of the fluid inside the glass and on collision events. Moss et al. [197] propose a simplified, physically inspired model for bubble creation, designed specifically for real-time applications. It uses the fluid surface curvature and velocity as parameters for bubble creation and a stochastic model for bubble sound synthesis based on Van den Doel's work [81]. However, the model is designed for a shallow water simulator, which greatly reduces interaction possibilities by allowing only surface waves, precluding splashes and object penetration.

Inspired by the physically based fluid sound synthesis work of Moss et al. [197], and utilizing a particle-based fluid model [194], we develop an efficient bubble generation technique and introduce a novel vibrotactile model. This enables rich body-fluid interactions with vibrotactile and multimodal cues.

8.3.0.4 Overview of the approach

When an object vibrates under an applied force, a pressure wave is generated at its surface, traveling to the subject's ears and mechanoreceptors. We motivate our vibrotactile approach, based on sound generation mechanisms, on the fact that acoustic and tactile feedback are both vibrations that share a common physical source.

By comparing film frames with the air-borne generated sound, Richardson [256] provides an explanation for the process of a projectile impacting and entering a fluid volume. The impact produces a "slap" and projects droplets, while the object penetration creates a cavity that is filled with air. The cavity is then sealed at the surface, creating an air bubble that vibrates due to pressure changes. Smaller bubbles can spawn from the fragmentation of the main cavity, as well as from the movement of the fluid-air interface, such as when the droplets return to the fluid volume.

Our vibrotactile model is therefore divided in three components, following the physical processes that generate sound during solid-fluid interaction [256, 100]: (1) the initial high frequency impact, (2) the small bubble harmonics, and (3) the main cavity oscillation. As a consequence, it is highly dependent on the efficient genera-

tion and simulation of air bubbles within the fluid. Hence, a real-time fluid simulator enhanced with bubble synthesis is required on the physical simulation side.

Figure 8.7 provides an overview of our approach. The physical simulator automatically detects the solid-fluid impacts and the creation of air bubbles caused by interaction between a solid (such as a foot, a hand or an object) and the fluid volume. For each of these events, it sends the corresponding message to the vibrotactile model, which synthesizes a vibrotactile signal according to the simulation parameters. The signal is then output through a specific vibrotactile device, such as an actuated tile for foot-fluid interaction, or a hand-held vibrator for hand-fluid interaction.

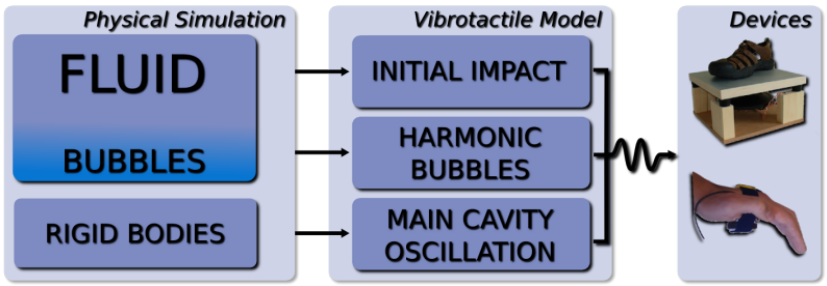

Fig. 8.7: Overview of our approach: the physical simulation computes the different parameters that are fed to the 3-step vibrotactile model, producing the signal sent to the various vibrotactile displays.

8.3.0.5 Fluid simulation with bubbles

The first building block of our approach is the fluid volume itself: we require a physically based real-time fluid simulation. Among existing fluid simulation techniques, the Smoothed-Particle Hydrodynamics (SPH) [194] model fulfills our requirements well, since the resulting fluid is unbounded, fast to compute and preserves small-scale details such as droplets. It is based on a set of particles discretizing the simulated media and conveying different physical properties, such as mass and viscosity. The motion of fluids is driven by the Navier-Stokes equations. Using the implementation of these equations in the SPH model [199], pressure and viscosity forces are computed at each time step. Rigid bodies are simulated as a constrained set of particles. For further details on SPH fluids, we refer the reader to [199].

As previously explained, in order to achieve vibrotactile interaction with fluids we need to simulate the bubbles inside the fluid. Since we only seek bubble creation events resulting in bubble sound synthesis, a bubble has a very short life span within our model, and can be seen more as an event than as the actual simulation of a pocket

of air. Hence, we adopt and simplify an existing SPH bubble synthesis algorithm [200] to obtain an efficient bubble creation and deletion mechanism.

A bubble is spawned when a volume of fluid entraps a volume of air. In order to detect this phenomenon within the SPH simulation, we compute an implicit color field c^p as in the method of Muller et al. [200]. This color field estimates the amount of neighboring particles (fluid, rigid and bubble) around any position in space, while its gradient ∇c^p estimates in which direction the surrounding particles are mainly located. At each timestep, we compute ∇c^p at each fluid particle position with:

$$\nabla c_i^p(\mathbf{x}_i) = \sum_j V_j \nabla W(\mathbf{x}_i - \mathbf{x}_j, h) \tag{8.5}$$

A fluid particle i triggers a bubble creation if the following conditions are fulfilled:

1. The vertical component of ∇c_i^p is positive: the fluid particle has most of its surrounding particles above it, creating a pocket of air under it.
2. The magnitude of the velocity of the particle is above a threshold: still or slow moving fluid particles do not generate bubbles.

A bubble is destroyed when it is no longer entrapped by fluid or held by a rigid body. Since we only use bubbles for triggering events, a bubble is also destroyed if it is alone in the surrounding media. To this end, we compute another implicit color field, c^b, which only considers bubble particles, thus estimating the amount of neighboring bubbles surrounding a point in space. A bubble i is destroyed if one of the following conditions is fulfilled:

1. The vertical component of ∇c_i^p is negative: the bubble particle has most of its surrounding particles under it, and the air cannot be trapped anymore.
2. The color field c_i^b is null: the particle is alone inside the media.

8.3.0.6 Vibrotactile model

Our vibrotactile model receives the events from the physical simulation, and can synthesise a signal consisting of three components: the initial high frequency impact, the small bubble harmonics, and the main cavity oscillation. This is illustrated in Figure 8.8.

Initial impact

During rigid body impacts on a fluid surface, Richardson [256] observed a damped high-frequency and low amplitude sound immediately after the impact, later explained as a guided acoustic shock [170]. To the best of our knowledge, no model provides the equations for air pressure oscillations due to a rigid body impact on a fluid surface. Previous work has been able to model the phenomenon to some extent, only for very simple shapes and specific penetration cases [130]. Nevertheless,

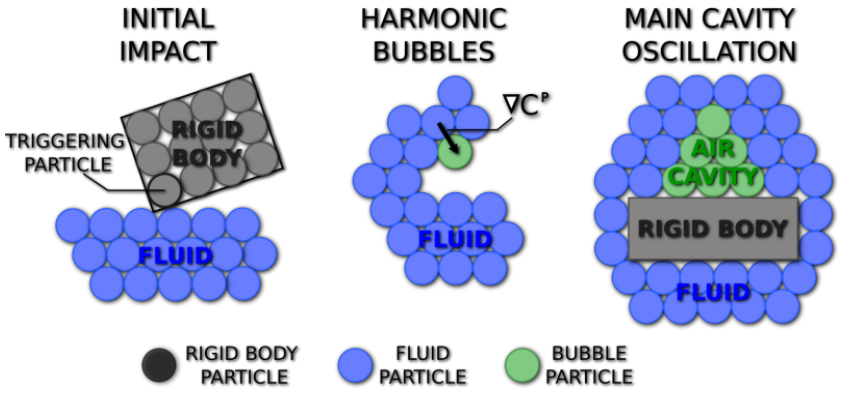

Fig. 8.8: The three components of our vibrotactile model.

the short duration of the impact does not justify a computationally expensive implementation. Hence, similar to previous work [83], we follow a physically inspired approach exploiting the short and burst-like nature of the vibration.

Synthesis

The impact signal is synthesized in a three step approach. A burst of white noise is first generated, spanning on the vibrotactile frequency range with a given base amplitude A. The signal is then fed to a simple envelope generator in order to modulate its amplitude. The signal rises exponentially during an attack time t_a, from nil to the original amplitude A, followed by an exponential decay of release time t_r, mimicking the creation and attenuation of the short and highly damped impact. Last, the modulated signal excites an elementary resonator. For this, a second-order resonant filter is used, creating a resonance peak around a central frequency w_0. The impact signal is therefore approximated as a resonating burst of white noise, with parameters to control its amplitude (A), duration (t_a, t_r) and central frequency (w_0).

Control

An impact event is triggered when the distance between a rigid body particle and a fluid particle is below the smoothing radius. Since only the particles at the surface of the rigid body have to be taken into account to avoid false triggers, a new implicit color field c^r is computed only considering rigid body particles: particles belonging to the lowest level sets of c^r belong to the surface. Richardson [256] observed that, in general, the intensity of the impact sound between a rigid body and a fluid is proportional to v^3, where v is the speed of the body at the moment of impact. Hence, after detecting an impact, we can synthesize an impact signal of amplitude A proportional to v^3. We use the same manually set duration and central frequency parameters for all impacts.

Harmonic bubbles

Small bubbles are generated by small pockets of air trapped under the water surface. Splashes and underwater cavity fragmentation are two causes for small bubble generation. By approximating all bubbles as spherical bubbles and relying on our SPH simulation enhanced with bubble generation, we can easily synthesize and control this component of the model.

Synthesis

Following van den Doel [81], we modeled the bubble as a damped harmonic oscillator. The pressure wave $p(t)$ of an oscillating spherical bubble is given by

$$p(t) = A_0 \sin(2\pi t f(t)) e^{-dt} \tag{8.6}$$

A_0 being the initial amplitude, $f(t)$ the resonance frequency and d a damping factor.

Minnaert's formula [189] approximates the resonance frequency f_0 of a spherical bubble in an infinite volume of water by $f_0 = 3/r$, where r is the bubble radius. In order to account for the rising in pitch due to the rising of the bubble towards the surface, Van den Doel [81] introduces a time dependent component in the expression of the resonant frequency: $f(t) = f_0(1 + \xi dt)$, with $\xi = 0.1$ found experimentally. Taking into account viscous, radiative and thermal damping, the damping factor d is set to $d = 0.13/r + 0.0072r^{-3/2}$. As for the initial amplitude A_0, previous work [176] suggests, after empirical observations, that $A_0 = \varepsilon r$ with $\varepsilon \in [0.01; 0.1]$ as a tunable initial excitation parameter. For a detailed explanation of the different hypothese and equations, we refer the reader to [197] and [81] .

Control

Our bubble vibration synthesis algorithm allows the generation of bubble sounds based on two input parameters: the bubble radius r and the initial excitation parameter ε. Using our SPH simulation, we couple the vibration synthesis with bubble creation events and automatically select the aforementioned parameters.

If we wanted to simulate the fluid and the bubbles at a scale where the particle radius matches the smallest bubble radius that generates a perceivable vibration (12mm for a 250Hz frequency), we would require around a million particles for a cubic meter of fluid. Achieving real-time performances with this number of particles is currently highly challenging for common hardware. Since we cannot directly link the particle radius to the resonating bubble radius, we transpose the physically inspired approach of Moss et al. [197] to determine the radius and excitation parameters from statistical distributions: power law distributions are used both for r and ε, within the ranges allowed by each parameter. When a bubble is created, values for r and ε are sampled, and sent to the signal synthesis algorithm.

Main cavity oscillation

The main cavity is a large bubble that produces a characteristic low-frequency bubble-like sound. By modeling the cavity as a single bubble with a large radius, we can rely on our harmonic bubble synthesis and control algorithms for this second component of our vibrotactile model.

Synthesis

As in the case of the harmonic bubble component, we use Equation 8.6 to synthesize the vibration produced by the oscillation of the main cavity. Since we will be using larger values for r, the resulting vibration will be of a much lower frequency, coherent with what we hear in real life. ε is set to 0.1 since no variability is desired.

Control

In order to detect the formation and collapsing of the main cavity during object penetration, we track the grouping of individual bubbles within our SPH simulation. Bubbles are spawned and stay alive when a cavity begins its closing and collapsing process, until they fill most of the cavity volume, as illustrated in Figure 8.8 and rendered in Figure **??** (right, bubbles in blue). At this point, there are bubbles within the cavity that are surrounded exclusively by other bubbles. These bubbles are detected when their color field c^b is above a threshold. If such a particle is detected, there is a potential cavity collapse.

Starting from the detected particle, we perform a search for neighboring bubbles to find the extent of the cavity. Bubble neighbors are added to the set of cavity bubbles, and the process is repeated on the new neighbors until no new neighbor is added. As the search is executed on the GPU, an iterative implementation is required, with one thread per new bubble neighbor, benefiting from our accelerated neighbor search algorithms. During our experiments, we required less than 5 search cycles to account for all the bubbles inside a cavity.

The total number N_b of cavity bubbles is proportional to the volume of the cavity. Since the cavity is modeled as a single large spherical bubble in the signal synthesis algorithm, its radius r can be deduced from the volume of the cavity. Hence, the number of cavity bubbles is mapped to the radius r of the spherical cavity, with user-defined minimal (r^{min}) and maximal (r^{max}) values: $[N_b^{min}, N_b^{max}] \rightarrow [r^{min}, r^{max}]$.

8.4 Multimodal rendering of fluids

Our fluid vibrotactile model is implemented in PureData, while the SPH fluid and bubble simulation are implemented on GPU [62]. The communication between the SPH simulation and the acoustic model is handled through the Open Sound Control (OSC) protocol. Each time a bubble, cavity or impact event is detected in the fluid

simulation, an OSC message is sent to the acoustic model with the corresponding parameters for sound synthesis. Since our vibrotactile model is built from sound generation mechanisms, we are able to produce acoustic feedback using the same model, by displaying the signal through a speaker and in the 12 Hz - 20 kHz range.

Kinesthetic feedback can also be rendered through a suitable haptic device, such as a multiple degrees-of-freedom force-feedback manipulator. The approach is described in previous work [62], using the same SPH fluid and rigid body simulation model.

We designed three scenarios representing three possible interaction conditions with multimodal feedback. See Figures 8.9 - 8.9. For the graphic rendering, we used a meshless screen-based technique optimized for high frequency rendering, described in previous work [62]. The scenarios were run on a Core 2 Extreme X7900 processor at 2.8 GHz, with 4 GB of RAM and an Nvidia Quadro FX 3600M GPU with 512 MB of memory.

Fig. 8.9: Active foot-water interaction (shallow pool).

Active foot-water interaction (shallow pool): This scene presents vibrotactile, acoustic and visual feedback (Figure 8.9). Our approach is particularly suited for foot-floor interaction, where the floor renders the vibrotactile feedback to the user's feet through appropriate vibrotactile transducers. Acoustic feedback can also be provided through speaker or headphones. We used a floor consisting of a square array of thirty-six 30.5×30.5 cm rigid vibrating tiles (see Chapters 2 and 3), rendering in the 20-750 Hz range. The virtual scene consisted of a virtual pool with a water depth of 20 cm filling the floor. The user's feet were modeled as parallelepiped rigid

bodies and tracked through the floor pressure sensors. The user could walk about, splashing water as he stepped on the pool as seen in Figure 8.9. Performance: 15,000 particles (1% bubbles), 152Hz.

Fig. 8.10: Passive foot-water interaction (beach shore).

Passive foot-water interaction (beach shore): This scenario integrates vibrotactile, acoustic and visual feedback (Figure 8.10). Using the same hardware setup as the previous scenario, we designed a tidal action scene in which the user stands still and experiences waves washing up on a sandy beach, as shown in Figure 8.10. Performance: 15,000 particles (6% bubbles), 147Hz.

Active hand-water interaction (water bucket): This scene incorporates vibrotactile, kinesthetic, acoustic and visual feedback (Figure 8.11). The user can interact with fluids with his hands using a hand-held vibrotactile transducer and a 6DoF force feedback device. In this scenario, a small vibrator was attached to one of the user's hands. The hand was tracked by a motion capture system, and modeled in the virtual world as a parallelepiped rigid body. He could feel the water sensations by plunging his hand into a cubic volume of fluid, as seen in Figure 8.11. Figure 8.12 shows the vibrotactile signal generated during a plunging movement. Performance: 7,000 particles (6% bubbles), 240Hz.

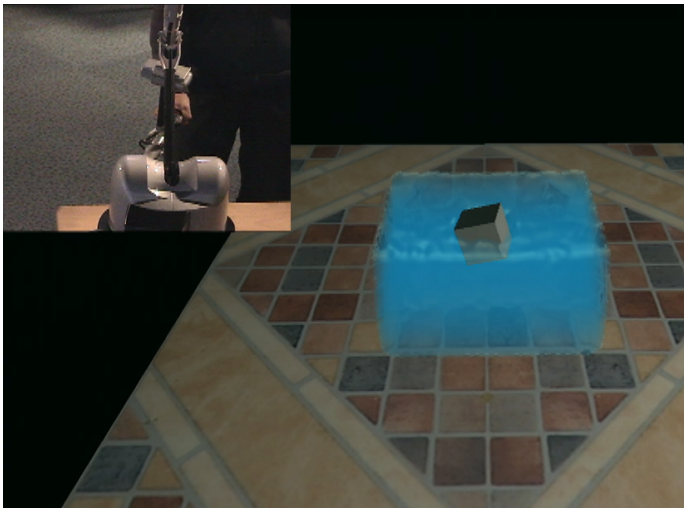

Fig. 8.11: Active hand-water interaction (water bucket).

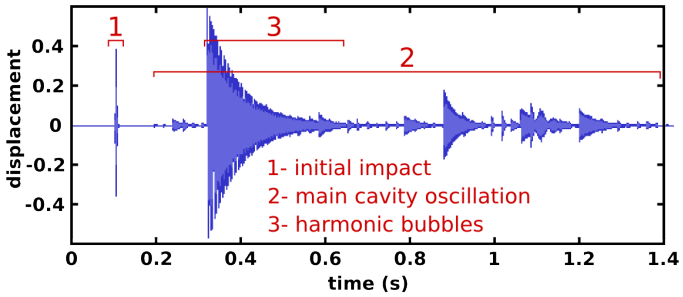

Fig. 8.12: Vibrotactile signal generated with our model during a plunging movement, with its three distinct components: (1) the initial impact, (2) the small bubble harmonics, and (3) the main cavity oscillation.

Chapter 9
Evaluation of multimodal ground cues

R. Nordahl, A. Lécuyer, S. Serafin, L. Turchet, S. Papetti, and F. Fontana

Abstract This chapter presents an array of results on the perception of ground surfaces via multiple sensory modalities, with special attention to non visual perceptual cues, notably those arising from audition and haptics, as well as interactions between them. It also reviews approaches to combining synthetic multimodal cues, from vision, haptics, and audition, in order to realize virtual experiences of walking on simulated ground surfaces or other features.

9.1 Introduction

The multisensory perception of objects and surfaces that are felt or manipulated with the hands has been extensively studied in the literature, and this has, to some extent, informed the design of new generations of complex, multimodal human-computer interfaces that utilize touch, vision, and sound to access and interact with digital information or virtual worlds. As noted in the preceding chapters, substantially less research in either human perception or human-computer interaction has been devoted to interacting via the feet.

Multimodality is an increasingly common feature of interactive systems. Whilst most studies focus on the interaction between vision and audition or between vision and touch, interaction between touch and audition is also significant because both sources of sensory information possess high temporal resolution, and thus are produced by and evidence similar mechanical properties and interactions. Prior literature has investigated many aspects of audio-tactile cross-modal interactions in perception; see [166, 143, 270, 45]. Other, more applied, studies have investigated audio-tactile effects to enhance interaction with virtual worlds [249, 79, 78, 219, 275, 21].

The purpose of this chapter is to review an array of results on the perception of ground surfaces via multiple sensory modalities, with special attention to non visual perceptual cues, notably those arising from audition and haptics, as well as interac-

tions between them. It also reviews approaches to combining synthetic multimodal cues, from vision, haptics, and audition, in order to realize virtual experiences of walking on simulated ground surfaces or other features.

9.2 Evaluating foot-floor multimodal interactions

An overview of the different studies considered in this chapter is given in Table 9.1. The table shows the large number of studies using various experimental protocols and different developed technologies described in the previous chapters. The main results obtained in these various experiments are described in the following subsections and summarized in the conclusions.

Modalities	**Technology**	**Type of experiment**
Haptic+Visual	Visual camera motion + Force in hands	Perception of self-motion (vection illusion)
Haptic (Tactile)+ + Haptic (Kinesthetic)	Variable compliance + Vibrations	Perception of stiffness
Tactile+Audio+ +Kinesthetic	Real materials	Perception of material type
Audio+Haptic	Footstep sounds (ears/helmet) + Vibratory shoes	Identification of ground type (with or without sensory conflict)
Audio+Haptic	Footstep sounds (loudspeakers) + Vibratory shoes	Illusory vibrotactile changes.
Audio+Haptic	Footstep sounds	Recognition of bumps and holes
Audio+Haptic	Friction simulation	Walking on a virtual rope
Audio+Haptic	Footstep sounds	Effect of ecological feedback on gait

Table 9.1: Overview of multimodal experiments described in this chapter.

9.3 Audio-haptic perception of real ground materials

The haptic perception of ground surface mechanical properties, such as softness or friction, or material types is essential in order to assure the stable regulation of dynamic posture and the control of locomotion in diverse environments. It is widely (often implicitly) assumed that kinesthetic (force-displacement) and visual perceptual cues dominate the sensorimotor control of locomotion over natural ground surfaces. However, a number of recent studies suggest that auditory and tactile cues acquired through the sole of the foot also contribute significantly to these perceptual processes.

Giordano et al. [112, 113] studied walkers' abilities to identify a variety of different walked-upon ground surfaces, comprising both solid materials (e.g., marble, wood) and granular media (e.g., gravel, sand) in different experimental conditions in which auditory, haptic, or audiohaptic information was available, and in a kinesthetic condition, where, during walking, tactile information was perturbed via vibromechanical noise to the sole of the foot. (Kinesthesia refers to the sense of movement and forces on the body.) Tactile masking was achieved using a novel shoe sole with integrated vibrotactile actuation (as described in Chapter 2). The authors found haptic and audio-haptic discrimination abilities to be equally accurate, and determined that auditory and kinesthetic abilities to discriminate ground surfaces to both be comparatively inaccurate. When walking on granular materials, which can shift underfoot, participants also appeared to focus preferentially on relatively inaccurate kinesthetic information when identifying the materials. The authors hypothesized that, although sub-optimal for the purpose of material identification, a focus on kinesthetic sensory channels indicates that attention was given preferentially to information that would most promptly signal postural instabilities.

9.3.1 Haptic-haptic cues: Plantar vibrotactile feedback effects on perceived ground stiffness

Visell et al. [312] investigated how the perception of ground surface compliance is altered by plantar vibration feedback. They conducted experiments in which 60 subjects walked in shoes over a rigid floor plate that provided supra- or near-threshold vibration feedback, and responded indicating how compliant it felt, either in subjective magnitude or via pairwise comparisons. In one experiment, the effect of plantar vibration feedback on ground compliance perception was measured via a novel apparatus that allowed both the mechanical stiffness of a floor plate and vibration feedback presented through it to be manipulated (see Figure 9.1).

Results showed that perceived compliance of the plate increased monotonically with vibration feedback intensity, and depended to a lesser extent on the temporal or frequency distribution of the feedback. When both plate stiffness (inverse compliance) and vibration amplitude were manipulated, the effect persisted, with both factors contributing to compliance perception. A significant influence of vibration was observed at low amplitudes (< 0.5 m/s^2) that were close to psychophysical detection thresholds for the stimuli. Taken together, the results of these experiments demonstrate that the perceived haptic compliance of a walking surface is increased in the presence of plantar cutaneous vibration feedback. The authors also found that an increased perception of compliance could be achieved with types of vibration feedback that differed in waveform, amplitude envelope, or the frequency distribution of their energy. None of the experiments involved training, and the effects observed did not require awareness that vibration feedback was being provided. It was concluded that vibration felt during stepping on a rigid surface is combined with the mechanical stiffness of the surface in the haptic perception of compliance. In ad-

dition, the results show that the variation of vibration feedback alone is sufficient to elicit a percept of compliance. One hypothesis consistent with the observations is that plantar vibration feedback simulated the effect of increased displacement during stepping. This interpretation is also consistent with a basic mechanical description of the mechanics of material deformation underfoot during stepping. These findings show that vibrotactile sensory channels are highly salient to the perception of ground surface compliance, and suggest that correlations between vibrotactile sensory information and motor activity may be of broader significance for the control of human locomotion than has been previously acknowledged. An article presenting these experiments is being prepared for journal submission.

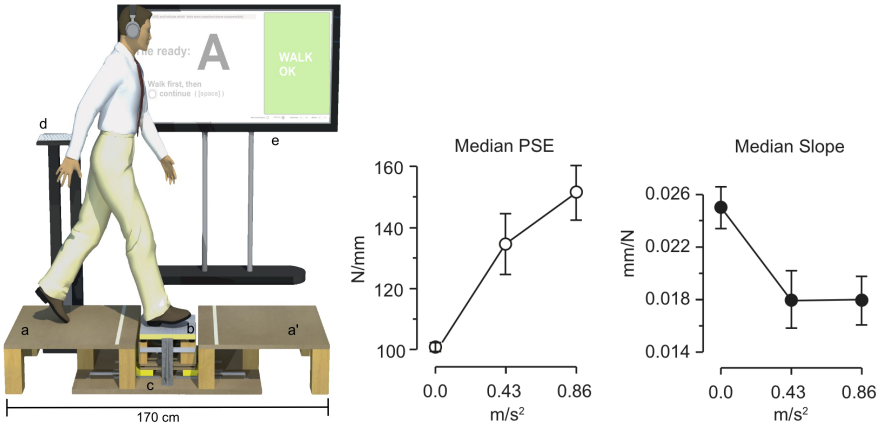

Fig. 9.1: Left: Vibrotactile floor interface from the experiment of Visell et al. [312]. Right: Point of subjective equality and psychometric curve slope for stiffness perception vs. vibration amplitude, based on fits to the experimental data.

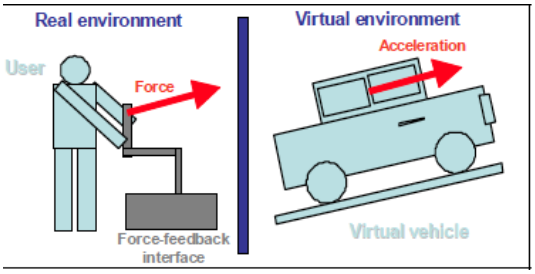

Fig. 9.2 Concept of Haptic motion: a force feedback corresponding to a virtual acceleration.

Fig. 9.3 Experimental apparatus used for generating Haptic Motion: A force-feedback is sent in the hands of the user in a synchronized way with visual feedback of motion in the VE.

9.4 Haptic-Visual cues: Perception of self motion with force feedback and visual motion

We have developed a new visuo-haptic method for navigation in virtual worlds called "Haptic motion". Haptic motion allows the user to feel an important sensation of displacement of his body by applying a force in his hands (see Figure 9.2). This force is coherently produced together with a visual 3D environment. We addressed the question of how haptic motion can influence the perception of self-motion compare with visual stimulation alone. We did not only want to measure qualitatively this influence but also quantitatively. To this aim, we designed two experiments.

In the first experiment we submitted the subject to step of virtual acceleration (see Figure 9.3). The visual and haptic displays are coherent physically, i.e. the visual acceleration correspond to the haptic force (inertial force).There were three different conditions in this experiment: haptic stimulation, visual stimulation and visuo-haptic stimulation. We found that the haptic force strongly influenced the occurrence, the onset and the duration of a well-known illusion of self-motion: the vection illusion.

To understand more deeply how haptic information is merged with visual information, in a second experiment we used different patterns of haptic force to observe in which fashion the fusion with the visual pattern is done. We found that the sensation of self-motion corresponding to haptic motion can be generated in more complex 3D trajectories, and is more important when subjects received a force in the hand proportional to the virtual acceleration instead of virtual speed.

Taken together, our results suggest that haptic motion could be used in various VR applications to enhance sensation of self-motion, such as in virtual reality and video games, or in driving simulators.

9.5 Visual+Haptic cues: Perception of self motion with visual and vibrotactile cues.

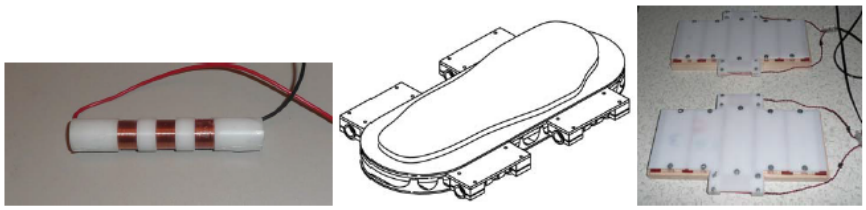

Fig. 9.4: Haptuator and vibrofoot design. Each vibrofoot has 2 haptuators for the stimulation of the sole.

The principle of the experiment is to investigate the role of vibrotactile stimulations in self motion perception. We used visual cues to represent more realistic stimulations. To this aim we design an immersive room where the experiment can be achieved. We tried different type of vibrotactile stimulation to find the one who give the most important sensation of self-motion. To test our hypothesis we designed a vibrotactile apparatus that can stimulate the two feet (see Figure 9.4).

The preliminary results suggest that some vibrotactile patterns have the ability to produce a stronger self motion sensation than others. These patterns could be good candidates to produce self-motion sensation in immersive room at a very low cost.

9.6 Visual-Audio cues: Perception of bumps and holes with camera motions and footstep sounds.

An experiment has also been conducted whose goal was to investigate the role of sound and vision in the recognition of different surface profiles of bumps and holes in a walking scenario.

Fifteen subjects participated to two within-subjects experiments where they were asked to interact with a desktop system simulating bumps, holes and flat surfaces by means of audio, visual and audio-visual cues. The visual techniques used to simulate the act of walking over bumps and holes were the same proposed in [299]: a straightforward modification of the cameras height (H), a modification of the cameras navigation velocity (V), a modification of the cameras orientation (O), and the combination of the three effects (HOV). The technique adopted to render bumps and holes at auditory level has been the placement of footsteps sounds at different temporal intervals.

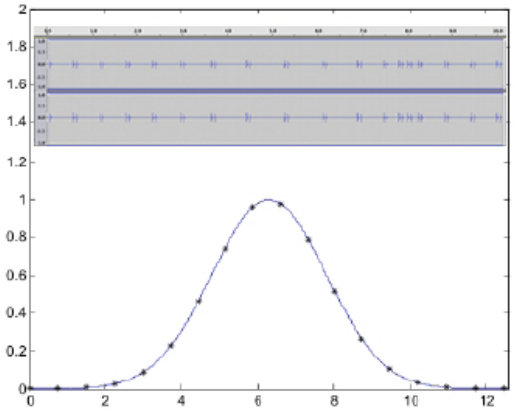

Fig. 9.5 Gaussian bump simulation with the indication of the points at which the footstep sounds occur, and stereo waveform of the corresponding sound file (above).

Results of the first experiment show that participants are able to successfully identify the surface profiles provided through all the proposed audio-visual techniques with very high success rates. The addition of audio stimuli did not produce higher percentages for the recognition of the surfaces rather than the visual only modality which is already very high and close to 100 %.

In addition, the role of dominance between audio and visual modalities has been investigated by means of a second experiment in which conflicting audio-visual stimuli were presented. Results show clearly that in presence of audio-visual conflicts audio is dominated by vision when H and O effects are presented. Conversely, vision is dominated by audio when V and HOV effects are presented. In particular the highest role of dominance has been found for audio stimuli respect visual stimuli provided by means of the Velocity effect. Last, a subjective questionnaire revealed, for the criteria investigated, a clear and significant preference for the bimodal stimuli respect to the stimuli presented in the single modalities. Details about this experiment can be found in [299].

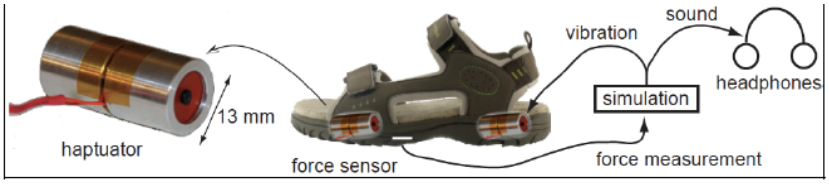

Fig. 9.6: Sandals enhanced with sensors and haptuators used in the experiment (see Chapter 2).

9.7 Audio-Haptic cues: Illusory vibrotactile changes induced by variable acoustic energy in the low frequency.

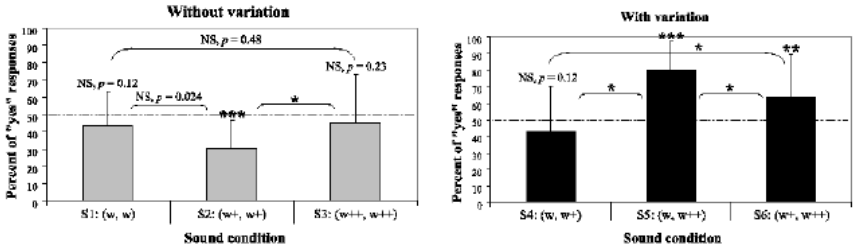

Fig. 9.7: (Left) Mean percentage of yes responses (bars represent std) for the without variation condition as a function of the sound configurations S1: (w,w), S2: (w+,w+), S3: (w++,w++). The difference from random (line at 50%) was tested using one-proportion (two-tailed) z-tests. The differences between the three sound conditions were tested with two-proportion z-tests (two-tailed and Bonferroni-adjusted alpha-level with p = 0:05=3 = 0:0167). (Right) Mean percentage of yes responses (bars represent std) for the with variation condition as a function of the sound configurations S4: (w,w+), S5: (w,w++), S6: (w+,w++). The difference from random (line at 50 %) was tested using one-proportion (two-tailed) z-tests. The differences between the three sound conditions were tested with two-proportion z-tests (two-tailed and Bonferroni-adjusted alpha-level with p = 0:05=3 = 0:0167). Legenda: *:$p < 0:05$, **: $p < 0:01$, ***:$p < 0:001$, NS: not significant. (Papetti et al., 2010b).

Making use of the augmented footwear system, an experiment was set up investigating the influence of low-frequency auditory cues on the perception of underfoot vibration during a walking task. Results show that vibrotactile perception is influenced by such cues. For each channel (i.e. left and right shoe), an audio-haptic signal was routed to three paths: two audio paths going to the speakers, and one haptic path going to two vibrotactile transducers (haptuators) embedded in the respective sandal. Concerning the audio path, the signal was split in two frequency bands: the upper band was routed to a mini-speaker mounted on the sandal, while the other band was sent to four broadband loudspeakers located at the experiment room corners. The cross-over frequency was chosen to take advantage of the precedence effect: thanks to this effect, the user heard an ecologically consistent sound of footsteps coming exclusively from the feet while walking with the augmented sandals. Finally, in order to enhance the sense of presence, environmental sounds of a forest (representing wind in the trees, birds singing and a river flowing) were superimposed to the auditory stimuli at foot level.

Subjects were asked to wear the augmented sandals and to walk with a regular pace along a predefined path. Starting from halfway, the intensity of the low frequency signal at the loudpspeakers could be changed. Before the experiment, subjects had been informed that a change in the intensity of the feedback could happen

halfway during each take, however they were not aware that only the audio feedback was altered. Overall the experiment lasted about 45 minutes and consisted of twelve experimental configurations corresponding to several combinations of low frequency levels: a set of six increments (namely, three unvaried conditions plus three increases) plus a set of six decrements (again, three unvaried conditions plus three decreases). In detail, every take consisted of a pair of low frequency levels: one for the first half of the path and another one for the second part. The level pairs used in the experiment are shown below:

- without-variation - S1: (w, w), S2: (w+, w+), S3: (w++, w++)
- with-variation - S4: (w, w+), S5: (w, w++), S6: (w+, w++)

Note that the unvaried conditions S1, S2 and S3 are the same for both increments and decrements, while the varied conditions S4, S5 and S6 are in reverse order for increments and decrements. Each condition was repeated four times, for a total of 48 trials. Decrements and increments were presented separately, that is, half subjects started with a randomized sequence of 24 decrements (i.e., twelve decrements and twelve no-variation trials) and half with a randomized sequence of 24 increments (i.e., twelve increments and twelve no-variation trials). At the end of each take, subjects had to write down whether they had felt any change in the vibrotactile feedback under their feet (answer: yes/no), and the corresponding confidence rating (from 1 to 7; 1: absolutely not confident, 4: moderately confident, 7: very confident).

For each participant, the percentages of yes responses were calculated for the twelve experimental conditions. The difference from random percentage (50and we used two-proportion (two-tailed) z-tests in order to check the differences between the experimental conditions. An alpha level of 0.05 was adopted. A first global analysis considered the percentages of yes responses in the stimulus conditions without-variation vs. with-variation. Results confirm that a cross-modal effect is present, and manifests itself as an audio-tactile illusion where audio low frequency influences the vibrotactile perception. The significant differences from random (50interpreted like a double proof of such audio-tactile illusion. In other words, we have a cause/effect relationship, where the cause is the intensity variation of the low frequency, and the effect is the illusion: when the cause is present the effect is present, furthermore when the cause is absent the effect is absent.

In a detailed analysis, we considered the percentages of yes responses for the two stimulus conditions without-variation vs with-variation as a function of the sound configurations. The results are presented in Figure 16. For the without-variation condition the percentage of yes responses was significantly different from random in the S2 condition, but not in the S1 and S3 conditions. For the with-variation condition the percentage of yes responses was significantly different from random in the S5 and S6 conditions, but not in the S4 condition. Furthermore there is an optimal association (sweet spot) for the audio-tactile illusion. In this regard, it is expected that the largest low frequency variation (amounting to 12 dB) represented by S5: (w,w++) corresponds to a stronger illusion. On the other hand, it is found that the same relative low frequency variation (6 dB) starting from different absolute levels namely S4: (w, w+) and S6: (w+, w++) result in considerably different effects. In

particular, a sweet spot is found for higher and more clearly perceivable absolute LFS levels. Also, a sweet spot for the without variation condition is represented by the S2: (w+, w+) condition: it is likely that a clearly perceivable low frequency level facilitated the participants to correctly feel the constancy of vibrotactile feedback.

9.8 Audio-haptic identification of ground surfaces

In this section we provide an overview of several experiments whose goal was to investigate the ability of subjects to recognize simulated surfaces delivered both auditorily and haptically.

All the experiments described in this section were carried out in an acoustically isolated laboratory. The walking area was approximately 18 square meters, delimited by the walls of the laboratory. The setup for the experiments consisted of the pair of sandals described in Chapter 2, an Arduino board, a Fireface soundcard, a laptop and a set of headphones (Sennheiser HD 650).

In the conditions with audio only, the haptic actuators were not used, and the pressure sensors were driving the synthesis engine only to provide auditory feedback.

In the conditions with haptics only, participants were asked to wear earplugs and sound protection headsets instead of headphones, in order to block any audible feedback produced by the actuators. Indeed such sounds were not in the same quality range of the sounds designed to be conveyed through the headphones, and they could have biased the judgments of the participants. The offline experiments were conducted by having subjects sitting and experiencing the feedback provided either to the shoes or to the ears. The experiments where the synthesis engine run in realtime were conducted by allowing subjects to walk in the laboratory, enabling the tight sensorymotor coupling which is natural during walking. In order to facilitate the navigation of the subjects, the wires coming out from the shoes in all setups, as well as the wires connecting the headphones to the soundcard, were linked to a bumbag or to snaplinks attached to trousers (see Figure 9.8).

9.8.1 Offline identification of virtual grounds

The goal of this experiment was to assess whether subjects were able to recognize surfaces simulated auditorily and haptically which were delivered by using the synthesis engine offline.

Procedure:

The participants were asked to wear the sandals previously described and the headphones, and to sit on a chair. In the condition with haptic only they wore earplugs and sound protection headsets. Participants were asked to recognize the stimuli they were exposed to. They were given a list of sixteen materials: wood, creaking wood, underbrush, snow, frozen snow, beach sand, gravel, metal, high grass, dry leaves, concrete, dirt, puddles, water, carpet and I don't know. Each of the four standard surfaces were presented twice in a randomized order. When presented one of the four standard stimuli, participants had to match it to one in the list and rated the realism and quality of the simulations. At the conclusion of the experiment, participants were asked to leave comments.

Participants:

The forty five volunteers (students and faculty at the Engineering college of Copenhagen; 31 men and 14 women; average age =24.5, st.d.=4.6) were randomly assigned to one of the three groups (audio only, haptic only or audio-haptic) for a total of 15 participants per condition. None reported hearing problems or other sensory impairments. In order for the size of sandals not to affect performance, subjects wore shoes sizes from 41 and 45 (as mentioned before, the sandals were size 43).

Fig. 9.8 A person wearing the sandals enhanced with pressure sensors and actuators.

Results and discussion:

The experiment shows that haptic cues alone give the subjects the possibility to recognize categories of surfaces with poor fine discrimination. A solid surface was not confused with an aggregate, and viceversa. The combination of auditory and haptic cues did not necessarily produce a better recognition performance. More details on the experiment are described in [211].

9.8.2 Online identification of virtual grounds

The goal of this experiment was to assess whether subjects were able to recognize auditory and haptically simulated surfaces which were provided by using the synthesis engine interactively, i.e., by walking in the laboratory using the actuated sandals.

Procedure:

During condition 1 and 3 the participants were asked to wear the pair of sandals and the headphones and to walk in the laboratory. During condition 2 they were asked to wear the pair of sandals, earplugs and sound protection headsets, and to walk in the laboratory. During the experiment, 8 stimuli were presented twice in randomized order. The stimuli consisted of audio and haptic simulations of footstep sounds on the following surfaces: beach sand, gravel, snow (in particular deep snow), forest underbrush (a forest floor composed by dirt, leaves and branches breaking), dry leaves, wood, creaking wood and metal. Participants were given a list of different surfaces to be held in one hand, presented as non-forced alternate choice. Such list included a range of materials wider than those presented in experiments. During the act of walking they listened simultaneously to footsteps sounds and/or vibrations on a different surface according to the stimulus presented.

Participants:

Thirty participants were divided in three groups (n = 10) to perform the between-subjects experiment. The three groups were composed respectively of 7 men and 3 women, aged between 20 and 35 (average age=24.6, st.d.=4.67), 9 men and 1 woman, aged between 20 and 31 (average age=23.4, st.d.=3.23), and 7 men and 3 women, aged between 21 and 25 (average age=22.7, st.d.=1.07). All participants reported normal hearing conditions.

Results and discussion:

The results of this experiment confirm the fact that the recognition task was more successful when subjects were exposed to auditory stimuli instead of haptic ones. As in the offline situation, the combination of auditory and haptic stimuli did not significantly enhance the recognition. More details on the experiment are described in [268].

9.8.3 Identification of virtual grounds with conflicting cues

We conducted an experiment whose goal was to investigate the role of dominance of the audio and haptic modalities during the use of our walking system. Subjects were asked to interact with the system and to recognize the different walking sounds and vibrations they were exposed to. The experiment consisted of both coherent and incoherent audio-haptic stimuli. In presence of coherent stimuli the same surface material was presented both at audio and haptic level. The provided incoherent stimuli consisted of different surface materials; in particular when audio level a solid surface was presented, while at haptic level an aggregate surface was delivered, and viceversa. One of our hypotheses was that the audio modality would have dominated the haptic one. Another was that the recognition would have slightly improved using coherent stimuli rather than the incoherent ones.

Procedure:

During the experiment participants were asked to wear the pair of sandals and the headphones previously described, and to walk in the laboratory. During the act of walking they listened simultaneously to footstep sounds and vibrations on a different surface according to the stimuli presented. The task consisted of recognizing the surfaces they were exposed to. As opposed to our previous research, participants were not provided with a forced list of possible choices. This was due to the fact that we wanted subjects to be somehow creative in their recognition of the surface, without guessing from a predefined list. Participants were exposed to 12 trials consisting of 4 coherent stimuli and 8 incoherent stimuli. The 12 audio-haptic stimuli were presented once in randomized order The modeled surfaces were 4 (2 solid and 2 aggregate): wood, metal, snow and gravel. In presence of incoherent stimuli the conflict was obtained by providing one of the solid surfaces by means of auditory feedback, and one of the aggregate surfaces at haptic level. Analogously, another set of incoherent stimuli consisted of delivering an aggregate surface at auditory level and a solid surface at haptic level.

Participants:

Ten participants, 7 male and 3 female, aged between 20 and 38 (mean = 25.81, std = 5.77), were involved in the experiment. All participants reported normal hearing conditions and all of them were naive with respect to the experimental setup and to the purpose of the experiment.

Results and discussion:

Results show that when conflicting cues are present, the auditory modality is dominant on the haptic one. Such results are consistent with the ones obtained in the previous experiments, were we encountered a higher recognition rate using auditory feedback as opposed to haptic feedback. More details on the experiment are described in [302].

9.9 Audio haptic walking over bumps and holes

Until now the audio-haptic experiments described consist of simulation of different flat surfaces.

We extended such research in order to assess if it is possible to simulate walking over bumps or holes using auditory and haptic cues. In particular, we investigated whether the timing between heel and toe and the timing between footsteps, varied at both auditory and haptic level, affected perception of walking on unflat surfaces. This simulation is motivated by the fact that when walking uphill people tend to decelerate, while walking downhill they accelerate.

Procedure

During all experiments subjects were sitting on a chair, listening to the sounds through headphones and feeling the haptic vibrations through the haptic shoes. They were given the list of three different surfaces (bump, hole, flat), presented as forced alternate choice. The task consisted of recognizing to which surface the walk corresponded after the presentation of the stimuli.

Participants

Forty-five participants were divided in three groups (n=15) to perform the three conditions of the experiment. The three groups were composed respectively of 11 men and 4 women, aged between 20 and 29 (mean = 23.6, std = 2.84), 11 men and 4 women, aged between 21 and 32 (mean = 24.86, std = 3.48) and 11 men

and 4 women, aged between 20 and 28 (mean = 23.06, std = 2.40). All participants reported normal hearing conditions. All participants were naive with respect to the experimental setup and to the purpose of the experiment.

Results and discussion

Results show that varying temporal aspects between footsteps allow to successfully simulating the act of walking on a bump, hole, or flat surface, especially in the auditory modality. Moreover, in the recognition task, haptic cues show to significantly reinforce auditory cues.

9.10 Walking on a virtual rope

We have recently started to explore the role of auditory and haptic feedback in facilitating task performance. In this particular study, we are interested in understanding whether auditory and haptic feedback facilitates the task of walking on a virtual rope.

Procedure

Subjects were asked to wear the haptic sandals and to walk blindfolded straight in order not to fall from a virtual plank. Figure 9.9 shows a subject performing the experiment. Specifically, subjects were give the following instructions: ”Imagine you are walking on a wooden plank. Your task is to walk from one side to the other. Walk slowly and pay attention to the feedback you receive in order to succeed on your task. If your feet are outside of the plank you will fall.” The same stimuli were provided for the auditory and haptic simulation and designed as follows: when a user was walking on top of the virtual plank, his position was detected by a motion capture system (Naturalpoint by Optitrack). In this case, the synthesis engine provides as a stimulus the sound and haptic feedback of a creaking wood. The physics based synthesis engine was implemented using the algorithms described in [24].

Participants

The experiment was performed by 15 participants, 14 men and 1 woman, aged between 22 and 28 (mean = 23.8, std = 1.97). All participants reported normal hearing conditions. All participants were naive with respect to the experimental setup and to the purpose of the experiment.

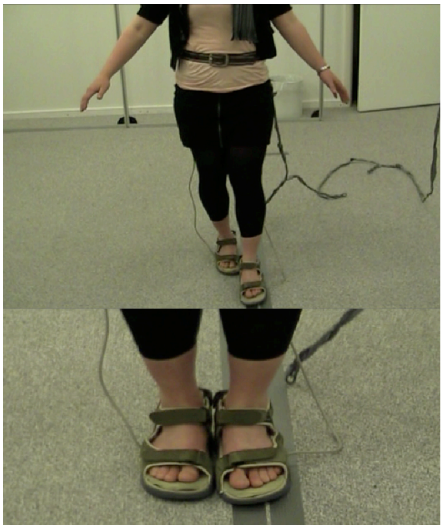

Fig. 9.9 A subject performing the experiment consisting of walking on a virtual rope.

Results and discussion

The results of the experiment do not provide clear indications on the role of the feedback to facilitate balance control. Indeed, feedback helps balance mostly when haptic stimuli are provided, although the differences are not significant.

9.11 Audio-haptic matching of offline footsteps simulation

We have conducted three between subjects audio-haptic experiments whose goal was to assess the ability of subjects in matching pairs of materials passively presented at auditory and haptic level.

Thirty-six participants were asked to evaluate the degree of coherence between the audio and haptic stimuli presented in each trial. In experiment 1 participants were asked to rate to which extent the haptic stimulus was coherent with the auditory stimulus. During experiment 2 they were asked to rate to which extent the auditory stimulus was coherent with the haptic stimulus. During experiment 3, participants were asked to rate to which extent the auditory and the haptic stimuli were coherent with each other.

Results show that on average audio-haptic pairs of materials belonging to the same typology (aggregate or solid) were considered as fitting well, while the pairs belonging to different typologies were judged not matching well. Participants were

not precise in scaling how well the materials belonging to the same typology matched each other. However the audio-haptic pairs presented with the same material were only in few cases judged as the most fitting.

It is possible to conclude that when simulating offline an audio-haptic stimulus by means of the proposed system, a solid material provided at auditory level fit well with a solid material (not necessarily the same) at haptic level, but not with an aggregate one; analogously for the aggregate case.

9.12 Effects of ecological auditory and vibrotactile underfoot feedback on human gait: a preliminary investigation

A pilot experiment was carried out [227] where subjects were asked to walk along a predefined path while wearing a pair of instrumented sandals which provide auditory and vibrotactile feedback. Three experimental conditions were set up, corresponding to different feedback: two conditions simulating different ground materials, and one neutral (i.e. control) condition without artificial feedback. Preliminary results indicate that non-visual interactive feedback in a walking task influences, although not significantly, the subjects' gait patterns.

In a related work [46] the authors have shown that gait patterns, accounting for specific emotional intentions, are affected by ecological auditory and vibrotactile underfoot feedback, albeit not to a statistically significant degree. The results of our experiment support such previous conclusions, overall suggesting that supplying subjects which walk on a neutral, solid floor with non-visual interactive cues representing virtual grounds may have perceptual salience, however not to the point to push them into changing their usual walking style.

Such results may be exploited in navigation aid applications, providing users with informative yet non-intrusive auditory and vibrotactile underfoot cues. For instance, virtual pathways may be defined by simulating different ground materials through non-visual cues, thus helping normally sighted as well as visually-impaired persons keep the right track in complex functional spaces such as airports, railway stations and so on.

Experiment

The experimental hypothesis was that human gait can be influenced by providing ecological audio-tactile feedback through the feet.

Eight subjects, seven males and one female, of Italian nationality participated in the experiment. Their average age was 22.3 years. Six subjects were right-handed and also considered their right foot as dominant. One subject was left-handed and one ambidextrous, also with regard to the use of feet. None of them reported any foot- or locomotion-related deficiencies.

The equipment used in the experiment consisted of the instrumented shoe presented in Chapter 2.

Three experimental conditions were set up, corresponding to different stimuli: one control condition (N) without additional feedback, and two conditions (S and M) providing artificial audio-tactile feedback. The latter was generated in real-time by driving two different physics-based sound models (refer to Chapter 7) with the data provided by the force sensors: two ground materials were simulated, respectively icy snow (S) and mud (M).

The participants were asked to wear the instrumented sandals and the backpack, and walk along a eight-shaped path in the experiment room. They were informed that a change in the multimodal feedback could occur at each trial, and no other instructions were given. In order to avoid biases due to the room configuration, half of the participants started walking from one of the shorter sides of the rectangular room and the other half from the other side.

The experiment considered 8 trials for each condition, resulting in 24 trials for each experimental session, which lasted about 15 minutes. The order of the trials was randomized for each subject: before each trial the experimenter switched the feedback among the three conditions N, S and M, accordingly to such order.

Results and discussion

The recorded force data were analyzed in order to extract the following inter-onset intervals (IOIs) during walk: heel-to-toe intervals between contacts at the heel and the toe, for the left and right foot (respectively labeled h2tL and h2tR); inter-foot heel-to-heel intervals between contacts at the right and left heel (h2h); inter-feet heel-to-toe intervals between contacts at the right heel and left toe (h2tRL). The contacts were detected making use of thresholds and taking into account the slope of the force curves.

A first one-way repeated measures ANOVA (RM-ANOVA) was performed on the data recorded in the neutral condition N, in order to verify whether the subjects walked with a regular pace when no stimuli were present. The different trials in the neutral condition N were considered as repeated measures for each subject, and the mean IOIs in each trial were used. The respective results for the four IOIs are shown in Table 9.2. The obtained p-values are very high, meaning that the subjects walked

h2tL	$F(7,7) = 1.36$, $p = 0.2420$
h2tR	$F(7,7) = 0.21$, $p = 0.9814$
h2h	$F(7,7) = 0.69$, $p = 0.6788$
h2tRL	$F(7,7) = 1.38$, $p = 0.2345$

Table 9.2: Results from RM-ANOVA for the neutral condition N.

with a very regular gait in the neutral condition N. In particular the h2tR interval appears extremely regular.

Considering the above results and since the majority of the participants (six over eight) were right-handed, we performed a second RM-ANOVA on such subjects only. As shown in Table 9.3, the IOIs from these subjects are much more irregular, except for the h2tR interval. These may indicate that only the dominant foot provides

h2tL	$F(7,5) = 2.30$, $p = 0.0485$
h2tR	$F(7,5) = 0.97$, $p = 0.4713$
h2h	$F(7,5) = 2.88$, $p = 0.0173$
h2tRL	$F(7,5) = 6.03$, $p = 0.0001$

Table 9.3: Results from RM-ANOVA for right-handed subjects in the neutral condition N.

reliable data. Also this may suggest that a confidence value $\alpha = 0.05$ can be assumed in the analysis, thus allowing to isolate the irregularities found for the right-handed subjects in the neutral condition N.

The IOIs in the three conditions N, S and M were also tested using a RM-ANOVA, considering the mean IOIs over all trials in each condition. The results of

h2tL	$F(2,7) = 2.22$, $p = 0.1452$
h2tR	$F(2,7) = 3.09$, $p = 0.0775$
h2h	$F(2,7) = 3.01$, $p = 0.0815$
h2tRL	$F(2,7) = 2.58$, $p = 0.1108$

Table 9.4: Results from RM-ANOVA for the conditions N, S and M.

Table 9.4 show that the subjects' gait was slightly affected by the audio-tactile feedback provided in the conditions S and M, as the IOIs are more irregular compared to the neutral condition N (see Table 9.2). This is clearly evident especially considering the result concerning the h2tR and h2h intervals. By assuming a confidence value $\alpha = 0.05$ as suggested above, the results from the h2tR and h2h intervals are indeed close to statistical significance.

However, the relatively high p-values indicate that such effect needs further investigation. In particular the experiment should be repeated with a larger number of subjects, as eight subjects do not guarantee the conditions for performing a proper ANOVA test. In a broader perspective, the lack of a clear statistical significance in the obtained results may have an alternative interpretation. In fact the ability to provide salient non-visual cues underfoot, which do not significantly alter one's walking style, may enable the design of foot interfaces supplying informative, meanwhile non-intrusive messages for guiding users across spaces otherwise difficult to navigate.

9.13 Conclusions

This chapter presented an overview of multimodal experiments performed in the context of foot-floor interactions. The experiments were performed with the goal of evaluating the different technologies developed, while at the same time achieving a better understanding of the role of the different modalities in performing discriminations tasks, ranging from recognizing the simulated surfaces, to recognize simulated bumps and holes, to illusory effects.

The main advantage provided by the technologies developed, such as shoes enhanced with sensors and actuators, or haptically enhanced platforms, is the fact that the different parameters of the simulations can be carefully controlled in laboratory settings, allowing to achieve a better understanding of the relationship between physical and perceptual parameters of the simulation.

The different experiments performed provide a better understanding of the relationship between auditory, haptic and visual cues when simulating ground events. As an example, the experiments show that subjects can recognize simulated surfaces both auditorily and haptically. The combination of auditory and haptic information does not significantly enhance the recognition. Moreover, subjects are able to recognize simulated bumps and holes when reproduced visually, auditorily and haptically. Moreover, auditory and haptic feedback slightly modifies subjects' gate, although not significantly. Using auditory and haptic feedback also allows to recreate some illusions, such as the sensation of the presence of haptic feedback when only auditory feedback is delivered. Moreover, auditory and haptic feedback can be used as indication for subjects to walk on a determined path, such as a straight line or a virtual rope. Taken together, these experiments provide some evidence of the importance of feedback in simulated environments, focusing on auditory and haptic feedback at the ground level, topic which has been rather unexplored in the virtual reality community.

References

1. *Proc. of the 4th Intl. Mobile Music Workshop*, Amsterdam, NL, May 2007.
2. A. Abu-El-Quran, R. A. Goubran, and A. D. C. Chan. Security monitoring using microphone arrays and audio classification. *IEEE Trans. on Instrumentation and Measurement*, 55(4), 2006.
3. M. Addlesee, A. Jones, F. Livesey, and F. Samaria. The orl active floor. *IEEE Personal Communications*, 4(5):35–51, 1997.
4. M. Addlesee, A. H. Jones, F. Livesey, and F. S. Samaria. The ORL active floor. *IEEE Personal Communications*, 4:35–41, 1997.
5. F. Adjémian and P. Evesque. Different regimes of stick-slip in granular matter: from quasi-periodicity to randomness. *EGS XXVII General Assembly, Nice, 21-26 April 2002*, 2002.
6. J. M. Adrien. The missing link: Modal synthesis. pages 269–297, 1991.
7. P. Agrawal, I. Rauschert, K. Inochanon, L. Bolelli, S. Fuhrmann, I. Brewer, G. Cai, A. MacEachren, and R. Sharma. Multimodal interface platform for geographical information systems (geomip) in crisis management. In *ICMI '04: Proceedings of the 6th international conference on Multimodal interfaces*, pages 339–340, New York, NY, USA, 2004. ACM.
8. H. J. Ailisto, M. Lindholm, J. Mantyjarvi, E. Vildjiounaite, and S.-M. Makela. Identifying people from gait pattern with accelerometers. In *Proc. SPIE – Biometric Technology for Human Identification II*, 2005.
9. M. Alava, P. Nukala, and S. Zapperi. Statistical models of fracture. *Advances in Physics*, 55(3):349–476, 2006.
10. P. Albinsson and S. Zhai. High precision touch screen interaction. In *Proceedings of the SIGCHI conference on Human factors in computing systems*, pages 105–112. ACM, 2003.
11. K. Aminian and B. Najafi. Capturing human motion using body-fixed sensors: outdoor measurement and clinical applications. *Journal of Visualization and Computer Animation*, 15(2):79–94, 2004.
12. R. Annies, E. Martinez Hernandez, K. Adiloglu, H. Purwins, and K. Obermayer. Classification schemes for step sounds based on gammatone-filters. 2007.
13. G. Arechavaleta, J.-P. Laumond, H. Hicheur, and A. Berthoz. The nonholonomic nature of human locomotion: a modeling study. In *Proceedings of IEEE International Conference on Biomedical Robotics and Biomechatronics*, pages 158–163, 2006.
14. S. Arulampalam, S. Maskell, and N. Gordon. A tutorial on particle filters for online nonlinear/non-gaussian bayesian tracking. *IEEE Transactions on Signal Processing*, 50:174–188, 2002.
15. D. Ashbrook and T. Starner. Learning significant locations and predicting user movement with gps. In *International Symposium on Wearable Computing*, Seattle, WA, October 2002.
16. D. Ashbrook and T. Starner. Using gps to learn significant locations and predict movement across multiple users. *Personal Ubiquitous Comput.*, 7(5):275–286, 2003.

17. K. J. Astrom. Optimal control of Markov decision processes with incomplete state estimation. *J. Math. Anal. Applic.*, 10:174–205, 1965.
18. J.-J. Aucouturier, B. Defreville, and F. Pachet. The bag-of-frame approach to audio pattern recognition: A sufficient model for urban soundscapes but not for polyphonic music. *Journal of the Acoustical Society of America*, 2007.
19. J.-J. Aucouturier, F. Pachet, P. Roy, and A. Beurivé. Signal + context = better classification. In *Proceedings of ISMIR 07*, pages 425–430, 2007.
20. T. Augsten, K. Kaefer, R. Meusel, C. Fetzer, D. Kanitz, T. Stoff, T. Becker, C. Holz, and P. Baudisch. Multitoe: High-precision interaction with back-projected floors based on high-resolution multi-touch input. In *Proceedings of the 23nd annual ACM symposium on User interface software and technology*, pages 209–218. ACM, 2010.
21. F. Avanzini and P. Crosato. Integrating physically based sound models in a multimodal rendering architecture: Research articles. *Comput. Animat. Virtual Worlds*, 17(3-4):411–419, 2006.
22. F. Avanzini and D. Rocchesso. Modeling collision sounds: non-linear contact force. In *Proc. Conf. on Digital Audio Effects (DAFX-01)*, pages 61–66, Limerick, December 2001.
23. F. Avanzini and D. Rocchesso. Modeling Collision Sounds: Non-linear Contact Force. *Proc. COST-G6 Conf. Digital Audio Effects (DAFX-01)*, pages 61–66, 2001.
24. F. Avanzini, S. Serafin, and D. Rocchesso. Interactive simulation of rigid body interaction with friction-induced sound generation. *Speech and Audio Processing, IEEE Transactions on*, 13(5):1073–1081, 2005.
25. E. Ayyappa. Normal human locomotion, part 2: Motion, ground reaction force. *J. Prosthetics and Orthotics*, 9(2), 1997.
26. A. Baldassarri, F. Dalton, A. Petri, S. Zapperi, G. Pontuale, and L. Pietronero. Brownian forces in sheared granular matter. *Physical Review Letters*, 96(11):118002, 2006.
27. L. Bao. Physical activity recognition from acceleration data under semi-naturalistic conditions. Technical report, Master's thesis, MIT, 2003.
28. L. Bao and S. Intille. Activity recognition from user-annotated acceleration data. *Pervasive 2004*, pages 1–17, April 2004.
29. S. Barrass and M. Adcock. Interactive granular synthesis of haptic contact sounds. In *AES 22nd International Conference on Virtual, Synthetic and Entertainment Audio*, 2002.
30. C. Basdogan and M. A. Srinivasan. *Handbook of Virtual Environments: Design, Implementation, and Applications*. CRC Press, 1 edition, Jan. 2002.
31. S. Basu, S. J. Schwartz, and A. Pentland. Wearable phased arrays for sound localization and enhancement. In *ISWC*, page 103, 2000.
32. L. E. Baum, T. Petrie, G. Soules, and N. Weiss. A maximization technique occurring in the statistical analysis of probabilistic functions of markov chains. *Ann. Math. Statist.*, 41(1):164–171, 1970.
33. R. K. Begg, M. Palaniswami, and B. Owen. Support vector machines for automated gait classification. *IEEE Transactions on Biomedical Engineering*, 52(5), 2005.
34. H. Benko, A. Wilson, and P. Baudisch. Precise selection techniques for multi-touch screens. In *Proceedings of the SIGCHI conference on Human Factors in computing systems*, pages 1263–1272. ACM, 2006.
35. B. Bhanu and X. T. Zou. Moving humans detection based on multi-modal sensor fusion. In *Object Tracking and Classification Beyond the Visible Spectrum*, page 136, 2004.
36. A. Bicchi, J. Salisbury, and D. Brock. Contact sensing from force measurements. *The Int J of Robotics Research*, 12(3):249, 1993.
37. C. M. Bishop. *Pattern Recognition and Machine Learning*. Springer, August 2007.
38. A. Bissacco, A. Chiuso, Y. Ma, and S. Soatto. Recognition of human gaits. *Computer Vision and Pattern Recognition, IEEE Computer Society Conference on*, 2:52, 2001.
39. A. Bissacco and S. Soatto. Modeling and learning contact dynamics in human motion. In *Proc. of Computer Vision and Pattern Recognition (CVPR)*, 2005.
40. R. E. Bland. Acoustic and seismic signal processing for footsetp detection. Master's thesis, Massachusetts Institute of Technology. Dept. of Electrical Engineering and Computer Science., 2006.

41. B. Blesser. An interdisciplinary synthesis of reverberation viewpoints. *J. of the Audio Engineering Society*, 49(10), 2001.
42. G. Borin, G. De Poli, and D. Rocchesso. Elimination of Delay-Free Loops in Discrete-Time Models of Nonlinear Acoustic Systems. *IEEE Trans. on Speech and Audio Processing*, 8(5):597–605, September 2000.
43. D. A. Bowman, E. Kruijff, J. J. LaViola, and I. Poupyrev. *3D User Interfaces: Theory and Practice*. Addison-Wesley Professional, 1 edition, 2004.
44. G. R. Bradski. Computer vision face tracking for use in a perceptual user interface. *Intel Technology Journal*, 2(2):12–21, 1998.
45. J.-P. Bresciani, M. O. Ernst, K. Drewing, G. Bouyer, V. Maury, and A. Kheddar. Feeling what you hear: Auditory signals can modulate tactile tap perception. *Experimental Brain Research*, 162:172–180, 2005.
46. R. Bresin, A. de Witt, S. Papetti, M. Civolani, and F. Fontana. Expressive sonification of footstep sounds. In R. Bresin, T. Hermann, and A. Hunt, editors, *Proc. of the Interaction Sonification workshop (ISon) 2010*, KTH, Stockholm, Sweden, Apr. 7 2010.
47. R. Bresin, S. Delle Monache, F. Fontana, S. Papetti, P. Polotti, and Y. Visell. Auditory feedback from continuous control of crumpling sound synthesis. In *CHI 2008 Workshop on Sonic Interaction Design*, Florence, Italy, Apr. 5-10 2008. ACM.
48. M. Brubaker, L. Sigal, and D. Fleet. Estimating Contact Dynamics. In *IEEE International Conference on Computer Vision (ICCV)*, 2009.
49. G. Bruder, F. Steinicke, and K. H. Hinrichs. Arch-Explore: a natural user interface for immersive architectural walkthroughs. In *IEEE Symposium on 3D User Interfaces, 2009. 3DUI 2009*, pages 75–82. IEEE, 2009.
50. M. Büchler, S. Allegro, S. Launer, and N. Dillier. Sound classification in hearing aids inspired by auditory scene analysis. 2005.
51. G. Burdea and M. Akay. *Force and touch feedback for virtual reality*. Wiley New York, 1996.
52. M. Casey. General sound classification and similarity in mpeg-7. *Organised Sound*, 6(2):153–164, 2001.
53. M. Casey. *Sound Classification and Similarity, in: Introduction to MPEG-7, Multimedia Content Description Interface*. John Wiley and Sons, Ltd., Jun 2002.
54. G. Casiez, D. Vogel, Q. Pan, and C. Chaillou. RubberEdge: reducing clutching by combining position and rate control with elastic feedback. In *Proceedings of the ACM symposium on User interface software and technology*, pages 129–138, Newport, Rhode Island, USA, 2007. ACM.
55. T. Chau. A review of analytical techniques for gait data. part 1: fuzzy, statistical and fractal methods. *Gait and Posture*, 13(1), 2001.
56. T. Chau. A review of analytical techniques for gait data. part 2: neural network and wavelet methods. *Gait and Posture*, 13(2), 2001.
57. J. Chen, A. H. Kam, J. Zhang, N. Liu, and L. Shue. Bathroom activity monitoring based on sound. *Pervasive Computing*, pages 47–61, 2005.
58. L. Cheng and S. Hailes. On-body wireless inertial sensing for foot control applications. In *IEEE 19th International Symposium on Personal, Indoor and Mobile Radio Communications 2008 (PIMRC 2008)*, 2008.
59. M. Chion. *Audio-Vision*. Columbia Univ. Press, New York, USA, 1994.
60. R. Christensen, J. Hollerbach, Y. Xu, and S. Meek. Inertial-force feedback for the treadport locomotion interface. *Presence: Teleoperators & Virtual Environments*, 9(1):1–14, 2000.
61. P. Chueng and P. Marsden. Designing Auditory Spaces to Support Sense of Place: The Role of Expectation. *CSCW Workshop: The Role of Place in Shaping Virtual Community*, 2002.
62. G. Cirio, M. Marchal, S. Hillaire, and A. Lecuyer. Six Degrees-of-Freedom haptic interaction with fluids. *IEEE Transactions on Visualization and Computer Graphics*, PP(99):1–1, Nov. 2011.
63. G. Cirio, M. Marchal, T. Regia-Corte, and A. Lécuyer. The magic barrier tape: a novel metaphor for infinite navigation in virtual worlds with a restricted walking workspace. In *Proceedings of the 16th ACM Symposium on Virtual Reality Software and Technology*, pages 155–162, Kyoto, Japan, 2009. ACM.

64. M. Civolani, F. Fontana, and S. Papetti. Efficient acquisition of force data in interactive shoe designs. In *Proc. 5th Int. Haptic and Auditory Interaction Design Workshop*, pages 129–138, Sept. 2010.
65. B. P. Clarkson and A. Pentland. Extracting context from environmental audio. In *ISWC*, pages 154–155, 1998.
66. P. R. Cook. Physically informed sonic modeling (PhiSM): Synthesis of percussive sounds. *Computer Music Journal*, 21(3):38–49, 1997.
67. P. R. Cook. Modeling Bill's gait: Analysis and parametric synthesis of walking sounds. In *Proc. Audio Engineering Society 22 Conference on Virtual, Synthetic and Entertainment Audio*, Espoo, Finland, July 2002. AES.
68. G. Courtine and M. Schieppati. Human walking along a curved path. i. body trajectory, segment orientation and the effect of vision. *Eu. J. of Neuroscience*, 18(1):177–190, 2003.
69. D. H. Cress. Terrain considerations and data base development for the design and testing of devices to detect intruder-induced ground motion. Technical Report M-78-1, U.S. Army Engineer Waterways Experiment Station, Vicksburg, Miss., 1978.
70. A. Crevoisier and P. Polotti. Tangible acoustic interfaces and their applications for the design of new musical instruments. In *NIME '05: Proceedings of the 2005 conference on New interfaces for musical expression*, pages 97–100, Singapore, Singapore, 2005. National University of Singapore.
71. A. Crossan, J. Williamson, and R. Murray-Smith. Haptic granular synthesis: Targeting, visualisation and texturing. In *Proc. Intl Symposium on Non-visual & Multimodal Visualization*, pages 527–532, 2004.
72. B. Dalton and M. Bove. Audio-based self-localization for ubiquitous sensor networks. In *118th Audio Engineering Society Convention*, 2005.
73. F. Dalton, F. Farrelly, A. Petri, L. Pietronero, L. Pitolli, and G. Pontuale. Shear stress fluctuations in the granular liquid and solid phases. *Physical Review Letters*, 95(13):138001, 2005.
74. R. Darken, W. Cockayne, and D. Carmein. The omni-directional treadmill: a locomotion device for virtual worlds. In *Proceedings of the 10th annual ACM symposium on User interface software and technology*, pages 213–221. ACM, 1997.
75. A. de Groot, R. Decker, and K. Reed. Gait enhancing mobile shoe (gems) for rehabilitation. In *Proceedings of World Haptics*, pages 190–195, 2009.
76. S. Delle Monache, P. Polotti, and D. Rocchesso. A toolkit for explorations in sonic interaction design. In *Proc. of the 5th Audio Mostly Conf.*, AM '10, pages 1:1–1:7, Pitea, Sweden, 2010. ACM.
77. A. P. Dempster, N. M. Laird, and D. B. Rubin. Maximum likelihood from incomplete data via the EM algorithm. *Proceedings of the Royal Statistical Society*, B-39:1–38, 1977.
78. D. DiFilippo and D. K. Pai. Contact interaction with integrated audio and haptics. In *Proceedings of the International Conference on Auditory Display, ICAD*, 2000.
79. D. E. DiFranco, G. L. Beauregard, and M. A. Srinivasan. The effect of auditory cues on the haptic perception of stiffness in virtual environments. *Proceedings of the ASME Dynamic Systems and Control Division.*, 1997.
80. S. Dixon and A. Cooke. Shoe-Surface Interaction in Tennis. *Biomedical engineering principles in sports*, page 125, 2004.
81. K. v. d. Doel. Physically based models for liquid sounds. *ACM Trans. Appl. Percept.*, 2(4):534–546, 2005.
82. L. Dominjon, A. Lecuyer, J. Burkhardt, G. Andrade-Barroso, and S. Richir. The "Bubble" technique: interacting with large virtual environments using haptic devices with limited workspace. In *Proceedings of World Haptics conference*, pages 639–640, 2005.
83. C. Drioli and D. Rocchesso. Acoustic rendering of Particle-Based simulation of liquids in motion. In *Proceedings of the Int. Conference on digital Audio Effects*, Como, Italy, Sept. 2009.
84. P. Dupont, V. Hayward, B. Armstrong, and F. Altpeter. Single state elastoplastic friction models. *IEEE Transactions on Automatic Control*, 47(5):787–792, 2002.

85. H. Durrant-Whyte and T. C. Henderson. Multisensor data fusion. In *Springer Handbook of Robotics*. Springer-Verlag, 2008.
86. A. Ebrahimpour, A. Hamam, R. L. Sack, and W. Patten. Measuring and modeling dynamic loads imposed by moving crowds. *Journal of Structural Engineering*, pages 1468–1474, 1996.
87. A. Ekimov and J. Sabatier. Vibration and sound signatures of human footsteps in buildings. *J. Acoust. Soc. Am.*, page 762, Jan 2006.
88. A. Ekimov and J. Sabatier. A review of human signatures in urban environments using acoustic and seismic methods. In *Proc. of IEEE Technologies for Homeland Security*, 2008.
89. A. Ekimov and J. M. Sabatier. Human motion analyses using footstep ultrasound and doppler ultrasound. *Journal of the Acoustical Society of America*, 2008(6), 123.
90. D. P. W. Ellis. *Prediction-driven computational auditory scene analysis*. PhD thesis, 1996. Supervisor-Barry L. Vercoe.
91. D. Engel, C. Curio, L. Tcheang, B. Mohler, and H. H. BÃŒlthoff. A psychophysically calibrated controller for navigating through large environments in a limited free-walking space. In *Proceedings of the 2008 ACM symposium on Virtual reality software and technology*, pages 157–164, Bordeaux, France, 2008. ACM.
92. A. J. Eronen, V. T. Peltonen, J. T. Tuomi, A. P. Klapuri, S. Fagerlund, T. Sorsa, G. Lorho, and J. Huopaniemi. Audio-based context recognition. *IEEE Transactions on Audio, Speech and Language Processing*, 14(1):321–329, 2006.
93. A. J. Farnell. Marching onwards – procedural synthetic footsteps for video games and animation. In *pd Convention*, 2007.
94. J. P. Fiene and K. J. Kuchenbecker. Shaping Event-Based haptic transients via an improved understanding of real contact dynamics. In *EuroHaptics Conference, 2007 and Symposium on Haptic Interfaces for Virtual Environment and Teleoperator Systems. World Haptics 2007. Second Joint*, pages 170–175. IEEE, 2007.
95. F. Fontana and R. Bresin. Physics-based sound synthesis and control: crushing, walking and running by crumpling sounds. In *Proc. Colloquium on Musical Informatics*, pages 109–114, Florence, Italy, May 2003.
96. F. Fontana, F. Morreale, T. Regia-Corte, A. Lécuyer, and M. Marchal. Auditory recognition of floor surfaces by temporal and spectral cues of walking. In *Proc. Int. Conf. on Auditory Display*, Budapest, Hungary, Jun. 20-24 2011.
97. D. Fox, J. Hightower, H. Kauz, L. Liao, and D. Patterson. Bayesian techniques for location estimation. In *Proceedings of The 2003 Workshop on Location-Aware Computing*, page 16, 2003.
98. D. Fox, J. Hightower, L. Liao, D. Schulz, and G. Borriello. Bayesian filtering for location estimation. *IEEE Pervasive Computing*, 2(3):24–33, 2003.
99. V. Fox, J. Hightower, L. Liao, D. Schulz, and G. Borriello. Bayesian filtering for location estimation. *Pervasive Computing, IEEE*, 2(3):24–33, July-Sept. 2003.
100. G. J. Franz. Splashes as sources of sound in liquids. *The Journal of the Acoustical Society of America*, 31(8):1080–1096, 1959.
101. Y. Freund and R. E. Schapire. Experiments with a new boosting algorithm. In *International Conference on Machine Learning*, pages 148–156, 1996.
102. P. Froehlich, R. Simon, and L. Baille. Mobile spatial interaction special issue. *Personal and Ubiquitous Computing*, (In press), 2008.
103. M. Fukumoto and T. Sugimura. Active click: tactile feedback for touch panels. In *CHI'01 extended abstracts*, pages 121–122. ACM, 2001.
104. T. Funkhouser, N. Tsingos, and J. Jot. Survey of methods for modeling sound propagation in interactive virtua l environment systems. 2003.
105. D. Gafurov, K. Helkala, and T. Sondrol. Biometric gait authentication using accelerometer sensor. *Journal of Computers*, 1(7):51–59, 2006.
106. D. Gafurov, K. Helkala, and T. Sondrol. Gait recognition using acceleration from mems. In *ARES*, pages 432–439, 2006.
107. F. Galbraith and M. Barton. Ground loading from footsteps. *Journal of the Acoustical Society of America*, Jan 1970.

108. W. W. Gaver. How Do We Hear in the World? Explorations in Ecological Acoustics. *Ecological Psychology*, 5(4):285–313, Apr. 1993.
109. W. W. Gaver. What in the world do we hear?: An ecological approach to auditory event perception. *Ecological psychology*, 5(1):1–29, 1993.
110. Z. Ghahramani and G. E. Hinton. Parameter estimation for linear dynamical systems. Technical Report (Short Note) CRG-TR-96-2, Department of Computer Science, University of Toronto, 1996.
111. Z. Ghahramani and G. E. Hinton. Parameter estimation for linear dynamical systems. Technical Report CRG-TR-96-2, University of Toronto, 1996.
112. B. Giordano, Y. Visell, H.-Y. Yao, V. Hayward, J. Cooperstock, and S. McAdams. Audio-haptic identification of ground materials during walking. *J. of the Acoustical Society of America*, 2011.
113. B. L. Giordano, S. McAdams, Y. Visell, J. R. Cooperstock, H. Yao, and V. Hayward. Non-visual identification of walking grounds. In *Proc. of Acoustics'08 in J. Acoust. Soc. Am.*, volume 123 (5), page 3412, 2008.
114. V. Hayward. Physically-based haptic synthesis. In M. Lin and M. Otaduy, editors, *Haptic Rendering: Foundations, Algorithms and Applications*. AK Peters, Ltd, 2007.
115. V. Hayward, O. Astley, M. Cruz-Hernandez, D. Grant, and G. Robles-De-La-Torre. Haptic interfaces and devices. *Sensor Review*, 24(1):16–29, 2004.
116. V. Hayward and K. Maclean. Do it yourself haptics, part I. *IEEE Robotics and Automation*, December 2007.
117. R. Headon and R. Curwen. Recognizing movements from the ground reaction force. In *Proceedings of the Workshop on Perceptive User Interfaces*, 2001.
118. M. Heintz. Real walking in virtual learning environments: Beyond the advantage of naturalness. In U. Cress, V. Dimitrova, and M. Specht, editors, *Learning in the Synergy of Multiple Disciplines*, volume 5794, pages 584–595. Springer Berlin Heidelberg, Berlin, Heidelberg, 2009.
119. E. A. Heinz, K. steven Kunze, S. Sulistyo, H. Junker, P. Lukowicz, and G. Tröster. Experimental evaluation of variations in primary features used for accelerometric context recognition. In *Proc. of the 1st European Symposium on Ambient Intelligence (EUSAI 2003*, pages 252–263, 2003.
120. H. Herrmann and S. Roux. *Statistical models for the fracture of disordered media*. North Holland, 1990.
121. E. Hoffmann. A comparison of hand and foot movement times. *Ergonomics*, 34(4):397, 1991.
122. J. A. Hogan. The past recaptured: Marcel Proust's aesthetic theory. *Ethics*, 49:187–203, January 1939.
123. J. Hollerbach. Locomotion interfaces and rendering. In M. Lin and M. Otaduy, editors, *Haptic Rendering: Foundations, Algorithms and Applications*. A K Peters, Ltd, 2008.
124. J. Hollerbach, D. Checcacci, H. Noma, Y. Yanagida, and N. Tetsutani. Simulating side slopes on locomotion interfaces using torso forces. In *Proceedings of International Symposium on Haptic Interfaces for Virtual Environment and Teleoperator Systems*, page 91, 2003.
125. J. Hollerbach, R. Mills, D. Tristano, R. Christensen, W. Thompson, and Y. Xu. Torso force feedback realistically simulates slope on treadmill-style locomotion interfaces. *International Journal of Robotics Research*, 20(12):939–952, 2001.
126. J. Hollerbach, Y. Xu, R. Christensen, and S. Jacobsen. Design specifications for the second generation sarcos treadport locomotion interface. In *Proceedings of Haptics Symposium*, pages 1293–1298, 2000.
127. S. H. Holzreiter and M. E. Köhle. Assessment of gait patterns using neural networks. *J. Biomech*, 26(6):645–51, 1993.
128. K. Houston and D. McGaffigan. Spectrum analysis techniques for personnel detection using seismic sensors. In *Proceedings of SPIE*, volume 5090, page 162, 2003.
129. K. M. Houston and D. P. McGaffigan. Spectrum analysis techniques for personnel detection using seismic sensors. *Proc. of SPIE*, 5090:162–173, 2003.

130. S. Howison, J. Ockendon, and J. Oliver. Deep- and shallow-water slamming at small and zero deadrise angles. *Journal of Engineering Mathematics*, 42(3):373–388, Apr. 2002.
131. K. H. Hunt and F. R. E. Crossley. Coefficient of restitution interpreted as damping in vibroimpact. *ASME J. Applied Mech.*, pages 440–445, June 1975.
132. T. Huynh and B. Schiele. Analyzing features for activity recognition. In *sOc-EUSAI '05: Proceedings of the 2005 joint conference on Smart objects and ambient intelligence*, pages 159–163, New York, NY, USA, 2005. ACM.
133. A. J. Ijspeert, J. Nakanishi, and S. Schaal. Learning attractor landscapes for learning motor primitives. In *Advances in Neural Information Processing Systems 15*, pages 1547–1554. MIT Press, 2003.
134. J. A. Ijspeert, J. Nakanishi, and S. Schaal. Learning rhythmic movements by demonstration using nonlinear oscillators. In *IEEE International Conference on Intelligent Robots and Systems (iros 2002)*, pages 958–963, 2002.
135. V. Interrante, B. Ries, and L. Anderson. Seven league boots: A new metaphor for augmented locomotion through moderately large scale immersive virtual environments. In *Proceedings of the IEEE Symposium on 3D User Interfaces*, pages 167—170, 2007.
136. A. Itai and H. Yasukawa. Personal identification using footstep detection based on wavelets. In *Proc. of ISPACS*, 2006.
137. A. Itai and H. Yasukawa. Footstep classification using wavelet decomposition. *Communications and Information Technologies, 2007. ISCIT '07. International Symposium on*, pages 551–556, Oct. 2007.
138. A. Itai and H. Yasukawa. Footstep classification using simple speech recognition technique. *Circuits and Systems, 2008. ISCAS 2008. IEEE International Symposium on*, pages 3234–3237, May 2008.
139. H. Iwata. Walking about virtual environments on an infinite floor. In *Proc. of IEEE Virtual Reality*, 1999.
140. H. Iwata, H. Yano, and F. Nakaizumi. Gait master: A versatile locomotion interface for uneven virtual terrain. In *Proceedings of IEEE Virtual Reality Conference*, pages 131–137, 2001.
141. H. Iwata, H. Yano, and H. Tomioka. Powered shoes. In *Proceedings of SIGGRAPH 2006 Emerging technologies*, page 28, 2006.
142. J. Jacko and A. Sears. *The human-computer interaction handbook: fundamentals, evolving technologies, and emerging applications*. Lawrence Erlbaum Assoc Inc, 2003.
143. V. Jousmaki and R. Hari. Parchment-skin illusion: sound-biased touch. *Current Biology*, 8(6):R190–R191, 1998.
144. R. Kalman and R. Bucy. New results in linear filtering and prediction theory. *ASME Transactions Part D J. Basic Engrg.*, pages 95–108, 1961.
145. M. Kaltenbrunner, T. Bovermann, R. Bencina, and E. Costanza. Tuio: A protocol for table-top tangible user interfaces. In *Proc of Gesture Workshop 2005*. Gesture Workshop, 2005.
146. J. Kekoni, H. Hämäläinen, J. Rautio, and T. Tukeva. Mechanical sensibility of the sole of the foot determined with vibratory stimuli of varying frequency. *Experimental brain research*, 78(2):419–424, 1989.
147. N. Kern and B. Schiele. Context-aware notification for wearable computing. In *ISWC*, pages 223–230. IEEE Computer Society, 2003.
148. N. Kern, B. Schiele, and A. Schmidt. Recognizing context for annotating a live life recording. *Personal and Ubiquitous Computing*, 11(4):251–263, 2007.
149. R. L. Klatzky, D. K. Pai, and E. P. Krotkov. Perception of material from contact sounds. *Presence: Teleoperators and Virtual Environment*, 9(4):399–410, 2000.
150. J. F. Knight, H. W. Bristow, S. Anastopoulou, C. Baber, A. Schwirtz, and T. N. Arvanitis. Uses of accelerometer data collected from a wearable system. *Personal Ubiquitous Comput.*, 11(2):117–132, 2007.
151. L. Kohli, E. Burns, D. Miller, and H. Fuchs. Combining passive haptics with redirected walking. In *Proceedings of the 2005 international conference on Augmented tele-existence*, pages 253–254, Christchurch, New Zealand, 2005. ACM.

152. P. Korpipää, M. Koskinen, J. Peltola, S.-M. Mäkelä, and T. Seppänen. Bayesian approach to sensor-based context awareness. *Personal and Ubiquitous Computing*, 7(2):113–124, 2003.
153. A. Krause, D. P. Siewiorek, A. Smailagic, and J. Farringdon. Unsupervised, dynamic identification of physiological and activity context in wearable computing. In *ISWC*, pages 88–97. IEEE Computer Society, 2003.
154. W. L. Kuan and C. Y. San. Constructivist physics learning in an immersive, multi-user hot air balloon simulation program (iHABS). In *ACM SIGGRAPH 2003 Educators Program*, page 1. ACM Press, 2003.
155. K. J. Kuchenbecker, J. Fiene, and G. Niemeyer. Improving contact realism through event-based haptic feedback. *IEEE Transactions on Visualization and Computer Graphics*, 12(2):219–230, 2006.
156. K. Kunze, P. Lukowicz, H. Junker, and G. Tröster. Where am i: Recognizing on-body positions of wearable sensors. In *In: LOCA'04: International Workshop on Locationand Context-Awareness*, pages 264–275. Springer-Verlag, 2005.
157. K. V. Laerhoven and O. Cakmakci. What shall we teach our pants? In *ISWC '00: Proceedings of the 4th IEEE International Symposium on Wearable Computers*, page 77, Washington, DC, USA, 2000. IEEE Computer Society.
158. K. V. Laerhoven and H.-W. Gellersen. Spine versus porcupine: A study in distributed wearable activity recognition. In *ISWC '04: Proceedings of the Eighth International Symposium on Wearable Computers*, pages 142–149, Washington, DC, USA, 2004. IEEE Computer Society.
159. J. J. LaViola, D. A. Feliz, D. F. Keefe, and R. C. Zeleznik. Hands-free multi-scale navigation in virtual environments. In *Proceedings of the ACM symposium on Interactive 3D graphics*, pages 9–15. ACM, 2001.
160. J. LaViola Jr, D. Feliz, D. Keefe, and R. Zeleznik. Hands-free multi-scale navigation in virtual environments. In *Proc of the 2001 symposium on Interactive 3D graphics*, pages 9–15. ACM New York, NY, USA, 2001.
161. A. Law, B. Peck, Y. Visell, P. Kry, and J. Cooperstock. A multi-modal floor-space for displaying material deformation underfoot in virtual reality. In *Proc. of the IEEE Intl. Workshop on Haptic Audio Visual Environments and Their Applications*, 2008.
162. A. Lécuyer. Simulating haptic feedback using vision: a survey of research and applications of pseudo-haptic feedback. *Presence: Teleoperators and Virtual Environments*, 18(1):39–53, 2009.
163. A. Lécuyer, J.-M. Burkhardt, and L. Etienne. Feeling bumps and holes without a haptic interface: the perception of pseudo-haptic textures. In *Proceedings of SIGCHI Conference on Human factors in computing systems*, pages 239–246, 2004.
164. A. Lécuyer, J.-M. Burkhardt, J.-M. Henaff, and S. Donikian. Camera motions improve sensation of walking in virtual environments. In *Proceedings of IEEE International Conference on Virtual Reality*, pages 11–18, 2006.
165. A. Lécuyer, J.-M. Burkhardt, J.-M. Henaff, and S. Donikian. Camera motions improve the sensation of walking in virtual environments. In *Proceedings of IEEE Virtual Reality*, pages 11–18, 2006.
166. S. Lederman. Auditory texture perception. *Perception*, 1979.
167. M.-Y. Lee, K.-S. Soon, and C.-F. Lin. New computer protocol with subsensory stimulation and visual/auditory biofeedback for balance assessment in amputees. *J. of Computers*, 4(10):1005–1011, Oct. 2009.
168. S.-W. Lee and K. Mase. Activity and location recognition using wearable sensors. *IEEE Pervasive Computing*, 1(3):24–32, 2002.
169. E. A. Lehmann. *Particle Filtering Methods for Acoustic Source Localisation and Tracking*. PhD thesis, Australian National University, 2004.
170. M. Lesser. Thirty years of liquid impact research: a tutorial review. *Wear*, 186-187(Part 1):28–34, July 1995.
171. J. Lester, T. Choudhury, N. Kern, G. Borriello, and B. Hannaford. A hybrid discriminative/generative approach for modeling human activities. In L. P. Kaelbling and A. Saffiotti,

editors, *IJCAI-05, Proceedings of the Nineteenth International Joint Conference on Artificial Intelligence, Edinburgh, Scotland, UK, July 30-August 5, 2005*, pages 766–772. Professional Book Center, 2005.
172. X. Li, R. J. Logan, and R. E. Pastore. Perception of acoustic source characteristics: Walking sounds. *Journal of the Acoustical Society of America*, 90(6):3036–3049, 1991.
173. L. Liao. *Location-based activity recognition*. PhD thesis, University of Washington, 1996.
174. L. Liao, D. Fox, and H. Kautz. Extracting places and activities from gps traces using hierarchical conditional random fields. *Int. J. Robotics Research*, 2007.
175. L. Liao, D. J. Patterson, D. Fox, and H. Kautz. Learning and inferring transportation routines. *Artificial Intelligence*, 171(5–6):311–331, 2007.
176. M. S. Longuet-Higgins. An analytic model of sound production by raindrops. *Journal of Fluid Mechanics*, 214:395–410, 1990.
177. P. Lukowicz, J. A. Ward, H. Junker, M. Stäger, G. Tröster, A. Atrash, and T. Starner. Recognizing workshop activity using body worn microphones and accelerometers. In A. Ferscha and F. Mattern, editors, *Pervasive Computing, Second International Conference, PERVASIVE 2004, Vienna, Austria, April 21-23, 2004, Proceedings*, volume 3001 of *Lecture Notes in Computer Science*, pages 18–32. Springer, 2004.
178. P. Lukowicz, J. A. Ward, H. Junker, M. Stäger, G. Tröster, A. Atrash, and T. Starner. Recognizing workshop activity using body worn microphones and accelerometers. In A. Ferscha and F. Mattern, editors, *Pervasive Computing, Second International Conference, PERVASIVE 2004, Vienna, Austria, April 21-23, 2004, Proceedings*, volume 3001 of *Lecture Notes in Computer Science*, pages 18–32. Springer, 2004.
179. A. MacEachren, G. Cai, R. Sharma, I. Rauschert, I. Brewer, L. Bolelli, B. Shaparenko, S. Fuhrmann, and H. Wang. Enabling collaborative geoinformation access and decision-making through a natural, multimodal interface. *International Journal of Geographical Information Science*, 19(3):293–317, 2005.
180. I. MacKenzie. Fitts' law as a research and design tool in human-computer interaction. *Human-Computer Interaction*, 7(1):91–139, 1992.
181. M. Mahvash and V. Hayward. Haptic rendering of cutting: A fracture mechanics approach. *Haptics-e*, 2(3):1–12, 2001.
182. J. Mantyjarvi, M. Lindholm, E. Vildjiounaite, S.-M. Makela, and H. J. Ailisto. Identifying users of portable devices from gait pattern with accelerometers. In *Proc. IEEE Intl. Conf. on Acoustics, Speech, and Signal Processing*, 2005.
183. M. J. Mathie, A. C. F. Coster, N. H. Lovell, and B. G. Celler. TOPICAL REVIEW: Accelerometry: providing an integrated, practical method for long-term, ambulatory monitoring of human movement. *Physiological Measurement*, 25:1–+, Apr. 2004.
184. G. P. Mazarakis and J. N. Avaritsiotis. A prototype sensor node for footstep detection. In *Wireless Sensor Networks, 2005. Proceeedings of the Second European Workshop on*, pages 415–418, 2005.
185. T. McGuine and J. Keene. The effect of a balance training program on the risk of ankle sprains in high school athletes. *The American journal of sports medicine*, 34(7):1103, 2006.
186. R. Meir and G. Rätsch. An introduction to boosting and leveraging. pages 118–183, 2003.
187. L. Middleton, A. Buss, A. Bazin, and M. Nixon. A floor sensor system for gait recognition. In *Proceedings of the Fourth IEEE Workshop on Automatic Identification Advanced Technologies*, pages 171–176, 2005.
188. T. Minka. Bayesian inference in dynamical models – an overview. Web published, Aug. 2008. `http://research.microsoft.com/users/minka/papers/dynamic.html`.
189. M. Minnaert. On musical air-bubbles and the sounds of running water. *Philosophical Magazine Series 7*, 16(104):235 – 248, 1933.
190. D. Minnen, T. Starner, J. Ward, P. Lukowicz, and G. Troster. Recognizing and discovering human actions from on-body sensor data. *Multimedia and Expo, IEEE International Conference on*, 0:1545–1548, 2005.
191. D. Mitrovic. Discrimination and retrieval of environmental sounds. Master's thesis, Vienna University of Technology, 2005.

192. T. Moeslund and E. Granum. A survey of computer vision-based human motion capture. *Computer Vision and Image Understanding*, 81(3):231–268, 2001.
193. T. Moeslund, A. Hilton, and V. Krueger. A survey of advances in vision-based human motion capture and analysis. *Computer vision and image understanding*, 104(2-3):90–126, 2006.
194. J. J. Monaghan. Smoothed particle hydrodynamics. *Annual Review of Astronomy and Astrophysics*, 30(1):543–574, Sept. 1992.
195. M. Morioka, D. Whitehouse, and M. Griffin. Vibrotactile thresholds at the fingertip, volar forearm, large toe, and heel. *Somatosensory & Motor Research*, 25(2):101–112, 2008.
196. H. Morishita, R. Fukui, and T. Sato. High resolution pressure sensor distributed floor for future human-robot symbiosis environments. In *IEEE/RSJ International Conference on Intelligent Robots and Systems (IROS 2002), Lausanne, Switzerland*, pages 1246–1251, 2002.
197. W. Moss, H. Yeh, J. Hong, M. C. Lin, and D. Manocha. Sounding liquids: Automatic sound synthesis from fluid simulation. *ACM Trans. Graph.*, 29(3):1–13, 2010.
198. A. Mostayed, M. M. G. Mazumder, S. Kim, and S. J. Park. Abnormal gait detection using discrete fourier transform. In *MUE*, pages 36–40, 2008.
199. M. Muller, D. Charypar, and M. Gross. Particle-based fluid simulation for interactive applications. In *Proceedings of the 2003 ACM SIGGRAPH/Eurographics symposium on Computer animation*, pages 154–159, San Diego, California, 2003. Eurographics Association.
200. M. Muller, B. Solenthaler, R. Keiser, and M. Gross. Particle-based fluid-fluid interaction. In *Proceedings of the 2005 ACM SIGGRAPH/Eurographics symposium on Computer animation*, pages 237–244, Los Angeles, California, 2005. ACM.
201. T. Murakita, T. Ikeda, and H. Ishiguro. Human tracking using floor sensors based on the Markov chain Monte Carlo method. In *Pattern Recognition, 2004. ICPR 2004. Proceedings of the 17th International Conference on*, volume 4, 2004.
202. K. Murphy. *Dynamic Bayesian Network : Representation, Inference and Learning*. PhD thesis, The University of California at Berkeley, 2002.
203. R. Murray-Smith, J. Williamson, S. Hughes, and T. Quaade. Stane: synthesized surfaces for tactile input. In M. Czerwinski, A. M. Lund, and D. S. Tan, editors, *Proceedings of the 2008 Conference on Human Factors in Computing Systems, CHI 2008, 2008, Florence, Italy, April 5-10, 2008*, pages 1299–1302. ACM, 2008.
204. A. Nashel and S. Razzaque. Tactile virtual buttons for mobile devices. In *Proceedings of CHI*, pages 854–855. ACM, 2003.
205. S. Nasuno, A. Kudrolli, A. Bak, and J. Gollub. Time-resolved studies of stick-slip friction in sheared granular layers. *Physical Review E*, 58(2):2161–2171, 1998.
206. S. Nasuno, A. Kudrolli, and J. Gollub. Friction in granular layers: hysteresis and precursors. *Physical Review Letters*, 79(5):949–952, 1997.
207. N. Nitzsche, U. D. Hanebeck, and G. Schmidt. Motion compression for telepresent walking in large target environments. *Presence: Teleoper. Virtual Environ.*, 13(1):44–60, 2004.
208. H. Noma. Design for locomotion interface in a large-scale virtual environment. atlas: Atr locomotion interface for active self-motion. In *Proceedings of the ASME Dynamic Systems and control division*, pages 111–118, 1998.
209. H. Noma, T. Sugihara, and T. Miyasato. Development of ground surface simulator for tel-e-merge system. In *Proceedings of IEEE Virtual Reality Conference*, page 217, 2000.
210. R. Nordahl. Increasing the motion of users in photorealistic virtual environments by utilizing auditory rendering of the environment and ego-motion. *Proceedings of Presence*, pages 57–62, 2006.
211. R. Nordahl, A. Berrezag, S. Dimitrov, L. Turchet, V. Hayward, and S. Serafin. Preliminary experiment combining virtual reality haptic shoes and audio synthesis. *Haptics: Generating and Perceiving Tangible Sensations*, pages 123–129, 2010.
212. R. Nordahl, S. Serafin, and L. Turchet. Sound Synthesis and Evaluation of Interactive Footsteps for Virtual Re ality Applications. In *Proc. IEEE Virtual Reality*, 2010.
213. D. Norman. *The Design of Future Things*. Basic Books, New York, 2007.
214. B. North, A. Blake, M. Isard, and J. Rittscher. Learning and classification of complex dynamics. *IEEE Transactions on Pattern Analysis and Machine Intelligence*, 22:1016–1034, 2000.

215. J. F. O'Brien and J. K. Hodgins. Graphical modeling and animation of brittle fracture. In *Proceedings of the 26th annual conference on Computer graphics and interactive techniques*, SIGGRAPH '99, pages 137–146, New York, NY, USA, 1999. ACM Press/Addison-Wesley Publishing Co.
216. A. M. Okamura, M. R. Cutkosky, and J. T. Dennerlein. Reality-based models for vibration feedback in virtual environments. *IEEE/ASME Transactions on Mechatronics*, 6(3):245–252, 2001.
217. A. M. Okamura, J. T. Dennerlein, and R. D. Howe. Vibration feedback models for virtual environments. In *1998 IEEE International Conference on Robotics and Automation, 1998. Proceedings*, volume 1, pages 674–679 vol.1. IEEE, 1998.
218. R. J. Orr and G. D. Abowd. The smart floor: a mechanism for natural user identification and tracking. In *ACM CHI extended abstracts*, pages 275–276, New York, NY, USA, 2000. ACM.
219. D. Pai, K. Doel, D. James, J. Lang, J. Lloyd, J. Richmond, and S. Yau. Scanning physical interaction behavior of 3d objects. In *Proceedings of the 28th annual conference on Computer graphics and interactive techniques*, pages 87–96, 2001.
220. A. Pakhomov and T. Goldburt. Seismic signals and and noise assesment for footstep detection range estimation in different environments. In *Proc. of SPIE*, volume 5417, 2004.
221. A. Pakhomov, A. Sicignano, M. Sandy, and T. Goldburt. Seismic footstep signal characterization. In *Proc. of SPIE*, volume 5071, pages 297–305, 2003.
222. T. Pakkanen and R. Raisamo. Appropriateness of foot interaction for non-accurate spatial tasks. In *CHI '04: CHI '04 extended abstracts on Human factors in computing systems*, pages 1123–1126, New York, NY, USA, 2004. ACM.
223. M. Palaniswami and R. Begg. *Computational Intelligence for Movement Sciences: Neural Networks and Other Emerging Techniques (Computational Intelligence and Its Applications Series)*. IGI Publishing, Hershey, PA, USA, 2006.
224. S. Papetti, F. Avanzini, and D. Rocchesso. Energy and accuracy issues in numerical simulations of a non-linear impact model. In *Proc. Conf. on Digital Audio Effects (DAFX-09)*, Como, Italy, September 2009.
225. S. Papetti, M. Civolani, F. Fontana, A. Berrezag, and V. Hayward. Audio-tactile display of ground properties using interactive shoes. In *Proc. 5th Int. Haptic and Auditory Interaction Design Workshop*, pages 117–128, Sept. 2010.
226. S. Papetti, F. Fontana, and M. Civolani. A shoe-based interface for ecological ground augmentation. In *Proc. 4th Int. Haptic and Auditory Interaction Design Workshop*, volume 2, Dresden, Germany, Sep. 10-11 2009.
227. S. Papetti, F. Fontana, and M. Civolani. Effects of ecological auditory and vibrotactile underfoot feedback on human gait: a preliminary investigation. In *Proc. 6th Int. Workshop on Haptic and Audio Interaction Design (HAID 2011)*, Kyoto, Japan, 2011.
228. J. Paradiso, C. Abler, K.-y. Hsiao, and M. Reynolds. The magic carpet: physical sensing for immersive environments. In *ACM CHI extended abstracts*, pages 277–278, New York, NY, USA, 1997. ACM.
229. J. Parkka, M. Ermes, P. Korpipää, J. Mäntyjärvi, J. Peltola, and I. Korhonen. Activity classification using realistic data from wearable sensors. *IEEE Transactions on Information Technology in Biomedicine*, 10(1):119–128, 2006.
230. R. D. Patterson, K. Robinson, J. Holdsworth, D. McKeown, C.Zhang, and M. H. Allerhand. Complex sounds and auditory images. In Y. Cazals, L. Demany, and K. Horner, editors, *Auditory Physiology and Perception*. Pergamon, 1992.
231. M. Pauly, R. Keiser, B. Adams, P. Dutré, M. Gross, and L. J. Guibas. Meshless animation of fracturing solids. In *ACM Transactions on Graphics (TOG)*, SIGGRAPH '05, New York, NY, USA, 2005. ACM. ACM ID: 1073296.
232. R. Pausch, T. Burnette, D. Brockway, and M. E. Weiblen. Navigation and locomotion in virtual worlds via flight into hand-held miniatures. In *Proceedings of ACM SIGGRAPH*, pages 399–400. ACM, 1995.

233. G. Pearson and M. Weiser. Of moles and men: the design of foot controls for workstations. In *Proc of the ACM SIGCHI conf on Human factors in Comp Sys*, pages 333–339. ACM New York, NY, USA, 1986.
234. T. Peck, M. Whitton, and H. Fuchs. Evaluation of reorientation techniques for walking in large virtual environments. In *Virtual Reality Conference, 2008. VR '08. IEEE*, pages 121–127, 2008.
235. L. Peltola, C. Erkut, P. R. Cook, and V. Välimäki. Synthesis of hand clapping sounds. *IEEE Trans. Audio, Speech and Language Proc.*, 15(3):1021–1029, 2007.
236. V. Peltonen, J. Tuomi, A. Klapuri, J. Huopaniemi, and T. Sorsa. Computational auditory scene recognition. In *Proc. of IEEE Conf. on Acoustics, Speech and Signal Processing (ICASSP'02)*, 2002.
237. S. Perreault and C. Gosselin. Cable-driven parallel mechanisms: Application to a locomotion interface. *Journal of Mechanical Design*, 130:102301, 2008.
238. J. Perry. *Gait analysis: normal and pathological function*. SLACK incorporated, 1992.
239. R. F. Pinkston. A touch sensitive dance floor/midi controller. *Journal of the Acoustical Society of America*, 96(5):3302–3302, 1994.
240. S. Pirttikangas, J. Suutala, J. Riekki, and J. Röning. Learning vector quantization in footstep identification. In *Proceedings of 3rd IASTED International Conference on Artificial Intelligence and Applications (AIA), IASTED*, 2003.
241. A. Polaine. The flow principle in interactivity. In *Proceedings of the 2nd Au. conf. on Interactive Entertainment*, page 158, 2005.
242. I. Potamitis, H. Chen, and G. Tremoulis. Tracking of multiple moving speakers with multiple microphone arrays. *Speech and Audio Processing, IEEE Transactions on*, 12(5):520–529, Sept. 2004.
243. R. L. Potter, L. J. Weldon, and B. Shneiderman. Improving the accuracy of touch screens: an experimental evaluation of three strategies. In *CHI '88: Proc of the SIGCHI conference on Human factors in computing systems*, pages 27–32, New York, NY, USA, 1988. ACM.
244. I. Poupyrev, S. Maruyama, and J. Rekimoto. Ambient touch: designing tactile interfaces for handheld devices. In *Proceedings of UIST*. ACM, 2002.
245. A. Quarteroni, R. Sacco, and F. Saleri. *Numerical Mathematics*. Springer, 2nd edition, 2007.
246. L. R. Rabiner and B. H. Juang. An introduction to hidden Markov models. *IEEE ASSP Magazine*, 3(1):4–16, Jan 1986.
247. R. Radhakrishnan and D. Divakaran. Generative process tracking for audio analysis. In *IEEE International Conference on Acoustics, Speech and Signal Processing*, 2006.
248. A. Rahimi. *Learning to transform time Series with a Few Examples*. PhD thesis, Massachussetts Institute of Technology, 2006.
249. C. Ramstein and V. Hayward. The pantograph: A large workspace haptic device for a multimodal human-computer interaction. In *Proceedings of the SIGCHI conference on Human factors in computing systems, CHI'04, ACM/SIGCHI Companion-4/94*, pages 57–58, 1994.
250. C. Randell and H. Muller. Context awareness by analyzing accelerometer data. In *ISWC '00: Proceedings of the 4th IEEE International Symposium on Wearable Computers*, page 175, Washington, DC, USA, 2000. IEEE Computer Society.
251. I. Rauschert, P. Agrawal, R. Sharma, S. Fuhrmann, I. Brewer, and A. MacEachren. Designing a human-centered, multimodal gis interface to support emergency management. In *GIS '02: Proceedings of the 10th ACM international symposium on Advances in geographic information systems*, pages 119–124, New York, NY, USA, 2002. ACM.
252. N. Ravi, N. Dandekar, P. Mysore, and M. L. Littman. Activity recognition from accelerometer data. *American Association for Artificial Intelligence*, 2005.
253. S. Razzaque, Z. Kohn, and M. Whitton. Redirected walking. In *Proc of EUROGRAPHICS*, pages 289–294, 2001.
254. S. Razzaque, Z. Kohn, and M. C. Whitton. Redirected walking. In *Proceedings of Eurographics*, 2001.
255. S. Razzaque, D. Swapp, M. Slater, M. C. Whitton, and A. Steed. Redirected walking in place. In *Proceedings of the workshop on Virtual environments 2002*, pages 123–130, Barcelona, Spain, 2002. Eurographics Association.

256. E. G. Richardson. The sounds of impact of a solid on a liquid surface. *Proceedings of the Physical Society. Section B*, 68(8):541–547, Aug. 1955.
257. I. Rius, X. Varona, F. X. Roca, and J. Gonzàlez. Posture constraints for bayesian human motion tracking. In *Articulated Motion and Deformable Objects*, pages 414–423. Springer Verlag, 2006.
258. D. Rocchesso and F. Fontana, editors. *The Sounding Object*. Edizioni di Mondo Estremo, Florence, Italy, 2003.
259. N. Roman and D. Wang. Binaural tracking of multiple moving sources. *Acoustics, Speech, and Signal Processing, 2003. Proceedings. (ICASSP '03). 2003 IEEE International Conference on*, 5:V–149–52 vol.5, April 2003.
260. S. Roweis and Z. Ghahramani. A unifying review of linear gaussian models. *Neural Computation*, 11(2):305–345, 1999.
261. S. Roweis and Z. Ghahramani. An em algorithm for identification of nonlinear dynamical systems. In *Proc. of Neural Information Processing Systems 13 (NIPS'00)*, 2000.
262. R. A. Ruddle and S. Lessels. The benefits of using a walking interface to navigate virtual environments. *ACM Trans. Comput.-Hum. Interact.*, 16(1):1–18, 2009.
263. K. Salisbury, F. Conti, and F. Barbagli. Haptic rendering: introductory concepts. *IEEE Computer Graphics and Applications*, 24(2):24– 32, 2004.
264. R. Sanders and M. Scorgie. The Effect of Sound Delivery Methods on a User's Sense of Presence in a Virtual Environment, 2002.
265. J. Schacher and M. Neukom. Ambisonics Spatialization Tools for Max/MSP. In *Proceedings of the International Computer Music Conference*, 2006.
266. R. M. Schafer. *The tuning of the world*. Random House Inc., 1977.
267. A. Schmidt, M. Strohbach, K. v. Laerhoven, A. Friday, and H.-W. Gellersen. Context acquisition based on load sensing. In *UbiComp '02: Proceedings of the 4th international conference on Ubiquitous Computing*, pages 333–350, London, UK, 2002. Springer-Verlag.
268. S. Serafin, L. Turchet, R. Nordahl, S. Dimitrov, A. Berrezag, and V. Hayward. Identification of virtual grounds using virtual reality haptic shoes and sound synthesis. In *Proceedings of Eurohaptics symposium on Haptic and Audio-Visual Stimuli: Enhancing Experiences and Interaction*, 2010.
269. J. P. Sethna, K. A. Dahmen, and C. R. Myers. Crackling noise. *Nature*, (410):242–250, Mar. 2001.
270. S. Shimojo and L. Shams. Sensory modalities are not separate modalities: plasticity and interactions. *Current Opinion in Neurobiology*, 11(4):505–509, 2001.
271. Y. Shoji, A. Itai, and H. Yasukawa. Personal identification using footstep detection in indoor environments. *IEICE Trans. Fundamentals*, E88-A(8), 2005.
272. R. H. Shumway and D. S. Stoffer. An approach to time series smoothing and forecasting using the em algorithm. *J. of Time Series Analysis*, 3(4), 1982.
273. J. Sinclair, P. Hingston, and M. Masek. Considerations for the design of exergames. In *Proc of the 5th Int ACM Conf on Comp Graphics and Interactive Techniques, Southeast Asia*, page 295, 2007.
274. M. Slater, M. Usoh, and A. Steed. Taking steps: The influence of a walking technique on presence in virtual reality. *ACM Trans. on Computer-Human Interaction*, 2(3):201–219, 1995.
275. J. Sreng, F. Bergez, J. Legarrec, A. Lécuyer, and C. Andriot. Using an event-based approach to improve the multimodal rendering of 6dof virtual contact. In *Proceedings of ACM Symposium on Virtual Reality Software and Technology (ACM VRST)*, pages 173–179, 2007.
276. M. A. Srinivasan and C. Basdogan. Haptics in virtual environments: Taxonomy, research status, and challenges. *Computers & Graphics*, 21(4):393–404, 1997.
277. M. Stäger, P. Lukowicz, N. Perera, T. von Büren, G. Tröster, and T. Starner. Soundbutton: Design of a low power wearable audio classification system. In *ISWC*, pages 12–17. IEEE Computer Society, 2003.
278. F. Steinicke, G. Bruder, J. Jerald, H. Frenz, and M. Lapp. Estimation of detection thresholds for redirected walking techniques. *IEEE Transactions on Visualization and Computer Graphics*, 16(1):17–27, 2009.

279. F. Steinicke, G. Bruder, T. Ropinski, and K. H. Hinrichs. Moving towards generally applicable redirected walking. In *Proceedings of the Virtual Reality International Conference (VRIC)*, pages 15—24. IEEE Press, 2008.
280. V. Stiles, I. James, S. Dixon, and I. Guisasola. Natural Turf Surfaces: The Case for Continued Research. *Sports Medicine*, 39(1):65, 2009.
281. R. L. Storms and M. J. Zyda. Interactions in Perceived Quality of Auditory-Visual Displays. *Presence: Teleoperators & Virtual Environments*, 9(6):557–580, 2000.
282. J. Su. Motion compression for telepresence locomotion. *Presence: Teleoper. Virtual Environ.*, 16(4):385–398, 2007.
283. A. Subramanya, A. Raj, J. Bilmes, and D. Fox. Recognizing activities and spatial context using wearable sensors. In *In Proc. of the Conference on Uncertainty in Artificial Intelligence (UAI*, 2006.
284. G. Succi, D. Clapp, R. Gampert, and G. Prado. Footstep detection and tracking. In *Proc. of SPIE*, 2001.
285. E. A. Suma, S. Clark, D. Krum, S. Finkelstein, M. Bolas, and Z. Warte. Leveraging change blindness for redirection in virtual environments. In *2011 IEEE Virtual Reality Conference (VR)*, pages 159–166. IEEE, 2011.
286. J. Suutala, K. Fujinami, and J. Roening. Gaussian Process Person Identifier Based on Simple Floor Sensors. In *Proceedings of the 3rd European Conference on Smart Sensing and Context*, page 68. Springer-Verlag, 2008.
287. J. Suutala and J. Röning. Combining classifiers with different footstep feature sets and multiple samples for person identification. In *IEEE International Conference on Acoustics, Speech, and Signal Processing (ICASSP)*, volume 5, 2005.
288. J. Suutala and J. Roning. Methods for person identification on a pressure-sensitive floor: Experiments with multiple classifiers and reject option. *Information Fusion*, 9(1), 2008.
289. M. Tanaka and H. Inoue. A study on walk recognition by frequency analysis of footsteps. *Trans. IEE of Japan*, 119-C(6), 1999.
290. E. M. Tapia, S. Intille, and K. Larson. Real-time recognition of physical activities and their intensities using wireless accelerometers and a heart rate monitor. In *Proceedings of the 11th International Conference on Wearable Computers (ISWC '07)*, 2007.
291. E. M. Tapia, S. S. Intille, and K. Larson. Activity recognition in the home using simple and ubiquitous sensors. pages 158–175. 2004.
292. J. Taylor and Q. Huang. *CRC handbook of electrical filters*. CRC, 1997.
293. J. Templeman, P. Denbrook, and L. Sibert. Virtual locomotion: Walking in place through virtual environments. *Presence*, 8(6):598–617, 1999.
294. J. N. Templeman, P. S. Denbrook, and L. E. Sibert. Virtual locomotion: Walking in place through virtual environments. *Presence: Teleoper. Virtual Environ.*, 8(6):598–617, 1999.
295. L. Terziman, A. Lécuyer, S. Hillaire, and J. M. Wiener. Can camera motions improve the perception of traveled distance in virtual environments? In *Proceedings of IEEE Virtual Reality Conference*, pages 131–134, 2009.
296. S. Thrun, W. Burgard, and D. Fox. *Probabilistic Robotics*. MIT Press, 2005.
297. S. Thrun, W. Burgard, and D. Fox. *Probabilistic Robotics (Intelligent Robotics and Autonomous Agents)*. The MIT Press, September 2005.
298. H. Tramberend, F. Hasenbrink, G. Eckel, U. Lechner, and M. Goebel. CyberStage – An Advanced Virtual Environment. *ERCIM News*, 31, October 1997.
299. L. Turchet, M. Marchal, A. Lécuyer, R. Nordahl, and S. Serafin. Influence of auditory and visual feedback for perceiving walking over bumps and holes in desktop vr. In *Proceedings of the 17th ACM Symposium on Virtual Reality Software and Technology*, pages 139–142. ACM, 2010.
300. L. Turchet, M. Marchal, A. Lécuyer, S. Serafin, and R. Nordahl. Influence of visual feedback for perceiving walking over bumps and holes in desktop vr. In *Proceedings of 17th ACM Symposium on Virtual Reality Software and Technology*, pages 139–142, 2010.
301. L. Turchet and S. Serafin. A preliminary study on sound delivery methods for footstep sounds. In *Proc. Conf. on Digital Audio Effects (DAFX-11)*, Paris, France, Sept. 2011.

302. L. Turchet, S. Serafin, S. Dimitrov, and R. Nordahl. Conflicting audio-haptic feedback in physically based simulation of walking sounds. *Haptic and Audio Interaction Design*, pages 97–106, 2010.
303. L. Turchet, S. Serafin, and R. Nordahl. Examining the role of context in the recognition of walking sounds. In *Proceedings of Sound and Music Computing Conference*, 2010.
304. L. Turchet, S. Serafin, and R. Nordahl. Physically based sound synthesis and control of footsteps sounds. In *Proc. Conf. on Digital Audio Effects (DAFX-10)*, Graz, Austria, Sep. 6-10 2010.
305. M. Usoh, K. Arthur, M. C. Whitton, R. Bastos, A. Steed, M. Slater, and J. Frederick P. Brooks. Walking > walking-in-place > flying, in virtual environments. In *Proceedings of the 26th annual conference on Computer graphics and interactive techniques*, pages 359–364. ACM Press/Addison-Wesley Publishing Co., 1999.
306. K. van den Doel, P. Kry, and D. Pai. FoleyAutomatic: physically-based sound effects for interactive simulation and animation. *Proceedings of the 28th annual conference on Computer graphics and interactive techniques*, pages 537–544, 2001.
307. Y. Visell and J. Cooperstock. Enabling gestural interaction by means of tracking dynamical systems models and assistive feedback. In *Proc. of the IEEE Intl. Conf. on Systems, Man, and Cybernetics*, Montreal, 2007.
308. Y. Visell and J. Cooperstock. Design of a Vibrotactile Display via a Rigid Surface. In *Proc. of IEEE Haptics Symposium*, 2010.
309. Y. Visell, J. Cooperstock, B. L. Giordano, K. Franinovic, A. Law, S. McAdams, K. Jathal, and F. Fontana. A vibrotactile device for display of virtual ground materials in walking. In *Proc. of Eurohaptics 2008*, 2008.
310. Y. Visell, F. Fontana, B. Giordano, R. Nordahl, S. Serafin, and R. Bresin. Sound design and perception in walking interactions. *International Journal of Human-Computer Studies*, 2009.
311. Y. Visell, F. Fontana, B. Giordano, R. Nordahl, S. Serafin, and R. Bresin. Sound design and perception in walking interactions. *Int. J. Human-Computer Studies*, (67):947–959, 2009.
312. Y. Visell, B. Giordano, G. Millet, and J. Cooperstock. Vibration influences haptic perception of surface compliance during walking. *PloS one*, 6(3):e17697, 2011.
313. Y. Visell, A. Law, and J. Cooperstock. Touch Is Everywhere: Floor Surfaces as Ambient Haptic Interfaces. *IEEE Transactions on Haptics*, 2009.
314. Y. Visell, A. Law, J. Ip, S. Smith, and J. R. Cooperstock. Interaction Capture in Immersive Virtual Environments via an Intelligent Floor Surface. In *Proc. of IEEE Virtual Reality*, 2010 (To appear).
315. Y. Visell, A. Law, S. Smith, R. Rajalingham, and J. Cooperstock. Contact sensing and interaction techniques for a distributed multimodal floor display. In *Proc. of IEEE 3DUI*, 2010.
316. Y. Visell, S. Smith, A. Law, R. Rajalingham, and J. Cooperstock. Contact sensing and interaction techniques for a distributed, multimodal floor display. In *3D User Interfaces (3DUI), 2010 IEEE Symposium on*, pages 75–78. IEEE, 2010.
317. E. Wan and R. van der Merwe. *The Unscented Kalman Filter*. Wiley Publishing, 2001.
318. E. A. Wan and R. V. D. Merwe. The unscented kalman filter for nonlinear estimation. *Adaptive Systems for Signal Processing, Communications, and Control Symposium 2000. AS-SPCC. The IEEE 2000*, pages 153–158, 2000.
319. J. Wang. Gaussian process dynamical models for human motion. *IEEE Trans. on Pattern Analysis and Machine Intelligence*, 30(2), 2008.
320. J. Wang, D. Fleet, and A. Hertzmann. Gaussian process dynamical models. In *Advances in Neural Information Processing Systems 18*, 2005.
321. J. A. Ward. *Activity monitoring: continuous recognition and performance evaluation*. PhD thesis, ETH Zürich, Switzerland, 2006.
322. J. A. Ward, P. Lukowicz, G. Troster, and T. E. Starner. Activity recognition of assembly tasks using body-worn microphones and accelerometers. *IEEE Trans. Pattern Analysis and Machine Intelligence*, 28(10):1553–1567, Oct. 2006.
323. B. G. Watters. Impact noise characteristics of female hard-heeled foot traffic. *J. Acoust. Soc. Am.*, 37:619–630, 1965.

324. L. Wauben, M. van Veelen, D. Gossot, and R. Goossens. Application of ergonomic guidelines during minimally invasive surgery: a questionnaire survey of 284 surgeons. *Surgical endoscopy*, 20(8):1268–1274, 2006.
325. E. Weinstein, K. Steele, A. Agarwal, and J. Glass. Loud: A 1020-node modular microphone array and beamformer for intelligent computing spaces. Technical report, Massachusetts Institute of Technology, 2004.
326. A. Westner and V. M. B. Jr. Applying blind source separation and deconvolution to real-world acoustic environments. In *Proc. of the AES*, 1999.
327. A. Westner and V. M. B. Jr. Blind separation of real world audio signals using overdetermined mixtures. In *Proc. Int. Conf. on Independent Component Analysis and Blind Source Separation*, pages 251–256, 1999.
328. B. Williams, G. Narasimham, B. Rump, T. P. McNamara, T. H. Carr, J. Rieser, and B. Bodenheimer. Exploring large virtual environments with an HMD when physical space is limited. In *Proceedings of the ACM symposium on Applied perception in graphics and visualization*, pages 41–48, Tubingen, Germany, 2007. ACM.
329. X. Xie, Q. Lin, H. Wu, G. Narasimham, T. P. McNamara, J. Rieser, and B. Bodenheimer. A system for exploring large virtual environments that combines scaled translational gain and interventions. In *Proceedings of the 7th symposium on Applied perception in graphics and visualization*, page 65. ACM Press, 2010.
330. H.-F. Xing, F. Li, and Y.-L. Liu. Wavelet denoising and feature extraction of seismic signal for footstep detection. *Wavelet Analysis and Pattern Recognition, 2007. ICWAPR '07. International Conference on*, 1:218–223, Nov. 2007.
331. T. Yamada, S. Nakamura, and K. Shikano. Robust speech recognition with speaker localization by a microphone array. In *Proc. ICSLP '96*, volume 3, pages 1317–1320, Philadelphia, PA, Oct. 1996.
332. K. Yin and D. K. Pai. Footsee: an interactive animation system. In *SCA '03: Proceedings of the 2003 ACM SIGGRAPH/Eurographics symposium on Computer animation*, pages 329–338, Aire-la-Ville, Switzerland, Switzerland, 2003. Eurographics Association.
333. C. A. Zanbaka, B. C. Lok, S. V. Babu, A. C. Ulinski, and L. F. Hodges. Comparison of path visualizations and cognitive measures relative to travel technique in a virtual environment. *IEEE Transactions on Visualization and Computer Graphics*, 11(6):694–705, 2005.
334. S. Zhai. *Human performance in six degree of freedom input control*. PhD thesis, University of Toronto, 1995.
335. Y. Zhang, J. Pettré, Q. Peng, and S. Donikian. Data based steering of virtual human using a velocity-space approach. In *Proceedings of Motion in Games*, Lecture Notes in Computer Science 5884, pages 170–181. Springer, 2009.